uOttawa

L'Université canadienne
Canada's university

FACULTÉ DES ÉTUDES SUPÉRIEURES ET POSTOCTORALES

uOttawa

L'Université canadienne
Canada's university

FACULTY OF GRADUATE AND POSDOCTORAL STUDIES

Jay Conrad

AUTEUR DE LA THÈSE / AUTHOR OF THESIS

Ph.D. (Chemistry)

GRADE / DEGREE

Department of Chemistry

FACULTÉ, ÉCOLE, DÉPARTEMENT / FACULTY, SCHOOL, DEPARTMENT

Design of Ru-Pseudohalic Catalysts for Olefin Metathesis

TITRE DE LA THÈSE / TITLE OF THESIS

Deryn Fogg

DIRECTEUR (DIRECTRICE) DE LA THÈSE / THESIS SUPERVISOR

CO-DIRECTEUR (CO-DIRECTRICE) DE LA THÈSE / THESIS CO-SUPERVISOR

EXAMINATEURS (EXAMINATRICES) DE LA THÈSE / THESIS EXAMINERS

David Bryce

Sandro Gambarotta

Robert Crutchely

Warren Piers

Gary W. Slater

Le Doyen de la Faculté des études supérieures et postdoctorales / Dean of the Faculty of Graduate and Postdoctoral Studies

Design of Ru-Pseudohalide Catalysts for Olefin Metathesis

Jay C. Conrad

Thesis submitted to the
Faculty of Graduate and Postdoctoral Studies
University of Ottawa
in partial fulfillment of the requirements for the degree of

Doctor of Philosophy

Ottawa-Carleton Chemistry Institute
Faculty of Science
University of Ottawa

Your file Votre référence
ISBN: 978-0-494-49334-2
Our file Notre référence
ISBN: 978-0-494-49334-2

Table of Contents

List of Figures

Chapter 1

Chapter 2

Chapter 3

Chapter 4

Chapter 5

Chapter 6

Appendix A – Catalytic Data

Appendix B – Oligomer Characterization

Appendix C – Fluorous Solvents

Appendix D – NMR Spectra

Appendix E – XRD

List of Tables

Chapter 2

Chapter 3

Chapter 4

Chapter 5

Chapter 6

Appendix A – Catalytic Data

Appendix B – Characterization of Oligomers

Appendix E – XRD Data

List of Schemes

Chapter 3

Chapter 4

Chapter 5

Chapter 6

Abstract

Ruthenium-catalyzed olefin metathesis is an exceptionally powerful method for the catalytic formation of new C=C bonds, recognized last year with the Nobel Prize. While the Grubbs-class catalysts $RuCl_2LL'(CHPh)$ have led to many advances, they offer limited selectivity and lifetimes. As these shortcomings are associated with the chloride ligands, we sought to incorporate "pseudohalide" ligands. Catalysts RuXX'(CHPh)(IMes)(py) were prepared by use of sterically undemanding ancillary ligands and electron-deficient aryloxides. Their modular structure permits control over selectivity via matching of catalyst and substrate reactivity. While their initiation efficiency lies between that of the second- and third-generation Grubbs catalysts, high efficiency is found in RCM of α,ω–dienes to form trisubstituted olefins, vinyl alcohols, α, β-unsaturated acrylates, macrolactones, ethers, tertiary amines, thioethers, and silanes. Their performance relative to the most active Grubbs systems is sometimes better, sometimes less so, with the optimum catalyst being a matter of trial and error (though the sustained activity of the aryloxide catalysts means that they often perform better in reactions that require long lifetimes). They are outstanding in enyne metathesis (enabling quantitative formation of tetrasubstituted olefins, a first in Ru-catalyzed metathesis) and in RCM synthesis of macrocycles. Examination of the much longer reaction time of the Grubbs systems led to the unexpected finding that oligomerization of α,ω-dienes is kinetically dominant, and that RCM products are liberated in a concentration-dependent backbiting reaction. This is extremely important, as oligomers are generally regarded as a dead end in metathesis. This finding completely revises our understanding of the context and protocols for construction of conformationally flexible, medium and large rings by RCM.

Acknowledgements

I would like to thank the following people: my parents for endless support and encouragement; Prof. Deryn Fogg, who has truly been the optimal catalyst for my education – enthusiastic and a pleasure to work with, she has furthered my education more than I thought possible (e.g. a picture may be worth a thousand words; however, I must concede, words are required to say this). In the Fogg lab I had the opportunity to work with a number of talented people from the outset. Jenn, Dino, and Sam took the time to show me the way, although Dino can feel free to take the coffee addiction back. Postdocs Ken and Melanie, graduate students Heather, Sebastien, Johanna and Nick, and undergraduate students Nicola, Henrietta, Maeve and Rylan continued to make coming to work fun and beer nights even more enjoyable. Nostalgic Thursday nights with Claudio, Pawel or Amir will be missed. As well, Glenn and Cheryl are acknowledged for their help with NMR experiments. Prof. Hillary Jenkins must be credited for giving me the headstart from a solid undergraduate experience. Claudio Carra is especially thanked for spending the time and effort to collaborate on the DFT calculations. Colin Masui (Symyx Technologies) is thanked for very useful discussions about high-throughput experiments. Crystallographers Scott Delgano, Hillary Jenkins, Pat Crewdson and Sean Xiang are gratefully acknowledged for handling XRD crystal structures. Effie and Lakota, I thank you both for the companionship while writing this thesis, the honest opinions and the former for being the one for me. Lastly this thesis was supported by scholarship funding from NSERC and the University of Ottawa.

List of Abbreviations

Ac	Acetyl
ADMET	Acyclic diene metathesis
BHT	2,6-di-(tert)-butyl-4-methyl-phenol
Bn	Benzyl
Brpy	3-bromopyridine
BTF	α,α,α-trifluorotoluene
COD	Cyclooctadiene
COE	Cyclooctene
Cp	Cyclopentadienyl
Cp*	Pentamethyl-cyclopentadienyl
CM	Cross metathesis
COSY	Correlation spectroscopy
DCE	1,2-dichloroethane
DFT	Density functional theory
DME	Dimethoxyether
DMF	*N,N*-dimethylformamide
DMSO	Dimethylsulfoxide
EM_k	Effective molarity (kinetic)
EM_K	Effective molarity (thermodynamic)
equiv	equivalents
ES-MS	Electrospray mass spectroscopy
EtOAc	Ethyl acetate
FC-72	perfluorohexane
GC	Gas chromatography
GPC	Gel permeation chromatography
H_2IMes	1,3-bis-(2,4,6-trimethylphenyl)imidazolin-2-ylidene
HMBC	Heteronuclear multiple bond correlation experiment
HPLC	High performance liquid chromatography
HRMS	High resolution mass spectroscopy

ICP-AES	Inductively coupled plasma atomic emission spectroscopy
IMe	1,3-dimethyl-imidazol-2-ylidene
IMes	1,3-bis-(2,4,6-trimethylphenyl)imidazol-2-ylidene
IPr	1,3-bis-(2,6-diisopropylphenyl)imidazol-2-ylidene
IR	Infrared
MALDI-TOF	Matrix Assisted laser desorption ionization-time of flight
MeCN	Acetonitrile
MS	Mass spectroscopy
NBE	Norbornene
NHC	*N*-heterocyclic carbene
NMP	*N*-methylpyrolidone
NMR	Nuclear magnetic resonance
OTf	trifluoroacetate
PDI	Polydispersity
PhCl	Chlorobenzene
PhMe	Toluene
$PhNO_2$	Nitrobenzene
ppm	parts per million (μg/g)
py	Pyridine
RCM	Ring closing metathesis
ROCM	Ring opening cross metathesis
ROMP	Ring opening metathesis polymerization
R_f	Retention factor
[S]	Substrate concentration
TES	Triethylsilyl
TFA	Trifluoroacetic acid
THF	Tetrahydrofuran
THN	1,2,3,4-tetrahydronaphthalene
TLC	Thin layer chromatography
TOF	Turnover frequency
TON	Turnover number

Ts	Toluene sulfonate
XRD	X-ray diffraction

List of Compounds

#	Compound	#	Compound	#	Compound
1	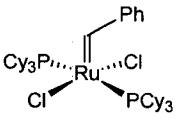	**2** NHC = **a**: IMes **b**: H_2IMes	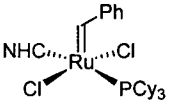	**3** L = **a**: py **b**: Brpy	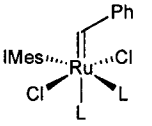
4 R = **a**: $CHCMe_2$ **b**: Ph	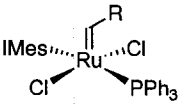	**5** R, R' = **a**: H, H **b**: Ph, H **c**: H, NO_2	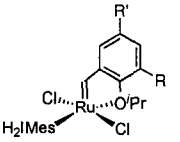	**6**	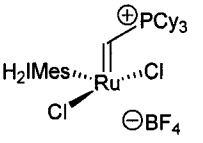
7	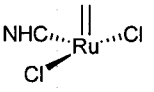	**8** X = **a**: Cl **b**: H	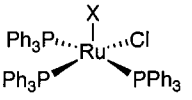	**9**	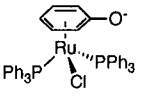
10	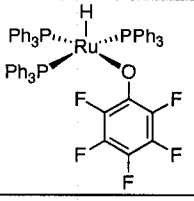	**11**	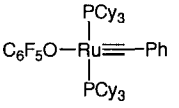	**12** L = **a**: py **b**: Brpy	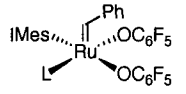
13	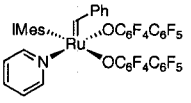	**14**	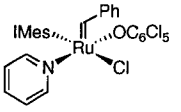	**15** L = **a**: py **b**: Brpy	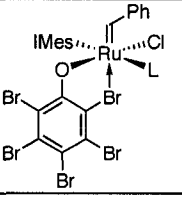
16b	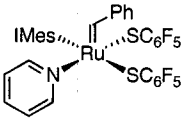	**17**	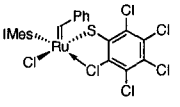	**18** X = **a**: NCS **b**: NCO **c**: CN	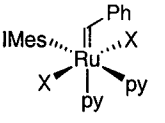
19 X = **a**: NCS **b**: NCO **c**: CN	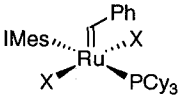	**20**		**21**	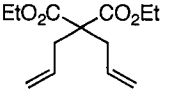
22	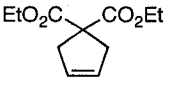	**23** X = **a**: O_2CCF_3 **b**: $O_2CC_3F_7$ **c**: OC_6F_5	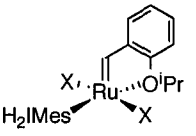	**24**	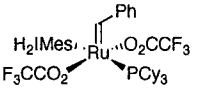

25 X = **a**: ^{t}Bu **b**: $CCF_3(CH_3)_2$ **c**: $C(CF_3)_3$	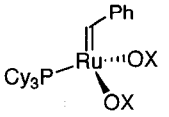	**26**	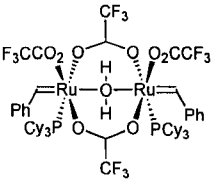	**27** R, R' = **a**: H, NO_2	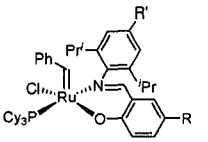
28	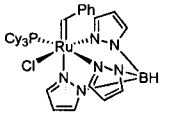	**29**	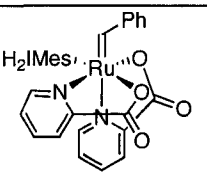	**30** L = **a**: PCy_3 **b**: py_2	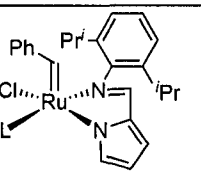
31 X = **a**: OTf **b**: SO_4 **c**: O_2CCF_3	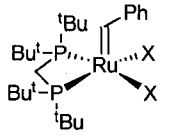	**32**	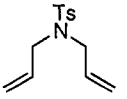	**33**	
34	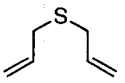	**35**		**36**	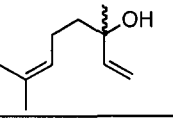
37	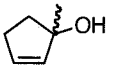	**38**	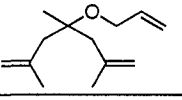	**39**	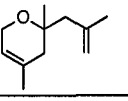
40	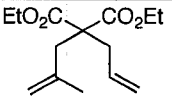	**41**	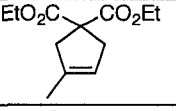	**42**	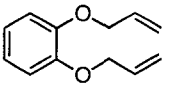
43	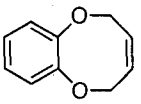	**44**	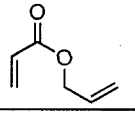	**45**	
46	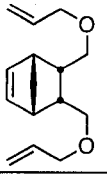	**47**	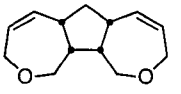	**48**	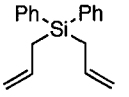
49	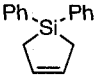	**50**	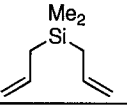	**51**	
52	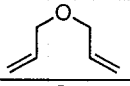	**53**		**54**	
55		**56**		**57**	
58	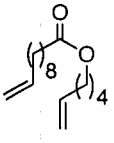	**59**	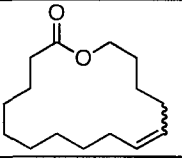	**60**	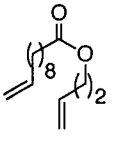

61	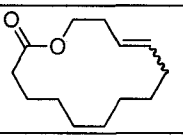	**62**	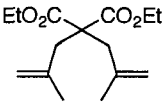	**63**	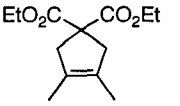
64	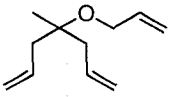	**65** n = **a**: 1 **b**: 2	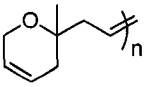	**66**	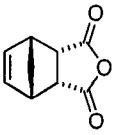
67		**68**	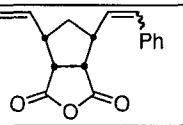	**69**	
70	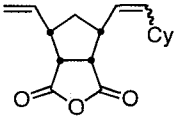	**71**	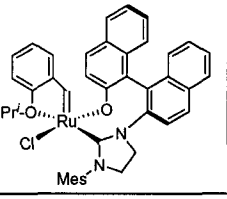	**72**	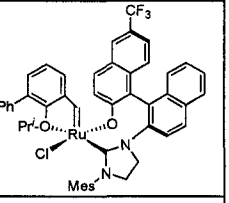
73	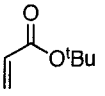	**74**	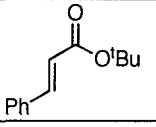	**75**	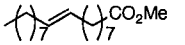
76	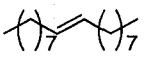	**77**		**78**	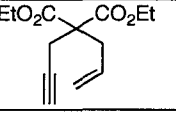
79	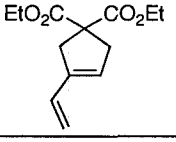	**80**	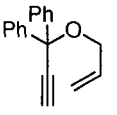	**81**	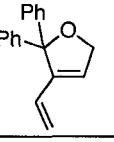
82	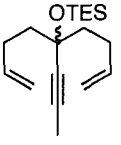	**83**	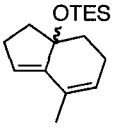	**84**	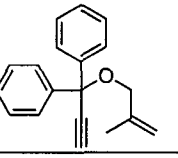
85	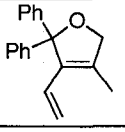	**86**	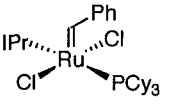	**87**	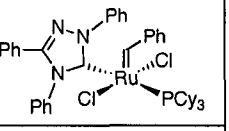
88	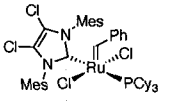	**89**	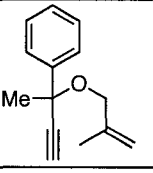	**90**	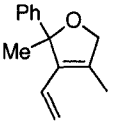
91	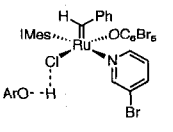	**92**	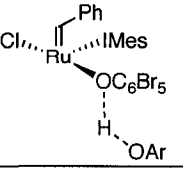	**93**	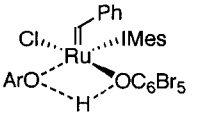

94	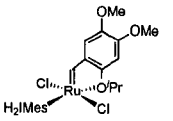	**95**	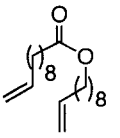	**96**	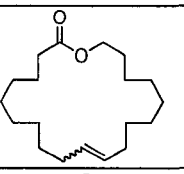
97	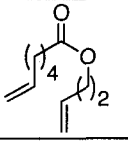	**98**	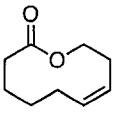	**99**	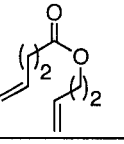
100	olig-**102**	**101**	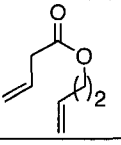	**102**	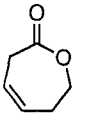
103	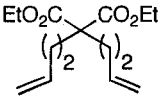	**104**	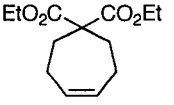	**105**	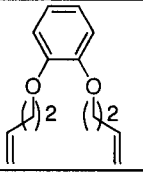
106	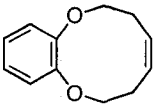	**107**	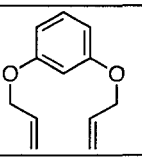	**108**	olig-**107**
109	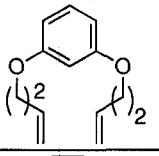	**110**	olig-**109**	**111**	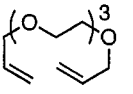
112	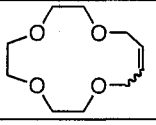	**113**	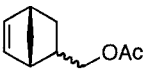	**114**	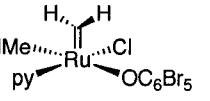
115	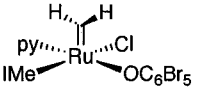	**116**	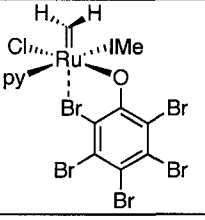	**117**	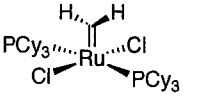
118	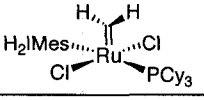	**119**	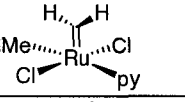	**120**	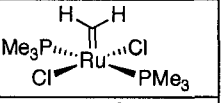
121	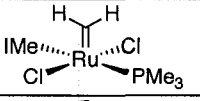	**122**	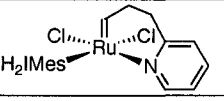	**123**	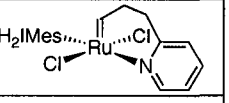
124	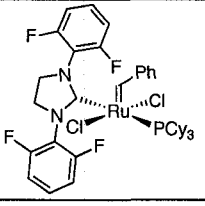	**125**	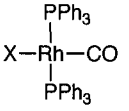		

1 Introduction

"No other technical principle combines economic and ecological values as closely as catalysis."[1] In an age of global concern over the state of the environment, the development of catalytic technologies is becoming increasingly important. The ability of a catalyst to lower the activation energy of a chemical transformation reduces energy costs (Figure 1), affording access to molecules that would otherwise be impractical to make, while minimizing the environmental footprint required.[2-4] Few catalytic methodologies offer the diversity and selectivity of transition-metal catalyzed olefin metathesis.[5,6]

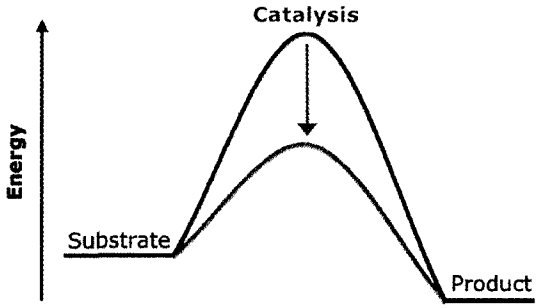

Figure 1. A catalyst lowers the energy needed to convert a substrate into a product.

1.1 Olefin Metathesis

Olefin metathesis describes reactions in which a metal complex catalyzes the skeletal reorganization of alkenes or alkynes. [5-10] Without a catalyst, the thermal [2+2] cycloaddition of two alkenes is symmetry forbidden.[11] Olefin metathesis research began with the use of ill-defined, multi-component catalysts. One of the first reports of metathesis polymerization used a mixture of $TiCl_4$ and EtMgBr as the catalyst.[12] At an early stage, metathesis polymerization was also found to be catalyzed by $WEt_3/AlEt_3$[13] or $RuCl_3$.[14] With these

catalyst formulations in hand, the metathesis of small molecules was explored. Propene, for example, was found to produce ethylene and 2-butene.[15]

Although these structurally ill-defined catalysts gave access to new materials, the reaction mechanism was not understood. In 1970, Chauvin proposed that olefin metathesis is catalyzed by metal alkylidenes, which undergo a [2+2] cycloaddition with an alkene to afford metallacyclobutane and, upon retro-addition, a new alkene (Scheme 1).[16] Compelling evidence for this mechanism emerged from subsequent labeling studies.[17]

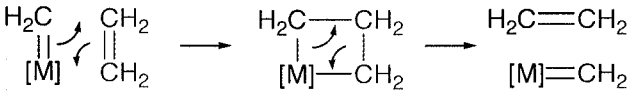

Scheme 1. The Chauvin mechanism for olefin metathesis uses a metal alkylidene as catalyst.

The different kinds of metathesis processes are summarized in Scheme 2. Cross metathesis (CM) exchanges the R-groups of acyclic alkenes. Related to CM, acyclic diene metathesis (ADMET) occurs when dienes undergo an intermolecular reaction to form oligomers.[18] The alternative intramolecular reaction of dienes results in cyclization, a process termed ring closing metathesis (RCM).[19,20] Ring-opening metathesis polymerization (ROMP) of cycloolefins (cycloalkenes) affords polymers. Finally, ene-yne (enyne) metathesis is the reaction of an alkyne and an alkene to form a 1,3-diene.[21] In these reactions, product distributions are determined by thermodynamic parameters. For example, ROMP is driven by the release of ring strain in the cyclic precursor, while CM or RCM processes can be driven by the volatilization of ethylene. The Chauvin mechanism illustrates that any metal-

alkylidene complex can catalyze all of these reactions, providing its reactivity and selectivity is sufficient.

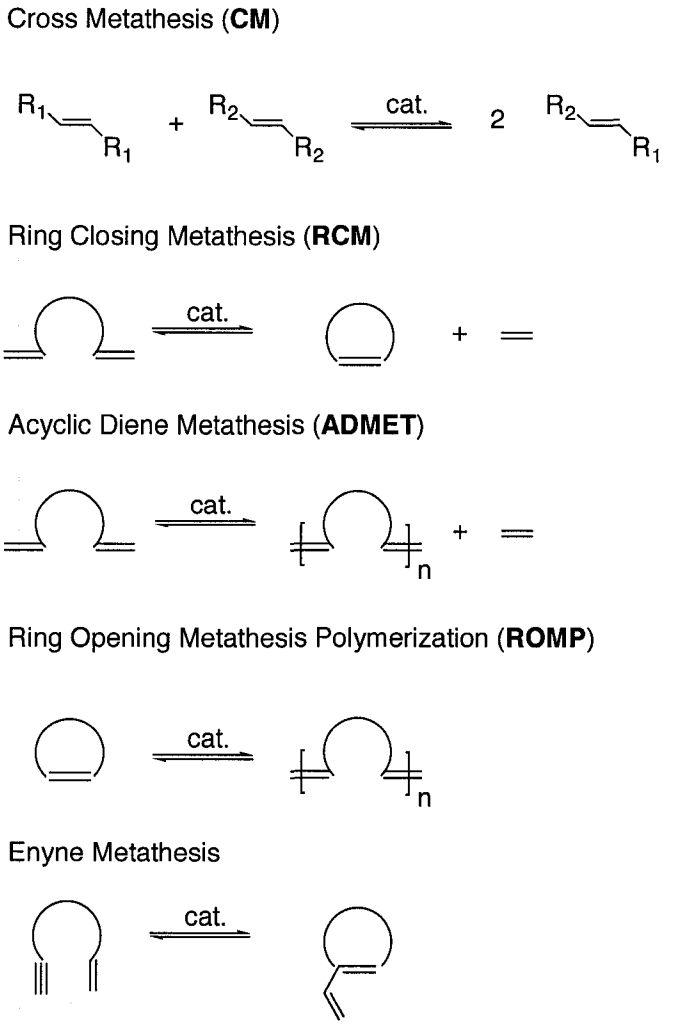

Scheme 2. Types of olefin metathesis reactions.

The diverse nature of these metathesis reactions led to many applications for the early catalysts, including the synthesis of α-olefins,[6] the preparation of macrolactones for perfumery applications,[22] and the production of industrially important polymers via ROMP

of cyclopentene, cyclooctene (Vestenemer), norbornene (Norsorex), and dicyclopentadiene (Metton, Telene, Pentam).[6] Selective reactions involving more complex substrates, however, required the development of structurally well-defined, more active catalysts.

Well-defined, single-component metathesis catalysts are complexes containing a metal-alkylidene. Low oxidation state complexes containing "Fischer carbenes" ([M]=CHOR),[23,24] are less reactive than the high oxidation state "Schrock carbenes" ([M]=CHR).[25] Intensive research by Schrock and coworkers led to the development of well-defined highly active Mo and W catalysts.[26,27] A key advance was the development of a ligand set that enabled fine-tuning of catalyst stereoelectronics. Modulation of the bulk and electronic properties of the imido and, in particular, the alkoxide or aryloxide anionic ligands permitted a high degree of control over reactivity and selectivity. Mo catalysts were used in RCM reactions to form oxygen[28] and nitrogen[29] heterocycles. Chiral catalysts (e.g. C, Figure 2) enabled the production of isotactic ROMP polymers[30] and chiral organic compounds via asymmetric RCM (Figure 2).[27]

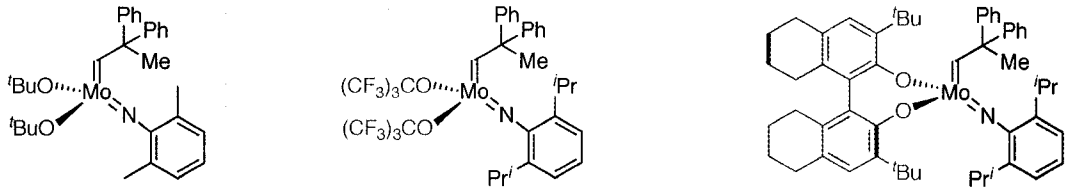

Figure 2. Representative examples of Schrock metathesis catalysts.

Despite the high metathesis activity and remarkable selectivity (including stereoselectivity) of the Group 6 catalysts, they are limited by their high sensitivity to air, water and protic or oxygen donor functional groups, as well as their thermal sensitivity. The

enormous recent expansion in use of metathesis technology is largely due to the development of highly active, easily handled ruthenium catalysts.[31] Ruthenium systems of the Grubbs type, $RuCl_2(CHR)LL'$ (**1**),[32,33] are more thermally stable and much less oxophilic than the Group 6 catalysts. They can thus be deployed in much less stringently controlled reaction conditions, though it should be recognized that the active catalyst is oxygen-sensitive.

Metathesis via **1** is initiated by loss of a neutral PCy_3 ligand, creating an empty coordination site for the incoming alkene. The alkene then undergoes a Chauvin [2+2] cycloaddition with the *cis*-disposed Ru=CHR moiety to generate a metallacyclobutane. NMR evidence for the Ru metallacyclobutane intermediate has recently been reported by Piers and co-workers.[34] A new alkene is obtained by retro-addition; after alkene dissociation, the active catalyst is reformed.

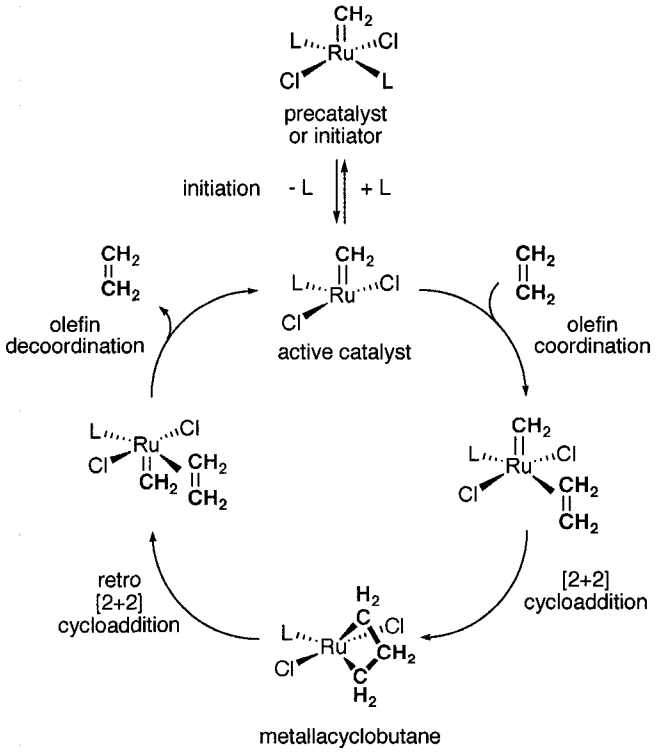

Scheme 3. Ru mediated olefin metathesis mechanism.

The catalytic activity of **1** was increased by replacing one PCy_3 with an *N*-heterocyclic carbene (NHC) group. The discovery of the powerful activating effect of NHC ligands in Ru catalyzed olefin metathesis is attributable to the research groups of Herrmann, Grubbs, and Nolan.[35] Most extensively studied are derivatives containing an IMes[35c,d] or H_2IMes[35e] ligand (**2a** or **2b** respectively; Figure 3). Depending on the substrate, either may be superior.[35-37] Since the H_2IMes version (**2b**) is now commercially available, however, it has become the default choice for "second generation" Ru catalysts, and is widely used by organic chemists. Organometallic chemists, however, tend to use **2a** as it is easier to prepare in high purity. The origin of the higher activity of the second generation catalysts vs. the Grubbs catalyst **1**, is not simply the greater electron-donating power of the NHC ligand, vs. PCy_3: For **2a/b**, the rate of initiation was found to be slower than that of **1**, but its reaction with an olefin was much faster. The result is a much more active catalyst.[38,39]

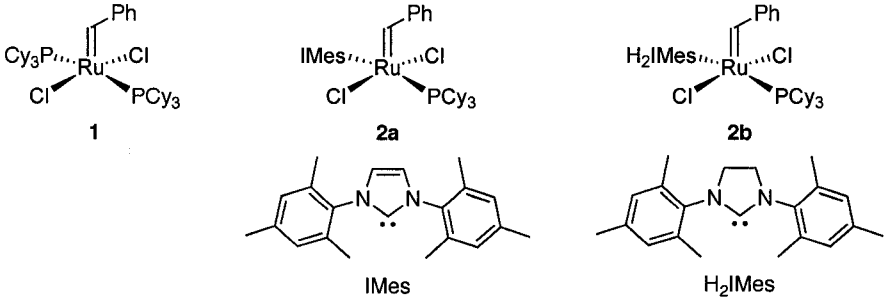

Figure 3. Grubbs' catalyst (**1**) and second generation catalysts containing *N*-heterocyclic carbenes as ligands (**2a/b**).

Since the development of **1** and **2a/b**, olefin metathesis has been widely employed as an exceptionally powerful tool for carbon-carbon bond formation. RCM and CM reactions have had major impact in organic synthesis, and feature as key steps in an increasing number

of natural product syntheses.[40-43] Heterocycles containing phosphorus,[44] sulfur,[44,45] oxygen,[46] nitrogen[46] and carbohydrates[47] are now routinely made by RCM methods. Key to the synthetic utility of the ruthenium metathesis catalysts is that they display orthogonal reactivity, that is, they preferentially react with alkenes leaving most other functional groups untouched. For example, **2b** displays orthogonal reactivity with bromostyrenes, allowing cross metathesis while leaving the aryl bromide untouched. In contrast, Pd cross-coupling catalysts react with both alkene and aryl bromide.[48]

Metathesis frequently offers greater atom economy[49] and higher yields than traditional C-C bond forming methods.[50] As well, the functional-group tolerance displayed by the ruthenium catalysts allows the metathesis step to be used at virtually any stage of a synthesis. This versatility has engaged many synthetic organic chemists, and metathesis is now a key technology for constructing complex molecules.[40] As one high-profile example, ciguatoxin (one of the largest molecules assembled by total synthesis), uses RCM at several key ring-forming steps (Scheme 4).[51]

In other important examples, of RCM in chemical synthesis, macrocycles such as the epothilones (anti-cancer drug candidates),[52,53] (–)-muscone,[54] and Exaltolide[55] (synthetic musk fragrances) have been obtained by RCM.[56] Applications of highly functionalized ROMP polymers include use as: drug delivery agents, nonlinear optical materials,[6] and neoglycopolymers.[57] Recently, olefin metathesis has been used to gain access to molecules with novel topologies, such as molecular gyroscopes[58] or bowl-shaped sumanenes,[59] the latter being a fullerene fragment.

References page 12

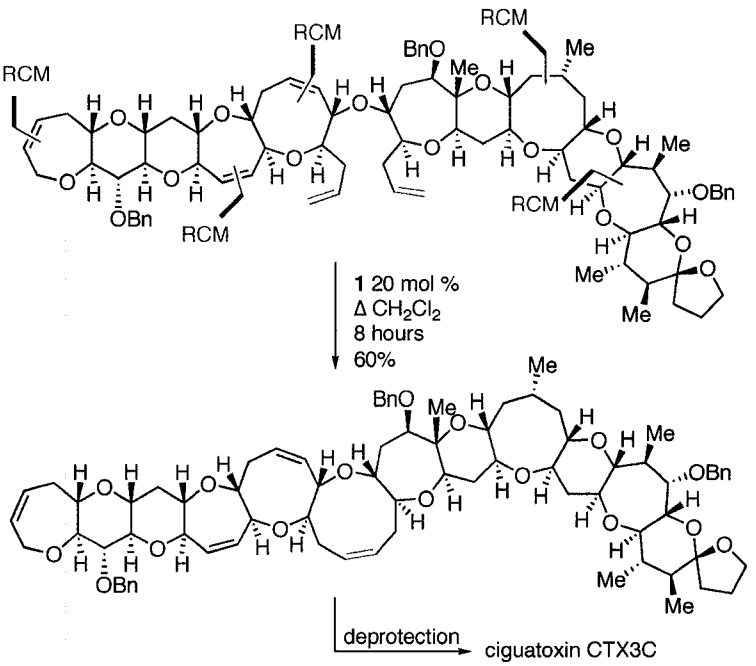

Scheme 4. A late-stage RCM step in the synthesis of ciguatoxin.

The importance of the science described above was recognized in 2005 with a Nobel prize being awarded to Chauvin, Schrock and Grubbs, pioneers of metathesis chemistry. The citation stated, in part, that:

"Catalysts for metathesis have been developed into enormously powerful and versatile tools in organic synthesis. The wealth of synthetic transformations that can be accomplished is astonishing."
-Nobel Prize Announcement 2005[60]

Despite the phenomenal success of Grubbs catalyst (**1**) and its NHC derivatives **2**, limitations include their short lifetimes and the inability to tune selectivity. Reduced catalyst loadings and increased catalyst productivity are needed before widespread industrial use is feasible. To date, however, the major focus of research has been improving catalyst activity. Increased activity has been achieved by making derivatives of **2** that contain ligands which

are more labile than PCy_3, such as: pyridine (**3**),[61] PPh_3 (**4**)[62] or a styrenyl ether (**5a**)[63] activated by steric (**5b**)[64] or electronic destabilization (**5c**)[65] of the chelate ring. An extreme example of this approach was the development of four-coordinate phosphonium alkylidene **6**.[66]

For all the above catalyst modifications, the anionic chloride ligand remains unchanged. Consequently, all converge on **7** as the active intermediate (Figure 4). Therefore, similar selectivity and deactivation pathways can be anticipated.

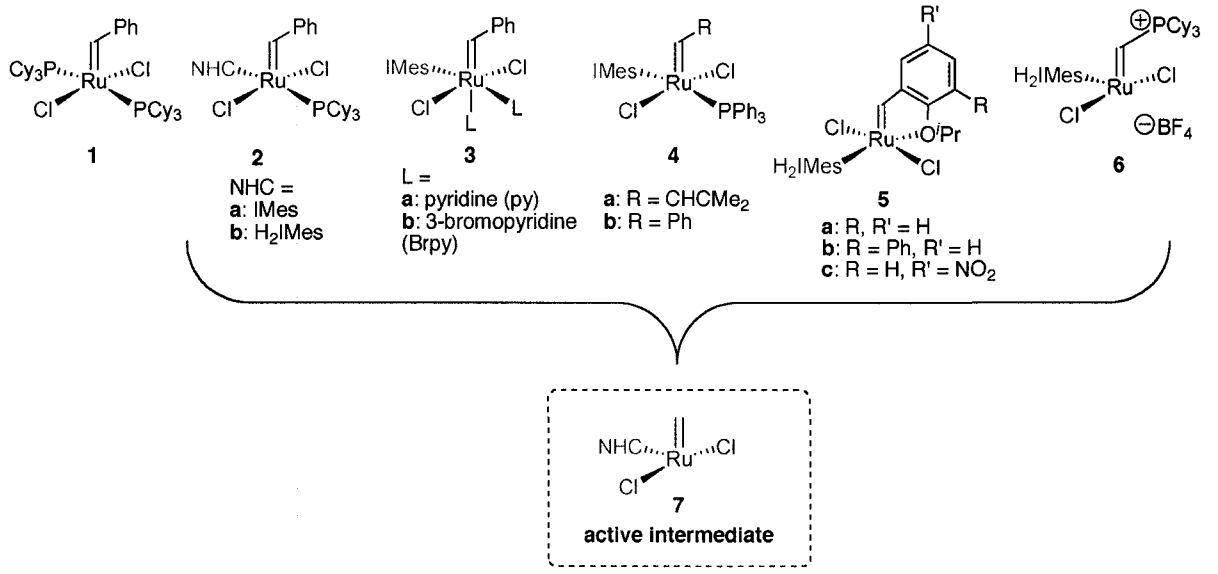

Figure 4. Metathesis catalysts that converge on 14-electron dichloride intermediate **7**.

Previous work form our group described the bimolecular decomposition of a range of $RuCl_2LL'(CHR)$ species into metathesis inactive dimers based on the $Ru_2(\mu\text{-}Cl)_3$ core.[67-69] Others have described the thermal decomposition of **2b**,[70] and the unimolecular decomposition of metallacyclobutane by reductive elimination (Scheme 5).[71] Advances in

the design of Ru metathesis catalysts require a new strategy to limit such decomposition pathways and to enable modulation of catalyst activity and selectivity.

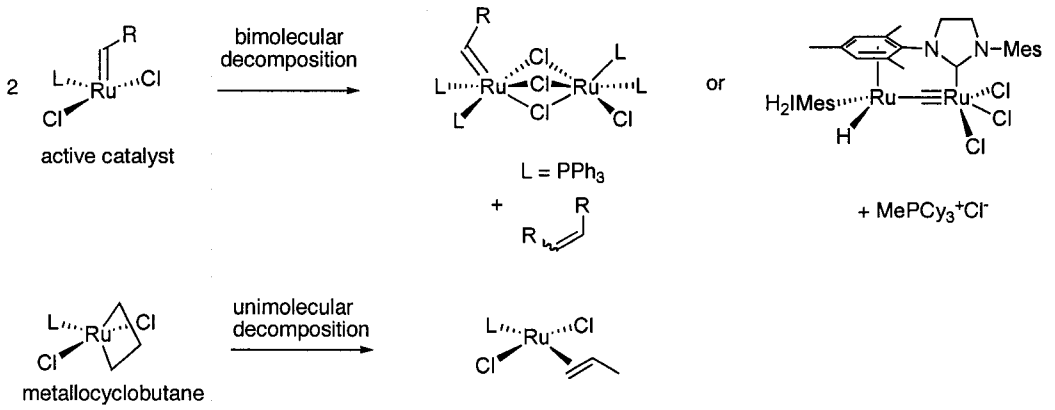

Scheme 5. Known decomposition routes of Grubbs-class metathesis catalysts.

The key design element we chose to change was the replacement of chloride with pseudohalides.[72] Work from the Schrock group, described above, showed that the definition of the catalyst active site, including prevention of bimolecular decomposition, could be accomplished with modular, tunable aryloxide or alkoxide ligands.[73] In comparison, the chloride ligands ubiquitous to Ru chemistry offer limited capacity for tuning. We were intrigued by the potential of a Ru catalyst family in which the chloride ligands were replaced with more readily tunable anionic ligands, such as aryloxides (Figure 5). The ability to tune catalyst selectivity, activity and productivity via better use of the anionic donors is an especially attractive prospect, because unlike the neutral donors, the anionic donors are much less likely to dissociate during metathesis. Therefore, they enhance the capacity for tuning catalyst sterics and electronics at all mechanistic steps, not just initiation. Stereoelectronic effects are found throughout chemistry: in catalysis, small differences in catalyst structure can mean the difference between success and failure.

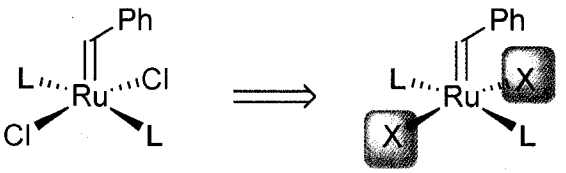

Figure 5. Conventional Ru metathesis catalysts contain chloride anionic ligands. A new variable design incorporates the anionic "X" ligands.

1.2 Scope of this Thesis

This thesis describes a new approach to the design of ruthenium metathesis catalysts aimed at enhancing catalyst performance and controlling selectivity. Depending on the application high activity or productivity is required. Experimental details are found in Chapter 2 and data not appearing in the main text is tabulated in the appendices. Chapter 3 describes the synthetic efforts directed at replacing the chloride ligands in the Grubbs type Ru catalysts with pseudohalides. Chapter 4 describes the screening of catalysts for ROMP activity, and testing of the optimal Ru-aryloxide catalysts for challenging reactions such as the formation of macrocycles or tetrasubstituted olefins. Modulation of these ligands permits control over catalyst selectivity and activity and enables the use of low catalyst loadings. In Chapter 5, ring-closing metathesis is examined in closer detail. An unrecognized fundamental interplay between ADMET and RCM chemistry is described, which has profound implications both for the design of appropriate experimental protocols, and for the validity of some data reported in the literature. Chapter 6 includes studies on the reactivity and mechanistic behavior of selected aryloxide catalysts using a combination of kinetic and theoretical methods. Finally, Chapter 7 offers suggestions for future work, including asymmetric metathesis.

1.3 References

(1) Herrmann, W.A., *ISHC 14 Program. Catalysis: Technology of the Future*. Technische Universität München: Munich, 2003.
(2) Cornils, B.; Herrmann, W.A.; Schlögl, R.; Wong, C., *Catalysis from A to Z: A Concise Encyclopedia*. Wiley: Weinheim, 2003.
(3) van Leeuwen, P.W.N.M., *Homogeneous Catalysis: Understanding the Art*. Kluwer Academic Publishers: Dordecht, 2004.
(4) Blaser, H.U.; Schmidt, E., *Asymmetric Catalysis on Industrial Scale*. Wiley: Weinheim, 2004.
(5) Ivin, K.J.; Mol, J.C., *Olefin Metathesis and Metathesis Polymerization*. Academic Press: New York, 1997.
(6) Grubbs, R.H., *Handbook of Metathesis*. Wiley-VCH: Weinheim, Germany, 2003.
(7) a) Calderon, N., *Acc.Chem. Res.*, **1972**, *5*, 127-132. b) Calderon, N.; Chen, H. Y.; Scott, K. W. *Tetrahedron Lett.*, **1967**, *34*, 3327-3329.
(8) Grubbs, R.H. *Tetrahedron* **2004**, *60*, 7117-7140.
(9) Grubbs, R.H.; Trnka, T.M.; Sanford, M.S. *Curr. Method. Inorg. Chem.* **2003**, *3*, 187-231.
(10) Rouhl, M. *Chem. Eng. News.* **2002**, *80*, 34-38.
(11) Carey, F.A.; Sundberg, R.J., *Advanced Organic Chemistry Part A: Structure and Mechanisms, 4 Ed.* Kluwer Academic: New York, 2000.
(12) Anderson, M. W.; Merckling, M. G., Polymeric bicyclo[2.2.1]hept-2-ene U.S. Pat. 2,721,189, 1955.
(13) Natta, G.; Dall'Asta, G.; Mazzenti, G. *Angew. Chem., Int. Ed.* **1964**, *3*, 723-729.
(14) Michelotti, F.W.; Keaveney, W.P. *J. Polym. Sci.* **1965**, 895-905.
(15) Banks, R.L.; Bailey, G.C. *Ind. Eng. Chem.* **1964**, *3*, 170.
(16) Herisson, J.L.; Chauvin, Y. *Makromol. Chem.* **1970**, *141*, 161-176.
(17) Grubbs, R.H.; Carr, C.; Hoppin, P.L.; Burk, P.L. *J. Am. Chem. Soc.* **1976**, *98*, 3478-3484.
(18) Wagener, K.B.; Boncella, J.M.; Nel, J.G. *Macromolecules* **1991**, *24*, 2649-2657.
(19) Villemin, D. *Tetrahedron Lett.* **1980**, *21*, 1715-1718.
(20) Tsuji, J.; Hashiguchi, S. *Tetrahedron Lett.* **1980**, *21*, 2955-2958.
(21) Katz, T.J.; Sivavec, T.M. *J. Am. Chem. Soc.* **1985**, *107*, 737-738.
(22) Mol, J.C. *J. Mol. Catal. A* **2004**, *213*, 39-45.
(23) Fischer, E.O.; Maasböl, A. *Angew. Chem., Int. Ed.* **1964**, *3*, 580-581.
(24) Cardin, D.J.; Cetinkaya, B.; Lappert, M.F. *Chem. Rev.* **1972**, *72*, 545-574.
(25) a) Schrock, R. R. *J. Am. Chem. Soc.* **1974**, *96*, 6796-6797. b) Schrock, R. R., *Acc. Chem. Res.* **1979**, *12*, 98-104.
(26) Bazan, G.C.; Schrock, R.R.; Cho, H.N.; Gibson, V.C. *Macromolecules* **1991**, *24*, 4495-4502.
(27) Schrock, R.R.; Hoveyda, A.H. *Angew. Chem., Int. Ed.* **2003**, *42*, 4592-4633.
(28) Fu, G.C.; Grubbs, R.H. *J. Am. Chem. Soc.* **1992**, *114*, 5426-5427.
(29) Fu, G.C.; Grubbs, R.H. *J. Am. Chem. Soc.* **1992**, *114*, 7324-7325.
(30) McConville, D.H.; Wolf, J.R.; Schrock, R.R. *J. Am. Chem. Soc.* **1993**, *115*, 4413-4414.
(31) Trnka, T.M.; Grubbs, R.H. *Acc. Chem. Res.* **2001**, *34*, 18-29.

(32) Schwab, P.; France, M.B.; Ziller, J.W.; Grubbs, R.H. *Angew. Chem., Int. Ed.* **1995**, *34*, 2039-2041.
(33) Schwab, P.; Grubbs, R.H.; Ziller, J.W. *J. Am. Chem. Soc.* **1996**, *118*, 100-110.
(34) Romero, P.; Piers, W. *J. Am. Chem. Soc.* **2005**, *127*, 5032-5033.
(35) (a) Weskamp, T.; Schattenmann, W. C.; Spiegler, M.; Herrmann, W. A. *Angew. Chem., Int. Ed.* **1998**, *37*, 2490-2493. Herrmann, W. A. *Angew. Chem., Int. Ed.* **1999**, *38*, 262. (b) Weskamp, T.; Kohl, F. J.; Hieringer, W.; Gleich, D.; Herrmann, W. A. *Angew. Chem., Int. Ed.* **1999**, *38*, 2416-2419. (c) Huang, J.; Stevens, E. D.; Nolan, S. P.; Peterson, J. L. *J. Am. Chem. Soc.* **1999**, *121*, 2674-2678. (d) Scholl, M.; Trnka, T. M.; Morgan, J. P.; Grubbs, R. H. *Tetrahedron Lett.* **1999**, *40*, 2247-2250. (e) Scholl, M.; Ding, S.; Lee, C. W.; Grubbs, R. H. *Org. Lett.* **1999**, *1*, 953-956.
(36) Fürstner, A.; Ackermann, L.; Gabor, B.; Goddard, R.; Lehmann, C.W.; Mynott, R.; Stelzer, F.; Thiel, O. *Chem. Eur. J.* **2001**, *7*, 3236-3253.
(37) Bielawski, C.W.; Grubbs, R.H. *Angew. Chem., Int. Ed.* **2000**, *39*, 2903-2906.
(38) Sanford, M.S.; Love, J.A.; Grubbs, R.H. *J. Am. Chem. Soc.* **2001**, *123*, 6543-6554.
(39) Sanford, M.S.; Ulman, M.; Grubbs, R.H. *J. Am. Chem. Soc.* **2001**, *123*, 749-750.
(40) Nicolaou, K.C.; Bulger, P.G.; Sarlah, D. *Angew. Chem., Int. Ed.* **2005**, *44*, 4490-4527.
(41) Maier, M.E. *Angew. Chem., Int. Ed.* **2000**, *39*, 2073-2077.
(42) Yet, L. *Chem. Rev.* **2000**, *100*, 2963-3007.
(43) Fürstner, A. *Angew. Chem., Int. Ed.* **2000**, *39*, 3012-3043.
(44) McReynolds, M.D.; Dougherty, J.M.; Hanson, P.R. *Chem. Rev.* **2004**, *104*, 2239-2258.
(45) Karsch, S.; Freitag, D.; Schwab, P.; Metz, P. *Synthesis* **2004**, 1696-1712.
(46) Deiters, A.; Martin, S.F. *Chem. Rev.* **2004**, *104*, 2199-2238.
(47) Roy, R.; Das, S.K. *Chem. Commun.* **2000**, 519-529.
(48) Chatterjee, A.K.; Toste, F.D.; Choi, T.-L.; Grubbs, R.H. *Adv. Syn. Catal.* **2002**, *344*, 634-637.
(49) Trost, B.M. *Science* **1991**, *254*, 1471-1477.
(50) Gaich, T.; Mulzer, J. *Org. Lett.* **2005**, *7*, 1311-1313.
(51) a) Hirama, M.; Oishi, T.; Uehara, H.; Inoue, M.; Maruyama, M.; Oguri, H.; Satake, M., *Science*, **2001**, *294*, 1904-1907. b) Inoue, M.; Miyazaki, K.; Uehara, H.; Maruyama, M.; Hirama, M., *Proc. Natl. Acad. Sci. USA*, **2004**, *101*, 12013-12016.
(52) Yang, Z.; He, Y.; Vourloumis, D.; Vallberg, H.; Nicolaou, K.C. *Angew. Chem., Int. Ed.* **1997**, *36*, 166-168.
(53) Rivkin, A.; Cho, Y.S.; Gabarda, A.E.; Yoshimura, F.; Danishefsky, S.J. *J. Nat. Prod.* **2004**, *67*, 139-143.
(54) Louie, J.; Bielawski, C.W.; Grubbs, R.H. *J. Am. Chem. Soc.* **2001**, *123*, 11312-11313.
(55) Fürstner, A.; Langemann, K. *Synthesis* **1997**, 792-803.
(56) Kraft, P.; Bajgrowicz, J.A.; Denis, C.; Frater, G. *Angew. Chem., Int. Ed.* **2000**, *39*, 2980-3010.
(57) Fraser, C.; Grubbs, R.H. *Macromolecules* **1995**, *28*, 7248-7255.
(58) Shima, T.; Hampel, F.; Gladysz, J.A. *Angew. Chem., Int. Ed.* **2004**, *43*, 5537-5540.
(59) Sakurai, H.; Daiko, T.; Hirao, T. *Science* **2003**, *301*, 1878.
(60) See 2006 Nobel Lectures from R.H. Grubbs, R. R. Schrock and Y. Chauvin: http://nobelprize.org, also see a) Chauvin, Y. *Angew. Chem., Int. Ed.*, **2006**, *45*, 3740-3747. b) Schrock, R.R. *Angew. Chem., Int. Ed.*, **2006**, *45*, 3748-3759. c) Grubbs, R. H. *Angew. Chem., Int. Ed.*, **2006**, *45*, 3760-3765.

(61) **3a**: Conrad, J. C.; Amoroso, D.; Czechura, P.; Yap, G. P. A.; Fogg, D. E. *Organometallics*, **2003**, *22*, 3634-3636. H_2IMes-**3a**: Sanford, M. S.; Love, J. A.; Grubbs, R. H., *Organometallics*, **2001**, *20*, 5314-5318. H_2IMes-**3b**: Love, J. A.; Morgan, J. P.; Trnka, T. M.; Grubbs, R. H. *Angew. Chem., Int. Ed.* **2002**, *41*, 4035-4037.
(62) **4a**: Conrad, J. C.; Yap, G. P. A.; Fogg, D. E. *Organometallics* **2003**, *22*, 1986-1988. H_2IMes **4b**: Sanford, M. S.; Love, J. A.; Grubbs, R. H. *Organometallics* **2001**, *20*, 5314-5318. **4b**: Huang, J.; Stevens, E. D.; Nolan, S. P.; Peterson, J. L. *Organometallics* **1999**, *18*, 5375-5380
(63) (a) Kingsbury, J. S.; Harrity, J. P. A.; Bonitatebus, P. J.; Hoveyda, A. H. *J. Am. Chem. Soc.* **1999**, *121*, 791-799. (b) Garber, S. B.; Kingsbury, J. S.; Gray, B. L.; Hoveyda, A. H. *J. Am. Chem. Soc.* **2000**, *122*, 8168-8179. (c) Hoveyda, A. H.; Gillingham, D. G.; Van Veldhuizen, J. J.; Kataoka, O.; Garber, S. B.; Kingsbury, J. S.; Harrity, J. P. A. *Org. Biomol. Chem.* **2004**, *2*, 8-23.
(64) a) Wakamatsu, H.; Blechert, S. *Angew. Chem., Int. Ed.*, **2002**, *41*, 794-796. b) Wakamatsu, H.; Blechert, S. *Angew. Chem., Int. Ed.*, **2002**, *41*, 2403-2405.
(65) (a) Grela, K.; Harutyunyan, S.; Michrowska, A. *Angew. Chem., Int. Ed.*, **2002**, *41*, 4038-4040. (b) Michrowska, A.; Bujok, R.; Harutyunyan, S.; Sashuk, V.; Dolgonos, G.; Grela, K. *J. Am. Chem. Soc.*, **2004**, *126*, 9318-9325. (c) Zaja, M.; Connon, S. J.; Dunne, A. M.; Rivard, M.; Buschmann, N.; Jiricek, J.; Blechert, S. *Tetrahedron* **2003**, *59*, 6545-6558.
(66) Romero, P.E.; Piers, W.E.; McDonald, R. *Angew. Chem., Int. Ed.* **2004**, *43*, 6161-6165.
(67) Amoroso, D.; Yap, G.P.A.; Fogg, D.E. *Organometallics* **2002**, *21*, 3335-3343.
(68) Amoroso, D.; Snelgrove, J.L.; Conrad, J.C.; Drouin, S.D.; Yap, G.P.A.; Fogg, D.E. *Adv. Syn. Catal.* **2002**, *344*, 757-763.
(69) Drouin, S.D.; Monfette, S.; Amoroso, D.; Yap, G.P.A.; Fogg, D.E. *Organometallics* **2005**, *24*, 4721-4728.
(70) Hong, S.H.; Day, M.W.; Grubbs, R.H. *J. Am. Chem. Soc.* **2004**, *126*, 7414-7415.
(71) van Rensburg, W.J.; Steynberg, P.J.; Meyer, W.H.; Kirk, M.M.; Forman, G.S. *J. Am. Chem. Soc.* **2004**, *126*, 14332-14333.
(72) Pseudohalogen – compounds that resemble the halogen elements, in their chemistry, e.g. cyanogen, thiocyanogen, iodine cyanide. Certain ions that have sufficient resemblance to halide ions are sometimes referred to as pseudohalide ions, e.g. (http://goldbook.iupac.org).
(73) Schrock, R.R. *J. Mol. Catal. A* **2004**, *213*, 21-30.

2 Experimental Methods

2.1 General Procedures

2.1.1 Reaction Conditions

Synthetic procedures were carried out at room temperature (22 °C) under an inert atmosphere in either an N_2 filled MBraun drybox or a Schlenk line filled with argon dried by passing it through a column of Drierite. Reactions carried out in air are indicated in the individual experimental procedures. Column chromatography of organic molecules was always carried out in air, following standard procedures.[1] All reactions were stirred with Teflon coated magnetic stir bars. For all reactions, the glassware used was heated to 110 °C in an oven and dried under vacuum.

2.1.2 Solvents

Dry, oxygen-free benzene (reagent grade), hexane (reagent grade), toluene (reagent grade), dichloromethane (HPLC grade), tetrahydrofuran (unstabilized) and diethyl ether (reagent grade) were obtained using an Anhydrous Engineering solvent purification system, and stored over Linde 4 Å molecular sieves. Other solvents were purified and degassed by standard methods, typically by distillation.[2] Pyridine was distilled from CaH_2 and 3-bromopyridine filtered 5 times through a short column of neutral alumina.

2.1.3 Deuterated Solvents

All deuterated solvents were purchased from Cambridge Isotope Laboratories Ltd. or Aldrich. For the collection of NMR spectra of organic molecules the deuterated solvents were used without further purification. For organometallic complexes or catalytic reactions dry degassed solvents were used. $CDCl_3$ was distilled from CaH_2 and stored over activated

Linde 4 Å molecular sieves. C_6D_6 was degassed by consecutive freeze/pump/thaw cycles and stored over activated sieves. Ampoules of CD_2Cl_2, toluene-d_8, and THF-d_8 were opened in the glovebox and used as is.

2.1.4 NMR Spectroscopy

^1H (300 or 500 MHz), ^{31}P NMR (121 or 202 MHz) ^{19}F (282 MHz) and ^{13}C NMR (75 or 125 MHz) spectra were recorded on a Bruker Avance-300 or Bruker Avance-500 spectrometer at 298 K. Spectral widths used for the acquisition of NMR spectra δ (ppm): ^1H, +25 to -35; ^{13}C +350 to 0; ^{31}P, +250 to -50. ^1H and ^{13}C NMR spectra were referenced to residual solvent peaks and recorded on the 300 MHz instrument unless stated otherwise. Coupling constants are given as absolute values. ^{31}P NMR spectra were calibrated to external standard of H_3PO_4 at δ 0 ppm; samples were externally referenced by inserting a capillary filled with 85% H_3PO_4 into an NMR tube containing the desired solvent and calibrating to δ 0 ppm. Alternatively, for some solvents, 0.1 M solutions of PPh_3 were used as the external standard, δ: C_6H_6 (-5.06 ppm), $CHCl_3$ (-5.64 ppm), CH_2Cl_2 (-5.46 ppm). In a similar manner, ^{19}F NMR spectra were referenced to trifluoroacetic acid (δ 0 ppm). Literature values referenced to CCl_3F, now a regulated chlorofluorocarbon, are shifted -76.53 ppm compared to TFA. $^{13}C\{^1H\}$ data for organic compounds are singlets unless stated otherwise.

2.1.5 Gas Chromatography

GC-FID analyses were performed on an Agilent 6890 Series GC-FID equipped with an Agilent 7683 Series autosampler. A Varian CP-wax 52 CB carbowax chemically bonded, 30 m length, 320 μm diameter column was used. The carrier gas was UHP grade helium. The analyte injection volume was 1 μl. The inlet septum was replaced every 200 injections or

References page 78

upon loss of a good baseline signal to noise ratio. The autosampler was set to rinse the syringe with methanol and dichloromethane five times each between runs.

2.1.6 Other instrumentation

IR spectra were measured on a Bomem MB100 IR spectrometer with NaBr salt plates. Organometallic complexes were typically analyzed as a nujol mull and only non overlapping peaks such as C=C and C=O stretches were reported. IR spectra of liquid organic molecules were recorded neat and the entire spectrum is reported.

Microanalyses and ICP-AES (inductively coupled plasma atomic emission spectrometry) analyses for Ru content were carried out by Guelph Chemical Laboratories Ltd., Guelph, Ontario.

Inert-atmosphere MALDI-MS analyses were performed on a Bruker Daltonics OmniFlex MALDI TOF mass spectrometer equipped with a nitrogen laser (337 nm), and interfaced to an MBraun LabMaster 130 glovebox. Data were collected in positive reflecting mode, with accelerating voltage held at 20 kV for all experiments, calibrating before each use with $[RuCl_2(dppe)_2]$: calculated $M^{+\cdot}$ *m/z* 968.11 and $[M\text{-}Cl]^+$ *m/z* 933.14. Matrix (pyrene) and analyte solutions were prepared in CH_2Cl_2 at concentrations of 20 mg/mL and 1 mg/mL, respectively; samples were mixed in a matrix:analyte ratio of 20:1 and spotted on the plate using the dried droplet method. Either Maeve Moriarty, Melanie Eelman or Johanna Blacquiere collected spectra. Electrospray mass spectra of organometallic complexes were acquired from THF solutions (1mg/mL).

Gel permeation chromatography (GPC) data were collected using a Waters 515 HPLC pump, Rheodyne 7725i injector fitted with a 200 μl injection loop, Waters styrogel HR3 and HR4 columns in series, an Optilab DSP refractometer and a Wyatt Dawn light-

scattering detector. HPLC grade dichloromethane was used as the eluent and sparged vigorously for 30 min with argon prior to use. Samples were dissolved in CH_2Cl_2 (1 mg/mL) and filtered through a 50 μm syringe filter.

2.2 Synthesis of Ligands

2.2.1 Modified synthesis of *N*-tosylhydrazone

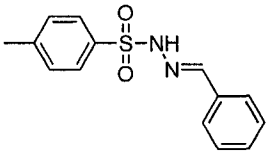

Reaction carried out in air. To a solution of 4-toluenesulfonehydrazide (18.322 g, 0.0984 mol) in MeOH (40 mL) was added benzaldehyde (10 mL, 0.0984 mol). After stirring for 5 min. a white precipitate formed. The mixture was cooled to 0 °C, filtered and washed with MeOH (10 mL). After drying under vacuum 24.034 g (89%) of white powder was collected. NMR data agrees with reported values.[3]

2.2.2 Modified synthesis of phenyl diazomethane

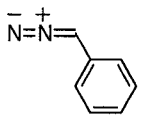

Reaction carried out in air. To a solution of *N*-tosylhydrazone (28 g, 0.107 mol) in triethyleneglycol (200 mL) was added solid KOH (8.16 g, 0.204 mol). The mixture was stirred at 70 °C for 1 hour. During this time the colour gradually changed to deep red. The reaction was quenched with cold water (100 mL). Red phenyl diazomethane was extracted with pentane (3 x 50 mL). The combined fractions were dried with $MgSO_4$, and cooled to –78 °C. The white solids that formed were removed by filtration. The red filtrate was reduced under vacuum to an oil, 3.14 g (25%). NMR data agrees with reported values.[3]

2.2.3 Modified synthesis of glyoxal-bis-(2,4,6-trimethylphenyl)imine

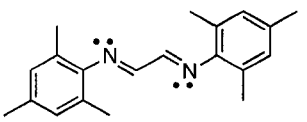

Reaction carried out in air. To a solution of 2,4,6-trimethylaniline (67.16 g, 0.5 mol) in n-propanol (150 mL) was added glyoxal (40 % wt solution in water, 36.3 g, 0.25 mol). After stirring at 60 °C for 4 h the yellow powder was filtered off, 57 g (78%). NMR data agree with reported values.[4]

2.2.4 Modified synthesis of 1,3-bis(2,4,6-trimethylphenyl)imidazolium chloride

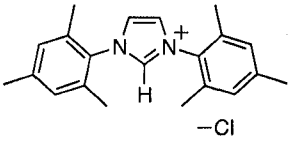

In a dry flask under an atmosphere of argon was added glyoxal-bis-(2,4,6-trimethylphenyl)imine (9 g, 0.0308 mol) and dry THF (100 mL). Next, chloromethylethyl ether (3.03 g, 0.0308 mol) was added by syringe. A vial of activated sieves was hung by a copper wire inside the flask. The reaction was stirred for 5 days, during which a white solid began to precipitate. The white solid was then collected by filtration, washed with THF (3 x 100 mL) then dried under vacuum, 7.068 g (68%). NMR data agree with reported values.[4]

2.2.5 Modified synthesis of IMes, 1,3-bis(2,4,6-trimethylphenyl)imidazol-2-ylidene

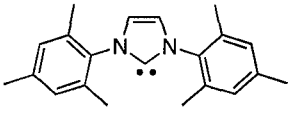

To a solution of 1,3-bis(2,4,6-trimethylphenyl)imidazolium chloride (5 g, 14.7 mmol) in THF (50 mL) was added solid KO^{t}Bu (1.939 g, 14.7 mmol). The reaction was stirred for 1.5 h. The solvent was then removed under vacuum and the white residue dissolved in benzene. The gummy residue was allowed to settle to the bottom and the liquid decanted into a large 3 cm coarse ground glass filter half filled with compacted Celite. The leftover glue was rinsed twice more with 15 mL benzene. The filtrate was then reduced under vacuum to dryness; a warm water bath was used to keep the benzene from freezing. The off-white solid was reprecipitated from hexane

(-35 °C) to give a white powder, which was filtered and dried under vacuum, 3.67 g (82%). NMR data agree with reported values.[4]

2.3 Synthesis of $RuCl_2(CHR)(L)(L')$ complexes and their precursors

2.3.1 Improved synthesis of $RuCl_2(PPh_3)_3$, **8a**

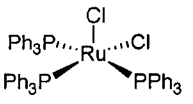

To a 500 mL Schlenk round bottom flask was added $RuCl_3(H_2O)_6$ (10 g, 0.0425 mmol) and dry methanol. The dark solution was heated to reflux for 1 h. Against the flow of nitrogen 6 equiv. of PPh_3 (67 g, 0.255 mol) were added, then heated again for 4 h. Using a Schlenk filter, the solid was then filtered off. *The purification is carried out with wet solvents in air.* The brown powder was washed with 500 mL of MeOH then 8 × 500 mL washes with hexanes or until no more PPh_3 was present by TLC. The powder was then dried under vacuum, 33 g (81 %). ^1H and $^{31}P\{^1H\}$ NMR data correspond with literature values.[5]

2.3.2 Improved synthesis of $RuHCl(PPh_3)_3$, **8b**

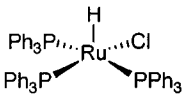

To a 500 mL Schlenk round bottom flask was added $RuCl_2(PPh_3)_3$ (2.00 g, 2.08 mmol) and 100 mL toluene. Then a solution of KH (50 mg, 2.08 mmol) in 2-propanol (20 mL) was added. The resulting solution was heated to reflux on a Schlenk line under Ar for 8 h. A purple suspension formed. The volume of solvent was reduced under vacuum to 2 mL. After adding 10 mL of hexane, purple $RuHCl(PPh_3)_3$ precipitated and was then filtered off, washed with hexanes (4-5 mL), methanol (4 x 3 mL) and then dried under vacuum; yield: 1.924 g (99%). ^1H and $^{31}P\{^1H\}$ NMR data agree with values reported.[5]

2.3.3 Larger scale synthesis of Grubbs' catalyst, $RuCl_2(CHPh)(PCy_3)_2$, **1a**

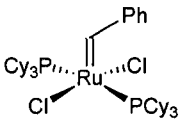

To a stirred, cooled solution (–78 °C) of $RuCl_2(PPh_3)_3$ (11.345 g, 11.8 mmol) in CH_2Cl_2 (275 mL) was added over 15 min. a solution of phenyl diazomethane (3.18 g, 23.6 mmol) in CH_2Cl_2 (100 mL). The colour turned brown. After warming to 0 °C with an ice bath (~30 min), a solution of PCy_3 (7.3 g, 26 mmol) in CH_2Cl_2 (20 mL) was added via syringe. The solution was then warmed to 21 °C and stirred for 45 min. The colour changed to purple. The solvent was removed under vacuum and the remaining dark purple residue was suspended in MeOH (100 mL) and filtered. *The following washes can be done in air with wet solvents.* The purple powder was washed and filtered with MeOH (2 x 100 mL) then 0 °C acetone (100 mL). The purple powder was collected on a filter and dried under vacuum, 6.8 g (70%). NMR data agree with reported values.[6] Characteristic peaks: ^{1}H NMR (C_6D_6): δ 19.94; ($CDCl_3$): δ 19.95. $^{31}P\{^1H\}$ NMR ($CDCl_3$): δ 36.9.

2.3.4 Improved yield synthesis of $RuCl_2(CHPh)(IMes)(PCy_3)$, **2a**

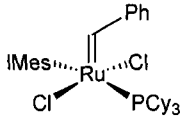

To a solution of $RuCl_2(CHPh)(PCy_3)_2$ (**1**, 6.68 g, 8.13 mmol) in toluene (40 mL) was added IMes (2.6 g, 8.54 mmol). Over 1.5 h the purple solution turned red and the toluene was removed under vacuum. The red residue was then dissolved in pentane (20 mL), and cooled to –78 °C, then filtered. The salmon pink powder was then dried overnight, 6.189 g (90%). NMR data agree with those reported.[7] Characteristic peaks; ^{1}H NMR ($CDCl_3$): δ 19.40 (s, 1H, RuC*H*); (C_6D_6): δ 19.92 (s, 1H, RuC*H*). $^{31}P\{^1H\}$ NMR ($CDCl_3$): δ 32.4 (s); ($CDCl_3$): δ 32.7 (s).

2.3.5 Synthesis of $RuCl_2(CHPh)(IMes)(py)_2$, **3a**

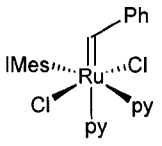

To a 50 mL round bottom flask, 5 g of $RuCl_2(CHPh)(IMes)(PCy_3)$ (**2a**) was dissolved in pyridine (~5 mL). A thick deep green solution was obtained. Addition of small amounts (0.5 mL) of pyridine was sometimes needed to completely dissolve the starting material. To help dissolve any clumps of unreacted starting material, the reaction was stirred vigorously for 15 min. The green precipitate was crashed out with 20 mL hexane and stirred again for 15 min. After cooling to –35 °C, the green solid was filtered off and dried under vacuum overnight, 6.17 g (96%). ^{1}H NMR (C_6D_6): δ 20.02 (s, 1H, RuC*H*), 9.33 (d, $^3J_{HH}$ = 4.3, 2H, py), 8.55 (d, $^3J_{HH}$ = 4.7, 2H, py), 8.25 (d, $^3J_{HH}$ = 7.5, 2H, Ph), 7.21–7.14 (m, 1H, Ph), 6.94 (t, $^3J_{HH}$ = 7.6, 2H, Ph), 6.78 (t, $^3J_{HH}$ = 7.2, 1H, py), 6.50 (s, 4H, Mes Ar*H*), 6.43 (t, $^3J_{HH}$ = 5.9, 1H, py), 6.30–6.27 (m, 3H, py, NC*H*), 6.00 (t, $^3J_{HH}$ = 6.2, 2H, py), 2.50 (s, 12H, CH_3), 1.99 (s, 6H, CH_3). ^{13}C{^{1}H} (C_6D_6): δ 317.8 (s, RuCH), 184.8 (s, NCN), 153.8 (s, Ar *C*), 152.5 (s, Ar *C*H), 150.9 (s, Ar *C*H), 138.4 (s, Ar *C*H), 138.3 (s, Ar *C*H), 137.7 (s, Ar *C*), 135.2 (s, Ar *C*), 134.1 (s, Ar *C*), 131.1 (s, Ar *C*H), 129.2 (s, Ar *C*H), 129.1 (s, Ar *C*H), 128.3 (s, Ar *C*H), 127.9 (s, Ar *C*H), 124.9 (s, Ar *C*H), 122.8 (s, Ar *C*H), 122.6 (s, Ar *C*H), 21.1 (s, *C*H_3), 19.5 (s, *C*H_3). IR (KBr, nujol, cm^{-1}): ν (C=C) 1593 (w). Anal. Calcd. $C_{38}H_{40}N_4Ru$: C, 62.98; H, 5.56; N, 7.73%. Found C, 63.21; H, 5.94; N, 7.61%.

2.3.6 Synthesis of $RuCl_2(CHPh)(IMes)(3\text{-Br-py})_2$, **3b**

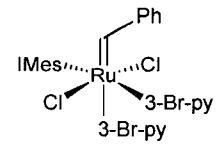

In a 50 mL round bottom flask 400 mg of $RuCl_2(CHPh)(IMes)(PCy_3)$ (**2a**, 48.4 mmol) was dissolved in 3-bromo-pyridine (~5 mL). (Note: To remove polar impurities (^{1}H NMR (C_6D_6): δ 11.5 ppm) immediately before use, 3-bromopyridine was filtered through a column of neutral alumina five times). A thick deep green solution was obtained. Addition of small amounts (0.5 mL) of 3-bromo-pyridine was

sometimes needed to completely dissolve the starting material. To help dissolve any clumps of unreacted starting material, the reaction was stirred vigorously for 15 min. The green precipitate was crashed out with 20 mL hexane and stirred again for 15 min. After cooling to –35 °C the green solid was filtered off and dried under vacuum overnight, 381 mg (89%). ^{1}H NMR (C_6D_6): δ 19.79 (s, 1H), 9.29 (br s, 1H), 8.98 (d, $^3J_{HH}$ = 13.3, 2H), 8.30 (br s, 1H), 8.15 (d, $^3J_{HH}$ = 7.4, 2H), 7.18 (s, 1H), 6.91 (t, $^3J_{HH}$ = 7.3, 3H) 6.54 (s, 4H), 6.38 (d, $^3J_{HH}$ = 6.8, 1H), 6.25 (br s, 1H), 6.10 (br s, 1H), 5.56 (br s, 1H), 2.46 (br s, 12H), 2.10 (s, 6H).

2.3.7 Synthesis of $RuCl_2(CHCHCMe_2)(PPh_3)_2$

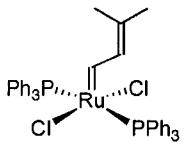

Reaction of $RuHCl(PPh_3)_3$ (1.00 g, 1.08 mmol) with an equimolar amount of 3-chloro-3-methyl-butyne (122 μL) in the presence of Proton Sponge, 1,8-bis(dimethylamino)naphthalene (231 mg, 1.08 mmol) in 10 mL CH_2Cl_2 caused an immediate color change to brown. Dilution with benzene (1 mL), concentration to ~1 mL and addition of hexanes (15 mL) precipitated a brown solid, which was filtered off, washed with methanol and hexanes (5 x 1 mL each), and dried under vacuum. Yield 0.305 g (55%); subsequent crops were contaminated with the reported dimer.[8,9] ^{1}H NMR ($CDCl_3$): δ 18.20 (q, $^3J_{HH}$ = $^3J_{HP}$ = 9.4 Hz, 1H, RuC*H*), 6.85–7.65 (m, 31H, Ar*H*, C*H*CH), 1.23 (s, 3H, CH_3), 0.96 (s, 3H, CH_3); ^{31}P{^{1}H} NMR ($CDCl_3$): δ 30.0 (s). ^{13}C{^{1}H} NMR (CD_2Cl_2): δ 291.4 (t, $^2J_{CP}$ = 10 Hz, RuCH), 152.1 (t, $^2J_{CP}$= 11 Hz, CHCH), 134.9 (t, $^4J_{CP}$ = 5.7 Hz, Ar), 132.1 (t, $^1J_{CP}$ = 20 Hz, Ph), 130.4 (s, Ph), 128.5 (t, J_{CP} = 4.7 Hz , Ph), 27.3 (s, CH_3), 20.9 (s, CH_3). IR (Nujol, cm^{-1}): ν (C=C) 1568 (m); anal. calcd. for $C_{41}H_{38}Cl_2P_2Ru$: C 64.40, H 5.01%; found: C 64.45, H 5.53%.

References page 78

2.3.8 Synthesis of $RuCl_2(CHCHCMe_2)(IMes)(PPh_3)$, **4a**

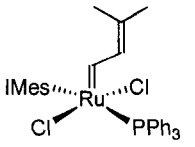

A solution of $RuCl_2(CHCHCMe_2)(PPh_3)_2$ (0.13 mmol) and IMes (0.13 mmol) in 40 mL benzene was stirred for 45 min. The solvent was removed and the residue precipitated from a minimum amount of benzene and pentane (20 mL). The product was filtered off and dried overnight, 81 mg (76%). ^{1}H NMR (C_6D_6): δ 19.40 (d, $^3J_{HH}$ = 10.8 Hz, 1 H; Ru=C*H*), 7.5-7.6 (m, 6 H, P*Ph*), 7.27 (d, $^3J_{HH}$ = 10.9 Hz, 1 H, CHC*H*), 6.9–7.1 (m, 9 H, P*Ph*), 6.77 (s, 2 H, Mes C*H*), 6.64 (s, 2 H, Mes C*H*), 6.22 (s, 2 H, NC*H*), 2.57 (s, 6 H, Mes CH_3), 2.34 (s, 6 H, Mes CH_3), 2.19 (s, 3 H, Mes CH_3), 1.99 (s, 3 H, Mes CH_3), 1.02 (s, 3 H, =CCH_3), 0.65 (s, 3 H, =CCH_3). ^{31}P{^{1}H} (C_6D_6) δ: 38.64 (s). ^{13}C{^{1}H} NMR (C_6D_6): δ 297.1 (d, $^2J_{CP}$ = 11.3 Hz, Ru=*C*H), 190.5 (d, $^2J_{CP}$ = 95.3 Hz, N*C*N), 147.4 (d, $^3J_{CP}$ = 3.6 Hz, =CH*C*H), 138.7–127.9 (multiple peaks: Ph and Mes *C*, *C*H; =*C*Me$_2$) 123.8 (d, $^4J_{CP}$ = 37.3 Hz, N*C*H), 27.2 (s, =*C*CH$_3$), 21.4 (overlapping s, Mes *C*H$_3$), 20.2 (s, =CCH$_3$), 18.9 (s, Mes *C*H$_3$). IR (Nujol, cm^{-1}): ν (C=C) 1607 (m), 1585 (s). Anal. Calcd. for $C_{44}H_{47}Cl_2N_2PRu$: C, 65.50; H, 5.87; N, 3.47%. Found: C, 65.09; H, 6.15; N, 3.13%.

2.3.9 Synthesis of $RuCl_2(CHCHCMe_2)(IMes)_2$

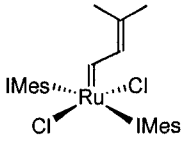

To a solution of $RuCl_2(CHCHCMe_2)(PPh_3)_2$ (0.13 mmol) in 40 mL toluene was added solid IMes (0.26 mmol). After stirring for 48 h, the reaction was judged complete by ^{31}P NMR. Free PPh_3 could not be separated from the highly soluble product. The solvent was removed under vacuum to yield a red oil. ^{1}H NMR (C_6D_6): δ 19.55 (d, $^3J_{HH}$ = 11.2 Hz, 1H, Ru=C*H*), 7.37 (d, $^3J_{HH}$ = 11.2 Hz, 1H, CHC*H*), 7.3–7.4 (m, 12H, free P*Ph*$_3$), 7.0–7.1 (m, 18 H, free P*Ph*$_3$), 6.65 (s, 8 H, Mes C*H*), 5.98 (s, 4 H, NC*H*), 2.36-2.13 (overlapping s, 36 H, Mes CH_3), 0.76 (s, 3 H, =CCH_3), 0.67 (s, 3 H, =CCH_3). ^{31}P{^{1}H} (C_6D_6, 298K): δ -5.06 (s, free PPh_3). ^{13}C{^{1}H} NMR (C_6D_6): δ 289.4 (s, Ru=*C*H), 192.4 (s, N*C*N),

146.9 (s, =CHCH), 138-120 (multiple peaks, Ph and Mes *C*, *C*H; NCH, =*C*Me$_2$), 27.8 (s, =C*C*H$_3$), 21.4 (s, Mes *p*-*C*H$_3$), 20.6 (s, =CC*H*$_3$), 19.2 (s, Mes *o*-*C*H$_3$). ES-MS (THF): m/z: 813 [M$^+$ - Cl]; the isotope pattern corresponds with that calculated.

2.3.10 Synthesis of $RuCl_2(CHPh)(IMes)_2$

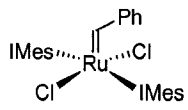

To a solution of $RuCl_2(CHPh)(IMes)(py)_2$ (**3a**, 392 mg, 0.54 mmol) in benzene (20 mL) was added solid IMes (0.54 mmol) and stirred for 8 h. Under vacuum, the red solution was reduced to dryness and reprecipitated from pentane (-78 °C) twice to yield a red powder, 407 mg (86 %). ^{1}H NMR (C_6D_6): δ 19.98 (s, 1H, Ru=C*H*), 9.44 (d, $^3J_{HH}$ = 8.1 Hz, 1H, Ph, *o*-C*H*), 7.04 (t, $^3J_{HH}$ = 7.3 Hz, 1H, Ph, *p*-C*H*), 6.84 (t, $^3J_{HH}$ = 7.1 Hz, 1H, Ph, *m*-C*H*), 6.70 (t, $^3J_{HH}$ = 6.5 Hz, 1H, Ph, *m*-C*H*), 6.63 (br s, 8H, Mes C*H*), 6.34 (d, $^3J_{HH}$ = 7.8 Hz, 1H, Ph, *o*-C*H*), 5.97 (s, 4H, NC*H*), 2.31 (s, 12H, Mes *p*-C*H*$_3$), 2.12 (br s, 24H, Mes *o*-CH$_3$). ^{13}C{^{1}H} NMR (C_6D_6): δ 296.1 (s, Ru=*C*H), 192.4 (s, N*C*N), 151.5 (s, Ph *ipso-C*), 137.6 (s, *Ar*), 137.2 (s, *Ar*), 137.3 (s, *Ar*), 132.0 (s, Mes *C*), 129.7 (s, *Ar*), 129.4 (s, *Ar*), 129.2 (s, *Ar*), 128.6 (s, *Ar*), 128.1 (s, Ph *C*H), 126.4 (s, Mes *m*-*C*H), 126.0 (s, Mes *m*-*C*H), 124.6 (s, N*C*H), 21.4 (s, Mes *C*H$_3$), 19.3 (s, Mes *C*H$_3$), 19.2 (s, Mes *C*H$_3$). IR (Nujol, cm^{-1}): ν (C=C) 1609 (m). Anal. Calcd. for $C_{49}H_{54}Cl_2N_4Ru$: C, 67.57; H, 6.25; N, 6.43%. Found: C, 68.06; H, 6.35; N, 6.50%. MALDI-TOF MS (dithranol): m/z: 869 [M$^+$ - H]; the isotope pattern corresponds with that calculated. ES-MS (THF): m/z: 869 [M$^+$ - H]; the isotope pattern suggests overlap of more than one ion. X-ray quality crystals were grown by slow evaporation of a toluene solution.

2.4 Decomposition of Ru-alkylidenes

2.4.1 $RuCl(PPh_3)_2(\mu\text{-}Cl)_3Ru(PPh_3)_2(CHCHCMe_2)$

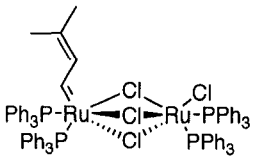

A suspension of $RuCl_2(CHCMe_2)(PPh_3)_2$ (200 mg, 0.26 mmol) in 0.75 mL C_6D_6 underwent 54% conversion to dimer over 11 days at 21 °C. ^1H NMR (C_6D_6): δ 15.86 (q, $^3J_{HH} = {}^3J_{HP} = 12.5$ Hz). $^{31}P\{^1H\}$ NMR (C_6D_6): δ 48.69 (br s, 1P), 43.89 (br s, 1P), 40.41 (br s, 2P).

2.4.2 2,7-dimethylocta-2,4,6-triene

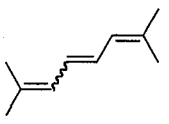

Same procedure as $RuCl(PPh_3)_2(\mu\text{-}Cl)_3Ru(PPh_3)_2(CHCHCMe_2)$. The product was detected by monitoring the olefinic signals between 6.5 and 5.9 ppm. *E*:*Z* = 3:1 ^1H NMR (C_6D_6): δ 6.55–6.50 (m, *Z* isomer), 6.49–6.43 (m, *E* isomer), 6.25–6.20 (m, *Z* isomer), 6.01–5.94 (m, *E* isomer). The spectra agree with the calculated spectra using ACD ^1H NMR simulator.

2.5 General Procedure for the synthesis of thallium salts.

Note: The toxicity of thallium (particularly in the +1 oxidation state) is well established, and the subject has been recently reviewed.[10] Care must be taken to prevent introduction into the body by inhalation, by ingestion via contaminated hands or gloves, or through the skin. All thallium reagents and wastes, including contaminated solvents, were handled using double-glove and secondary containment procedures, with separate disposal of all wastes in accordance with government regulations. Thallium ethoxide is a very dense a clear liquid. This reagent was weighed instead of syringed. Over time TlOEt degrades forming a black precipitate that is easily decanted off.

References page 78

To an oven-dried flask containing a solution of HOC_6X_5 (X = H, F, Cl, Br; 5.0 g scale) in 100 mL dry toluene was added 1.0 equiv TlOEt. The solution was stirred for 8 h, after which the solvent was removed under vacuum. The resulting white solid was washed with hexanes (3 × 8 mL), then dried under vacuum to yield a fine white powder, which was handled under nitrogen in a drybox. Yield 80–90%. Diethyl ether was used for phenols that were not soluble in toluene.

2.6 Model reactions with $RuHCl(PPh_3)_3$ (8a) or $RuCl_2(PPh_3)_3$ (8b)

2.6.1 Improved synthesis of $RuCl(\eta^5OC_6H_5)(PPh_3)_2$, **9**

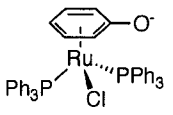

To a stirred purple solution of $RuCl_2(PPh_3)_3$ (**8a**, 200 mg, 0.21 mmol) in 4 mL dichloromethane was added solid $TlOC_6H_5$ (1 equiv). After stirring for 48 h at 21 °C, the orange solution was filtered through Celite, concentrated, and precipitated with 4 mL of hexanes, filtered off, washed with hexanes (4 mL), and dried under vacuum. Yield: 132 mg (83%). NMR data agree with the values reported.[11,12] Crystals were obtained from a concentrated solution of dichloromethane.

2.6.2 Attempted Synthesis of $RuH(OC_6H_4\text{-}4\text{-}NO_2)(PPh_3)_3$

Solid $TlOC_6H_4\text{-}4\text{-}NO_2$ (14 mg, 0.1 mmol) was added to stirred purple solution of $RuCl_2(PPh_3)_3$ (**8a**, 100 mg, 0.11 mmol) in 4 ml dichloromethane. After 48 h at 21 °C, new signals consistent with the desired product appeared: ^{1}H NMR (C_6D_6): δ -17.71 (q, $^3J_{PP}$ = 30 Hz, Ru*H*). $^{31}P\{^1H\}$ NMR (C_6D_6): δ 79.4 (t, $^3J_{PP}$ = 27.0 Hz, 1P), 43.6 (d, $^3J_{HP}$ = 27.0 Hz, 2P). The product was not stable enough to isolate. Formation of the π-bound product is inferred from the liberation of PPh_3.

References page 78

2.6.3 $RuH(OC_6F_5)(PPh_3)_3$, **10**

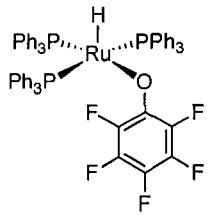

Thallium pentafluorophenoxide (176 mg, 0.45 mmol) was added to a purple solution of $RuHCl(PPh_3)_3$ (**8b**, 420 mg, 0.45 mmol) in 20 mL of THF. The mixture was stirred for 3 h, over which time it turned red. The solvent was removed under reduced pressure, and the resulting oil was dissolved in benzene and filtered through Celite to remove TlCl. The filtrate was concentrated and treated with pentane to precipitate a red solid, which was filtered off. Yield after drying in vacuo: 392 mg (81%). Blocklike crystals suitable for X-ray analysis were grown by slow evaporation of a saturated THF solution. ^1H NMR (C_6D_6): δ 7.40–7.31 (m, 17H, Ar), 6.94–6.90 (m, 10H, Ar), 6.85–6.80 (m, 18H, Ar), -22.29 (q of t, $^2J_{PH}$ = 27.9 Hz, $^5J_{FH}$ = 7.2 Hz, 1H, Ru*H*). $^{31}P\{^1H\}$ NMR (298 K, C_6D_6): δ 47 (br s). $^{31}P\{^1H\}$ NMR (248 K, C_7D_8): δ 87.1 (t, $^2J_{PP}$ = 26 Hz, 1P), 40.9 (d, $^2J_{PP}$ = 26 Hz, 2P). $^{13}C\{^1H\}$ NMR (C_6D_6): δ 144.7–139.6 (m, OC_6F_5), 136.6–136.1 (m, Ph), 134.9–134.6 (m, Ph), 132.5 (d, J_{PC} = 9.6 Hz, Ph), 129.2 (s, Ph). $^{19}F\{^1H\}$ NMR (282.4 MHz, C_6D_6): δ -93.5 to -93.6 (m, 2F), -94.6 to -94.9 (m, 2F), -107.8 to -101.9 (m, 1F). $^{19}F\{^1H\}$ NMR (223 K, C_7D_8): δ -88.8 to -88.9 (m, 1F, o-F), -92.01 (t, $^3J_{FF}$ = 20.9 Hz, 1F, m-F), -93.38 (t, $^3J_{FF}$ = 22.0 Hz, 1F, m-F), -102.5 to -102.6 (m, 1F, o-F), -106.9 to -107.0 (m, 1F, p-F). A low-temperature ^{19}F-^{19}F COSY experiment shows the following correlations (ppm): -89 and -93; -92 and -102; -92 and -107; -93 and -107. IR (Nujol): ν(Ru-H) 2089 cm-1. Anal. Calcd for $RuC_{60}H_{46}P_3OF_5$: C, 67.22; H, 4.33. Found: C, 66.88; H, 4.05.

References page 78

2.7 Aryloxide Derivatives

2.7.1 Representative test reaction on NMR scale

To a 1 dram vial equipped with a stir bar solid $TlOC_6F_5$ (22 mg, 55.2 μmol) was added to a solution of $RuCl_2(CHPh)(IMes)(py)_2$ (**3a**, 20 mg, 27.6 μmol) in C_6D_6 (1 mL). Reaction progress was determined using the RuCHPh ^1H NMR handle (δ 15-21 ppm). The reactions were monitored after 15 min, 3, 8 and 24 hours. $RuCl_2(CHPh)(IMes)(py)_2$ (**3a**) 19.97 ppm → $Ru(OC_6F_5)_2(CHPh)(IMes)(py)$ (**12a**) 18.96 ppm.

2.7.2 $Ru(OC_6F_5)_2(CHPh)(IMes)(py)$, **12a**

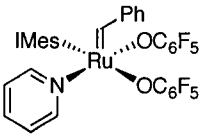

Two equivalents of $TlOC_6F_5$ (470 mg, 1.21 mmol) were added to a green solution of $RuCl_2(CHPh)(IMes)(py)_2$ (440 mg, 0.607 mmol) in 20 mL toluene and stirred overnight. The suspension was filtered through Celite, which was then washed with CH_2Cl_2 (5 mL). The filtrate was stripped to dryness, and the residue precipitated from a minimum volume of CH_2Cl_2 by addition of pentane (20 mL). The green product was filtered off and dried under vacuum. Yield 526 mg (92%). ^1H NMR ($CDCl_3$): δ 18.76 (s, 1H, Ru=C*H*), 7.96 (d, $^3J_{HH}$ = 5.2 Hz, Ph, 2H), 7.47–7.38 (m, 4H, C*H*), 7.15 (s, 2H, C*H*), 7.10 (t, $^3J_{HH}$ = 7.7 Hz, 2H, C*H*), 7.03 (s, 2H, C*H*), 6.81 (t, $^3J_{HH}$ = 6.9, 2H, C*H*), 6.66 (s, 2H, NC*HCH*), 2.37 (s, 6H, CH_3), 2.27 (s, 6H, CH_3), 1.58 (s, 6H, CH_3). $^{13}C\{^1H\}$ (C_6D_6): δ 313.9 (s, Ru=*C*H), 183.5 (s, N*C*N), 154.4–123.9 (s, Ar, ArF), 21.5 (s, CH_3), 18.4 (s, CH_3), 17.5 (s, CH_3). $^{19}F\{^1H\}$ NMR ($CDCl_3$) δ -86.4 to -86.5 (m, 2F), -86.7 to -86.7 (m, 2F), -94.3 (t, $^3J_{FF}$ = 22.3, 2F), -94.5 (t, $^3J_{FF}$ = 22.5, 2F), -104.8 to -105.0 (m, 1F), -105.8 to -106.0 (m, 1F). IR (nujol, cm^{-1}): ν(C=C) 1646. Anal. Calcd. for $C_{43}H_{55}F_{10}N_3O_2Ru$: C, 57.45; H, 3.75; N, 4.47%. Found: C, 57.46; H, 3.65; N, 4.56%. X-ray quality crystals were grown by slow evaporation of a saturated toluene solution.

2.7.3 $Ru(OC_6F_5)_2(CHPh)(IMes)(3\text{-}Br\text{-}py)$, **12b**

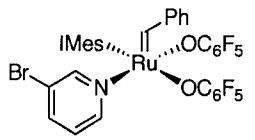

Two equivalents of $TlOC_6F_5$ (409 mg, 1.05 mmol) were added to a green solution of $RuCl_2(CHPh)(IMes)(3\text{-}Br\text{-}py)_2$ (**3b**, 465 mg, 0.526 mmol) in 20 mL toluene and stirred overnight. The suspension was filtered through Celite, which was then washed with CH_2Cl_2 (5 mL). The filtrate was stripped to dryness, and the residue precipitated from a minimum volume of CH_2Cl_2 by addition of pentane (20 mL). The green product was filtered off and dried under vacuum. Yield 451 mg (84%). ^1H NMR (C_6D_6): δ 18.84 (s, 1H, Ru=C*H*), 8.14 (m, 1H, py C*H*), 7.85 (d, J_{HH} = 5.8, 1H, py C*H*), 7.60 (d, J_{HH} = 7.6, 2H, Ph C*H*), 7.19 - 7.14 (m, 1H, Ph, C*H*), 6.98 - 6.88 (m, 4H, Ph, Mes C*H*), 6.59 - 6.54 (m, 1H, py C*H*), 6.48 (s, 2H, Mes C*H*), 6.05 (s, 2H, NC*H*), 5.66 (dd, $^3J_{HH}$ = 8.2; $^3J_{HH}$ = 5.8, 1H, py C*H*), 2.23 (s, 6H, CH_3), 2.15 (s, 6H, CH_3), 1.51 (s, 6H, CH_3). $^{13}C\{^1H\}$ NMR ($CDCl_3$): δ 313.4 (s, Ru=*C*H), 182.8 (s, N*C*N), 155.4 (s, Ar *C*H), 153.0 (s, Ar *C*H), 152.0 (s, Ar *C*) 143.3 - 134.9 (m, Ar *C*F), 140.0 (s, Ar *C*), 137.7 (s, Ar *C*H), 136.6 (s, Ar *C*), 136.2 (s, Ar *C*), 134.9 (s, Ar *C*), 129.6 (s, Ar *C*H), 129.2 (s, Ar *C*H), 128.0 (s, Ar *C*H), 124.9 (s, Ar *C*H), 123.8 (s, NC*H*CHN), 119.4 (s, Ar *C*), 21.6 (s, *C*H_3), 18.4 (s, *C*H_3), 17.6 (s, *C*H_3). $^{19}F\{^1H\}$ $CDCl_3$ -87.2 to -87.4 (m, 4F), -95.4 to -95.6 (m, 4F), 105.4 (tt, $^3J_{FF}$ = 22.6, $^4J_{FF}$ = 8.5, 1F), -106.8 (tt, $^3J_{FF}$ = 25.4 $^4J_{FF}$ = 8.5, 1F). Anal. Calcd for $C_{43}H_{54}F_{10}BrN_3O_2Ru$: C, 53.00; H, 3.11; N, 3.99%. Found C, 52.68; H, 3.36; N, 4.12%.

2.7.4 Attempted synthesis of $Ru(CHPh)(OC_6H_4\text{-}4\text{-}NO_2)_2(IMes)(py)$

To $RuCl_2(CHPh)(IMes)(py)_2$ (**3a**, 20 mg) stirring in 1 mL of C_6D_6 was added two equivalents of $TlOC_6H_4\text{-}4\text{-}NO_2$ (15 mg). After 15 min the signal for **3a** was reduced and after 3 hours no signal for alkylidene was observed.

2.7.5 Attempted synthesis of $Ru(CHPh)(OC_6H_4F)_2(IMes)(py)$

To $RuCl_2(CHPh)(IMes)(py)_2$ (**3a**, 20 mg) stirring in 1 mL of C_6D_6 was added two equivalents of $TlOC_6H_4F$ (13 mg). After 3 hours, 3 new alkylidenes appeared: ^1H NMR (C_6D_6) δ 19.76, 19.55 and 19.45 ppm. After 12 hours all alkylidene signals had disappeared.

2.7.6 Attempted synthesis of $Ru(CHPh)(OC_6H_5)_2(IMes)(py)$

To $RuCl_2(CHPh)(IMes)(py)_2$ (**3a**, 20 mg) stirring in 1 mL of C_6D_6 was added two equivalents of $TlOC_6H_4$ (17 mg). After 24 hours no alkylidene signals were observed. New peaks for phenol ~12 ppm and π-bound aryl complexes appeared in a similar location to $RuCl(\eta^5\text{-}OC_6H_5)(PPh_3)_2$ (**9**): ^1H NMR (C_6D_6) δ 5.5–4.30 ppm.

2.7.7 Attempted synthesis of $Ru(CHPh)(OC_6H_3\text{-}3,5\text{-}(CF_3)_2)_2(IMes)(py)$

To $RuCl_2(CHPh)(IMes)(py)_2$ (**3a**, 15 mg) stirring in 1 mL of C_6D_6 was added two equivalents of $TlOC_6H_3\text{-}3,5\text{-}(CF_3)_2$ (18 mg). A new product appeared within 3 hours but decomposed after 3 more hours. ^1H NMR (C_6D_6): δ 18.69 (s, 1H, Ru=*CH*), 7.80 (d, $^3J_{HH}$ = 7.7, 2H, Ar*H*), 7.39 (d, $^3J_{HH}$ = 7.7, 2H, Ar*H*), 6.96–6.94 (m, 4H, Ar*H*), 6.89–6.84 (m, 3H, Ar*H*), 6.78 (s, 2H, Ar*H*), 6.67–6.63 (m, 2H, Ar*H*), 6.46 (s, 2H, Ar*H*), 6.34 (s, 1H, Ar*H*), 6.09–6.04 (m, 2H, Ar*H*), 6.03 (s, 2H, Ar*H*), 2.18 (s, 6H, CH_3), 1.41 (s, 12H, CH_3).

2.7.8 Attempted synthesis of $Ru(CHPh)(OC_6F_4\text{-}4\text{-}CF_3)_2(IMes)(py)$

To $RuCl_2(CHPh)(IMes)(py)_2$ (**3a**, 20 mg) stirring in 1 mL of C_6D_6 was added two equivalents of $TlOC_6F_4\text{-}4\text{-}CF_3$ (24 mg). Within 15 minutes two new benzylidenes appeared, ^1H NMR (C_6D_6): δ 19.93 and 18.71 ppm. The products were inseparable by precipitation with hexane.

2.7.9 Attempted synthesis of $Ru(CHPh)(OC_6F_4\text{-}3\text{-}CF_3)_2(IMes)(py)$

To $RuCl_2(CHPh)(IMes)(py)_2$ (**3a**, 15 mg) stirring in 1 mL of C_6D_6 was added two equivalents of $TlOC_6F_4\text{-}3\text{-}CF_3$ (15 mg). New benzylidene signals appeared within 1 hour ^1H NMR (C_6D_6): δ 20.11, 19.91, 19.84. After 12 hours all alkylidene signals were gone.

2.7.10 $Ru(CHPh)(OC_6F_4\text{-}4\text{-}C_6F_5)_2(IMes)(py)$, **13a**

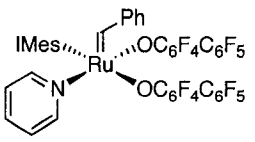

To $RuCl_2(CHPh)(IMes)(py)_2$ (**3a**, 200 mg) stirring in 20 mL of C_6H_6 was added two equivalents of $TlOC_6F_4\text{-}4\text{-}C_6F_5$ (296 mg). After stirring overnight, the reaction was complete and an emerald green solution with white precipitate was obtained. Thallium chloride was removed by filtration through Celite. The product was isolated from the filtrate by reducing the solvent volume to 1 mL and precipitating with pentane (10 mL). Reprecipitation from a minimum amount of toluene and pentane (10 mL) cooled to –35°C followed by filtration yielded 230 mg of green powder (67%). ^1H NMR (C_6D_6): δ 18.62 (s, 1H, Ru=C*H*), 8.10 (d, $^3J_{HH}$ = 5.1, 2H, Ar*H*), 7.83 (d, $^3J_{HH}$ = 7.5, 2H, Ar*H*), 7.02 (t, $^3J_{HH}$ = 7.8, Ar*H*), 6.96 (s, 2H, Ar*H*), 6.65–6.58 (m, 2H, Ar*H*), 6.49 (s, 2H, Ar*H*), 6.14–6.10 (m, 4H, Ar*H*), 2.18 (s, 3H, CH_3), 2.12 (s, 3H, CH_3), 1.51 (s, 3H, CH_3). $^{13}C\{^1H\}$ NMR (C_6D_6): δ 317.6 (s, Ru*C*H), 183.3 (s, N*C*N), 153.7 (s, Ar*C*H), 152.1 (s, Ar*C*), 147.7–146.6 (m, Ar*C*F), 143.8–143.3 (m, Ar*C*F), 140.1 (s, Ar*C*), 139.6–139.3 (m, Ar*C*F), 137.0 (s, Ar*H*), 136.4 (s, Ar*H*), 135.6 (s, Ar*C*H), 135.5 (s, Ar*H*), 134.1 (s, Ar*C*), 130.8 (s, Ar*C*H), 129.8 (s, Ar*C*H), 129.7 (s, Ar*C*H), 128.3 (s, Ar*C*H), 124.7 (s, Ar*C*H), 123.7 (s, Ar*C*H), 20.8 (s, *C*H_3), 18.0 (s, *C*H_3), 17.0 (s, *C*H_3). $^{19}F\{^1H\}$ NMR ($CDCl_3$): δ -62.2 to -62.3 (m, 2F), -62.5 to -62.6 (m, 2F), -70.5 to -70.6 (m, 2F), -71.2 to -71.3 (m, 2F), -79.1 (t, J_{FF} = 21.0, 1F), -79.2 (t, J_{FF} = 21.1, 1F), -86.0 (d, J_{FF} = 17.6, 2F), -87.1 to -87.4 (m, 6F). Anal. Calcd. for $C_{57}H_{35}F_{18}O_2N_3Ru$: C, 55,35; H, 2.85; N, 3.40%. Found: C, 55.73; H, 8.12; N,

3.31%. Single crystals suitable for X-ray diffraction were grown from a slowly evaporating solution of THF layered with decane.

2.7.11 $RuCl(OC_6Cl_5)(CHPh)(IMes)(py)$, **14**

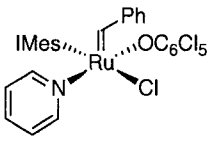

To a solution of $RuCl_2(CHPh)(IMes)(py)_2$ (**3a**, 200 mg, 0.276 mmol) in 20 mL benzene was added solid $TlOC_6Cl_5$ (130 mg, 0.276 mmol). The reaction was stirred for 8 h, then filtered through Celite and stripped to dryness. The green residue was redissolved in toluene (5 mL) and filtered through neutral alumina. The filtrate was concentrated to ~0.5 mL, after which 40 mL of hexanes were added over 5 minutes. The mixture was cooled to –35 °C. A green precipitate deposited over a period of 5 hours. This was filtered off and dried under high vacuum. Yield 170 mg (70%). Yields are limited by high solubility. ^{1}H NMR (C_6D_6): δ 19.78 (s, RuC*H*, 1H), 8.42–7.89 (br m, 4H, py), 7.15–7.11 (m, 2H, Ph), 6.88 (t, $^3J_{HH}$ = 9.0, 2H, Ph), 6.74 (s, 2H, C*H*Mes), 6.33 (s, 2H, C*H*Mes), 6.18 (t, $^3J_{HH}$ = 7.2, 1H, py), 6.15 (s, 2H, NC*H*), 5.90 (t, $^3J_{HH}$ = 6.3, 2H, py), 2.46 (s, 6H, Mes CH_3), 2.07 (s, 6H, Mes CH_3), 2.00 (s, 6H, Mes CH_3). ^{13}C{^{1}H} NMR (C_6D_6): δ 314.9 (s, Ru*C*H), 181.4 (s, N*C*N), 161.5 (s, Ar *C*), 152.7 (s, Ar *C*), 151.5 (s, Ar *C*H), 138.9 (s, Ar *C*), 137.1 (s, Ar *C*), 137.0 (s, Ar *C*), 135.7 (s, Ar *C*H), 129.9 (s, Ar *C*H), 129.2 (s, Ar *C*H), 129.1 (s, Ar *C*H), 129.0 (s, Ar *C*H), 127.9 (s, Ar *C*H), 127.8 (s, Ar *C*H), 124.3 (s, Ar *C*H), 122.9 (s, NCH*C*HN), 20.9 (s, *C*H_3), 18.6 (s, *C*H_3), 17.9 (s, *C*H_3). Anal. Calcd. $C_{39}H_{35}Cl_6N_3ORu$: C, 53.50; H, 4.03; N, 4.80%. Found C, 53.94; H, 3.99; N, 4.81%.

References page 78

2.7.12 $RuCl(OC_6Br_5)(CHPh)(IMes)(py)$, **15a**

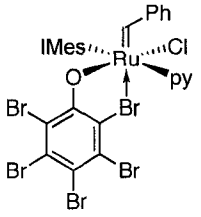

To a solution of $RuCl_2(CHPh)(IMes)(py)_2$ (**3a**, 200 mg, 0.276 mmol) in 20 mL benzene was added $TlOC_6Br_5$ (191 mg, 0.276 mmol). The reaction was stirred overnight, then filtered through Celite and stripped of solvent. The green powder was redissolved in 0.5 mL toluene, then 20 mL hexanes was added over 5 min. The mixture was cooled to –35 °C for several hours, over which time a green precipitate deposited. This was filtered off and dried under vacuum. Yield 257 mg (85%). ^{1}H NMR (C_6D_6): δ 19.68 (s, 1H, Ru=C*H*), 8.55–7.85 (br m, 4H, py), 7.16–7.11 (m, 2H, Ph), 6.87 (t, $^3J_{HH}$ = 7.5, 2H, Ph), 6.75 (s, 2H, C*H*Mes), 6.36 (s, 2H, C*H*Mes), 6.12–6.13 (m, 3H, NC*H*, Ph), 5.96–5.84 (m, 2H, py), 2.46 (s, 6H, CH_3), 2.10 (s, 6H, CH_3), 1.98 (s, 6H, CH_3). ^{13}C{^{1}H} NMR ($CDCl_3$): δ 315.6 (s, Ru=*C*H), 181.5 (s, N*C*N), 163.2 (s, Ar *C*), 152.5 (s, Ar *C*), 151.3 (s, Ar *C*H), 139.3 (s, Ar *C*), 137.5 (s, Ar *C*), 137.1 (s, Ar *C*), 136.1 (s, Ar *C*H), 133.7 (s, Ar *C*), 129.9 (s, Ar *C*H), 129.7 (s, Ar *C*H), 129.4 (s, Ar *C*H), 129.1 (s, Ar *C*H), 128.2 (s, Ar *C*), 127.8 (s, Ar *C*H), 125.5 (s, Ar *C*), 124.8 (s, Ar *C*H), 123.3 (s, NCHCHN), 120.1 (s, Ar *C*), 116.4 (s, Ar *C*), 107.8 (s, Ar *C*), 21.3 (s, CH_3), 18.8 (s, CH_3), 17.9 (s, CH_3). Anal. Calcd for $C_{39}H_{35}Br_5ClN_3ORu$: C, 42.67; H, 3.21; N, 3.83%. Found C, 42.77; H, 3.12; N, 3.81%.

2.7.13 $RuCl(OC_6Br_5)(CHPh)(IMes)(3\text{-Br-py})$, **15b**

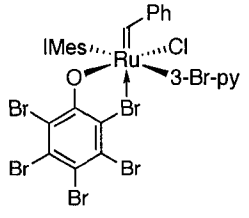

Solid $TlOC_6Br_5$ (111 mg, 0.161 mmol) was added to a solution of $RuCl_2(CHPh)(IMes)(3\text{-Br-py})_2$ (**3b**, 142 mg, 0.161 mmol) in benzene (20 mL). The green solution was stirred overnight, after which the white precipitate of TlCl was removed by filtration through Celite. The Celite was washed with toluene (5 mL) and the combined solutions were reduced to dryness under vacuum. The residue was taken up in the minimum volume of toluene and precipitated by addition of cold

pentane (-35 °C, 20 mL). The product was isolated as a green powder by filtering and drying under vacuum. Yield 172 mg (91%). ^{1}H NMR (C_6D_6): δ 19.55 (s, 1H, Ru=C*H*), 8.64 (br s, 1H, Ar C*H*), 7.98 (br s, 1H, Ar C*H*), 7.16–7.07 (m, 3H, Ar C*H*), 6.84 (t, $^3J_{HH}$ = 7.9, 2H, Ar C*H*), 6.72 (s, 2H, Ar C*H*), 6.34 (s, 2H, Mes Ar C*H*), 6.27 (br s, 1H, Ar C*H*), 6.11 (s, 2H, Ar C*H*), 5.48 (br s, 1H, Ar C*H*), 2.42 (s, 6H, C*H*$_3$), 2.15 (s, 6H, C*H*$_3$), 1.97 (s, 6H, Mes C*H*$_3$). ^{13}C{^{1}H} NMR (C_6D_6): δ 311.5 (s, Ru=*C*H), 180.4 (s, N*C*N), 163.7 (s, Ar *C*), 153.5 (s, Ar *C*), 153.1 (s, Ru=CH*C*), 150.1 (s, Ar *C*), 139.4 (s, Ar *C*), 138.8 (s, Ar *C*H), 137.6 (s, Ar *C*), 137.6 (s, Ar *C*), 137.2 (s, Ar *C*), 137.2 (s, Ar *C*), 130.3 (s, Ar *C*H), 129.8 (s, Ar *C*H), 129.7 (s, Ar *C*H), 129.5 (s, Ar *C*H), 129.4 (s, Ar *C*), 128.4 (s, Ar *C*H), 128.3 (s, Ar *C*H), 126.5 (s, Ar *C*), 126.1 (s, Ar *C*), 124.8 (s, Ar *C*H), 124.2 (s, N*C*H*C*HN), 120.7 (s, Ar *C*), 119.6 (s, Ar *C*), 116.7 (s, Ar *C*), 108.9 (s, Ar *C*), 21.4 (s, *C*H$_3$), 19.1 (s, *C*H$_3$), 18.3 (s, *C*H$_3$). Anal. Calcd for $C_{39}H_{34}Br_6N_3ORu$: C, 39.81; H, 2.91; N, 3.57%. Found C, 39.29; H, 2.87; N, 3.18%.

2.8 Thioaryloxide Derivatives

2.8.1 Attempted synthesis of $Ru(SC_6H_5)_2(CHPh)(IMes)(py)$

To a solution of $RuCl_2(CHPh)(IMes)(py)_2$ (**3a**, 20 mg) stirring in 1 mL of C_6D_6 were added two equivalents of $TlSC_6H_5$ (223 mg). After 3.5 h a new singlet appeared: ^{1}H NMR (C_6D_6): δ 17.93 ppm. Decomposition, as judged by loss of the alkylidene ^{1}H NMR signals, was complete after 12 hours.

2.8.2 $Ru(SC_6F_5)_2(CHPh)(IMes)(py)$, **16**

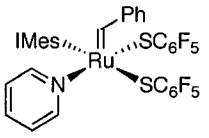

To a solution of $RuCl_2(CHPh)(IMes)(py)_2$ (**3a**, 200 mg) stirring in 20 mL of C_6H_6 was added two equivalents of $TlSC_6F_5$ (223 mg). Reaction was complete after 15 min and the colour changed from green to red (observed by ^{1}H and ^{19}F

NMR). Reactions was complete after 30 min. Stirring for a longer time decomposed the compound to presumably the *cis* isomer noted by the appearance of a new benzylidene and an additional set of peaks in the ^{19}F spectrum. High solubility hampered isolation. After filtering through Celite to remove TlCl, the solvent was removed under vacuum. The red residue was then precipitated from 10 mL of pentane at –78°C. The brown powder was collected on a filter and dried overnight, yield 55 mg (20% **16a**). The *cis* isomer **16b** was obtained after a solution of **16a** was left standing in C_6D_6 for 5 days, 3:1. *Trans*-**16a** ^1H NMR (C_6D_6): δ 19.19 (s, 1H, RuC*H*), 8.54 (s, $^3J_{HH}$ = 7.53, 2H, Ar*H*), 7.60 (br s, 2H, Ar*H*), 7.23 (t, $^3J_{HH}$ = 7.1, 1H, Ar*H*), 6.42 (br s, 1H, Ar*H*), 6.19 (br s, 2H, Ar*H*), 5.84 (br s, 1H, Ar*H*), 5.41 (s, 2H, NC*H*), 2.85–2.34 (br s, 12H, CH_3), 2.34–1.97 (br s, 6H, CH_3). *Cis*-**16b** ^1H NMR (C_6D_6): δ 18.20 (s, 1H, RuC*H*). $^{19}F\{^1H\}$ C_6D_6 δ -56.2 (d, $^3J_{FF}$ = 26.82, 2F), -88.6 (t, $^3J_{FF}$ = 21.74, 1F), -91.0 (t, $^3J_{FF}$ = 22.3, 2F). Single crystals of the *cis* isomer **16b** suitable for X-ray diffraction were obtained by slow evaporation of a concentrated THF solution layered with decane.

2.8.3 $Ru(SC_6Cl_5)Cl(CHPh)(IMes)$, **17**

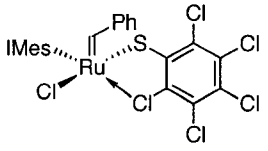

One equivalent of $TlSC_6Cl_5$ (168 mg, 0.345 mmol) was added directly to $RuCl_2(CHPh)(IMes)(py)_2$ (**3a**, 250 mg, 0.345 mmol) in benzene (20 mL). After stirring overnight, the white TlCl precipitate was removed by filtration through Celite. Then the solvent was removed under vacuum. The green residue was then precipitated from a minimum amount of toluene and pentane. Reprecipitation from toluene pentane and filtration followed by and drying under vacuum yields 152 mg (54%) of green powder. ^1H NMR (C_6D_6): δ 17.74 (s, RuC*H*), 7.13–6.95 (m, 1H), 6.82 (t, $^3J_{HH}$ = 8.1, 2H), 6.78–6.65 (m, 2H), 6.37–6.26 (m, 1H), 6.25–6.17 (m, 2H), 6.14–5.98 (m, 4H), 4.25 (s,

1H), 2.48 (br s, 6H), 2.29 (br s, 6H), 2.01 (br s, 6H).$^{13}C\{^1H\}$ NMR (C_6D_6): δ 310.9 (s, Ru=*C*H), 178.0 (s, N*C*N), 153.3 (s, Ar*C*), 152.3 (s, Ar*C*), 152.1 (s, Ar*C*), 139.0 (s, Ar*C*), 139.0 (s, Ar*C*), 137.2 (s, Ar*C*), 135.8 (s, Ar*C*H), 129.8 (s, Ar*C*H), 129.1 (s, Ar*C*), 128.3 (s, Ar*C*H), 124.8 (s, Ar*C*H), 123.1 (s, Ar*C*H), 122.6 (s, Ar*C*), 21.1 (s, *C*H_3), 19.2 (s, *C*H_3). MALDI-MS $[M]^{+\bullet}$ 811.82 *m/z*. Addition of excess pyridine and stirring for 30 min did not change the chemical shift of the benzylidene resonance in the ^1H NMR spectrum.

2.9 Linear Pseudohalides

2.9.1 $Ru(NCS)_2(CHPh)(IMes)(py)_2$, **18a**

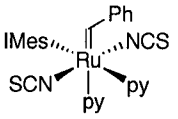

Two equivalents of AgSCN (91.6 mg, 0.552 mmol) were added directly to $RuCl_2(CHPh)(IMes)(py)_2$ (**3a**, 200 mg, 0.276 mmol) in benzene (20 mL). The suspension was stirred for 16 hours. The off white AgCl precipitate was removed by filtration through Celite. The filtrate was concentrated under vacuum and the green residue was precipitated from a minimum amount of benzene and pentane (40 mL). After drying under vacuum overnight 184 mg (97%) of green powder was obtained. ^1H NMR ($CDCl_3$): δ 17.99 (s, RuC*H*, 1H), 8.38 (d, $^3J_{HH}$ = 3.9, 2H, Ar*H*), 7.69 (d, $^3J_{HH}$ = 4.0, 2H, Ar*H*), 7.56 (d, $^3J_{HH}$ = 5.5, 2H, Ar*H*), 7.34–7.24 (m, 2H, Ar*H*), 7.09–6.88 (m, 3H, Ar*H*), 6.86–6.82 (m, 4H, ArH, NC*H*), 6.58 (t, $^3J_{HH}$ = 6.1, 2H, Ar*H*), 6.43 (s, 4H, Ar*H*), 2.09 (s, 12H, CH_3), 1.96 (s, 6H, CH_3). $^{13}C\{^1H\}$ ($CDCl_3$): δ 324.2 (s, Ru*C*H), 180.3 (s, N*C*N), 151.8 (s, Ar*C*), 150.7 (s, Ar*C*H), 149.9 (s, Ar*C*H), 139.1 (s, Ar*C*), 137.0 (br s, S*C*N), 136.6 (s, Ar*C*),136.3 (s, Ar*C*H), 135.0 (s, Ar*C*H), 131.1 (s, Ar*C*H), 130.5 (s, Ar*C*H), 128.9 (s, Ar*C*H), 128.3 (s, Ar*C*H), 128.2 (s, Ar*C*H), 125.0 (s, N*C*H), 123.8 (s, Ar*C*H), 20.9 (s, p*C*H_3), 17.8 (s, o*C*H_3). IR (nujol, cm^{-1}): ν (SCN) 2095 (s), (C=C) 1600 (m). Anal. Calcd for $C_{40}H_{40}SN_6Ru$: C, 62.39; H, 5.24; N,

10.91%. Found C, 62.58; H, 4.84; N, 10.46%. Single crystals suitable for X-ray diffraction were made by slow evaporation of a concentrated THF solution layered with decane.

2.9.2 Attempted synthesis of $Ru(CN)_2(CHPh)(IMes)(py)_2$

Two equivalents of AgCN (7.2 mg, 0.0552 mmol) were added directly to $RuCl_2(CHPh)(IMes)(py)_2$ (**3a**, 20 mg, 0.0276 mmol) in C_6D_6 (1 mL). After 1 hour a mixture of starting material and five new alkylidenes were observed. ^1H NMR (C_6D_6): δ 19.84, 19.80, 19.31, 17.97, 17.75 ppm.

2.9.3 Attempted synthesis of $Ru(NCO)_2(CHPh)(IMes)(py)_2$

Two equivalents of AgOCN (8 mg, 0.0552 mmol) were added directly to $RuCl_2(CHPh)(IMes)(py)_2$ (**3a**, 20 mg, 0.0276 mmol) in C_6D_6 (1 mL). The solution was stirred overnight and the colour changed to red. ^1H NMR (C_6D_6): δ 19.11 (s, 1H), 8.82 (d, $^3J_{HH}$ = 3.3, 2 H), 8.08 (d, $^3J_{HH}$ = 5.4, 2H), 7.96 (d, $^3J_{HH}$ = 7.5, 2H), 7.15 (s, 2H), 6.92 (t, $^3J_{HH}$ = 8.1, 2H), 6.38 (s, 4H), 6.32–5.88 (m, 7H), 2.34 (s, 12H), 1.89 (s, 6H). An inseparable side product in up to 25% was observed, ^1H NMR (C_6D_6): δ 19.60 ppm.

2.9.4 Attempted synthesis of $Ru(NCS)_2(CHPh)(IMes)(PCy_3)$

Two equivalents of AgNCS (8 mg, 0.0472 mmol) were added directly to $RuCl_2(CHPh)(IMes)(PCy_3)$ (**2a**, 20 mg, 0.0236 mmol) in C_6D_6 (1 mL). After 24 hours a green powder was obtained. The ^1H NMR spectrum showed no alkylidene signals. A weak ^{31}P NMR spectrum was obtained. $^{31}P\{^1H\}$ NMR (C_6D_6): δ 45.37 (d, $^2J_{PP}$ = 45), 40.17 (d, $^2J_{PP}$ = 40).

2.9.5 Attempted synthesis of $Ru(CN)_2(CHPh)(IMes)(PCy_3)$

Two equivalents of AgCN (7 mg, 0.0472 mmol) are added directly to $RuCl_2(CHPh)(IMes)(PCy_3)$ (**2a**, 20 mg, 0.0236 mmol) in C_6D_6 (1 mL). After 12 hours no change was observed.

2.9.6 $Ru(NCO)_2(CHPh)(IMes)(PCy_3)$, **19b**

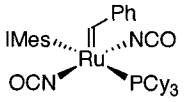

Two equivalents of AgNCO (177 mg, 0.118 mmol) were added directly to $RuCl_2(CHPh)(IMes)(PCy_3)$ (**2a**, 500 mg, 0.0591 mmol) in C_6D_6 (50 mL). After stirring overnight the solution turned brown. The AgCl precipitate was removed by filtering through Celite. The solvent was then reduced to 1 mL under vacuum. An orange powder was precipitated with 10 mL of hexane. A side-product appears at ^1H NMR (C_6D_6): δ 19.37 ppm and was difficult to remove. The powder was reprecipitated twice more from CH_2Cl_2/ether. The powder was collected on a filter and washed with 10 mL hexane then dried under vacuum, 210 mg (41%). ^1H NMR (C_6D_6): δ 18.39 (s, 1H), 9.5–9.1 (br s, 2H), 7.43 (d, $^3J_{HH}$ = 6.0, 2H), 7.17 (s, 2H), 7.06–6.98 (m, 3H), 6.97 (d, $^3J_{HH}$ = 6.0, 1H), 6.40–5.60 (br s, 1H), 2.60–0.76 (m, 51H). $^{13}C\{^1H\}$ NMR (C_6D_6): δ 299.0 (s, Ru*C*H), 187.0 (d, $^2J_{HH}$ = 47.1), 151.0 (s, Ar*C*), 150.6 (s, Ar*C*), 129.9–128.4 (m, Ar*C*, Ar*C*H), 124.2 (s, Ar*C*H), 32.8–25.7 (m, Cy, Me). Single crystals suitable for X-ray diffraction were made by slow evaporation of a concentrated a toluene solution layered with decane.

2.10 Ruthenium Carbynes

2.10.1 Improved Synthesis of $RuCl_3(PPh_3)_2(\equiv CCHCMe_2)$

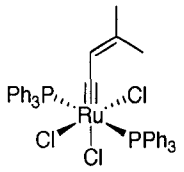

Addition of 3-chloro-3-methyl-1-butyne (244 μL, 2.16 mmol) to a stirred purple solution of $RuCl_2(CHCMe_2)(PPh_3)_2$ (500 mg, 0.27 mmol) in 5 mL THF caused an immediate color change to brown. After 7 days, orange solids precipitated, and no further $RuCl_2(CHCMe_2)(PPh_3)_2$ was evident by ^{31}P NMR analysis. The solution was diluted with hexanes (10 mL), and orange product filtered off, washed with hexanes (5 x 2 mL) and dried under vacuum. yield: 0.405 g (94%). NMR data agree with those reported.[8]

2.10.2 $Ru(\equiv CPh)(OC_6F_5)(PCy_3)_2$, **11**

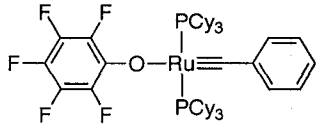

Addition of $TlOC_6F_5$ (566 mg, 1.46 mmol) in 7 mL toluene to a purple solution of $RuCl_2(CHPh)(PCy_3)_2$ (**1a**, 600 mg, 0.73 mmol) in 7 mL benzene resulted in quantitative reaction (NMR) within 3 hours, accompanied by a change in color to dark green. The suspension was filtered through Celite and the filtrate concentrated to dryness under vacuum. On redissolving the residue in cold (-35 °C) ether, a green powder slowly deposited. This was filtered off and washed with cold ether. Yield 395 mg (56 %); yields are limited by the high solubility in ether. Slow decomposition to unknown products occurred in benzene; decomposition is immediate in chlorinated solvents ($CDCl_3$, CD_2Cl_2). ^1H NMR (C_6D_6): δ 7.68 (d, $^3J_{HH}$ = 7.6 Hz, 2H, Ph), 6.97 (t, $^3J_{HH}$ = 7.5, 1H, Ph), 6.75 (t, $^3J_{HH}$ = 7.9, 2H, Ph), 2.23–2.18 (m, 8H, Cy), 1.94–1.54 (m, 36H, Cy), 1.30–1.15 (m, 8H, Cy), 1.08–0.90 (m, 8H, Cy). $^{31}P\{^1H\}$ NMR (C_6D_6): δ 42.59. $^{13}C\{^1H\}$ NMR (C_6D_6) δ 250.2 (Ru≡*C*Ph, located by HMBC; using the 500 MHz instrument), 153–125 (Ar), 35.6–26.6 (Cy). $^{19}F\{^1H\}$ NMR (C_6D_6): δ -90.27 (dd, $^3J_{FF}$ = 22.6, 11.3 Hz, 2F), -93.35 (t, $^3J_{FF}$ = 22.1,

2F), -106.73 to -106.98 (m, 1F). Anal. Calcd. for $C_{49}H_{71}F_5OP_2Ru$: C, 63.00; H, 7.66%. Found: C, 62.74; H, 8.12%. X-ray quality crystals were grown by slow evaporation of a saturated benzene solution.

2.11 Chiral Catalysts

2.11.1 $Ru(O_2C_{20}H_4F_8)(CHPh)(IMes)(py)\cdot THF$

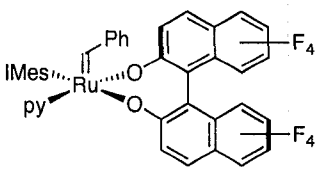

To a solution of $RuCl_2(CHPh)(IMes)(py)_2$ (**3a**, 668 mg, 0.922 mmol) in 20 mL benzene was added $Tl_2O_2C_{20}H_4F_8$ (772 mg, 0.922 mmol). The reaction was stirred overnight, then filtered through Celite flushed with 20 mL THF. The filtrate was then reduced to dryness under vacuum. In a test-tube the brown powder was redissolved in the minimum amount of THF and an equal amount of decane layered on top. The tube was then sealed with a septum. A small hole permitted THF to gradually evaporate and left emerald green crystals as the THF solvate. Yield, 512mg (66%). The phenyl protons were distinguished from pyridine by HMBC correlation of Ru=*C*H to the ortho phenyl proton resonances. Carbon assignments based on DEPT-135, HMQC and HMBC correlations. Due to fluorine coupling some ^{13}C resonances are very broad. ^1H NMR (THF-*d8*): δ 19.23 (s, 1H, RuC*H*), 7.85 (d, $^3J_{HH}$ = 9.3 Hz, 1H, OCC*H*), 7.81 (dd, $^3J_{HH}$ = 5.1, $^4J_{HH}$ = 3.0, 2H, ortho py), 7.51 (tt, $^3J_{HH}$ = 7.5, $^4J_{HH}$ = 3.0, 1H, para py), 7.40 (s, 2H, NC*H*), 7.35 (d, $^3J_{HH}$ = 9.3 Hz, 1H, OCC*H*), 7.16–7.11 (m, 3H, ortho and para Ph), 7.08 (d, $^3J_{HH}$ = 9.3 Hz, 1H, OCCHC*H*), 7.04 (br s, 2H, Mes Ar), 6.97 (br s, 2H, Mes Ar), 6.91 (br t, $^3J_{HH}$ = 7.2 Hz, 2H, py), 6.80 (t, $^3J_{HH}$ = 7.8 Hz, meta Ph), 6.57 (d, $^3J_{HH}$ = 9.3 Hz, 1H, OCCHC*H*), 3.64–3.58 (m, 2H, THF), 2.55 (s, 6H, Me), 2.13 (s, 6H, Me), 1.851.75 (br s and m overlapping, 8H, Me, THF).$^{13}C\{^1H\}$ NMR (THF-*d8*): δ 310.2 (s, Ru=*C*H), 184.6 (s, N*C*N), 172.3 (s, O*C*), 166.5 (s, O*C*), 156.3 (s, C*H*, ortho py), 155.2 (s,

Ar*C*), 140.6 (s, *C*, Mes), 138.4 (s, *C*, Mes), 137.2 (s, *C*, Mes), 137.0 (m, Ar*C*), 135.7 (m, Ar*C*), 131.0 (m, Ar*C*), 130.3 (m, Ar*C*), 129.5 (m, Ar*C*), 128.8 (m, Ar*C*), 128.6 (m, Ar*C*), 128.5 (m, Ar*C*), 127.8 (m, Ar*C*), 127.4 (m, Ar*C*), 127.0 (s, *C*H, binol), 126.2 (s, *C*H, NC*C*N), 124.6 (s, *C*H, binol), 124.3 (m, Ar*C*), 123.0 (br, *C*, binol), 118.5 (m, *C*H, binol), 114.0 (m, *C*, binol), 113.8 (m, *C*, binol), 21.3 (s, *C*H_3, Mes), 18.3 (s, *C*H_3, Mes), 18.2 (s, *C*H_3, Mes). $^{19}F\{^1H\}$ NMR (THF-*d8*): -73.09 (t, $^3J_{FF}$ = 16.0, 1F), -73.26 (t, $^3J_{FF}$ = 15.6, 1F), -80.72 to -80.87 (m, 2F), -91.47 (t, $^3J_{FF}$ = 18.7, 1F), -92.15 (t, $^3J_{FF}$ = 19.0, 1F), -98.03 (d, $^3J_{FF}$ = 19.7, 1F), -98.17 (d, $^3J_{FF}$ = 19.3, 1F). IR (nujol, cm^{-1}) υ (C=C) 1663, 1601, 1565 cm^{-1}. Anal calc: $RuC_{53}H_{39}F_8N_3O_2$ C, 63.47; H, 3.92; N, 4.19. Found C, 64.14; H, 3.61; 4.23%. MALDI-TOF MS [M-py(79)]$^{+\bullet}$ = 924 *m/z*. Using the same procedure starting from (*R*)-$TlO_2C_{20}H_4F_8$, (*R*)-$Ru(O_2C_{20}H_4F_8)$(CHPh)(IMes)(py) was made and was characterized by X-ray diffraction. X-ray quality crystals were grown by liquid diffusion from a saturated THF solution with an equal amount of decane layered on top.

2.11.2 $Ru(O_2C_{22}H_8F_8)$(CHPh)(IMes)(py)·THF

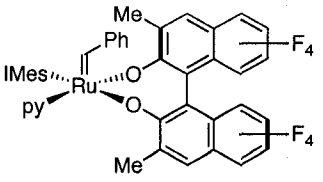

To a solution of $RuCl_2$(CHPh)(IMes)$(py)_2$ (**3a**, 59 mg, 0.0814 mmol) in 5 mL toluene was added $Tl_2O_2C_{22}H_8F_8$ (70 mg, 0.0814 mmol). The reaction was stirred overnight, then filtered through Celite flushed with 50 mL THF, then reduced to 1 mL under vacuum. The green powder was precipitated with 10 mL pentane, filtered and dried under vacuum. 55 mg (66 %). In a test-tube the brown powder was redissolved in the minimum amount of THF and an equal amount of decane layered on top. The tube was then sealed with a septum and vented through a small hole allowing the THF to gradually evaporate and leave emerald green crystals as the THF solvate. ^1H NMR (THF-*d8*): δ 17.24 (s, RuC*H*), 8.59–8.52 (br s, 1H), 8.2

–8.20 (m, 3H), 7.57–7.45 (m, 5H), 7.19–6.96 (m, 5H), 6.34 (s, 1H), 6.55 (s, 1H), 6.48 (s, 1H), 6.08 (s, 1H), 2.67 (s, 3H), 2.34–2.11 (m, 12H), 1.83–1.76 (m, 6H), 0.87 (s, 3H).

2.12 Substrates and Products

2.12.1 4-(allyloxy)-2,4,6-trimethylhepta-1,6-diene, **38**

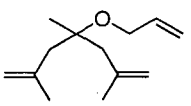

The same procedure as for 4-Allyloxy-4-methyl-hepta-1,6-diene (**64**, see below), using 2 g of 2,4,6-trimethylhepta-1,6-dien-4-ol. The product was purified by flash column chromatography on silica gel 10% EtOAc / hexane (R_f 0.90), and distilled under vacuum, yield 2.1 g (83%). ^{1}H NMR ($CDCl_3$): δ 5.94–5.82 (m, 1H), 5.25 (dq, $^2J_{HH}$ = 17.1, $^3J_{HH}$ = 1.8, 1H), 5.09–5.04 (m, 1H), 4.84–4.82 (m, 2H), 4.71–4.69 (m, 2H), 3.92 (dt, $^3J_{HH}$ = 5.1, $^3J_{HH}$ = 1.5, 2H), 2.22 (s, 4H), 1.80 (s, 6H), 1.15 (s, 3H). ^{13}C{^{1}H} ($CDCl_3$): δ 143.3, 136.0, 115.5, 114.6, 77.5, 62.7, 46.7, 24.7, 23.6. IR ν cm^{-1} (neat): 3077 (s), 2972 (s), 2939 (s), 2918 (s), 2857 (s), 2728 (w), 1792 (w), 1644 (s), 1454 (s), 1374 (s), 1317 (m), 1253 (m), 1140 (m), 1094 (s), 1064 (s), 1028 (m), 994 (m), 913 (s), 891 (s), 736 (s). HRMS (EI) *m/z*: Calculated for $[M\text{-}C_4H_7]^{+\bullet}$ 139.1123, found 139.1121.

2.12.2 2,4-dimethyl-2-(2-methylallyl)-3,6-dihydro-2*H*-pyran, **39**

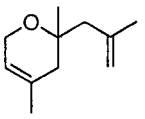

To 4-(allyloxy)-2,4,6-trimethylhepta-1,6-diene (300 mg, 1.54 mmol) in 15 mL CH_2Cl_2 was added 1 mol% $RuCl_2$(CHPh)(IMes)(PCy_3) (**2a**, 13mg, 0.154 mmol). After heating to reflux for 4 h, quantitative conversion was observed by ^{1}H NMR. Purification was accomplished by silica gel chromatography (25% EtOAc / hexanes, R_f 0.92). Residual EtOAc was removed by azeotrope with CH_2Cl_2 to yield 172 mg (67%) yellow volatile oil. ^{1}H NMR (C_6D_6): δ 5.15 (s, 1H), 4.91–4.90 (m, 1H), 4.77–4.76 (m, 1H), 4.01–3.99 (m, 2H), 2.27 (d, $^3J_{HH}$ = 13.5, 1H), 2.12 (d, $^3J_{HH}$ = 13.5, 1H), 1.97 (d, $^3J_{HH}$ = 16.8,

1H), 1.87 (s, 3H), 1.52–1.46 (m, 4H), 1.11 (s, 3H). $^{13}C\{^1H\}$ NMR (C_6D_6): δ 143.5, 130.4, 119.2, 114.5, 72.2, 61.1, 48.9, 40.0, 24.8, 23.5, 22.9. IR (neat) ν (cm^{-1}) 3072 (m), 3017 (m), 2969 (s), 2930 (s), 2826 (s), 2728 (m), 2706 (m), 1686 (m), 1642 (s), 1448 (s), 1372 (s), 1351 (m), 1260 (m), 1236 (m), 1154 (s), 1109 (s), 1028 (m), 1011 (s), 963 (w), 939 (w), 888 (s), 786 (m), 759 (s), 681 (w), 606 (m). HRMS (EI) *m/z*: Calculated for $[M\text{-}C_4H_7]^{+\bullet}$ = 111.0810, found 111.0780. Enantiomers separated by chiral GC-FID using a Chirasil-DEX CB column.

2.12.3 4-Allyloxy-4-methyl-hepta-1,6-diene, **64**

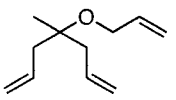

To diallylethanol, 1.4g (11.1mmol) in 20 mL of DMF was added 1 eq. of sodium hydride (0.266 g). The colour immediately changed to red brown. After stirring for two hours 1.1 equivalents of allylbromide were added and stirred overnight, and the colour turns orange. The reactions was quenched with 1 M NaOH (50 mL) and extracted three times with ether (100 mL). The organic layer was dried over sodium sulfate, filtered and concentrated under vacuum. The product was purified by flash column chromatography with 10% EtOAc / hexane (R_f 0.91). The product was then distilled under vacuum, 3.2 g (72 %). ^1H NMR ($CDCl_3$): δ 5.91–5.75 (m, 3H), 5.29–5.00 (m, 6H), 3.91 (d, $^3J_{HH}$ = 5.4, 2H), 2.25 (d, $^3J_{HH}$ = 7.5, 4H), 1.24 (s, 3H). $^{13}C\{^1H\}$ ($CDCl_3$): δ 135.7, 134.2, 117.5, 115.8, 62.5, 42.6, 23.03. IR ν cm^{-1} (neat): 3081(s), 2986 (s), 2929 (s), 2864 (s), 1842 (w), 1716 (w), 1645 (s), 1454 (m), 1443 (m), 1379 (s), 1312 (m), 1291 (m), 1267 (m), 1124 (m), 1058 (s), 997 (s), 906 (s), 742 (s), 649 (m). HRMS (EI) *m/z*: Calculated for $[M\text{-}C_3H_5]^{+\bullet}$ 125.0966, found 125.0973.

References page 78

2.12.4 2-allyl-2-methyl-3,6-dihydro-2*H*-pyran, **65a**

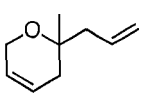

To 144 mg (8.66×10^{-4} mol) of 4-(allyloxy)-4-methylhepta-1,6-diene in 17 mL CH_2Cl_2 was added 1 mol % **12a** (8 mg), and heated to reflux for 2 hours. The reaction was then allowed to cool to room temperature. The brown solution was purified by adding silica (500 mg), stirring for 5 min and then filtering the brown solid off. After removing the solvent under vacuum, a volatile yellow oil was isolated 107 mg (89%). The brown residue can be removed by column chromatography, 5% EtOAc/hexanes, R_f 0.36, isolating to yield 38% of colorless product. ^{1}H NMR ($CDCl_3$): δ 5.89-5.51 (m, 3H), 5.10-4.92 (m, 2H), 4.16-3.96 (m, 2H), 2.38-2.08 (m, 2H), 2.08-1.72 (m, 2H), 1.11 (s, 3H). $^{13}C\{^1H\}$ NMR ($CDCl_3$): δ 129.2, 127.5, 125.6, 123.4, 72.1, 61.5, 43.3, 34.8, 24.0. IR (neat) ν (cm^{-1}): 3077 (s), 2979 (s), 2933 (s), 2862 (m), 1725 (m), 1664 (m), 1641 (s), 1516 (m), 1439 (m), 1376 (m), 1314 (w), 1292 (w), 1254 (m), 1123 (s), 1065 (s), 997 (s), 915 (s). HRMS (EI) *m/z*: calculated $[M-C_3H_5]^{+\bullet}$ 97.0653, found 97.0641.

2.12.5 1,4-bis(2-methyl-3,6-dihydro-2*H*-pyran-2-yl)but-2-ene, **65b**

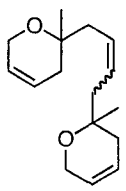

To 4-Allyloxy-4-methyl-hepta-1,6-diene (500 mg , 3.0 mmol) in a r.b. flask equipped with a stir bar was added 5 mol % $RuCl_2(CHPh)(IMes)(PCy_3)$ (**2a**, 127 mg, 0.15mmol) in 30 mL chloroform. After refluxing for 2 hours the solvent was removed under vacuum to afford a brown oil. Purification by flash silica gel chromatography 10 % EtOAc / hexane (R_f 0.55) afforded a colourless oil as a mixture of *E* and *Z* isomers (80:20), combined yield 330 mg (88%). ^{1}H NMR ($CDCl_3$): δ 5.73–5.7 (m, 4H), 5.64–5.59 (m, 2H), 5.53–5.50 (m, 2H), 4.13–4.11 (m, 4H), 2.29–1.85 (m, 8H), 1.17 (s, 9H). $^{13}C\{^1H\}$ NMR ($CDCl_3$): *E* isomer δ 129.1, 125.6, 123.3, 71.9, 61.3, 43.3, 34.8, 23.9; *Z* isomer δ

129.1, 127.4, 125.6, 72.1, 61.3, 37.6, 34.7, 23.8. IR (neat) ν (cm^{-1}) 3036 (s), 2976 (s), 2930 (s), 2896 (s), 2833 (s), 2703 (w), 1909 (w), 1819 (w), 1658 (m), 1607 (w), 1447 (m), 1429 (m), 1389 (s), 1373 (s), 1334 (m), 1262 (m). 1184 (s), 1084 (s), 1016 (m), 977 (m), 907 (s), 826 (m), 743 (s), 650 (s). HRMS (EI) m/z: Calculated for $[M\text{-}CH_3]^{+\bullet}$ 233.1542 found 233.1554.

2.12.6 1,4-bis(2-methyl-3,4-dihydro-2*H*-pyran-2-yl)but-2-ene

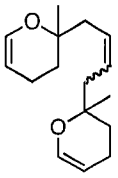

To 4-Allyloxy-4-methyl-hepta-1,6-diene, 500 mg (1.2 mmol) of in benzene (12 mL) were added 10 mol % $RuCl_2(CHPh)(IMes)(PCy_3)$ (**2a**, 102 mg). The reaction was then heated to 60 °C for 4 hours. Then K_2CO_3 (83 mg, 0.3 mmol) was added and heated for a further 24 hours. ^1H NMR yield 60%. The isolated yield was low due to the difficulty in removing small amounts side products and sensitivity to acid. Purification was accomplished by silica gel columns chromatography, 5 % EtOAc/hexane (R_f 0.83), 98 mg (26%). ^1H NMR (C_6D_6): δ 6.49 (dt, $^3J_{HH}$ = 6.3, $^3J_{HH}$ = 1.8, 2H), 5.65–5.61 (m, 2H), 4.69–4.63 (m, 2H), 2.46–2.30 (m, 4H), 1.96–1.87 (m, 4H), 1.68–1.59 (m, 2H), 1.52–1.41 (m, 2H), 1.26 (s, 6H). $^{13}C\{^1H\}$ NMR (C_6D_6): δ 143.0, 129.2, 98.9, 75.3, 43.2, 31.5, 24.1, 18.0. IR (neat) ν (cm^{-1}) 2937 (s), 2873 (m), 1717 (w), 1700 (w), 1684 (w), 1652 (m), 1647 (m), 1559 (w), 1541 (w), 1507 (w), 1456 (s), 1375 (s), 1355 (m), 1276 (w), 1223 (w), 1125 (s), 1067 (s), 1025 (s), 975 (s), 953 (s), 911 (w), 868 (w), 849 (w), 732 (m). HRMS (EI) *m/z*: Calculated for $[M]^{+\bullet}$ 248.1776 found 248.1768.

2.12.7 1-Propenyloxydecoxy-propene

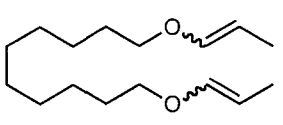

Method A, high dilution: A solution of 30 mg (0.14 mmol) 3-(10-Allyloxy-decyloxy)-propene in benzene (10 mL) and separate

solution of 8.3 mg (7 μmol) $RuCl(OC_6Br_5)(CHPh)(IMes)(py)$ (**15a**) in benzene (10 mL) were both added slowly via dropping funnel to refluxing benzene (10 mL) over 15 min. Final concentration of substrate is 0.05 M. After 1.5 hours full conversion to vinyl ether was observed (GC-FID).

Method B: To 500 mg 3-(10-Allyloxy-decyloxy)-propene in 40 mL $CHCl_3$ were added 83 mg $RuCl_2(CHPh)(IMes)(PCy_3)$ (**2a**). The solution was heated to reflux for 2 hours, quantitative conversion by GC was observed. The product was purified by flash column chromatography, 5% EtOAc / hexane (R_f = 0.8), 306 mg (61%). Three products were obtained, *EE*, *ZZ* and *EZ* (60% *Z* content as observed by comparing olefinic ^{1}H NMR coupling constants). Using method A or B no evidence for macrocycle or ADMET oligomer was observed. ^{1}H NMR ($CDCl_3$): δ 6.18 (dd, $^3J_{HH}$ = 12.6, $^2J_{HH}$ = 1.5, *E* 2H), 5.92 (dd, $^3J_{HH}$ = 6.20, $^2J_{HH}$ = 1.6, *Z* 2H), 4.78–4.67 (m, *E* 2H), 4.36 (p, $^3J_{HH}$ = 6.9, *Z* 2H), 3.68 (t, $^3J_{HH}$ = 6.6, *Z* 4H), 3.58 (t, $^3J_{HH}$ = 6.6, *E* 4H), 1.69–1.52 (m, 10H), 1.53–1.31 (m, 12H). $^{13}C\{^1H\}$ NMR ($CDCl_3$): δ 146.6, 146.6, 100.7, 98.2, 72.1, 69.1, 29.8, 29.5, 29.3, 26.0, 25.8, 12.6, 9.2. IR ν cm^{-1} (neat): 3085 (m), 3013 (m), 2930 (s), 2854 (s), 1842 (w), 1728 (w), 1645 (s), 1458 (m), 1397 (m), 1348 (m), 1264 (m), 1106 (s), 994 (m), 921 (s), 724 (w). HRMS (EI) *m/z*: Calculated for $[M]^{+\bullet}$ 254.2246, found 254.2131.

2.12.8 ((prop-1-enyloxy)methyl)benzene

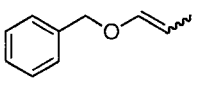

To allylbenzyl ether (1.0 g , 6.75 mmol) in 67.5 mL of toluene was added 5 mol% $RuCl_2(CHPh)(IMes)(PCy_3)$ (**2a**, 285 mg, 0.338 mmol) and 10 mol% K_2CO_3 (93 mg, 0.675 mmol). After heating to reflux for 24 hours the solvent was removed under vacuum to afford a brown oil. The product was purified by flash column chromatography 5 % EtOAc/hexane (R_f = 0.95) to yield 890 mg (89%) as a 0.78:1 mixture

of *E*/*Z* isomers. *E* isomer: ^{1}H NMR ($CDCl_3$): δ 7.62–7.44 (m, 5H), 6.55–6.51 (m, 1H), 5.14–5.03 (m, 1H), 4.86 (s, 2H), 1.77 (dd, $^{3}J_{HH}$ = 6.9, $^{4}J_{HH}$ = 1.8, 3H). $^{13}C\{^{1}H\}$ NMR ($CDCl_3$): δ 147.0, 138.1, 128.6, 128.3, 128.1, 99.8, 71.5, 10.0. *Z* isomer: ^{1}H NMR $CDCl_3$ δ 7.62 – 7.44 (m, 5H), 6.23–6.20 (m, 1H), 4.92 (s, 2H), 4.68 (p, $^{3}J_{HH}$ = 6.6, 1H), 1.88 (dd, $^{3}J_{HH}$ = 6.6, $^{4}J_{HH}$ = 1.8, 3H). $^{13}C\{^{1}H\}$ NMR ($CDCl_3$): δ 145.9, 138.5, 128.6, 128.3, 127.8, 102.2, 74.0, 13.2. IR ν cm^{-1} (neat): 3088 (m), 3063 (s), 3034 (s), 2922 (s), 2864 (s), 1668 (s), 1607 (m), 1496 (s), 1454 (s), 1403 (m), 1376 (m), 1356 (s), 1289 (m), 1270 (m), 1207 (m), 1176 (s), 1126 (s), 1075 (s), 1028 (m), 986 (m), 930 (s), 734 (s), 697 (s). HRMS (EI) *m/z*: Calculated for $[M]^{+\bullet}$ 148.0888, found 148.0893.

2.12.9 (1-(2-methylallyloxy)prop-2-yne-1,1-diyl)dibenzene, **84**

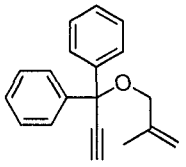

To a 250 ml 3 neck round bottom flask equipped with septa, under an argon atmosphere was added NaI (10 mg), 7.5 g (36 mmol) of 1,1-Diphenyl-2-propyn-1-ol (Aldrich) and 180 mL anhydrous DME. After cooling to 0 °C, solid NaH (950 mg, 39.6 mmol) was added and vigorous bubbling occurred. After warming to 21 °C and stirring for a further 30 minutes 3-bromo-2-methylpropene was added (7.3 mL, 72 mmol) and stirred for another 12 hours. The reaction was quenched with ice water and the organic phase extracted with ether (2 x 200 mL). The organic fractions were combined and dried over magnesium sulfate. After filtration the supernatant was concentrated under vacuum to yielding a yellow oil. The product was purified by flash column chromatography 10% EtOAc/hexane (R_f 0.75) and distilled under vacuum, 5.5 g (58%). ^{1}H NMR ($CDCl_3$): δ 7.57–7.52 (m, 4H), 7.42–7.28 (m, 6H), 5.19 (s, 1H), 4.99 (s, 1H), 4.02 (s, 2H), 3.52 (s, 1H), 1.87 (s, 3H). $^{13}C\{^{1}H\}$ NMR ($CDCl_3$): δ 143.2, 142.2, 128.2, 127.7, 126.5, 111.2, 83.2, 79.9, 77.6, 68.4, 19.9. IR (neat) ν (cm^{-1}): 3285 (s), 3061 (s), 3026 (s), 2973 (s), 2915 (s), 2857 (s),

2111 (m), 1946 (m), 1884 (m), 1810 (m), 1657 (s), 1597 (s), 1490 (s), 1449 (s), 1375 (m), 1317 (m), 1277 (m), 1191 (s), 1178 (s), 1157 (w), 1050 (s), 1003 (w), 973 (m), 936 (w), 903 (s), 770 (s), 654 (s), 641 (s). HRMS (EI) *m/z*: Calculated $[M]^{+\bullet}$ 262.1358, found 262.1355.

2.12.10 (2-(2-methylallyloxy)but-3-yn-2-yl)benzene, **89**

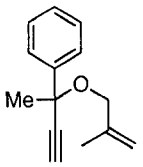

To a 500 mL 3 neck round bottom flask equipped with 3 septa under an argon atmosphere was added NaI (10 mg), 1-methyl-1-phenyl-2-propyn-1-ol (10 g, 8.4 mmol) and 350 mL anhydrous DME. After cooling to 0 °C, solid NaH (1.8 mg, 75.2 mmol) was added and vigorous bubbling occurred. After warming to 21 °C and then stirring for a further 30 minutes, 3-bromo-2-methylpropene was added (18.5 g ml, 137 mmol). After stirring for 12 hours the reaction was quenched with ice water and the organic phase extracted with ether (2 x 200 ml). The organic fractions were combined and dried over magnesium sulfate. After filtering off the white solid, the solvent was removed under vacuum to yield a clear oil. The product was purified by flash column chromatography using a solvent gradient 1-5% EtOAc/hexane (R_f 0.9 in 5% EtOAc/hexane) and distilled under vacuum, 9.8 g (72%). ^{1}H NMR ($CDCl_3$): δ 7.62–7.60 (m, 2H), 7.37–7.34 (m, 2H), 7.30–7.29 (m, 1H), 5.01 (s, 1H), 4.85 (s), 4.00 (d, $^3J_{HH}$ = 11.5, 1H), 3.55 (d, $^3J_{HH}$ = 11.5, 1H), 2.71 (s, 1H), 1.76 (s, 3H), 1.73 (s, 3H). $^{13}C\{^1H\}$ NMR ($CDCl_3$): δ 142.6, 142.3, 128.4, 127.8, 125.7, 111.4, 84.0, 75.8, 75.4, 68.8, 32.8, 19.9. IR (neat) ν (cm^{-1}): 3301 (s), 3063 (s), 2994 (s), 2937 (s), 2910 (s), 2858 (s), 2743 (w), 2108 (m), 1948 (w), 1887 (w), 1811 (w), 1658 (s), 1599 (m), 1488 (m), 1446 (s), 1368 (s), 1310 (w), 1223 (s), 1175 (s), 1096 (s), 1027 (s), 899 (s), 764 (s), 700 (s). HRMS (EI) *m/z*: Calculated $[M\text{-}CH_3]^{+\bullet}$ 185.0966, found 185.0962.

2.12.11 4-methyl-2,2-diphenyl-3-vinyl-2,5-dihydrofuran, **85**

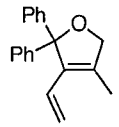

To a 1 dram screw cap vial was added (1-(2-methylallyloxy)prop-2-yne-1,1-diyl)dibenzene (**84**, 200 mg, 0.762 mmol), BHT (134mg, 0.610 mmol), 1.524 mL CH_2Cl_2 and 5 mol% catalyst **15b** (45 mg, 0.0381 mmol). The solution was heated to reflux for 6 hours after which the vial was opened and the solvent removed under vacuum. The product was purified by silica gel flash column chromatography, 5% EtOAc/hexane (R_f 0.31; BHT, R_f 0.89) to yield a clear oil, 189 mg (95%). ^{1}H NMR ($CDCl_3$): δ 7.35–7.19 (m, 10H), 6.36 (dd, $^3J_{HH}$ = 18.0, 11.7, 1H), 5.19 (d, $^3J_{HH}$ = 11.7, 1H), 5.07 (d, $^3J_{HH}$ = 18.0, 1H), 4.74 (s, 1H), 2.15 (s, 3H). ^{13}C{^{1}H} NMR ($CDCl_3$): δ 143.9, 135.5, 135.2, 128.8, 128.3, 128.1, 127.9, 127.8, 127.7, 127.3, 118.0, 96.1, 77.1, 11.6. IR (neat) ν (cm^{-1}): 3058 (s), 3023 (m), 2976 (m), 2921 (s), 2861 (s), 1758 (s), 1673 (w), 1599 (m), 1490 (m), 1446 (s), 1375 (w), 1265 (m), 1225 (m), 1175 (m), 1054 (s), 1032 (s), 990 (s), 931 (m), 760 (s), 736 (m), 700 (s), 627 (w). HRMS (EI) *m/z*: Calculated $[M]^{+\bullet}$ 262.1358, found 262.1361.

2.12.12 2,4-dimethyl-2-phenyl-3-vinyl-2,5-dihydrofuran, **90**

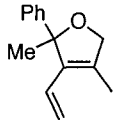

To a 1 dram screw cap vial was added (2-(2-methylallyloxy)but-3-yn-2-yl)benzene (**89**, 200 mg, 0.999 mmol) a stir bar, BHT (176 mg, 0.799 mmol), 1.565 mL CH_2Cl_2 and then 5 mol% catalyst **15b** (59 mg, 0.0305 mmol). The solution was heated to reflux for 6 hours after which the vial was opened and the solvent removed under vacuum. The product was purified by silica gel flash column chromatography, 10% EtOAc/hexane (R_f 0.67; BHT, R_f 0.95) to yield a clear oil, 165 mg (83%). ^{1}H NMR ($CDCl_3$): δ 7.30-7.26 (m, 5 H), 6.34 (dd, $^3J_{HH}$= 18.0, 11.4, 1H), 5.05 (d, $^3J_{HH}$ = 11.4, 1H), 4.89 (d, $^3J_{HH}$ = 18.0, 1H), 4.70 (s, 2H), 1.89 (s, 3H), 1.83 (s, 3H). ^{13}C{^{1}H} NMR ($CDCl_3$): δ 144.7, 136.3, 133.7, 128.1, 127.3, 127.2, 126.1, 116.2, 91.3, 77.0, 24.2, 10.6. IR (neat) ν (cm^{-1}): 3088 (s), 3058 (s), 2978

(s), 2925 (s), 2856 (s), 2827 (s), 1657 (s), 1601 (s), 1493 (m), 1446 (s), 1369 (s), 1238 (s), 1036 (s), 989 (m), 908 (m), 864 (w), 763 (s), 697 (s). HRMS (EI) *m/z*: Calculated $[M\text{-}CH_3]^{+\bullet}$ 185.0966, found 185.0950.

2.12.13 (*E*)-4-styryl-6-vinyl-tetrahydro-3a*H*-cyclopenta[*c*]furan-1,3-dione, **(*E*)-68**

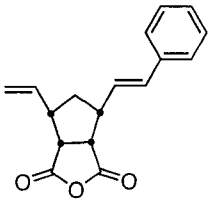

To a small flask charged with 6 mL CH_2Cl_2 was added (*endo*)-norbornene anhydride (100 mg, 609 μM), styrene (317 mg, 3.05 mM) and catalyst $Ru(OC_6F_5)_2(CHPh)(IMes)(3\text{-Br-py})$ (**12b**, 5 mg, 30.5 μM). The vessel was sealed then heated to 65 °C. After one hour the reaction was opened to air and solvent was removed to yield a brown oil. The product was purified by flash column chromatography, 3:1 hexane:EtOAc (R_f: Z = 0.35, E = 0.2). Yield, 124 mg (76 %, E:Z = 1.6:1). The *E*-isomer agrees with reported values.[13] ^{1}H NMR ($CDCl_3$): δ 7.41–7.20 (m, 5H), 6.50 (d, $^3J_{HH}$ = 15.9, 1H), 6.32–6.23 (m, 1H), 6.00–5.88 (m, 1H), 5.21–5.16 (overlapping s and d, $^3J_{HH}$ = 6.0, 2H), 3.52–3.48 (m, 2H), 3.13–2.95 (m, 2H), 2.09 (dt, $^3J_{HH}$ = 12.9, 7.2, 1H), 1.56 (q, $^3J_{HH}$ = 12.9, 1H). $^{13}C\{^1H\}$ NMR ($CDCl_3$): δ 170.7, 170.6, 136.6, 134.8, 132.2, 128.6, 128.5, 127.7, 126.4, 117.3, 49.8, 49.7, 49.3, 46.7, 46.2, 46.1, 36.5. IR neat NaCl ν (cm^{-1}): 2924 (s), 2851 (s), 1940 (w), 1854 (s), 1779 (s), 1667 (w), 1607 (w), 1519 (w), 1496 (w), 1448 (s) 1411 (m), 1350 (w), 1322 (w), 1258 (m), 1203 (s), 1091 (m), 1062 (w), 1030 (w), 999 (s), 968 (s), 919 (s), 823 (w), 804 (m), 790 (w), 695 (m).

2.12.14 (*Z*)-4-styryl-6-vinyl-tetrahydro-3a*H*-cyclopenta[*c*]furan-1,3-dione, **(*Z*)-68**

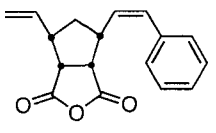

Isolated as a co-product from the reaction above: ^{1}H NMR ($CDCl_3$): δ 7.41–7.20 (m, 5H), 6.70 (d, $^3J_{HH}$ = 11.4, 1H), 6.32–6.23 (ddd, $^3J_{HH}$ = 16.8, 10.8, 7.5, 1H), 5.64 (dd, $^3J_{HH}$ = 11.4, 9.9 Hz, 1H), 5.19–5.12 (m, 2H), 3.45–3.40 (m,

3H), 3.05-2.85 (m, 1H), 2.05–2.00 (m, 1H), 1.46 (q, $^3J_{HH}$ = 7.8, 1H). $^{13}C\{^1H\}$ NMR ($CDCl_3$): δ 170.5, 170.5, 136.8, 134.7, 132.5, 128.4, 128.3, 127.3, 126.4, 117.3, 50.0, 49.5, 46.7, 41.2, 37.8. IR (neat) NaCl ν (cm^{-1}): 3081 (w), 2924 (s), 2859 (s), 1856 (s) 1777 (s), 1641 (w), 1449 (m), 1416 (w), 1324 (m), 1258 (m), 1204 (s), 1146 (w), 1091 (m), 1000 (s), 919 (s), 890 (w), 808 (w), 791 (w) 752 (w), 725 (w). HRMS (EI) *m/z*: Calculated for $[M]^{+\bullet}$ 268.1099; found 268.1086. The diastereoisomers were separated by HPLC: Chiracel AS-H 5% IPA/Hexane, 0.65 mL/min, 60 min.

2.12.15 (*E*)-4-(2-cyclohexylvinyl)-6-vinyl-tetrahydro-3a*H*-cyclopenta[*c*]furan-1,3-dione, **(*E*)-70**

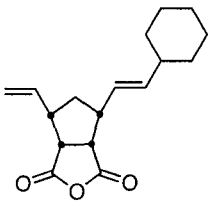

To a small flask charged with 6 mL CH_2Cl_2 is added (endo)-norbornene anhydride (100 mg, 609 μM), vinylcyclohexane (335 mg, 3.05 mM) then catalyst $Ru(O_2C_{20}H_4F_8)(CHPh)(IMes)(py)$ (3.3 mg, 0.5 mol%). The vessel was sealed then heated in an oil bath and heated to 65 °C. After one hour the reaction is opened to air and solvent is removed followed by silica gel column chromatography (2 × 15 cm, 3:1 hexane:EtOAc (R_f: *Z* = 0.43, *E* = 0.36). Combined yield 120 mg (72%); *E*:*Z*, 1:1. NMR data for the *E* isomer correspond with literature values.[13] ^1H NMR ($CDCl_3$): δ 5.98–5.86 (m, 1 H), 5.49–5.39 (m, 2H), 5.27–5.12 (m, 3H), 3.51–3.21 (m, 3H), 3.03–2.94 (m, 1H), 2.22–2.19 (m, 1H), 2.00–1.92 (m, 1H), 1.73–1.01 (m, 10H). $^{13}C\{^1H\}$ NMR ($CDCl_3$): δ 170.9, 170.5, 139.3, 135.0, 123.8, 117.1, 49.6, 46.6, 45.8, 40.6, 36.4, 32.8, 32.7, 26.0, 25.9. IR neat NaCl ν (cm^{-1}): 2924 (s), 2851 (s), 1854 (s), 1779 (s), 1667 (w), 1607 (w), 1519 (m), 1448 (s), 1411 (m), 1350 (m), 1332 (m), 1258 (m), 1203 (s), 1091 (m), 999 (s), 968 (m), 919 (s), 804 (m), 695 (w).

References page 78

2.12.16 (*Z*)-4-(2-cyclohexylvinyl)-6-vinyl-tetrahydro-3a*H*-cyclopenta[*c*]furan-1,3-dione, (**Z**)-**70**

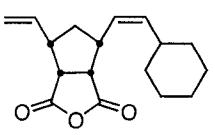

Isolated as a co-product from the reaction above. ^{1}H NMR ($CDCl_3$): δ 5.98–5.87 (m, 1H), 5.54–5.38 (m, 2H), 5.17–5.11 (m, 2H), 3.43 (p, $^3J_{HH}$ = 7.2, 2H), 2.98–2.87 (m, 2H), 2.02–1.90 (m, 2H), 1.71–1.62 (m, 5H), 1.40 (q, $^3J_{HH}$ = 12.9, 1H), 1.29–0.85 (m, 5H). ^{13}C{^{1}H} NMR ($CDCl_3$): δ 170.7, 170.4, 139.5, 134.9, 123.6, 117.2, 49.6, 46.8, 40.7, 37.9, 37.0, 33.4, 33.2, 26.0, 25.8. IR neat NaCl ν (cm^{-1}): 3081 (w), 2924 (s), 2805 (s), 1856 (s) 1777 (s) 1642 (w), 1449 (m), 1416 (w), 1324 (w), 1258 (m), 1204 (s), 1146 (w), 1091 (m), 1000 (s), 967 (m), 919 (s), 808 (w), 791 (m), 752 (w), 725 (w). HRMS (EI) *m/z*: Calculated for $[M]^{+\bullet}$ 274.1569; found 274.1583.

2.13 General Procedures for Catalytic Reactions

All substrates and monomers were distilled before use (b.p. < 125 °C, trap to trap distillation; b.p. > 125 °C vacuum distillation). Substrates were degassed using consecutive freeze pump thaw cycles. Either ^{1}H NMR or GC-FID was used to determine the outcome of catalytic reactions. The commercial sources or references for literature substrates are given in Table 1. For GC-FID, the identity of substrates and products was confirmed by GC-MS analysis. GC-FID yields were determined from the calibrated peak area responses in reference to internal standard THN (1,2,3,4-tetrahydronaphthalene). Calibration curves, using 5-10 points, were constructed in the concentration regime of the analyte to be monitored. The FID response was kept between 100-2000 pA with an analyte concentration range of 0.005-0.0001 M. An inlet split ratio of 10:1 was used. For reactions producing ADMET oligomers the amount of oligomerization was determined by difference. When ^{1}H NMR was used, the conversion was calculated by the integrated difference between olefinic signals. $CDCl_3$ or C_6D_6 were used as the solvent. ^{1}H NMR was not used to determine the

conversion for substrates known to form undistinguishable side products such as macrocyclization reactions. Agreement between 2 to 4 replicate runs with ± 3 % error was maintained. All reactions were put together in a nitrogen filled glove box.

Typically, a large (200 mg substrate) mother reaction was set up and then distributed to several small vials. The timed opening of the small vials enabled the monitoring of reactions over time without perturbing the reaction. For regular metathesis reactions one-dram vials equipped with PTFE lined screw tops were used. Once sealed, the reactions were brought out of the glove box for heating, the workflow for this type of reaction screening is shown in Figure 1. Reactions were heated in a drilled out aluminium block equilibrated to the desired temperature on a stirring hot plate and were stirred at 750 rpm. To ensure efficient heat transfer the holes in the aluminium block were made as small as possible. The temperature was monitored in a blank vial filled with silicon oil, (Figure 1).

2.13.1 Calculation of reaction concentrations

For reactions where the concentration of substrate is ≤ 0.1 M the density of the catalyst and substrate was not taken into account. At concentrations > 0.1M the density of catalyst and substrate is approximated to be 1 mg/μl and the volume created by the substrate and catalyst is accounted for in the calculation of reaction concentration.

1. A large solution containing solvent and internal standard is prepared.
2. An aliquot is removed for the time 0 reference (t_0).
3. Catalyst is added and the reaction is distributed to several vials.

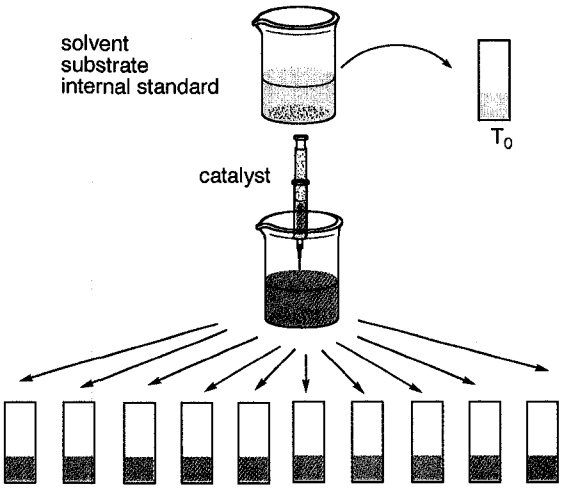

4. The reactions are closed and heated in an aluminum block.

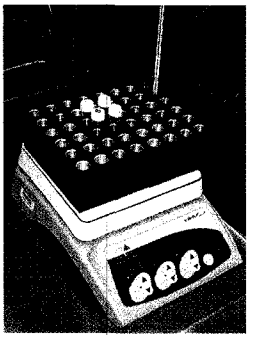

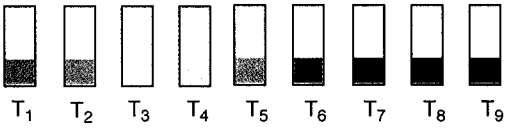

5. The vials were then opened at set time intervals and analyzed immediately by GC-FID or ^{1}H NMR.

Figure 1. Workflow for setting up RCM reactions to be monitored over time.

Table 1. Commercial sources and literature references for substrates and products.[a]

#	Compound	source or reference
20		Cyclooctene (COE) Aldrich
21	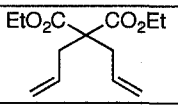	Aldrich "DEDAM"
32	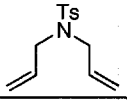	16,17

#	Compound	source or reference
poly-**20**	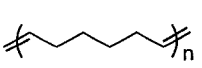	Vestenamer14
22	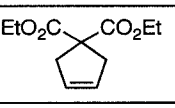	15
33	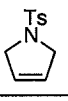	16

34	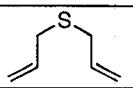	Lancaster
36	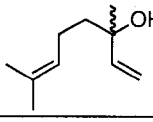	Linalool-Aldrich
40	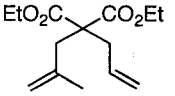	27
42	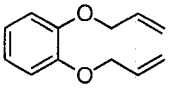	22
44	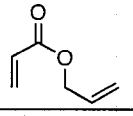	Lancaster
46	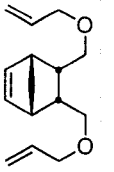	24
48	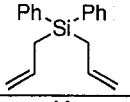	Lancaster
50	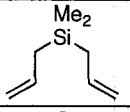	Lancaster
53		29
58	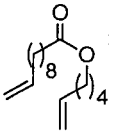	26
60	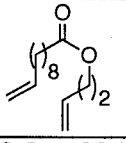	26
62	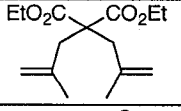	20
66	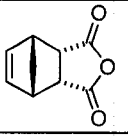	30
68	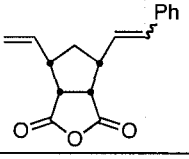	31

35		18
37	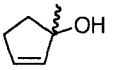	19
41	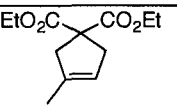	20,21
43	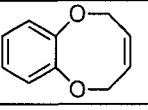	22
45		23
47	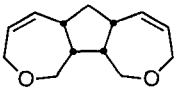	24
49	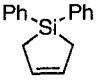	25
52	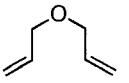	Aldrich
54		29
59	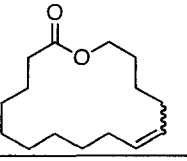	26
61	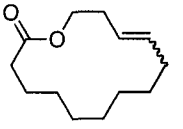	26
63	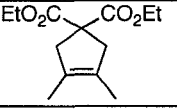	20
67		Aldrich
69		Aldrich

70	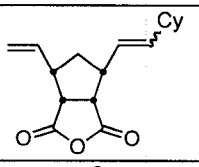	31
74	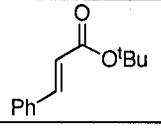	32
77	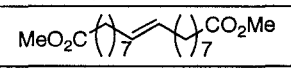	33
78	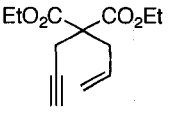	34
80	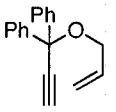	35
82	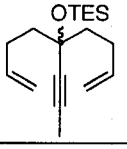	36
95	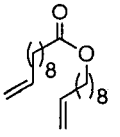	27
97	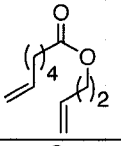	37
99	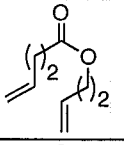	38
101	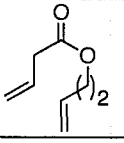	38
103	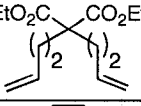	37
105	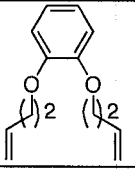	37
73	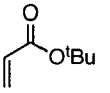	Aldrich
75	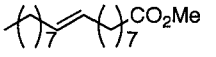	Aldrich
76	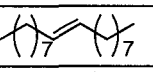	33
79	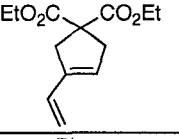	34
81	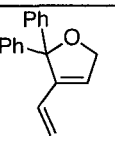	35
83	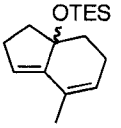	36
96	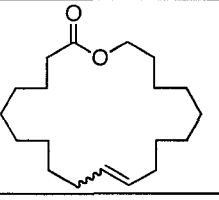	27
98	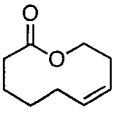	37
100	0 % RCM	
102	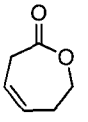	37
104	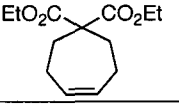	37
106	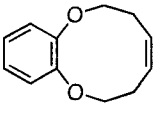	37

107	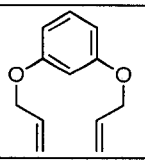	37
111	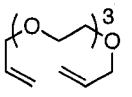	39
113	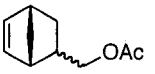	NBE-CH2OAc Promerus

109	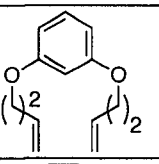	37
112	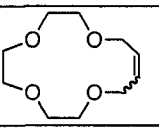	39
Poly-**113**	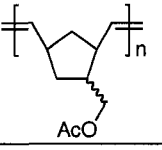	Promerus

[a]Substrates **40**, **42**, **46**, **62**, **66**, **78**, **82**, **105**, **107**, **111** were obtained from Dr. Jennifer Snelgrove of this lab. Substrates **97**, **99**, **101**, **103** were obtained from Sebastien Monfette of this lab. Monomer **117** was obtained from Dr. Dino Amoroso, Promerus LLC (Cleveland, OH).

2.14 Ring Closing Metathesis (RCM)

2.14.1 General method to monitor RCM, Enyne or CM with 5 mol% catalyst

To a small 1 dram vial containing 0.1 mmol of substrate and 1 mL of solvent was added 0.05 mmol of catalyst (final [S] = 0.1 M, [C] = 0.05 M). The rapidly-stirred reaction mixture was heated to 62 °C. For GC analysis internal standard was added prior to adding catalyst. Reactions to be monitored by NMR spectroscopy were in $CDCl_3$ or C_6D_6 solvent.

2.14.2 General method to monitor RCM or Enyne reactions with 0.05 or 0.5 mol% catalyst

To a small 1 dram vial containing 0.1 mmol of substrate and 1 mL of solvent was added a stock solution of catalyst, 0.0005 or 0.005 mmol (final [S] = 0.1 M, [C] = 0.0005 or 0.005 M). The rapidly-stirred reaction mixture was heated to 62 °C. For GC analysis internal standard was added prior to adding catalyst. Reactions to be monitored by NMR spectroscopy were in $CDCl_3$ or C_6D_6 solvent.

2.14.3 Representative RCM reaction, [substrate] = 0.1 M, monitored over time

In a nitrogen filled glovebox a 5-dram vial was charged with hex-5-enyl undec-10-enoate (**58**, 266 mg, 1 mmol) internal standard THN (66 mg) and CH_2Cl_2 (10 mL). A 10 μL sample was removed for T_0 and diluted to 5 mM for GC analysis. The reaction was then treated with $RuCl_2(CHPh)(IMes)(PCy_3)$ (**2a**, 42 mg, 0.05 mol). The reaction was stirred vigorously and 1.5 mL was transferred to 6 1-dram screw top vials. For the 5 minutes needed to transfer the reaction to the small vials, the reaction was open to the nitrogen of the glovebox atmosphere. The vials were then sealed and stirred for 10 more minutes at 21 °C. After this initial 15 minute mixing time at 21 °C the vials were brought out of the glovebox and heated to reflux. A vial was sampled once at different set time intervals: 15, 30, 45 min, 1, 1.5, and 2 h. Vials were then cooled to room temperature, opened and the GC spectrum recorded. The yield over time was determined by calibrated peak area response in reference of diene to internal standard at T_0 (Chapter 5, Figure 8; Appendix A, Table 9).

2.14.4 Representative RCM reaction at low concentration, [substrate] = 5 mM, monitored over time

In a nitrogen filled glovebox a 20 dram vial was charged with hex-5-enyl undec-10-enoate (**58**, 20 mg, 0.0751 mmol), internal standard THN (10 mg), and 15 mL CH_2Cl_2. A 1 mL aliquot was removed for the T_0 reference. Then 5 mol% $RuCl_2(CHPh)(IMes)(PCy_3)$ was added from a stock solution (295 μL, 3.50×10^{-6} mol from 10 mg **2a** in 1 mL CH_2Cl_2, 11.8 mM). The reaction was stirred vigorously and 1 mL was distributed to 8 1-dram screw top vials. For the 5 minutes needed to transfer the reaction to small vials the reaction was open to the nitrogen of the glovebox atmosphere. The vials were then sealed and stirred for 10 more minutes at 21 °C. After this initial 15 minute mixing time at 21 °C the vials were brought out

of the glovebox and heated to reflux. A vial was sampled once at different set time intervals: 15, 30, 45 min, 1, 1.5, 2, 3 and 5 h. Vials were cooled to room temperature and the GC spectrum recorded. The yield over time was determined by calibrated peak area response in reference of diene to internal standard at T_0 (Chapter 5, Figure 8; Appendix A, Table 8).

2.14.5 Representative RCM reaction, [substrate] = 0.1 M, then diluted to 5 mM, monitored over time

In a nitrogen filled glovebox a 1-dram vial was charged with a solution of hex-5-enyl undec-10-enoate (**58**, 40 mg, 1.50×10^{-4} mol), internal standard THN (20 mg) and CH_2Cl_2 (1.502 mL). A 751 μL sample was removed for T_0 and diluted to 5 mM for GC analysis. The remaining reaction was treated with 31.7 μL of a stock solution of $RuCl_2(CHPh)(IMes)(PCy_3)$ (100 mg **2a** in 1 mL CH_2Cl_2, 0.118 M). After stirring at 21 °C for 15 minutes, 251 μL was removed for GC analysis and the remainder diluted to 5 mM with 9.5 mL CH_2Cl_2. After stirring briefly the reaction was put into 5 separate 1-dram screw cap vials. Then the vials were brought out of the glovebox and heated to reflux. A vial was sampled once at different set time intervals: 15, 30, 45 min, 1, 1.5, 2, 3 and 5h. Vials were cooled to room temperature and the GC recorded. The yield over time was determined by calibrated peak area response in reference of diene to internal standard at T_0, (Appendix A, Table 10 and Figure 10).

2.14.6 Representative RCM of macrocycles dropwise addition of substrate and catalyst.

Under an atmosphere of argon, a three-neck round-bottom flask charged with 20 mL CH_2Cl_2 was fitted with a condenser and two equalizing-pressure addition funnels. Solutions of diene hex-5-enyl undec-10-enoate (**58**, 80 mg, 0.3 mmol with internal standard THN (10 mg)) and catalyst $RuCl_2(CHPh)(IMes)(PCy_3)$ (**2a**, 13 mg, 1.5×10^{-5} mol), each in 20 mL CH_2Cl_2, were

added drop-wise over 15 min. (During the preparation of the diene solution a 100 μL sample is removed and diluted to 5 mM for the T_0 reference). Beginning at 15 minutes, aliquots were removed via a gas-tight syringe, for quantification by GC at set time intervals of 15, 30, 45 min, 1, 1.5, 2, 3 5 and 9h. The yield over time was determined by calibrated peak area response in reference of diene to internal standard at T_0, (Chapter 5, Figure 5; Appendix A Table 7).

2.15 Analysis of ADMET Oligomers

2.15.1 Analysis of ADMET polymers by TLC

The reaction in 2.14.1 was prepared, except internal standard was not added. The solution was heated to reflux for 30 minutes. After cooling, the reaction was opened and a sample spotted on a TLC sheet. Separation was achieved with 10% EtOAc/hexanes and the spots were developed with anisaldehyde stain: diene R_f 75-95, polymer R_f 0-53 (Chapter 5, Figure 6).

2.15.2 Reaction followed by TLC

The procedure in 2.14.3 was followed, except internal standard was not added. The vials were opened at set time intervals and then when the reaction was finished all of the different reaction times were spotted on a TLC plate and eluted with 10% EtOAc/hexane. The spots were developed with anisaldehyde stain: **58** R_f 95; **59**, R_f 82; poly-**58** R_f 0-53 (Appendix B, Figure 18).

2.15.3 Analysis of ADMET Oligomers by ^{1}H NMR

The procedure in 2.14.1 was followed, except internal standard was not added. After the reaction was complete the oligomers were isolated by removing the solvent under vacuum

and drying the white greasy material under vacuum overnight then recording the ^1H NMR in $CDCl_3$ (Appendix B, Table 20).

2.15.4 MALDI-TOF Mass Spectrum of poly-**58**

The reaction in 2.14.1 was prepared, except internal standard was not added. The solution was heated to reflux for 30 minutes. Under reduced pressure the solution was reduced to a greasy solid. The material was then dissolved in dichloromethane (1 mg/mL). This was mixed 1:20 with a matrix solution (20 mg/mL, dithranol/CH_2Cl_2). The solution was then spotted on a sample plate, allowed to dry and analyzed. Analyses were performed using a Bruker Daltonics OmniFlex MALDI-TOF mass spectrometer equipped with a nitrogen laser (337 nm). (Chapter 5, Figure 7; Appendix B, Figure 17).

2.15.5 MALDI-TOF Mass Spectrum of poly-**58** formed during an RCM reaction using the Dropwise Addition Protocol

The reaction in 2.14.4 was carried out as above without internal standard. After the 15 minute addition period the reaction was opened to air and stirred until the solution turned brown. Under reduced pressure the solution was reduced to a greasy solid. The material was then dissolved in dichloromethane (1 mg/mL). This was mixed 1:20 with a matrix solution (20 mg/mL, pyrene/CH_2Cl_2). The solution was then spotted on a sample plate, allowed to dry and analyzed. Analyses were performed using a Bruker Daltonics OmniFlex MALDI-TOF mass spectrometer equipped with a nitrogen laser (337 nm). The full spectrum is shown in the Appendix B, Figure 16.

2.16 Tandem RCM - Isomerization

2.16.1 Representative procedure for tandem RCM isomerization

To a 1 dram screw top containing 118 μL C_6D_6 and a stirbar was added 5 mol % **2a** (5 mg, 5.91 μmol). *N*-tosyldiallylamine **32** (30 mg, 0.118 mmol) was then added, [S] = 0.1 M, [C] = 5 mM. after the 15 minutes to effect complete RCM solid K_2CO_3 (0.81 mg, 0.0204 mmol) was added and heated to reflux for 4 h. 100 % yield of cyclic vinyl amine by ^{1}H NMR. Same procedure for the formation of **54** from **51**.

2.17 Ring Opening Metathesis Polymerization (ROMP)

2.17.1 Representative procedure for synthesis of ROMP polymers

To a rapidly-stirred solution of initiator $RuCl(OC_6Br_5)(CHPh)(IMes)(3\text{-Br-py})$ (**15b**) in CH_2Cl_2 (7.1 mg, 1.0 mM) was added 100 equiv of NBE-CH_2OAc (**113**) monomer (final substrate concentration = 0.1 M). ROMP was allowed to continue for up to 24 h, depending on the initiator. Polymers were then precipitated by concentrating the solution and adding it dropwise to rapidly stirring methanol. The precipitates were filtered off, washed with methanol and hexanes, and dried under vacuum.

2.17.2 Representative procedure for measurement of ROMP kinetics

To cyclooctene (**20**, 50 μL, 0.385 mmol) and 3.85 mL of $CDCl_3$ was added 1.925 μmol of $Ru(OC_6F_5)_2(CHPh)(IMes)(py)$ (**12a**) as a solution in $CDCl_3$ (0.1925 M). After vigorous stirring for one minute, 0.75 mL of the solution was transferred to an NMR tube and set to spin at 20 Hz in the NMR probe. Conversions were determined at regular time intervals by monitoring the integrated intensities of olefinic signals for the monomer and polymer in time array ^{1}H NMR experiments. Rates and turnover frequencies (TOF; h^{-1}) were determined at

50% conversion, as the solution became slightly viscous at higher conversions. Polymerization data is tabulated in Appendix A: cyclooctene **20**, Table 1; NBE-CH_2OAc **113**, Table 24.

2.17.3 Determination of k_p/k_i (Chapter 6, Equation 1)

To a rapidly-stirred solution of initiator $Ru(OC_6Br_5)Cl(CHPh)(IMes)(3\text{-}Br\text{-}py)$ (**15b**, 10 mg, 8.5 umol) in $CDCl_3$ (0.5 mL) was added 10 equivalents of COE (**20**, 9.4 mg, 85 μmol) as a solution in $CDCl_3$ (0.35 mL). The initiator concentration was 0.01 M and the monomer concentration was 0.1 M. The integrated intensity of the alkylidene peaks was monitored by ^1H NMR, Table 2 and Figure 2. The relative peak integrations were used to determine k_p/k_i according to Equation 1 (Chapter 6).[40]

Table 2. Alkylidene ^1H NMR resonances for H_α δ ppm ($CDCl_3$).

Initiator		[Ru]-COE	[Ru]-NBE-CH_2OAc
$RuCl_2(CHPh)(PCy_3)_2$	**1**	19.29 (t, $^3J_{HH}$ = 5.2 Hz)	18.67–18.90 (m)
$RuCl_2(CHPh)(IMes)(PCy_3)$	**2a**	18.85 (br)	18.78–18.55 (br s)
$RuCl_2(CHPh)(IMes)(py)_2$	**3a**	19.32 (t, $^3J_{HH}$ = 5.5 Hz)	18.91–18.78 (m)
$RuCl_2(CHPh)(IMes)(3\text{-}Br\text{-}py)_2$	**3b**	19.36–19.27 (m)	18.81–18.78 (m)
$Ru(OC_6Br_5)Cl(CHPh)(IMes)(py)$	**15a**	18.73–18.57 (m)	18.75–18.67 (m)
$Ru(OC_6Br_5)Cl(CHPh)(IMes)(3\text{-}Br\text{-}py)$	**15b**	18.73–18.66 (m)	18.77–18.68 (m)

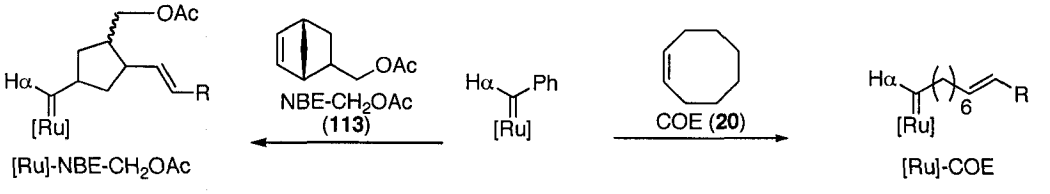

Figure 2. Determination of k_p/k_i by monitoring of H_α during the ROMP of 10 equivalents of COE or NBE-CH_2OAc.

2.18 Self Metathesis of Methyl Oleate

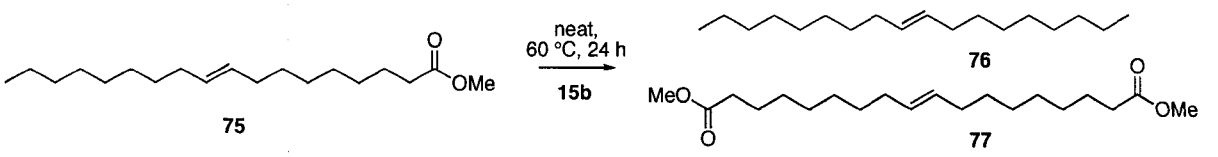

To a 1 dram screw top vial was added 200 mg of methyl oleate (6.75×10^{-4} mol). Catalyst **15b** was added as a stock solution as indicated in Table 3. After adding the catalyst the top was secured and the reaction was heated for 24 h at 60 °C. For analysis, 20 mg of the reaction mixture was removed and diluted with 10 mL CH_2Cl_2 and quantified by calibrated GC-FID (HP-1 column). The products were also identified by GC-MS (*m/z*): **75**, 296.27; **76**, 252.29; **77**, 340.26. Reaction yield and error on replicate experiments are tabulated in Appendix A, Table 25.

Table 3. Amount of catalyst (**15b**) added to 200 mg of methyl oleate (6.75×10^{-4} mol).

[S]/[C]	Catalyst stock solution	Composition	Amount added
40,000	4.25×10^{-4} M	10 mg (8.50×10^{-6} mol) / 20 mL CH_2Cl_2	40 μL (1.68×10^{-8} mol)
100,000	4.25×10^{-4} M	10 mg (8.50×10^{-6} mol) / 20 mL CH_2Cl_2	16 μL (6.75×10^{-9} mol)
1,000,000	8.50×10^{-6} M	10 mg (8.50×10^{-6} mol) / 10 mL CH_2Cl_2, diluted 100 μL / 9.9 mL	79 μL (6.75×10^{-10} mol)
2,000,000	8.50×10^{-6} M	10 mg (8.50×10^{-6} mol) / 10 mL CH_2Cl_2, diluted 100 μL / 9.9 mL	40 μL (3.38×10^{-10} mol)

References page 78

2.19 High Throughput Experiments

2.19.1 General Procedures

Fully integrated Symyx Technologies' screening equipment and software housed at the University of Ottawa Centre for Catalysis Research and Innovation was used to carry out parallel experiments in 96 well format. Reactions were designed using Library Studio software. Arrays of reactions were set up with the coordinates A1-H12 (1-96). Variables were changed along the A-H or 1-12 axis. The total volume of solvent per reaction was between 300 and 500 μL. Reactions were assembled in a glovebox from stock solutions of catalyst and substrate. To avoid waste from wash cycles, stock solutions were made as dilute as possible. The stock solutions for catalyst were made fresh for each run. For solutions with a concentration of 0.1 M or greater the solute was assumed to have a density of 1 g/mL. For solutions below 0.1 M the volume of the solute was assumed to be 0. For dispensing volumes < 100 μL, a Cavro liquid handling robot controlled by Impressionist software was used. The backing solvent for the liquid handling robots was toluene. The minimum dispense volume used for the liquid handling robots was 20 μL. When larger amounts of solvent were needed, a 12-tip 200 or 300 μL Eppendorf was used. Reactions were carried out in 7 × 30 mm glass cylinder inserts and were agitated with Parylene coated stir bars - 1.67 × 2.01 × 4.80 mm.

The inserts were arrayed 8 × 12 in a Symyx machined, anodized, aluminium block. Heating was accomplished with a Julabo heater/cooling unit interfaced with a Tecan reaction deck. The reactions were sealed with Teflon and then rubber sheets. The covers made from plastic were not compatible with 1,2-dichloroethane or THF and were not used with these solvents. The covers were held on tightly by a screwed down aluminium top. When solvent

needed to be removed, reactions were evaporated down in a vacuum centrifuge modified to accommodate the aluminium blocks.

Reactions were diluted to 0.02 M with methanol before GC analysis. The analysis was done using an Agilent GC-FID fitted with a GC-PAL autosampler. Both were controlled by Symyx engineered Epoch software. The GC was calibrated externally with a 10-point calibration curve using authentic starting material and product. The GC was fitted with an HP-1 column. To shorten analysis times, the GC method was optimized as much as possible, short (< 3 min) isocratic elutions were used. Under these conditions analysis of all 96 wells was complete in less than 6 hours. The data, stored on the RAS server and viewed through Polyview was exported to Excel for averaging and error analysis.

2.19.2 Solvent Screen Procedure

The following anhydrous grade solvents, purchased from Aldrich, were used: 1,2-dichloroethane, chlorobenzene, FC-72 (perfluorohexane), perfluorobenzene, ααα–trifluorotoluene (BTF), decane, dimethoxyethane (DME), *N,N*-dimethylformamide (DMF), *N*-methylpyrolidone (NMP), nitrobenzene, acetonitrile and dimethylsulfoxide (DMSO). Solvents THF, dichloromethane, toluene and benzene, were purified by solvent system as described in Section 1. All solvents were further prepared by degassing with a nitrogen sparge for 30 minutes and dried with activated Linde 4Å molecular sieves. Stock solutions of 8 different catalysts in dichloromethane were prepared, the amounts are tabulated below. The catalyst solutions were distributed in the rows A-H (40 μL, 2×10^{-7} mol). Several plates were daughtered at once. The solvent was removed under vacuum leaving the catalyst residues. The plates were covered so that they could be used at a later time. A picture of a plate containing catalyst is shown below in Figure 3.

Table 4. Solvent screen amount of catalyst dissolved in 5 ml CH_2Cl_2 to make 5×10^{-3} M stock solutions.

Row	Catalyst	Amount (mg)
1	**1**	21
2	**2a**	21
3	**3a**	18
4	**3b**	20
5	**12a**	24
6	**12b**	26
7	**15a**	27
8	**15b**	29

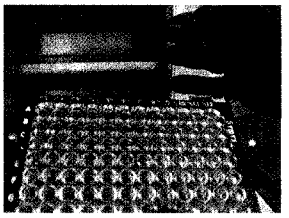

Figure 3. A reaction plate containing catalyst after the solvent has been removed.

To the inserts containing catalyst and stir bars was added the desired solvent. A 12-channel Eppendorf pipette was used to add different solvents (360 μL) across the columns 1-12. Next diethyldiallyl malonate (**20**) was added as a stock solution in toluene (40 μL of a 1 M solution, 1.201 g in 3.791 mL of toluene). The final reaction volume was 400 μL with a substrate concentration of 0.1 M. The catalyst loading was 0.5 mol%. After sealing the reaction block it was heated to 75 °C and stirred for 3 hours at 500 rpm. The reaction was then brought out of the glove box and after cooling to room temperature, opened. 120 μL was removed with a 12 channel Eppendorf and put into an analysis plate. The reaction mixtures were then diluted with 480 μL of methanol, total volume 600 μL, concentration 0.02 M. The plate was then mounted on the autosampler and the reactions were analyzed by GC-FID. Due to phase separation between FC-72 and methanol the methanol layer

containing the product was extracted off the top and analyzed. Figure 4 shows the work-flow for the solvent screen.

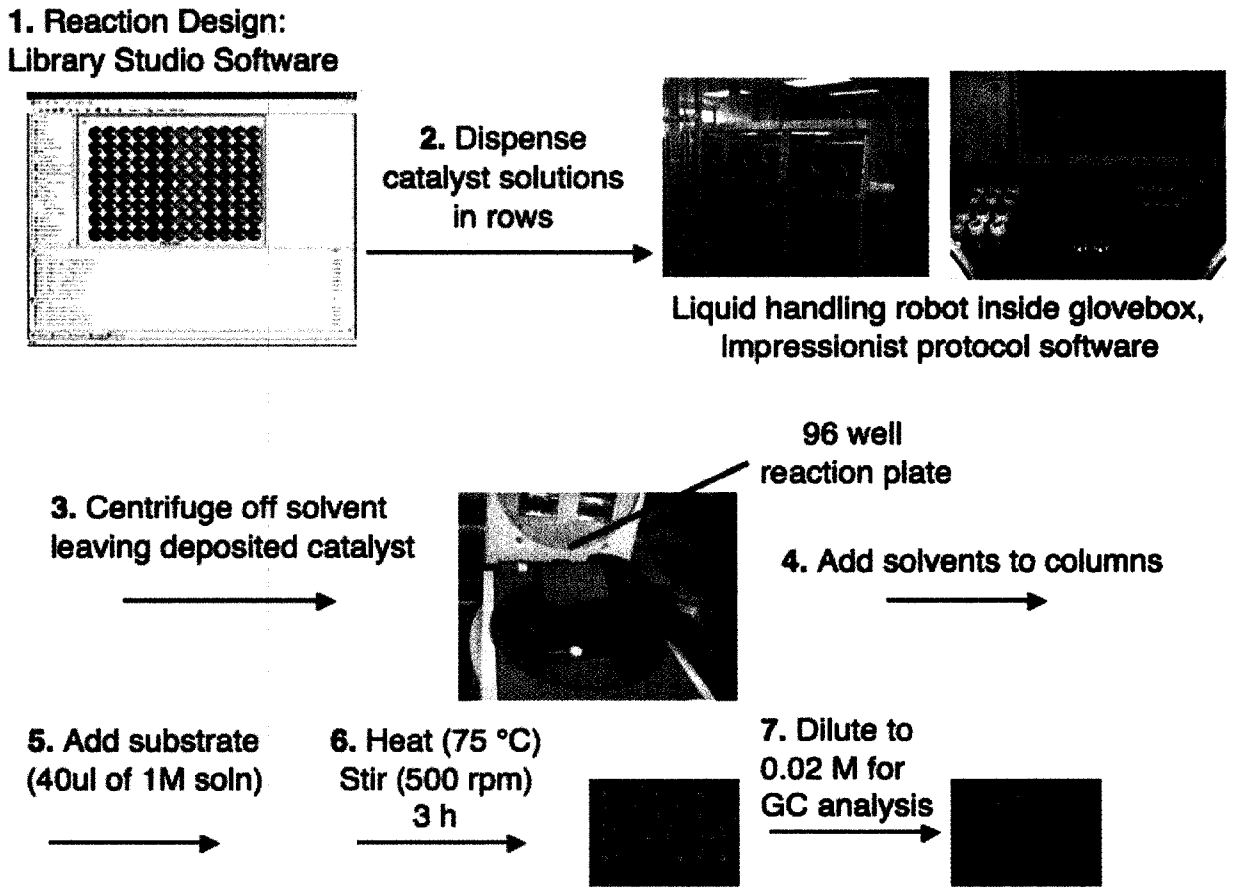

Figure 4. Work flow for RCM solvent screen.

To analyze the reactions a 10-point calibration curve was constructed for diethyldiallyl malonate **20** and the ring closed product, **21**. The yield was determined by the difference in calibrated peak area. The data was handled in Polyview and then exported to Microsoft Excel. The solvent screen data is plotted in Chapter 4, Figure 1 and the data are tabulated in Appendix A, Table 2 and Figures 1-9. The work-flow for the high throughput reaction analysis is shown in Figure 5.

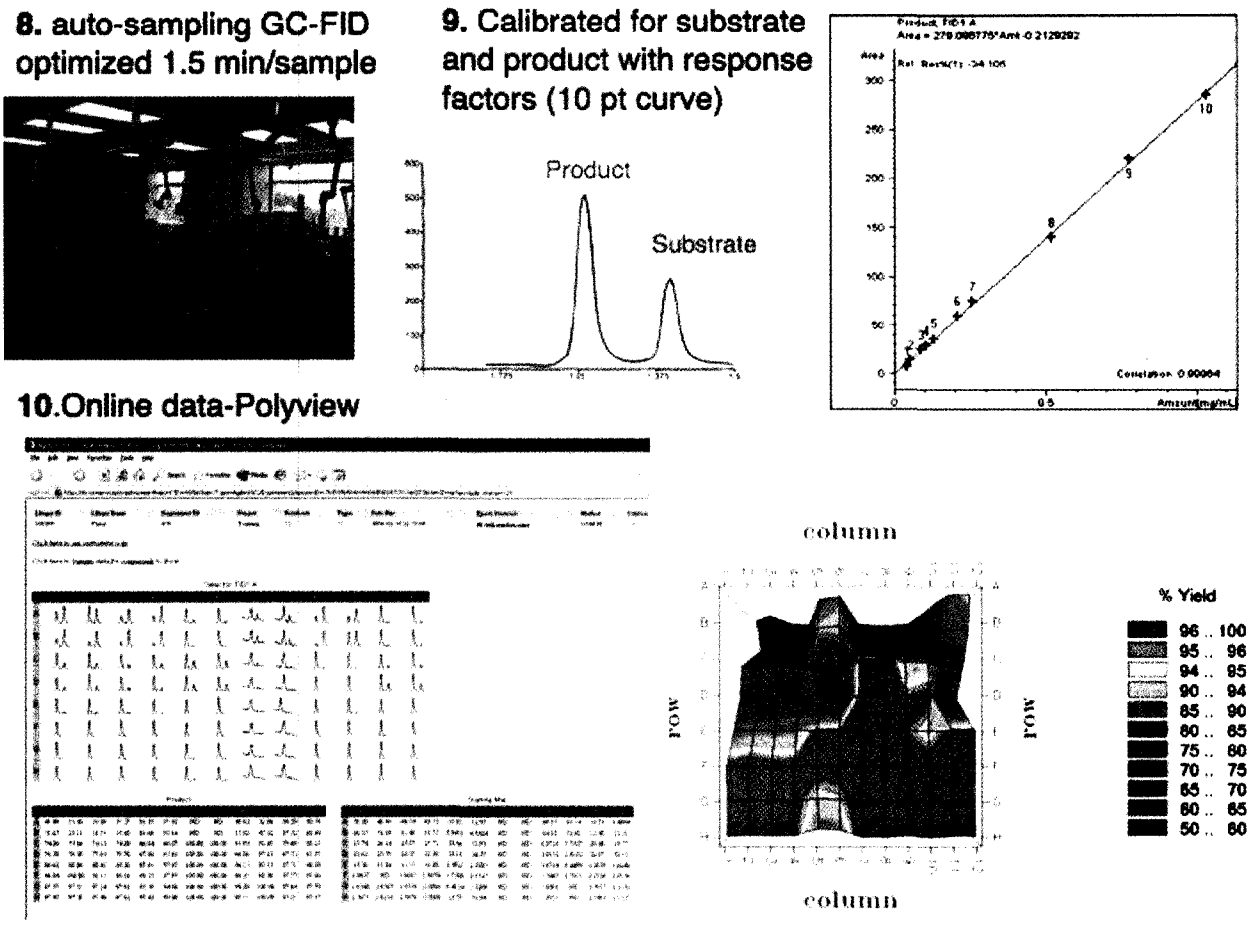

Figure 5. Analysis of reactions by calibrated GC-FID.

2.19.3 Primary Acid Additive Screen for Enyne Metathesis.

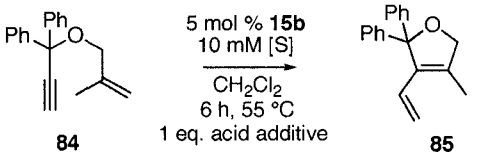

84 **85**

Stock solutions of additives (Aldrich) were prepared with a concentration of 0.1 M. The amounts used are shown in Table 5. The ratio of additive to substrate **84** was 1:1. To a series of wells was added 40 μL of additive (4 μmol, 0.1M). The solvent was then removed under vacuum. Next CH_2Cl_2 (320 μL) was added followed by substrate, 40 μL (4 μmol) of a stock 0.1 M solution (105 mg, in 3.9 mL of CH_2Cl_2). The catalyst, $RuCl(OC_6Br_5)(CHPh)(IMes)(3-$

Br-py) (**15b**), was added last, 40 μL from a 0.005 M stock solution (23 mg in 3.98 mL CH_2Cl_2). The total reaction volume was 400 μL, with a substrate final concentration of 0.01 M. The reactions were heated for 6 h at 55 °C. Then the reactions were allowed to cool to room temperature. An analysis plate was made with 300 μL from each well topped off with 300 μL of methanol for a total volume of 600 μL, and a concentration of 0.005 M. The diluted analysis plate was then analyzed by externally calibrated GC-FID. The data are tabulated in Appendix A, Table 3 and the corresponding graph is shown in Chapter 4, Figure 8.

Table 5. Additive solutions for primary screen, 0.1 M.

Additive	Amount (mg)	Solvent (2 mL)
Blank	0	CH_2Cl_2
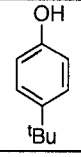	30	CH_2Cl_2
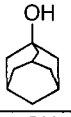	30	CH_2Cl_2
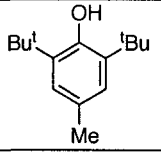	67	CH_2Cl_2
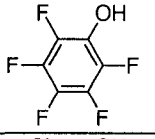	37	CH_2Cl_2
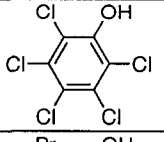	53	THF
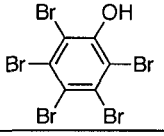	98	THF
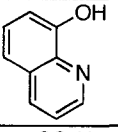	29	CH_2Cl_2
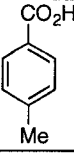	31	DMSO
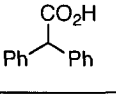	42	DMSO
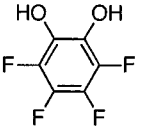	34	CH_2Cl_2
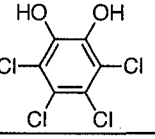	50	CH_2Cl_2
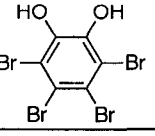	85	THF
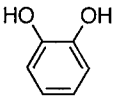	22	CH_2Cl_2

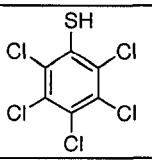	57	THF		14	DMSO
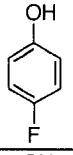	22	CH_2Cl_2	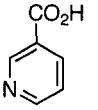	25	DMSO
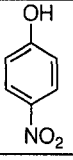	28	CH_2Cl_2		24	DMSO
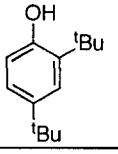	41	CH_2Cl_2	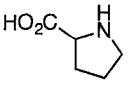	23	DMSO
NH_4PF_6	21	DMSO	NH_3SO_3H	19	DMSO
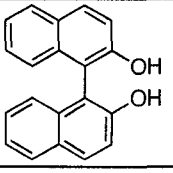	57	THF	NH_4Cl	11	DMSO

2.19.4 Narrowed Additive Screen for Enyne Metathesis

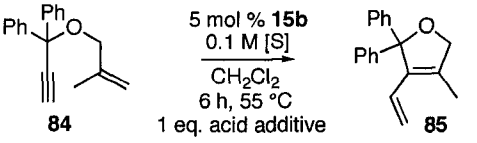

Stock solutions of additives were prepared according to Table 6. The additives were dispensed first, 100 μL each. Substrate **84** was then dispensed to each reaction, 100 μL from a 1 M solution (205 mg in 5 mL CH_2Cl_2). Next catalyst **15b** was added, 60 μl of a 0.025 M solution (59 mg in 1.94 mL CH_2Cl_2). For 6h the reactions were stirred and heated (55 °C). Next the reactions were removed from the glovebox and allowed to cool. For analysis, 50 μL was removed from each well and diluted with 450 μL of methanol to make a final concentration of 0.005 M. The data are tabulated in Appendix A, Table 4 and the corresponding graph is in Chapter 4, Figure 8.

Table 6. Composition of additive solutions (1 M) for the narrowed enyne metathesis screen.

Additive	Amount (mg)	CH_2Cl_2 (mL)
Blank	-	2.00
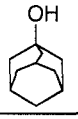	304	1.70
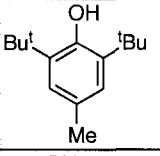	441	1.56
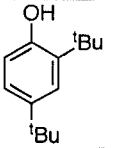	413	1.51
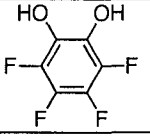	364	1.64

2.19.5 Screen for amount of BHT to add for enyne metathesis

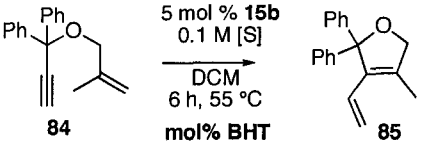

To an array of reaction wells was dispensed 100 μL of a 0.4 M stock solution of substrate, (**84**, 299 mg in 2.7 mL of CH_2Cl_2). Two stock solutions of BHT were made 0.06 M (13 mg in 3.99 mL CH_2Cl_2) and 0.6 M (132 mg in 3.87 mL). The amount dispensed is shown in Table 7. Next CH_2Cl_2 was added. Catalyst **15b**, added last, was then dispensed (27 μL) from a stock solution 0.075 M in CH_2Cl_2 (132 mg, 1.37 mL). The reaction was then sealed, then stirred and heated (55 °C) for 6 h. For analysis, 50 μL was removed form each well and diluted with 450 μL of methanol to make a final concentration of 0.005 M. The data are tabulated in Appendix A, Table 5 and the corresponding graph is in Chapter 4, Figure 8.

Table 7. Amount of CH_2Cl_2 and BHT added from 0.6 or 0.06 M stock solutions.

BHT (mol %)	Dispensed volume from 0.6 M stock solution	Dispensed volume from 0.06 M stock solution	Volume of CH_2Cl_2 added to make the final reaction volume 400 μL
0	0	0	273
10	0	67	206
20	0	134	139
30	20	0	253
40	27	0	246
50	34	0	239
60	40	0	233
70	47	0	226
80	54	0	219
90	60	0	213
100	67	0	206

2.19.6 Concentration of substrate screen

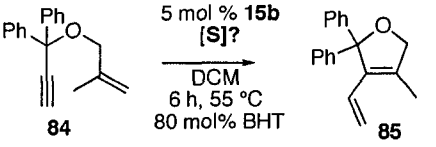

To 5 vials was added 20 mg of substrate, (1-(2-methylallyloxy)prop-2-yne-1,1-diyl)dibenzene (**84**, 7.62×10^{-5} mol). Next 0.8 equivalents of BHT was added (13 mg). Then, in amounts given in Table 8, solvent was added. Catalyst **15b** was added last, 5 mol% (4.5 mg, 3.81×10^{-6} mol). For this screen the density of catalyst, substrate and BHT were assumed to be 1mg/μL. For analysis, aliquots were removed from each well and diluted to a final concentration of 0.005 M. The data are tabulated in Appendix A, Table 6 and the corresponding graph is in Chapter 4, Figure 8.

Table 8. Amount of solvent added to make the dilutions for the screening of reaction concentration.

Final [S] M	Total reaction volume (μL)	Amount of CH_2Cl_2 added (μL)
0.1	762	724
0.25	305	267
0.5	114	114
0.75	102	64
1.0	76	38

2.19.7 Optimized reaction validation on bench scale (200 mg)

To a 1 dram vial was added 200 mg of substrate **84** (7.62×10^{-4} mol), 0.8 equivalents of BHT (130 mg, 6.10×10^{-4} mol) and 1.52 mL CH_2Cl_2. Next, 5 mol % catalyst **15b** was added (45 mg, 3.81×10^{-4} mol). The reaction was sealed and then heated to 60 °C in an aluminium block for 6 h. The yield was determined by GC-FID (100 %) and the isolated yield was also obtained after column chromatography (95 %). The characterization of this product is in Section 2.12.20. The reaction was repeated without using an additive and the yield was reduced to 87 % GC yield and 83 % isolated yield.

2.20 Removal of Ru Catalyst Residues from Organic Products

2.20.1 Representative procedure for the quantification of residual Ru in organic products after column chromatography

To a 20 mL screw top vial containing 200 mg of diethyldiallyl malonate, **21**, (8.32×10^{-4} mol) and 8.32 mL CH_2Cl_2 was added catalyst **15b** (50 mg, 4.16×10^{-5} mol). After closing the vial the reaction was heated to reflux for 15 minutes. The reaction was then opened to air and concentrated under vacuum. The ring closed product, **22**, was isolated by flash column chromatography.[1] A 1 cm diameter column was packed with 10 cm of silica. The product was eluted with 5% EtOAc/hexanes and fractions collected in 1 mL glass test tubes (**22** R_f 0.29). The fractions containing product were combined and concentrated under vacuum to give a clear oil, 79 mg (90%). The sample was sent to Guelph Chemical (Chemisar) for Ru analysis: < 10 ppm.

References page 78

2.20.2 RCM in Fluorous Reaction Media

To a 1-dram vial was added 1.66 mL FC-72 (perfluorohexane), 200 mg (8.32×10^{-4} mol) diethyldiallyl malonate, **21**, and 100 mg (8.32×10^{-5} mol) of catalyst **15b**. The substrate formed a layer on top and the catalyst sank to the bottom. The vial was sealed and heated to 60 °C. Upon heating the substrate and catalyst dissolved in FC-72. After 1h the reaction was cooled to room temperature and then opened, by GC analysis ring closing was complete. The ring-closed product was extracted with 4 × 4 mL hexanes. To induce separation between hexane and FC-72 the mixture was cooled for 1 minute in liquid nitrogen. To ensure the removal of Ru residues, the combined organic fractions were filtered through a 0.5 × 2 cm plug of silica. The filtrate was then concentrated under vacuum to yield to a clear oil, 150 mg (85 %). The residual ruthenium was 203 ppm.

2.21 Synthesis of $Rh(X)(CO)(PPh_3)_2$ complexes (125a-y)

To 10 mg (1.45×10^{-5} mol) of $[Rh(Cl)(CO)(PPh_3)_2]$ (**125m** Strem) in 1 mL THF was added 1 equiv of MX salt. The amounts and reaction times are given in Table 9. The reactions were judged complete by comparison to the $^{31}P\{^1H\}$ NMR of $[Rh(Cl)(CO)(PPh_3)_2]$. The reactions were worked up by filtering off the MCl salt by passing it through Celite and then removing the solvent under vacuum. The latter two steps could be performed in air. IR spectra of the new complexes were then recorded as a Nujol mull. The IR and data appears in Chapter 6, Table 10.

Table 9. Reaction times and amounts of MX salt added to $[RhCl(CO)(PPh_3)_2]$ **124** to yield $RhX(CO)(PPh_3)_2$ **125a-y**.

Reaction	MX Salt	Amount Added (mg)	Reaction Time (h)	Colour	$^{31}P\{^1H\}$ δ (ppm)	$^3J_{Rh\text{-}P}$ (Hz)
a	AgCN	2	3	red	30.4	broad
b	AgNCS	3	3	yellow	30.1	123.9
d	$TlSC_6F_5$	6	3	yellow	30.2	130.0
e	AgNCO	3	3	yellow	30.5	128.2
f	NaI	3	3	yellow	28.9	122.7
g	$TlOC_6F_4C_6F_5$	8	3	yellow	30.2	133.8
i	$TlOC_6F_4$-p-CF_3	7	3	yellow	31.1	132.4
j	$TlSC_6Cl_5$	7	3	green	29.1	131.2
k	$TlOC_6F_5$	6	18	yellow	30.2	134.3
l	$TlOC_6H_3$-m,m-$(CF_3)_2$	7	3	yellow	30.9	136.1
m	Cl (Strem Chemicals)	–	–	yellow	30.4	127.6
n	$TlSC_6H_5$	5	3	yellow	37.9	155.5
r	$TlOC_6H_4$-p-NO_2	5	3	yellow	30.3	134.9
s	$TlOC_6H_5$	5	3	yellow	28.1	139.5
t	$TlOC_6H_4$-m-CF_3	6	3	yellow	29.5	136.8
v	$TlOC_6H_4$-p-F	5	3	yellow	28.1	138.7
w	$TlOC_6Cl_5$	7	3	yellow	31.4	135.4
x	$TlOC_6H_2$-o,o-Br_2-p-NO_2	8	3	yellow	31.8	134.9
y	$TlOC_6Br_5$	10	3	yellow	30.0	137.3

2.22 DFT Calculations

The structures were calculated by Dr. Claudio Carra, a postdoctoral researcher in the Scaiano lab at the University of Ottawa. All calculations were performed using the Gaussian 03 package.[41] The stationary points on the potential energy surface (PES) were located with the B3LYP[42] hybrid density functional method. The LanL2DZ basis set[43] augmented with an f-polarization[44] function was used for the Ru atom, while the standard 6-31G* basis set was used for the remaining atoms.[45] The dissociation energy was corrected to account for the basis set superposition error (BSSE) using the Boys-Bernardi counterpoise method.[46] Atomic charges were calculated with the natural order (NBO) population analysis.[47]

References page 78

2.23 References

(1) Still, W.C.; Kahn, M.; Mitra, A. *J. Org. Chem.* **1978**, *43*, 2923-2925.
(2) Armarego, W.; Perrin, D., *Purification of Common Laboratory Chemicals 4th ed.* Butterworth-Heinemann: Boston, 1997.
(3) Creary, X. *"Tosylhydrazone Salt Pyrolyses: Phenydiazomethanes"* Organic Syntheses, 1990, Collective Vol. 7, p.438; 1986, Annual Vol. 64, p.207. available at http://www.orgsyn.org.
(4) Arduengo, A.J.; Krafczyk, R.; Schmutzler, R.; Craig, H.A.; Goerlich, J.R.; Marshall, W.J.; Unverzagt, M. *Tetrahedron* **1999**, *55*, 14523-14534.
(5) Hoffmann, P.R.; Caulton, K.G. *J. Am. Chem. Soc.* **1975**, *97*, 4221-4228.
(6) Schwab, P.; Grubbs, R.H.; Ziller, J.W. *J. Am. Chem. Soc.* **1996**, *118*, 100-110.
(7) Huang, J.; Stevens, E.D.; Nolan, S.P.; Petersen, J.L. *J. Am. Chem. Soc.* **1999**, *121*, 2674-2678.
(8) Amoroso, D.; Snelgrove, J.L.; Conrad, J.C.; Drouin, S.D.; Yap, G.P.A.; Fogg, D.E. *Adv. Synth. Catal.* **2002**, *344*, 757-763.
(9) Conrad, J.C.; Yap, G.P.A.; Fogg, D.E. *Organometallics* **2003**, *22*, 1986-1988.
(10) Galvan-Arzate, S.; Santamaria, A. *Tox. Lett.* **1998**, *99*, 1-13.
(11) a) Cole-Hamilton, D. J. ; Young, R. J. ; Wilkinson, G., *J. Chem. Soc., Dalton Trans.* **1976**, 1995-2001. b) Yamamoto, T.; Miyashita, S.; Naito, Y.; Komiya, S.; Ito, T.; Yamamoto, A., *Organometallics*, **1982**, *1*, 808-812.
(12) Snelgrove, J.L.; Conrad, J.C.; Yap, G.P.A.; Fogg, D.E. *Inorg. Chim. Acta.* **2003**, *345*, 268-278.
(13) Van Veldhuizen, J.J.; Gillingham, D.G.; Garber, S.B.; Kataoka, O.; Hoveyda, A.H. *J. Am. Chem. Soc.* **2003**, *125*, 12502-12508.
(14) Trademark of Degussa-Hüls AG.
(15) Nugent, W.A.; Feldman, J.; Calabrese, J.C. *J. Am. Chem. Soc.* **1995**, *117*, 8992-8998.
(16) Cerezo, S.; Cortes, J.; Moreno-Manas, M.; Pleixats, R.; Roglans, A. *Tetrahedron* **1998**, *54*, 14869-14884.
(17) Varray, S.; Lazaro, R.; Martinez, J.; Lamaty, F. *Organometallics* **2003**, *22*, 2426-2435.
(18) Spagnol, G.; Heck, M.-P.; Nolan, S.P.; Mioskowski, C. *Org. Lett.* **2002**, *4*, 1767-1770.
(19) Hoye, T.R.; Zhao, H. *Org. Lett.* **1999**, *1*, 1123-1125.
(20) Kirkland, T.A.; Grubbs, R.H. *J. Org. Chem.* **1997**, *62*, 7310-7318.
(21) Schweizer, E.E.; O'Neill, G.J. *J. Org. Chem.* **1965**, *30*, 2082-2083.
(22) Miller, S.J.; Kim, S.-H.; Chen, Z.-R.; Grubbs, R.H. *J. Am. Chem. Soc.* **1995**, *117*, 2108-2109.
(23) Freeman, R. *Mol. Phys.* **1962**, *5*, 499-508.
(24) Zuercher, W.J.; Hashimoto, M.; Grubbs, R.H. *J. Am. Chem. Soc.* **1996**, *118*, 6634-6640.
(25) Schmidt, B.; Pohler, M.; Costisella, B. *J. Org. Chem.* **2004**, *69*, 1421-1424.
(26) Fürstner, A.; Langemann, K. *Synthesis* **1997**, 792-803.
(27) Litinas, K.E.; Salteris, B.E. *J. Chem. Soc., Perkin Trans. 1* **1997**, 2869-2872.
(28) Fürstner, A.; Picquet, M.; Bruneau, C.; Dixneuf, P.H. *Chem. Comm.* **1998**, 1315-1316.
(29) Hong, S.H.; Sanders, D.P.; Lee, C.W.; Grubbs, R.H. *J. Am. Chem. Soc.* **2005**, *127*, 17160-17161.

(30) Hall, H.K., Jr.; Nogues, P.; Rhoades, J.W.; Sentman, R.C.; Detar, M. *J. Org. Chem.* **1982**, *47*, 1451-1455.
(31) Garber, S.B.; Kingsbury, J.S.; Gray, B.L.; Hoveyda, A.H. *J. Am. Chem. Soc.* **2000**, *122*, 8168-8179.
(32) Huang, Z.-Z.; Ye, S.; Xia, W.; Yu, Y.-H.; Tang, Y. *J. Org. Chem.* **2002**, *67*, 3096-3103.
(33) Forman, G.S.; McConnell, A.E.; Hanton, M.J.; Slawin, A.M.Z.; Tooze, R.P.; Van Rensburg, W.J.; Meyer, W.H.; Dwyer, C.; Kirk, M.M.; Serfontein, D.W. *Organometallics* **2004**, *23*, 4824-4827.
(34) Chatani, N.; Morimoto, T.; Muto, T.; Murai, S. *J. Am. Chem. Soc.* **1994**, *116*, 6049-6050.
(35) Fürstner, A.; Ackermann, L.; Gabor, B.; Goddard, R.; Lehmann, C.W.; Mynott, R.; Stelzer, F.; Thiel, O.R. *Chem. Eur. J.* **2001**, *7*, 3236-3253.
(36) Kim, S.-H.; Zuercher, W.J.; Bowden, N.B.; Grubbs, R.H. *J. Org. Chem.* **1996**, *61*, 1073-1081.
(37) Conrad, J.C.; Eelman, M.D.; Monfette, S.; Silva, J.; Snelgrove, J.L.; Parnas, H.H.; Fogg, D.E. *J. Am. Chem. Soc.* **2006**, 1024-1025.
(38) Lombardo, L. *Tetrahedron Lett.* **1985**, *26*, 381-384.
(39) Marsella, M.J.; Maynard, H.D.; Grubbs, R.H. *Angew. Chem. Int. Ed.* **1997**, *36*, 1101-1103.
(40) (a) Gold, L. *J. Chem. Phys.* **1958**, *28*, 91-99. (b) Rempp, R.; Merrill, E. W. *Polymer Synthesis*, Huethig and Wepf : New York, 1986. (c) Bazan, G. C.; Khosravi, T.; Schrock, R. R.; Feast, W. J.; Gibson, V. C.; O'Regan, M. B.; Thomas, J. K.; Davis, W. M. *J. Am. Chem. Soc.*, **1990**, *112*, 8378-8387.
(41) Gaussian 03, Revision B.04, M. J. Frisch, G. W. Trucks, H. B. Schlegel, G. E. Scuseria, M. A. Robb, J. R. Cheeseman, J. A. Montgomery, Jr., T. Vreven, K. N. Kudin, J. C. Burant, J. M. Millam, S. S. Iyengar, J. Tomasi, V. Barone, B. Mennucci, M. Cossi, G. Scalmani, N. Rega, G. A. Petersson, H. Nakatsuji, M. Hada, M. Ehara, K. Toyota, R. Fukuda, J. Hasegawa, M. Ishida, T. Nakajima, Y. Honda, O. Kitao, H. Nakai, M. Klene, X. Li, J. E. Knox, H. P. Hratchian, J. B. Cross, C. Adamo, J. Jaramillo, R. Gomperts, R. E. Stratmann, O. Yazyev, A. J. Austin, R. Cammi, C. Pomelli, J. W. Ochterski, P. Y. Ayala, K. Morokuma, G. A. Voth, P. Salvador, J. J. Dannenberg, V. G. Zakrzewski, S. Dapprich, A. D. Daniels, M. C. Strain, O. Farkas, D. K. Malick, A. D. Rabuck, K. Raghavachari, J. B. Foresman, J. V. Ortiz, Q. Cui, A. G. Baboul, S. Clifford, J. Cioslowski, B. B. Stefanov, G. Liu, A. Liashenko, P. Piskorz, I. Komaromi, R. L. Martin, D. J. Fox, T. Keith, M. A. Al-Laham, C. Y. Peng, A. Nanayakkara, M. Challacombe, P. M. W. Gill, B. Johnson, W. Chen, M. W. Wong, C. Gonzalez, and J. A. Pople, Gaussian, Inc., Pittsburgh PA, 2003.
(42) a) Becke, A. D. *J. Chem. Phys.* **1993**, *98*, 5648-5652. b) Miehlich, B.; Savin, A.; Stoll, H.; Preuss, H. *Chem. Phys. Lett.* **1989**, *157*, 200-206. c) Lee, C.; Yang, W.; Parr, G. *Phys. Rev. B* **1988**, *37*, 785-789.
(43) a) Dunning Jr., T. H.; Hay, P. J. *Modern Theoretical Chemistry Vol. 3*, Ed. H. F. Schaefer III, Plenum: New York, 1976, p1-28. b) Hay, P. J.; Wadt, W. R. *J. Chem. Phys.* **1985**, *82*, 270-283. c) Wadt, W. R.; Hay, P. J. *J. Chem. Phys.* **1985**, *82*, 284-298. d) Hay, P. J.; Wadt, W. R. *J. Chem. Phys.* **1985**, *82*, 299-310.
(44) Hollwarth, A.; Bohme, M.; Dapprich, S.; Ehlers, A.W.; Gobbi, A.; Jonas, V.; Kohler, K.F.; Stegmann, R.; Veldkamp, A.; Frenking, G. *Chem. Phys. Lett.* **1993**, *208*, 237-240.

(45) a) Ditchfield, R.; Hehre, W. J.; Pople, J. A. *J. Chem. Phys.* **1971**, *54*, 724-728. b) Hehre, W. J.; Ditchfield, R.; Pople, J. A. *J. Chem. Phys.* **1972**, *56*, 2257-2261. c) Hariharan, P. C.; Pople, J. A. *Mol. Phys.* **1974**, *27*, 209-214. d) Gordon, M. S., *Chem. Phys. Lett.* **1980**, *76*, 163-168.
(46) Boys, S.F.; Bernardi, F. *Mol. Phys.* **1970**, *19*, 553-566.
(47) Reed, A.E.; Curtiss, L.A.; Weinhold, F. *Chem. Rev.* **1988**, *88*, 899-926.

3 Development of Ru-Pseudohalide Catalysts for Olefin Metathesis

3.1 Introduction

The availability of robust, easily handled ruthenium catalysts for olefin metathesis has had a tremendous impact on organic synthesis. To date, the major goal in Ru catalyst design has been to increase the activity of Grubbs' catalyst **1**[1-3] or second generation catalysts containing an NHC ligand, **2a/b**. Derivatives of **2** containing a more labile donor such as **3-6** improved catalyst initiation but have not resolved the fact that they all focus on the same ruthenium dichloride intermediate **7**. As other halides (e.g. Br and I) are reported to reduce the metathesis activity type **1** or **2** class catalysts,[4] it was decided to exchange the ubiquitous chloride anionic ligands for a potentially better pseudohalide.

This chapter describes a program of study directed at understanding the parameters needed to construct a stable Ru-O bond, and the use of this insight to assemble a platform that enables modulation of the stereoelectronic properties of the target metathesis catalysts. General, and high-yield synthetic methods were targeted as a means of gaining efficient access to diverse catalyst structures.

3.2 Model Studies

3.2.1 Reaction Methodology and Catalyst Discovery

Exploratory reactions aimed at generating novel Ru-pseudohalide complexes were first carried out on small scale (20 mg of ruthenium precursor). NMR spectroscopy was used almost exclusively to monitor these reactions *in situ*, as this proved to be an effective means

of surveying a large amount of chemistry. Scout reactions were followed using various NMR "handles." For phosphine complexes, $^{31}P\{^{1}H\}$ NMR analysis (δ range: -10 to +100 ppm) was optimal, as deuterated solvent was not required.[a] Characteristic of alkylidene complexes are ^{1}H NMR signals far downfield (δ 17-21 ppm). Monitoring of the alkylidene peaks by ^{1}H NMR analysis allowed reactions to be followed where no ^{31}P nucleus was present. Complexes containing hydride were also useful. When *trans* to another ligand, hydride signals are found from δ -5 to -15 ppm; they appear as far upfield as -35 ppm when *trans* to a vacant site. In some cases ^{19}F NMR was useful for determining the ligand coordination mode, *vide infra.*

Test reactions were carried out in C_6D_6 at 21 °C with 20 mg of ruthenium precursor. If a new alkylidene and a reasonably clean ^{1}H NMR spectrum persisted in solution for at least 3 hours, the reaction was scaled up (> 200 mg) for additional characterization, as well as catalytic screening (results of the latter are described in Chapter 4). Complexes not stable enough to survive for 3 hours in solution, or to withstand isolation by precipitation, were abandoned. This time window was established using as a benchmark the behaviour of the most active catalysts known prior to this study (**3b** or **4a**).

3.2.2 Reactions with $RuHCl(PPh_3)_3$: Hydride as a Proxy for Alkylidene

Ligand architecture is critical in determining catalyst lifetime, selectivity and ultimately catalyst utility. Two design priorities for the anionic ligand were established at the outset: 1) the ligand should be tunable in terms of sterics and electronics and 2) its steric

[a] N.B. New NMR spectrometers, such as the Bruker Avance series spectrometers, do not show folded in peaks when the sweep window is too narrow. Instead, digital filtering is applied, and signals outside this window will not be observed.

References page 104

demand should not be excessive, as work by other groups has shown that bulky donors can block the catalyst active site, attenuating activity (see, e.g. $[Ru(O^tBu)_2(CHPh)(PCy)_3]$).[5] Phenol was chosen as an initial platform for study. To better understand the requirements to create a stable Ru-O bond, stability studies of Ru-O bonds in combination with labile ligands were investigated. For this work, $Ru(X)Cl(PPh_3)_3$ (**8a**, X = Cl; **8b**, X = H) provided a convenient model. Not only is the complex square pyramidal, with labile ligands, as in **1-5**, the high *trans* effect of hydride places this ligand in the apical site while eliminating any potentially misleading chemistry arising from the alkylidene itself. One chloride was easily replaced via salt metathesis to form a new Ru-OR bond in a labile coordination environment. This allowed us to isolate the question of whether a given ligand is appropriate for consideration as a halide surrogate.[6]

Calorimetric and reactivity studies[7-9] have led to a reevaluation of the assumption that late-transition-metal-oxygen bond energies are inherently low, as the Pearson "hard-soft" formalism would suggest. Previous work in the Fogg group,[10] however, demonstrates that the well-established stability of the Ru-OAr bond within complexes of the type[7] $Ru(\sigma\text{-}OAr)_2(PMe_3)_4$ is a function of the nonlability of the PMe_3 ligands. Thus, related complexes containing labile PPh_3 groups (e.g. $RuCl(\sigma\text{-}OAr)(PPh_3)_3$, $RuH(\sigma\text{-}OAr)(PPh_3)_3$; Ar = Ph, p-$^tBuC_6H_4$) are not isolable, owing to a facile $\sigma \rightarrow \pi$ isomerization, accompanied by loss of phosphine, to generate coordinatively saturated 18-electron π-aryloxide derivatives (e.g. **9**, Figure 1). Other examples of such behaviour in Ru chemistry include the formation of $RuH(\pi\text{-}ArO)(PR_3)_2$ by reaction of phenols with $RuH_2(PR_3)_4$.[11] For metathesis catalysts, which undergo initiation by loss of *labile* ligand, the PPh_3 model complexes are more

References page 104

relevant than those containing non-labile PMe_3 groups. Therefore, the isomerization to a coordinatively saturated π-aryl complex must be prevented by some other way.

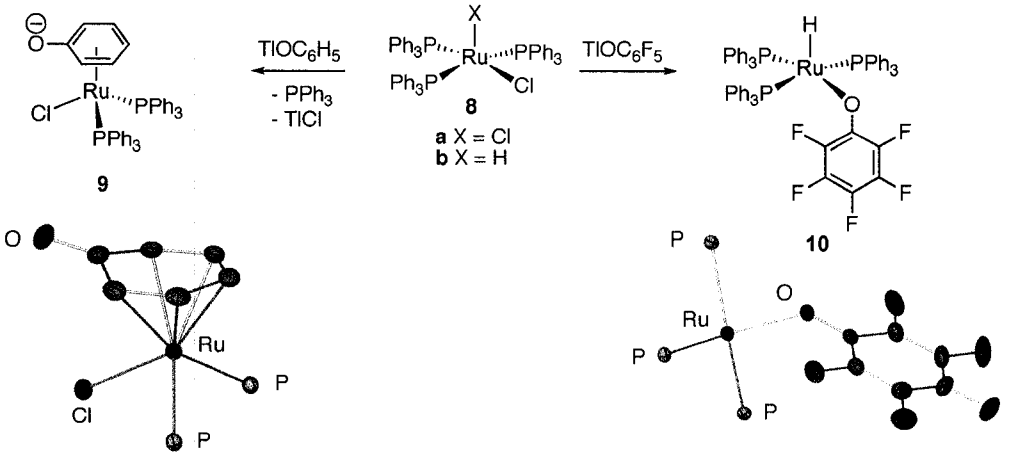

Figure 1. Electronic control over σ–π isomerization and ORTEP representations of crystal structures (For full details, see Appendix E). Thermal ellipsoids are shown at 30% probability level, hydrogen atoms and solvates omitted. Ph groups on PPh_3 omitted for clarity.

A plausible alternative means of preventing isomerization to the π-bonding mode is reduction of the electron density available within the aryl ring. With the intention of clarifying this possibility in PPh_3 systems via direct comparison with the complexes already examined (**9**), reaction of the labile precursor **8b** with perfluoroaryloxide anion was explored. In contrast to reactions with phenoxide, reaction of **8b** with thallium pentafluoroaryloxide effected complete conversion to the σ-aryloxide complex (Figure 1, **10**) within 3 h at 22 °C in THF. Similar behavior was observed with sodium pentafluoroaryloxide, but the reaction was only ca. 30% complete at 3h (100%, 48 h). The accelerating effect of Ag^+ and Tl^+ salts in halide substitution of metal complexes has been attributed to electrophilic "pull" by the heavy-metal cations, possibly via direct electrophilic

References page 104

attack on the halogen atom,[12] or interaction with the metal itself.[13] As well, the reaction is driven by the insolubility of TlCl in THF.

The red product was isolated in ca. 80% yield, and both NMR and combustion analysis were consistent with the formulation of the complex as $RuH(OC_6F_5)(PPh_3)_3$ (**10**). Room-temperature $^{31}P\{^1H\}$ NMR analysis revealed a broad singlet centered at δ 47 ppm, which resolved into an A_2B pattern at -50 °C, δ (C_7D_8): 87.1 (t, $^2J_{PP}$ = 26, 1P), 40.9 (d, $^2J_{PP}$ = 26, 2P). This confirmed retention of all three triphenylphosphine ligands. The hydride signal was observed as a quartet of triplets, split by long-range coupling to two ^{19}F nuclei, as well as the expected two-bond coupling to phosphorus, δ (C_6D_6): -22.29 (q of t, $^2J_{PH}$ = 27.9 Hz, $^5J_{FH}$ = 7.2 Hz. The coupling assignments were supported by $^1H\{^{19}F\}$ and $^1H\{^{31}P\}$ NMR experiments, which revealed the hydride signal as a quartet and a triplet, respectively.^{19}F NMR analysis of **10** revealed signals at chemical shifts similar to those found for free perfluorophenol and its thallium salt. In comparison, signals for the π-bound perfluoroaryloxy ring in $[Cp^*Ru(\eta^5\text{-}C_6F_5O)]$ or $[CpRu(\eta^6\text{-}C_6F_5OH)]^+$ are found 10-20 ppm upfield.[14]

Table 1 summarizes all the ^{19}F NMR data collected. All of the σ–bound perfluoroaryl rings appear downfield from the π-bound complexes, providing a useful method for determining the bonding mode for this class of ligand. The coordination mode of the aryloxide ligand within **10** was confirmed by X-ray analysis of crystals obtained by slow evaporation of a concentrated THF solution (Figure 1). Bond lengths and angles are discussed together at the end of this chapter. In contrast to the corresponding phenoxide species **9**, complex **10** showed no tendency to isomerize. It was stable in solution for more than 12 hours, and for four years when stored as a solid under inert atmosphere.

References page 104

Table 1. $^{19}F\{^{1}H\}$ NMR values for perfluorophenol and its metal complexes.[a]

Compound	Solvent	δ_F (ppm)
HOC_6F_5	$CDCl_3$	-87.7 to -88.1 (m, 4F) -92.1 to -92.6 (m, 1F)
$TlOC_6F_5$[b]	$CDCl_3$	-81.8 to -84.1 (m, 2F) -88.5 to -88. 7(m, 2F) -99.6 to -99.8 (m, 1F)
$TlOC_6F_5$	C_6D_6	-84.2 to -84.6 (m, 2F) -90.1 to -90.3 (m 2F) -101.8 to -101.9 (m 1F)
$RuH(OC_6F_5)(PPh_3)_3$ **10**	C_6D_6	-93.5 to -93.6 (m, 2 F) -94.6 to -94.9 (m, 2F) -107.8 to -101.9 (m, 1F)
$Ru(OC_6F_5)_2(CPh)(PCy_3)_2$ **11**	$CDCl_3$	-90.3 (dd, J_{FF} = 22.6, 11.3 Hz, 2F) -93.4 (t, J_{FF} = 22.1, 2F) -106.7 to -107.0 (m, 1F)
$Ru(OC_6F_5)_2(CHPh)(IMes)(py)$ **12a**	$CDCl_3$	-86.4 to -86.5 (m, 2F) -86.7 to -86.7 (m, 2F) -94.3 (t, J_{FF} = 22.3, 2F) -94.5 (t, J_{FF} = 22.5, 2F) -104.8 to -105.0 (m, 1F) -105.8 to -106.0 (m, 1F)
$Ru(OC_6F_5)_2(CHPh)(IMes)(Brpy)$ **12b**	$CDCl_3$	-87.2 to -87.4 (m, 4F) -95.4 to -95.6 (m, 4F) -105.4 (tt, J_{FF} = 22.6, J_{FF} = 8.5, 1F) -106.8 (tt, J_{FF} = 25.4 J_{FF} = 8.5, 1F)
$Ru(OC_6F_4C_6F_5)_2(CHPh)(IMes)(py)$ **13**	$CDCl_3$	-62.2 to -62.3 (m, 2F) -62.5 to -62.6 (m, 2F) -70.5 to -70.6 (m, 2F) -71.2 to -71.3 (m, 2F) -79.1 (t, J_{FF} = 21.0, 1F) -79.2 (t, J_{FF} = 21.1, 1F) -86.0 (d, J_{FF} = 17.6, 2F) -87.1 to -87.4 (m, 6F)
$Ru(SC_6F_5)_2(CHPh)(IMes)(py)$ **16a**	$CDCl_3$	-56.2 (d, J_{FF} = 26.82, 2F) -88.6 (t, J_{FF} = 21.74, 1F) -91.0 (t, J_{FF} = 22.3, 2F)
$[Cp^*Ru(\eta^5C_6F_5O)]$	$CDCl_3$[c]	-108.4 (m, 2F) -112.3 (m, 2F) -119.0 (m, 1F)

References page 104

Table 1 continued...

$[CpRu(\eta^6C_6F_5OH)]^+$	$CDCl_3$ [c]	-98.4 (m, 2F) -100.6 (m, 2F) -103.6 (m, 1F)

[a]282 MHz, 298K Referenced to external trifluoroacetic acid at 0 ppm, the patterns show second order effects.[b] The values are rather similar in C_6D_6 (-84.4 (m, 2F), -90.2 (m, 2F), -101.8 (m, 2F)). [c] Original values converted from δ $CFCl_3$ = 0 to δ TFA = 0 (δ_F Φ 76.5 ppm).[14]

Less electron-withdrawing aryloxides derived from 4-nitrophenol or 4-fluorophenol underwent rapid isomerization, with loss of PPh_3, to yield π-OAr complexes of type **9**.[10] From this difference in behavior, it was concluded that in order create a stable Ru-OAr bond, it is necessary to remove as much electron density as possible from the aryl ring, thus inhibiting the capacity of the ring to act as a π-donor to ruthenium. The electron deficiency of the aryloxide ligand can be gauged from the pK_a of the parent phenol. Thus, the following order of pK_a values is found: phenol, 10; 4-fluorophenol, 9.95; 4-nitrophenol, 7.14; pentafluorophenol, 5.52.[15]

3.3 Synthesis of Ru-Pseudohalide Alkylidene Catalysts

3.3.1 Improved Synthesis of Ruthenium Precursors

During the synthesis of **12a** from **3a**, the preparation of several Ru complexes and precursors was improved. In most cases the reactions have been scaled up relative to the reported procedures. Where possible, steps that would normally be carried out under inert atmosphere were carried out in air using solvents that had not been subjected to drying or deoxygenating procedures. While **2b** is commercially available, its cost is nearly 100 times greater than the $RuCl_3 \cdot 6H_2O$ starting material (Schemes 1-3). We focused on the IMes complexes **2a** and **3a**; for comparison with the H_2IMes (e.g. **2b**) complexes see Chapter 1.

References page 104

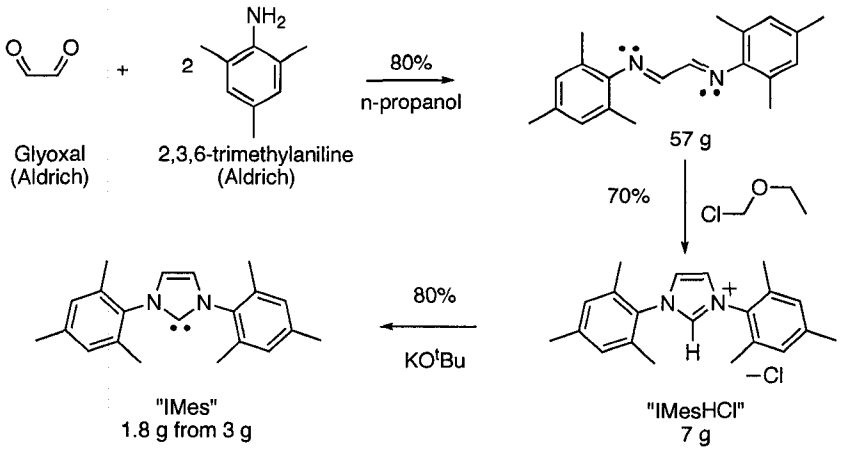

Scheme 1. Synthesis of the 1,3-bis(2,5,6-trimethylphenyl)imidazol-2-ylidene ligand, "IMes."

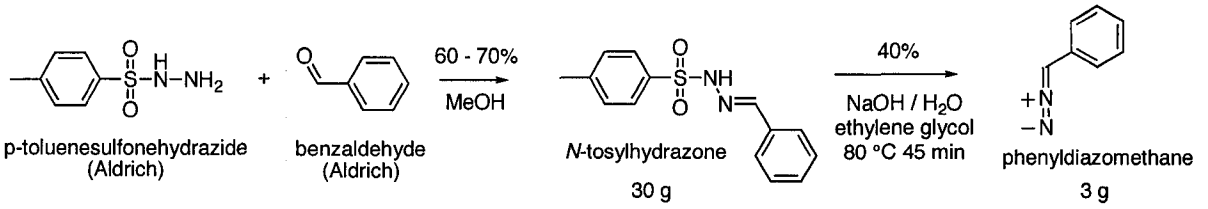

Scheme 2. Synthesis of phenyldiazomethane.

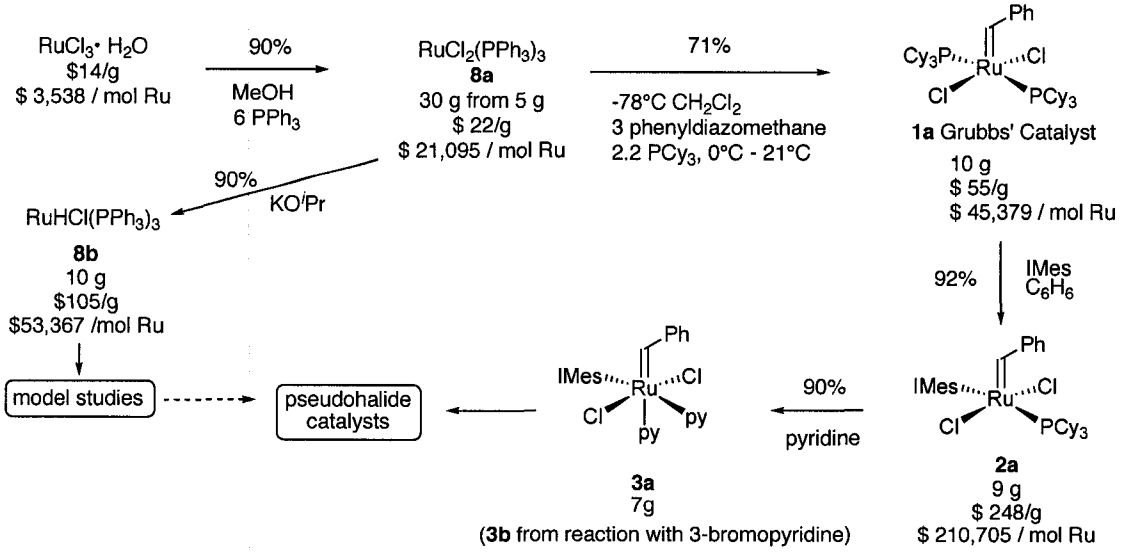

Scheme 3. Synthesis of ruthenium precursors (**1**, **3a**) used to generate pseudohalide catalysts. The scale of the reaction is indicated in grams. Prices from commercial sources are indicated in $/g and $/mol Ru.

3.3.2 Electron-Deficient Perfluoroaryloxide Complexes

The behaviour described in section 3.2.2 confirmed the efficacy of electronic parameters in determining the coordination mode of the aryloxide entity. This opened the door to incorporation of an aryloxide group within a ruthenium metathesis catalyst. Upon direct reaction of two equivalents of $TlOC_6F_5$ with **1**, however, alkylidyne **11** was obtained via deprotonation of the benzylidene ligand and liberation of phenol (Figure 2). Similar behavior was noted earlier on reaction of $RuCl_2(P^iPr_3)_2(CHPh)$ with NaOPh.[16] Given the higher acidity of pentafluorophenol, relative to phenol, it was speculated that the reaction might be driven by steric interactions between the aryloxide, PCy_3 and alkylidene ligands. In related work, Schrock observed α-elimination of bulky neopentyl groups to yield Ta alkylidenes.[17] Complex **11** was isolated as a green, air-stable, ether-soluble powder; its high solubility limited yields to ca. 60%.[b] The compound was unstable in solution, with a half-life of only a few hours. The carbyne resonance (δ 250.2 ppm) was therefore located by a proton-detected HMBC experiment rather than conventional $^{13}C\{^1H\}$ NMR analysis. The approximately square-planar molecular structure (Figure 2b) closely resembles that reported by the Caulton group for $Ru(CPh)(OPh)(P^iPr_3)_2$.[16] The carbyne complex was sufficiently stable in the solid state to obtain satisfactory combustion analysis.

[b] Synthesis and crystallographic characterization of complex **11** was carried out by Dino Amoroso of this research group.

References page 104

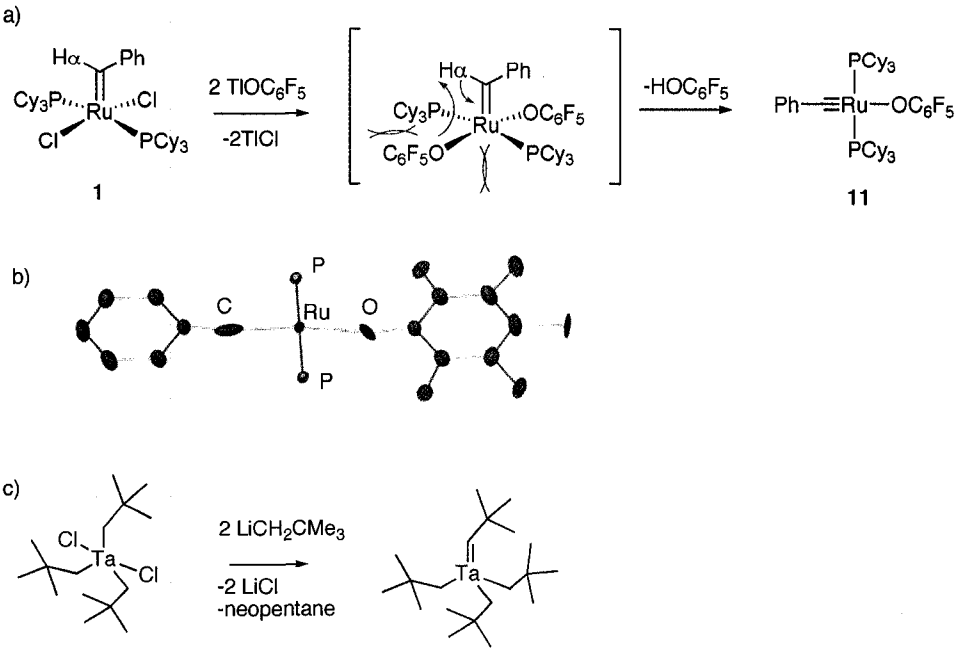

Figure 2. a) Treatment of **1** with $TlOC_6F_5$ yields α-elimination product **11**. b) ORTEP representation of **11**. Thermal ellipsoids are given at 30% probability level. Hydrogen atoms, benzene solvate, and Cy groups of PCy_3 omitted for clarity. (For details, see Ref 18). Aryloxide and alkylidyne ligands are disordered by a center of inversion at Ru. c) Synthesis of a Schrock carbene via α-elimination.

By reducing the three-dimensional bulk of the ancillary ligands (replacing PCy_3, cone angle 180°, with an essentially two-dimensional ligand set IMes/py) α-elimination was prevented, enabling the selective synthesis of five-coordinate alkylidene complexes. Thus, treatment of **3a** with $TlOC_6F_5$ in benzene at 21 °C effected quantitative conversion to **12a**, within 3 h at 22 °C (Figure 3). Reaction with KOC_6F_5 was much slower and the prolonged reaction times needed (18 h) resulted in competing decomposition of **3a**. The consumption of **3a** at this time was incomplete and new signals attributable to neither **3a** or **12a** appeared in the aromatic and aliphatic regions of the ^1H NMR spectrum.

Complex **12a** was isolated in 92% yield, and characterized by spectroscopic, microanalytical, and crystallographic analysis. Its geometry is square pyramidal, with the

References page 104

alkylidene occupying the apical site (Figure 3). This geometry is consistent with the high *trans* effect of this ligand. Retention of the potentially labile pyridine ligand within **12a** attests to the absence of steric constraints in this five-coordinate complex. Importantly, it also signifies the presence of an incipient coordination site for incoming substrate. The ^{19}F and ^{19}F-^{19}F COSY NMR spectra of **12a** reveal two sets of peaks, one set each for the chemically different OC_6F_5 groups. The signals appear in the typical range for σ-bound OC_6F_5 (Table 1).

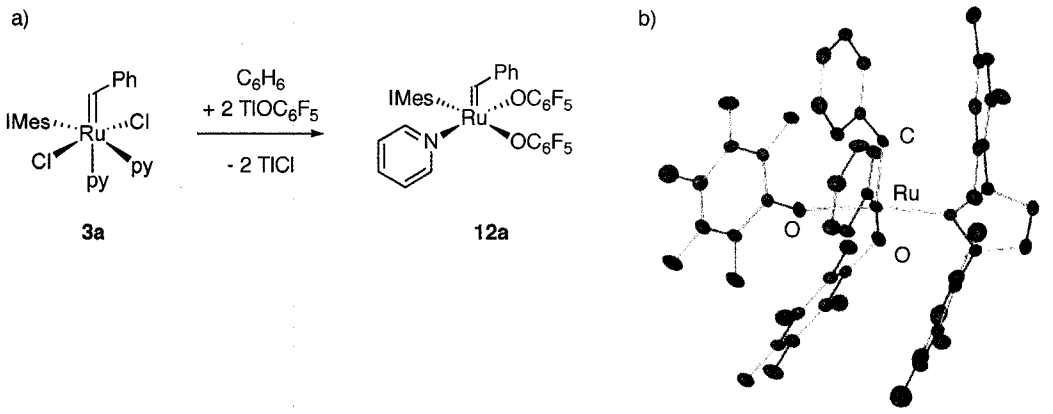

Figure 3. a) Synthesis of pseudohalide metathesis catalyst, **12a**. b) ORTEP representation of **12a** (For full details, see Appendix E). Thermal ellipsoids are shown at 30% probability level; hydrogen atoms and toluene solvate omitted for clarity.

A key feature observed during the synthesis of **12a** was the isomerization of the anionic ligands from their *trans*-disposition in **3a** to the *cis* disposition in **12a**. The *trans* to *cis* transformation presumably occurs with isomerization at some stage, but the process is not fully understood. The reaction has been followed by arrayed ^1H NMR experiments. A singlet at δ 18.92 ppm, observed within minutes, disappears over 8 hours (Figure 4). This signal is tentatively assigned to the *trans* isomer of **12a**. The driving force for the isomerization is

References page 104

likely a decrease in energy resulting from placement of the aryloxide ligand *trans* to pyridine. The increased stability may be a function of the higher π-basicity of oxygen vs. chloride, as well as its lower σ-donor ability (Pauling electronegativities: O, 3.44; Cl, 3.16).[19] The σ-donor and π*-acceptor character of the pyridine ligand, in conjunction with the π-basicity of the aryloxide ligand, is expected to create a push-pull interaction. The three-orbital four-electron interaction is shown in Figure 5.[20] (A possible consequence is attenuated lability for pyridine *trans* to aryloxide, as discussed in Chapter 6). The *cis*-arrangement of aryloxide ligands in **12a** makes the complex more polar, and it is only soluble in relatively polar organic solvents such as THF, CH_2Cl_2, or $CHCl_3$.

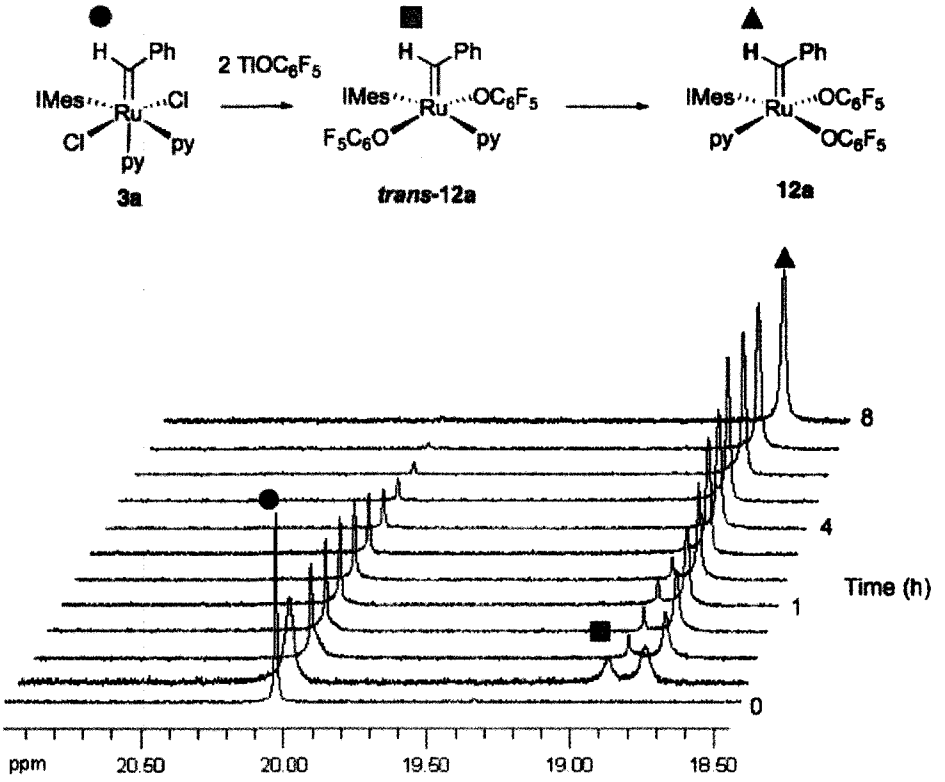

Figure 4. Arrayed ^{1}H NMR spectra (300 MHz, C_6D_6) showing conversion of **3a** (20 ppm) to **12a** (18.64 ppm), via the proposed intermediate ***trans*-12a** (18.92ppm).

References page 104

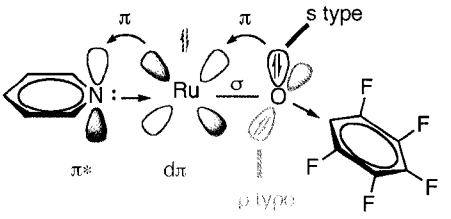

Figure 5. Model for py-Ru-OAr through bonding, the driving force for isomerization to the *cis* isomer **12a.**

3.4 Scope of Pseudohalide Catalysts Accessible from 3

3.4.1 Failed Reactions of **3a** with Aryloxides

Following the successful synthesis of **12a**, reaction of **3a** with a range of other aryloxide salts was undertaken (Figure 6). For all of the examples shown in Figure 6b, rapid loss of the alkylidene was observed (^{1}H NMR) presumably via σ→π isomerization of these less electron deficient aryloxides. During the reaction of **3a** with TlOPh, for example, ^{1}H NMR resonances for π-bound phenoxide (δ 5.50-4.30 ppm) were apparent, at a location similar to that seen for **9**. These results underscore the need for electron-withdrawing substituents able to deactivate the aryloxide ring toward π-donation. Thus, we turned to the exploration of additional perhaloaryloxides as possible pseudohalide ligands.

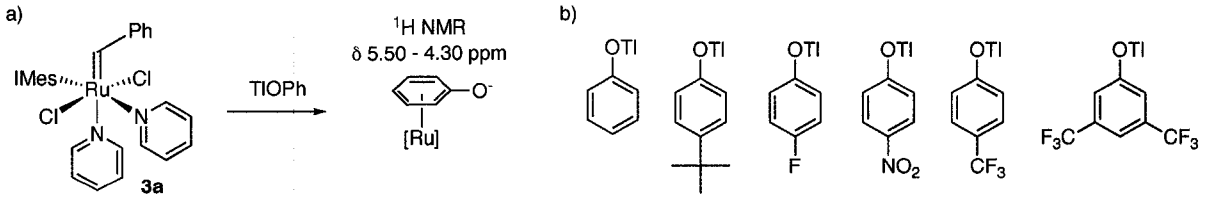

Figure 6. a) Reaction of **3a** with TlOPh. b) Aryloxides surveyed for which π-OAr coordination was observed.

References page 104

3.4.2 Perfluorinated Aryloxides

Given the limited solubility of **12a** in non-chlorinated solvents, installation of OC_6F_4-4-C_6F_5 was undertaken in the hope of increasing catalyst solubility in organic or fluorous solvents. As with **12a**, reaction of **3a** with two equivalents of $TlOC_6F_4$-4-C_6F_5 proceeded smoothly. ^1H and ^{13}C NMR, X-ray diffraction and combustion analysis confirmed the identity of the product as **13** (Figure 7). Complex **13** proved to be soluble in toluene, from which it was precipitated with pentane at -35 °C, albeit in only moderate (ca. 70%) yield.

Use of other fluorinated aryloxide salts, including $TlOC_6F_4$-4-CF_3 and $TlOC_6H_3$-3,5-CF_3, proved less successful. Treatment of **3a** with two equivalents of $TlOC_6F_4$-4-CF_3 produced a 1:1 mixture of two complexes with alkylidene resonances (C_6D_6) at δ 19.93 and 18.71 ppm. These could not be separated, and their use was not pursued further. Treatment of **3a** with two equivalents of $TlOC_6H_3$-3,5-CF_3 produced a new alkylidene complex (δ_H 18.69 ppm; C_6D_6) which decomposed upon workup.

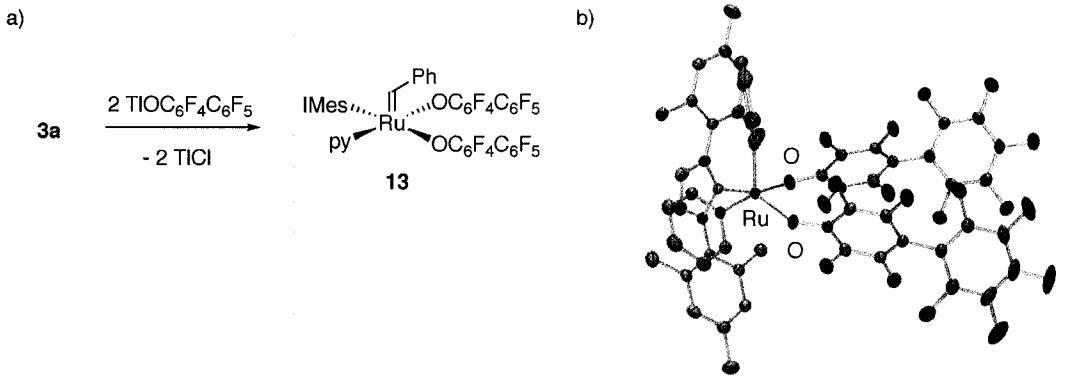

Figure 7. a) Synthesis of **13**. b) ORTEP representation of **13** (For full details, see Appendix E). Thermal ellipsoids shown at 30% probability level; hydrogen atoms and THF solvate omitted for clarity.

References page 104

3.4.3 Other Perhaloaryloxides as Pseudohalide Ligands

While chloride and bromide are less electronegative than fluoride, the decrease in overlap between the filled halide p-orbital and the aryl π system in HOC_6X_5 makes the perchloro and perbromo phenols more acidic than perfluorophenol (Pauling electronegativities: F, 3.89; Cl, 3.16; Br, 2.96).[19] A balance of inductive and mesomeric effects is evident from the calculated pK_a's (pK_a HOC_6X_5: X = H, 10; F, 5.86; Cl, 4.70; Br, 4.57).[21] Reaction of **3a** with $TlOC_6Cl_5$ or $TlOC_6Br_5$ yielded **14a** or **15a**, respectively, (Figure 8). Both **14a** and **15a** were green powders isolated in 70% and 85% yield respectively. The two complexes are stable when stored as powders and survive in (degassed) solution for many hours (>12 h). In C_6D_6, diagnostic alkylidene resonances appeared at δ_H 19.78 or 19.68 ppm. Due to the increased bulk of these perhaloaryloxide ligands, relative to perfluoroaryloxide, only one chloride ligand is replaced, as indicated by NMR and combustion analysis. ^{1}H NMR analysis revealed broad peaks in the aryl region for the pyridine and phenyl protons, which remain poorly resolved down to -70 °C. Similar dynamic behavior was reported for the phenyl protons in **2a/b**[22c] and (to a lesser extent) **3a**. This feature hints at catalyst activity, as discussed in Chapter 6.

3.4.4 More Labile 3-Bromopyridine Derivatives

To increase the activity of this new class of catalysts, 3-bromo-pyridine was used in place of pyridine.[23] Treatment of a homogeneous green solution of **3b** in toluene with one or two equivalents, respectively, of solid $TlOC_6X_5$ (X = F, Br) resulted in minimal color change, but after 1 h a white precipitate of thallium chloride deposited. Conversion to **12b** or **15b** was complete after 12 h at 21 °C (Figure 8), as judged by ^{1}H NMR analysis. Removal of

References page 104

the TlCl byproduct was accomplished by filtering the reaction mixture through Celite. This operation was complicated for **12b** by a low solubility in toluene, which necessitated extracting the Celite with methylene chloride in order to recover the product. Indeed, complexes **12a/b** and **15a/b** displayed opposite solubility properties, the former being preferentially soluble in chlorinated solvents, and the latter in aromatics. In both cases, the bromopyridine derivatives proved more soluble. Following precipitation from CH_2Cl_2 or toluene, respectively, with cold pentane, complexes **12b** and **15b** were obtained as green powders in 85-90% yield. NMR and combustion analyses were consistent with the proposed formulations. The room-temperature ^1H NMR spectrum also points toward the higher lability of the pyridine ligand in **15b**, compared to **12b** or **3b**. A broad singlet, centered at 8.64 and 7.98 ppm, was observed for the ortho protons (cf. a value of 8.14 ppm for **3b**), which remained incompletely resolved down to –70 °C. Other NMR data agree well with values for the pyridine analogues: notable is the location of the singlet due to the benzylidene proton in C_6D_6, at 18.84 (**12b**) or 19.55 ppm (**15b**), very close to the corresponding values for **12a** (18.64 ppm) and **15a** (19.68 ppm).

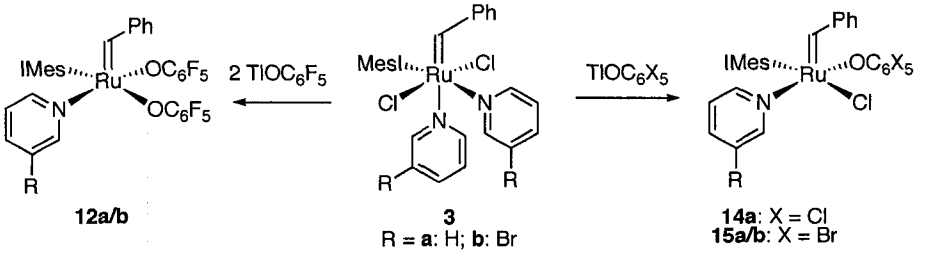

Figure 8. Synthesis of catalysts containing the more labile 3-bromopyridine ligands.

References page 104

3.4.5 Sulfur Analogues: Thioaryloxide Complexes

To determine the effect of a more nucleophilic sulfur atom on these pseudohalide ligands, reaction of **3a** with thioaryloxides was undertaken.[24,25] Addition of two equivalents of $TlSC_6F_5$ to **3a** in C_6H_6 caused a rapid colour change from green to red. After 15 minutes, NMR signals for **3a** had completely disappeared. As a single set of fluorine resonances indicated that the two SC_6F_5 rings were chemically equivalent, the complex was identified as the *trans*-isomer **16a**. This isomer degraded slowly over 12 hours to give an unknown decomposition product and the *cis* isomer **16b**, the latter giving rise to two sets of ^{19}F NMR signals. Each of complexes **16a** and **16b** proved difficult to isolate, but a saturated THF solution layered with decane and left to stand for several weeks deposited crystals of the *cis* isomer **16b** (Figure 9).

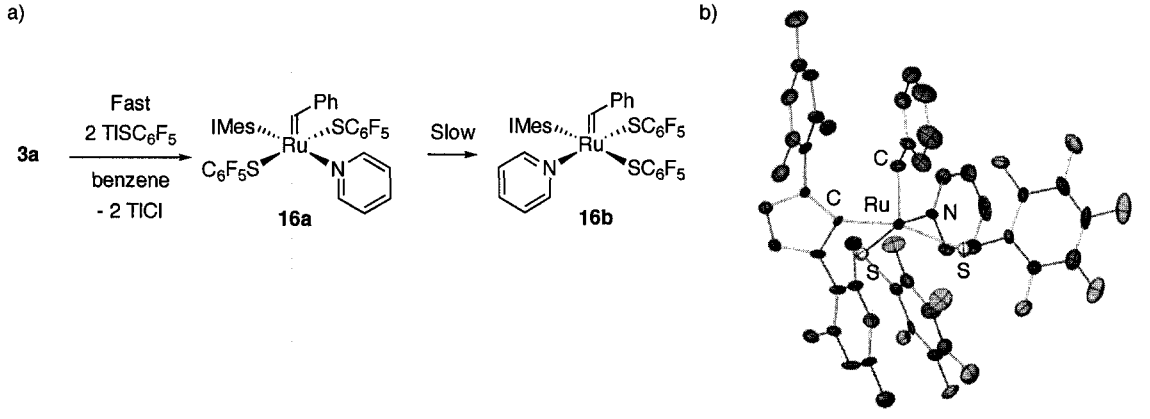

Figure 9. a) Reaction of **3a** with $TlSC_6F_5$. b) ORTEP representation of **16b** (For full details, see Appendix E). Thermal ellipsoids are shown at 30% probability level; hydrogen atoms, THF solvate omitted for clarity.

The corresponding reaction of **3a** with two equivalents of $TlSC_6H_5$ caused a new alkylidene signal to appear (δ_H 17.93 ppm; C_6D_6), which decomposed upon stirring for 8 hours further, indicated by decomposition of the alkylidene. Reaction of **3a** with $TlSC_6Cl_5$

gave a new product, **17**, (δ_H 17.74 ppm; C_6D_6). The green powder was isolated in 54% yield. ^{1}H NMR analysis indicated that pyridine was not present, perhaps suggesting formation of a chelate structure **17a**. Addition of excess pyridine had no effect, however, and alternative possibilities therefore include dimeric **17b** or **17c** (Figure 10). Complexes similar to **17a**, **17b** and **17c** are known, as discussed further in Chapter 6.[24,26] Efforts to grow single crystals were unsuccessful.

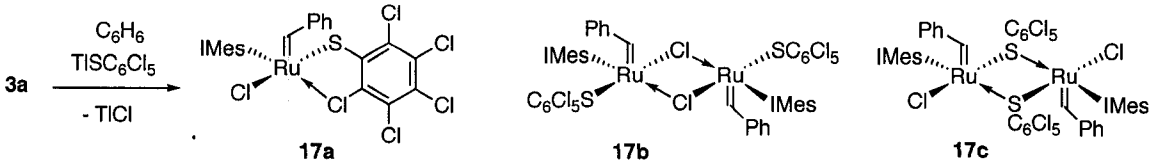

Figure 10. Synthesis and proposed structures for **17**.

3.4.6 Linear Pseudohalide Ligands

Linear anionic ligands such as thiocyanate, cyanate and cyanide have been extensively deployed in coordination chemistry.[27] These ligands are interesting for their linkage isomerization possibilities: the preference for binding at the more nucleophilic or more electronegative end affords an empirical gauge into the electron density at Ru. Reaction of **3a** with two equivalents of AgSCN resulted in emergence of a new alkylidene signal over 16 h at 22 °C (δ_H 18.46 ppm; C_6D_6). Complex **18a** (Figure 11) was isolated in high yield (97%) and was characterized by ^{1}H and ^{13}C NMR and combustion analysis. Owing to the smaller size of this ligand, both pyridine groups from **3a** were retained. Unexpectedly, the X-ray structure revealed that the ligands were N-bound not S-bound. The preference for the more electronegative element (Pauling electronegativities: N, 3.04; S, 2.58)[19] presumably

reflects the electron-rich character of the metal. Ru complexes containing the Ru-SCN linkage isomer are usually electron-poor.[28] This finding further suggests that electron-withdrawing ligands are more favorable for the formation of stable Ru-X complexes.

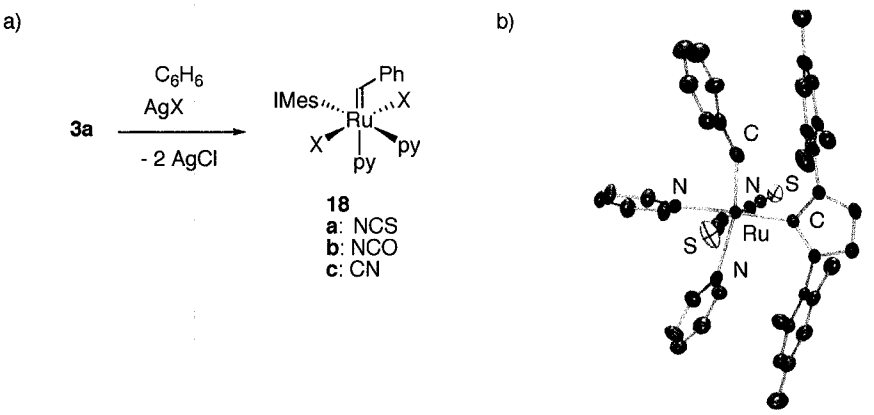

Figure 11. a) Synthesis of **18a-c**. b) ORTEP representation of **18a** (For full details, see Appendix E). Thermal ellipsoids are shown at 30% probability level; hydrogen atoms and THF solvate omitted for clarity.

On treatment of **3a** with AgOCN or AgCN, two new alkylidene resonances emerged over one hour. For the cyanate complex **18b**, after stirring overnight, two new products were observed (δ_H 19.11 and 19.60 ppm; C_6D_6). As the electronegativities of oxygen and nitrogen are quite close, the mixture may reflect the presence of both linkage isomers. Based on the stability of the *trans* orientation of NCS in **18a** the extra signals were not assigned as the *cis* isomer. For the cyanide derivative **18c**, five new alkylidene signals were observed (δ_H 19.84-17.75; C_6D_6), the complicated mixture of products was not investigated further.

The smaller steric demand of these linear anionic ligands permitted testing of our hypothesis that formation of the carbyne complexes is due to sterically-induced α-elimination. Surprisingly, reaction of **2a** with two equivalents of AgSCN or AgCN in benzene gave rise to no new alkyidene signals within 16 hours. Use of two equivalents of

AgOCN instead resulted in two new alkylidene signals (δ_H 18.39, 19.37 ppm, 10:1 ; C_6D_6). Crystals of **19b** suitable for X-ray diffraction were obtained from a saturated toluene solution layered with decane (Figure 12). The crystal structure has Ru bound through nitrogen. Werner has made similar cyanato complexes, also bound through nitrogen.[29] Clearly in the case of sterically undemanding anionic donors, the pseudohalide ligands can be incorporated into **2a**.

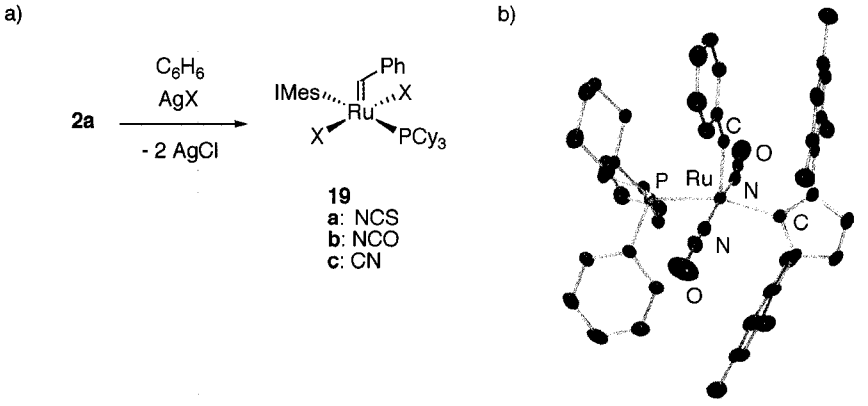

Figure 12. a) Synthesis of **19a-c**. b) ORTEP representation of **19b** (For full details, see Appendix E). Thermal ellipsoids are shown at 30% probability level; hydrogen atoms omitted for clarity.

3.5 Structural Parameters of Pseudohalide Complexes

3.5.1 X-ray Structures

The solid-state structures of those pseudohalide complexes for which X-ray quality crystals were obtained reveal similarities and some key differences. All structures have identical Ru=CHPh and Ru-IMes distances. All structures have distorted square pyramid or octahedral structures; in the former the basal ligands are bent downwards by 5-15°. The Ru-py distances are slightly longer for **16**, a function of the increased nucleophilicity of the

thioaryloxide ligand. In the case of **13**, the elongated steric bulk of $OC_6F_4C_6F_5$ ligand causes the aryl rings to flare out. It is tempting to comment on the inferred π-donor capabilities from the Ru-X-C bond angle, however, several papers have cautioned that such an analysis is not possible.[20,30] For oxygen, the presence of both an s- and a p-type lone pair means that the interaction of the former with the metal is independent of bond angle. However, when the Ru-O-R angle approaches 180°, overlap is maximized. In the case of four-coordinate **11** the oxygen is able to donate both lone pairs. This would account for the relative stability of the compound which can be regarded, in the extreme, as an 18-electron complex.

In some structures containing an XC_6F_5 group there is a distant non-bonding interaction between Ru and the *ortho* fluoride atoms: **10**, 3.50 Å; **12a**, 2.83 Å; **16b**, 3.61. The Grubbs group has reported a similar interaction where the arm of a fluorinated NHC ligand is found to be 3.2 Å from the Ru center.[31] For comparison, the average Ru···F distance found in the CCDC is 3.08 Å.[31] The effect of such dative interactions influencing catalyst initiation is discussed in detail in Chapter 6. This feature is absent in **13**, stacking of the two $OC_6F_4C_6F_5$ rings is found instead. The coplanarity of the aryl rings are 10.9° and 8.6°. The distance between the two C_6F_4 rings closest to Ru is 3.7 Å. This π-stacking feature likely minimizes the steric bulk of the large $OC_6F_4C_6F_5$ ligands. This feature is found in other complexes with large ligands, in $RuCl_2(CHPh)(IMes)_2$ the excess size of the IMes ligands is alleviated by π-stacking of the mesityl rings with the benzylidene (3.2 Å apart and within 8° of coplanarity).[32]

Mean values of the key Ru–L and Ru–X bond lengths, obtained from the Cambridge Structural Database, are collected in Table 3. The bond lengths within the pseudohalide complexes are very close to the average values, and are within the limits reported (Table 2).

References page 104

One small deviation from the average value for a Ru–N bond length (2.08 Å) is the elongated Ru–py bond in **18a** (2.33 Å). A similarly long bond for pyridine *trans* to benzylidene has been observed for **3b** (2.37 Å).[4b] The hydride complex **10** has the standard Y-shape common to d^6 ML_5 complexes.[33]

Table 2. Structural features of pseudohalide catalysts, $RuX_2(CHPh)(IMes)(L)$.[a]

	12a	**14**	**16b**	**18a**[b]	**19b**[b]
X	OC_6F_5	$OC_6F_4C_6F_5$	SC_6F_5	NCS	NCO
L	py	py	py	py_2	PCy_3
Ru – X_1 (Å)	2.08	2.08	2.36	2.04	2.09
Ru – X_2 (Å)	2.11	2.05	2.37	2.05	2.10
Ru – L (Å)	2.06	2.07	2.13	2.19 (2.33)[c]	2.45
Ru – X_1 – C (°)	120	134	111	173	174
Ru – X_2 – C (°)	125	141	113	170	169

[a]All Ru=CHPh 1.84 Å, Ru-IMes = 2.05 Å [b]Anionic ligands are trans. [c]py *trans* to alkylidene.

Table 3. Ruthenium structural parameters from the Cambridge Structural Database.

	Ru–C (Å)	Ru–N (Å)	Ru–O (Å)	Ru=C (Å)	Ru–S (Å)	Ru–NCS (Å)	Ru–NCO (Å)
Average	1.95	2.08	2.08	1.89	2.36	2.05	2.12
Max	3.23	2.49	2.65	2.17	2.82	2.11	2.19
Min	1.47	1.64	1.70	1.67	2.06	1.90	2.06

3.5.2 Characteristic ^1H and ^{13}C NMR Signals for Ru Metathesis Catalysts

Key NMR signals for the Ru precursors and pseudohalide complexes studied are summarized in Table 4. The range for the benzylidene proton is δ_H 17-20 ppm. For pseudohalide complexes the benzylidene proton appears upfield of its value in the corresponding dichloride complex. Values are given preferably in C_6D_6, or if solubility in C_6D_6 was poor, $CDCl_3$ was used. The NHC carbon appears between δ 185–180 ppm

compared to δ_C 216.3 ppm (THF-*d*8) for the free carbene.[34] The alkylidene ^{13}C NMR signals appear between δ_C 324-310 ppm. For comparison, the carbyne signal for **11** appears at δ_C 250.2 ppm.

Table 4. Characteristic ^1H NMR signals for alkylidene.

	Catalyst	δ_H (ppm) Ru=C*H*	
		C_6D_6	$CDCl_3$
1a	$RuCl_2(CHPh)(PCy_3)_2$	19.94	19.95
2a	$RuCl_2(CHPh)(IMes)(PCy_3)$	19.92	19.40
3a	$RuCl_2(CHPh)(IMes)(py)_2$	20.02	19.47
3b	$RuCl_2(CHPh)(IMes)(Brpy)_2$	19.79	19.28
12a	$Ru(OC_6F_5)_2(CHPh)(IMes)(py)$	18.64	18.76
12b	$Ru(OC_6F_5)_2(CHPh)(IMes)(Brpy)$	18.84	18.90
14a	$Ru(OC_6Cl_5)Cl(CHPh)(IMes)(py)$	19.78	
15a	$Ru(OC_6Br_5)Cl(CHPh)(IMes)(py)$	19.68	19.28
15b	$Ru(OC_6Br_5)Cl(CHPh)(IMes)(Brpy)$	19.55	
16a	$Ru(SC_6F_5)_2(CHPh)(IMes)(py)$	19.19	
16b	$Ru(SC_6F_5)_2(CHPh)(IMes)(py)$	18.20	
17	$Ru(SC_6Cl_5)Cl(CHPh)(IMes)(py)$	17.74	
13a	$Ru(OC_6F_4C_6F_5)_2(CHPh)(IMes)(py)$	18.62	
18a	$Ru(NCS)_2(CHPh)(IMes)(py)_2$	18.34	17.99
19b	$Ru(NCO)_2(CHPh)(IMes)(PCy_3)$	18.39	18.63
18c	$Ru(CN)_2(CHPh)(IMes)(py)_2$	19.80	

3.6 Conclusion

The coordination chemistry of Ru alkylidenes is rich and varied. Depending on the ligands present, these complexes may be rather stable or may decompose quickly. Our survey of these compounds was initiated by model studies in which we isolated the issue of the stability of the Ru=CHPh moiety as the key to the synthesis of new Ru-pseudohalide metathesis catalysts. Two variables emerged: Firstly, that the π-donor ability of the aryl ring must be curbed, in this case by introduction of electron withdrawing groups on the ring;

References page 104

Secondly, the steric bulk of either the ancillary ligands or anionic donors must be limited in order to prevent α-elimination reactions.

3.7 References

(1) Nguyen, S. T.; Grubbs, R. H.; Ziller, J. W. *J. Am. Chem. Soc.*, **1993**, *115*, 9858-9859.
(2) Schwab, P.; Grubbs, R. H.; Ziller, J. W. *J. Am. Chem. Soc.*, **1996**, *118*, 100-110.
(3) Schwab, P.; France, M. B.; Ziller, J. W.; Grubbs, R. H. *Angew. Chem. Int. Ed.*, **1995**, *34*, 2039-2041.
(4) Sanford, M. S.; Love, J. A.; Grubbs, R. H. *J. Am. Chem. Soc.*, **2001**, *123*, 6543-6554.
(5) Sanford, M. S.; Henling, L. M.; Day, M. W.; Grubbs, R. H. *Angew. Chem., Int. Ed.*, **2000**, *39*, 3451-3453.
(6) Marchenko, A. V.; Huffman, J. C.; Valerga, P.; Jimenez Tenorio, M.; Puerta, M. C.; Caulton, K. G. *Inorg. Chem.*, **2001**, *40*, 6444-6450.
(7) Fulton, J. R.; Holland, A. W.; Fox, D. J.; Bergman, R. G. *Acc. Chem. Res.*, **2002**, *35*, 44-56.
(8) Bryndza, H. E.; Tam, W. *Chem. Rev.*, **1988**, *88*, 1163-1188.
(9) Holland, P. L.; Andersen, R. A.; Bergman, R. G.; Huang, J.; Nolan, S. P. *J. Am. Chem. Soc.*, **1997**, *119*, 12800-12814.
(10) Snelgrove, J. L.; Conrad, J. C.; Yap, G. P. A.; Fogg, D. E. *Inorg. Chim. Acta*, **2003**, *345*, 268-278. (b) Snelgrove, J. L., Ph.D. Thesis, University of Ottawa: 2005.
(11) Cole-Hamilton, D. J.; Young, R. J.; Wilkinson, G. *J. Chem. Soc., Dalton Trans.*, **1976**, 1995-2001.
(12) Danopoulos, A. A.; Wilkinson, G.; Sweet, T. K. N.; Hursthouse, M. B. *Polyhedron*, **1994**, *13*, 2899-2905.
(13) Casado, M. A.; Perez-Torrente, J. J.; Lopez, J. A.; Ciriano, M. A.; Lahoz, F. J.; Oro, L. A. *Inorg. Chem.*, **1999**, *38*, 2482-2488.
(14) (a) Koelle, U.; Hörnig, A.; Englert, U., *Organometallics*, **1994**, *13*, 4064-4066. (b) Curnow, O. J.; Hughes, R. P., *J. Am. Chem. Soc.*, **1992**, *114*, 5895-5897.
(15) Streitwieser, A. J.; Heathcock, C. H. Introduction to Organic Chemistry; 2nd ed.; McMillan: New York, 1981.
(16) Coalter, J. N.; Bollinger, J. C.; Eisenstein, O.; Caulton, K. G. *New J. Chem.*, **2000**, *24*, 925-927.
(17) a) McLain, S. J.; Wood, C. D.; Schrock, R. R., *J. Am. Chem. Soc.*, **1977**, *99*, 3519-3520. b) Schrock, R. R., *Chem. Commun.*, **2005**, 2773-2777. c) Schrock, R. R., *Chem. Rev.*, **2002**, *102*, 145-179.
(18) Conrad, J. C.; Amoroso, D.; Czechura, P.; Yap, G. P. A.; Fogg, D. E. *Organometallics*, **2003**, *22*, 3634-3636.
(19) Pauling, L., *The Nature of the Chemical Bond.* Cornell Univeristy Press: Ithica, 1960.
(20) Caulton, K. G. *New J. Chem.*, **1994**, *18*, 25-41.
(21) Aptula, A. O.; Netzeva, T. I.; Valkova, I. V.; Cronin, M. T. D.; Schultz, T. W.; Kuhne, R.; Schuurmann, G. *QSAR*, **2002**, *21*, 12-22.
(22) (a) Weskamp, T.; Schattenmann, W. C.; Spiegler, M.; Herrmann, W. A. *Angew. Chem. Int. Ed.* **1998**, *37*, 2490-2493. (b) Herrmann, W. A. *Angew. Chem. Int. Ed.* **1999**, *38*, 262. (c)

References page 104

Weskamp, T.; Kohl, F. J.; Hieringer, W.; Gleich, D.; Herrmann, W. A., *Angew. Chem. Int. Ed.,* **1999**, *38*, 2416-2419. (d) **2a**: Huang, J.; Stevens, E. D.; Nolan, S. P.; Peterson, J. L. *J. Am. Chem. Soc.* **1999**, *121*, 2674-2678. (d) **2b** Scholl, M.; Trnka, T. M.; Morgan, J. P.; Grubbs, R. H. *Tetrahedron Lett.* **1999**, *40*, 2247-2250. (e) Scholl, M.; Ding, S.; Lee, C. W.; Grubbs, R. H. *Org. Lett.* **1999**, *1*, 953-956.
(23) Love, J. A.; Morgan, J. P.; Trnka, T. M.; Grubbs, R. H. *Angew. Chem., Int. Ed.,* **2002**, *41*, 4035-4037.
(24) Catala, R. M.; Cruz-Garritz, D.; Hills, A.; Hughes, D. L.; Richards, R. L.; Sosa, P.; Torrens, H. *Chem. Commun.,* **1987**, 261-262.
(25) Salcedo, R.; Torrens, H. *Transition Metal Chemistry,* **1980**, *5*, 247-249.
(26) Fries, G.; Ilg, K.; Pfeiffer, M.; Stalke, D.; Werner, H. *Eur. J. Inorg. Chem.,* **2000**, 2597-2601.
(27) Nagao, H.; Ooyama, D.; Hirano, T.; Naoi, H.; Shimada, M.; Sasaki, S.; Nagao, N.; Mukaida, M.; Oi, T. *Inorg. Chim. Acta.,* **2001**, *320*, 60-66.
(28) Tabatabaeian, K.; Downing, P.; Adams, H.; Mann, B. E.; White, C. *J. Organomet. Chem.,* **2003**, *688*, 75-81.
(29) Jung, S.; Ilg, K.; Brandt, C. D.; Wolf, J.; Werner, H. *Eur. J. Inorg. Chem.,* **2004**, 469-480.
(30) Schrock, R. R. *Polyhedron,* **1995**, *14*, 3177-3195.
(31) Ritter, T.; Day, M.; Grubbs, R. *J. Am. Chem. Soc.,* **2006**, *128*, 11768-11769.
(32) Conrad, J. C.; Yap, G. P. A.; Fogg, D. E. *Organometallics,* **2003**, *22*, 1986-1988.
(33) Riehl, J. F.; Jean, Y.; Eisenstein, O.; Pelissier, M. *Organometallics,* **1992**, *11*, 729-737.
(34) Arduengo, A. J.; Harlow, R. L.; Kline, M. *J. Am. Chem. Soc.,* **1991**, *113*, 361-363.

References page 104

4 Olefin Metathesis via Ru-Pseudohalide Catalysts

4.1 Introduction

Chapter 3 described the synthesis of a family of new olefin metathesis catalysts containing pseudohalide ligands. Changing chloride for alternative anionic donors has the potential to transform metathesis behaviour. At the minimum, a change in catalyst activity (i.e. turnover frequency, TOF) or productivity (turnover number, TON) can be expected. This chapter describes experiments directed at evaluating the activity of the new catalysts, and benchmarking their productivity relative to the chloride-containing Grubbs catalysts with a range of substrates. A recurring theme is that of catalyst loading, and the related issue of catalyst lifetime. At the outset of this work, the standard metathesis reactions used 5 mol % catalyst. As this technology enters the industrial arena, metathesis reactions that can be executed with <0.5 mol % catalyst become increasingly important, requiring a concomitant increase in catalyst productivity.

Other areas of enormous interest include the development of catalysts or catalytic protocols that enable metathesis of challenging substrates. These include substrates containing potentially poisoning functionalities; macrocycles and medium-sized rings; and, in particular, sterically encumbered, geminally-disubstituted olefins. All of these substrates require long reaction times for metathesis to proceed to completion, even for highly reactive catalysts. As high catalyst activity is frequently associated with short lifetimes, this highlights the importance of achieving a balance between catalyst activity and productivity. Finally, a balance between activity and selectivity is also desirable. High activity is not always necessary, some applications requiring slower catalysts that will react with substrates

References page 147

in a controlled fashion. A major potential advantage of the aryloxide catalysts lies in their modular nature, a key aspect of the tunable selectivity of the Schrock Mo catalysts. This Chapter describes exploration of all of these features for the aryloxide family of catalysts.

4.2 Catalyst Screening

4.2.1 Evaluating Catalyst Activity in ROMP of Cyclooctene

ROMP of cyclooctene **20** provides an excellent primary reaction in screening for catalyst activity. As the olefinic signals for cyclooctene appear ca. 1 ppm upfield from those due to the ring-opened polymer, the reaction is easily monitored by queued ^{1}H NMR experiments. Rate profiles (Appendix B) were constructed by evaluating the integrated intensities of these peaks over time. Catalyst activity is expressed in terms of the turnover frequency in Table 1, though mass transport limitations (particularly at high conversions) mean that these data reflect a lower limit. In order to minimize the effect of increased viscosity, TOF values are calculated at 50 % conversion. For screening purposes, the independent rates of initiation and propagation were not assayed. These parameters are explored in more detail in Chapter 6.

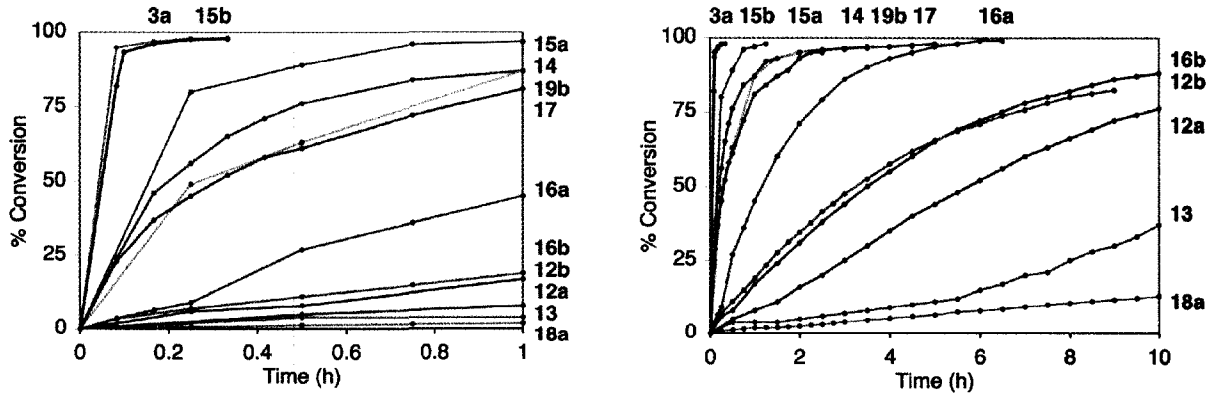

Figure 1. Evaluation of activity of RuXX'(CHPh)(IMes)(L) in ROMP of cyclooctene.

Table 1. Evaluation of activity of RuXX'(CHPh)(IMes)(L) in ROMP of cyclooctene.

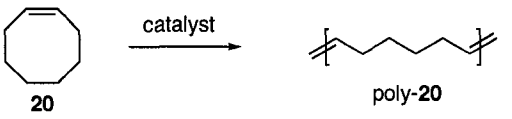

Catalyst	X	X' (if ≠ X)	L	TOF(min^{-1})[a]	Rel. rate
3a	Cl		py_2	38.2	294
15b	OC_6Br_5	Cl	3-Br-C_5H_4N	32.9	253
15a	OC_6Br_5	Cl	py	10.7	223
19b	NCO		PCy_3	7.99	166
14a	OC_6Cl_5	Cl	py	6.67	139
17	SC_6Cl_5	Cl	py	5.05	105
16a	SC_6F_5		py	1.33	28
12b	OC_6F_5		3-Br-C_5H_4N	0.48	10
16b	SC_6F_5		py	0.48	10
12a	OC_6F_5		py	0.28	6
13	$OC_6F_4C_6F_5$		py	0.13[b]	3
18a	NCS		py	0.048[b]	1

[a] TOF at 50 % conversion. [b] Extrapolated value.

The data of Table 1 indicate that **15b** is most active of the pseudohalide catalysts, and that all of these are less reactive in ROMP of COE than the "third-generation" Grubbs catalyst **3a**[1,2] (though the reverse is true for other substrates: Section 4.3.3). Use of pyridine in place of 3-bromopyridine (**15a**) retards ROMP. Catalysts **14a**, **19b**, **17** and **16a** exhibited moderately high ROMP activities; catalysts **12b**, **16a** and **12a**, intermediate activity, while catalysts **13** and **18a** were essentially inactive. From this selection, **15a** and **15b** were chosen for further study in applications requiring a high activity. For applications in which different metathesis manifolds are accessible, and selectivity is therefore important, **12a/12b** were used. The linear pseudohalide (**18**, **19**), thioaryloxide (**16**, **17**) and perfluorobiaryloxide (**13**) catalysts were not investigated further.

References page 147

4.2.2 Effect of Solvent on Catalyst Productivity

The importance of solvent effects in reaction chemistry, and in homogeneous catalysis in particular, cannot be overstated.[3] The solvent is typically, and overwhelmingly, the most abundant portion of a reaction mixture, and the choice of solvent often determines the success of a reaction. For reactions involving polar transition states, for example, a polar solvent can lower the activation energy. Selectivity can also be dramatically affected, as found for Mo-catalyzed asymmetric metathesis carried out in THF, vs. benzene.[4] Interaction of solvent molecules with the metal center in transition-metal catalysis can play an important role in ligand dissociation[5] or, conversely, catalyst poisoning. Metal-bound halogens can also function as hydrogen-bond acceptors,[6] a point discussed in more detail below.

The impact of solvent on the metathesis activity of aryloxide catalysts **12a/b** and **15a/b** was evaluated with diethyldiallyl malonate **21** as substrate, and compared with the behaviour of dichloride catalysts **1**, **2a**, **3a** and **3b** (Scheme 1). Low catalyst loadings were chosen, to amplify the impact of the different solvents on RCM performance. An array of solvents was investigated (Figure 3; data tabulated in Appendix B). The weakly coordinating solvents THF and dimethoxyethyl ether (DME) generally reduced activity, while all catalysts tested were poisoned by DMSO, MeCN, nitrobenzene, *N*-methylpyrrolidone (NMP) and *N*,*N*-dimethylformamide (DMF). ROMP via **2b** was earlier shown to be strongly retarded by polar additives such as nitriles, secondary amines and thiocyanates.[7] As the Ru catalysts decompose in alcohol solvents, these were not included in the solvent screen.[8-11]

Chlorinated solvents of intermediate polarity were generally best. The sole exception was **12a/b** in CH_2Cl_2, this probably reflecting the effect of the low boiling point of this solvent (40 °C), limiting efficient catalyst initiation. The good performance of the Grubbs

catalysts **1** and **2a** in a wide range of solvents is due in part to their high solubility in both chlorinated and hydrocarbon solvent. The lower solubility of aryloxide catalysts in hydrocarbon solvents diminishes their performance in these media. The extreme of this effect is found for the perfluoroaryloxide catalysts **12a** and **12b**, which are much less soluble in decane, toluene and benzene. Best performance for these catalysts was found in $CDCl_3$. The acidity of $CDCl_3/CHCl_3$ is the highest of the solvents tested (pK_a 18), raising the possibility that small amounts of acid may play a role in catalyst activation. In fact, many of the less active pseudohalide catalysts reported in the literature (next section) may be activated in this way.

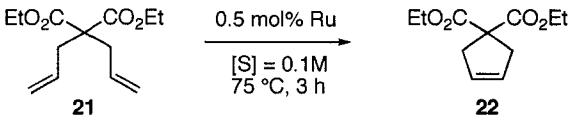

21 22

Scheme 1.

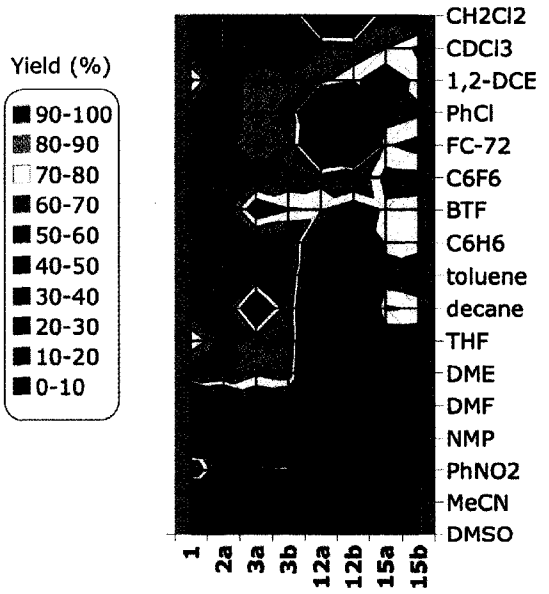

Figure 2. Contour plot showing RCM yield as a function of solvent. Average error ±2%, for details, see Appendix A (Contours are meant to be visual aids for identifying trends for catalysts or solvents but do not represent solvent mixtures).

References page 147

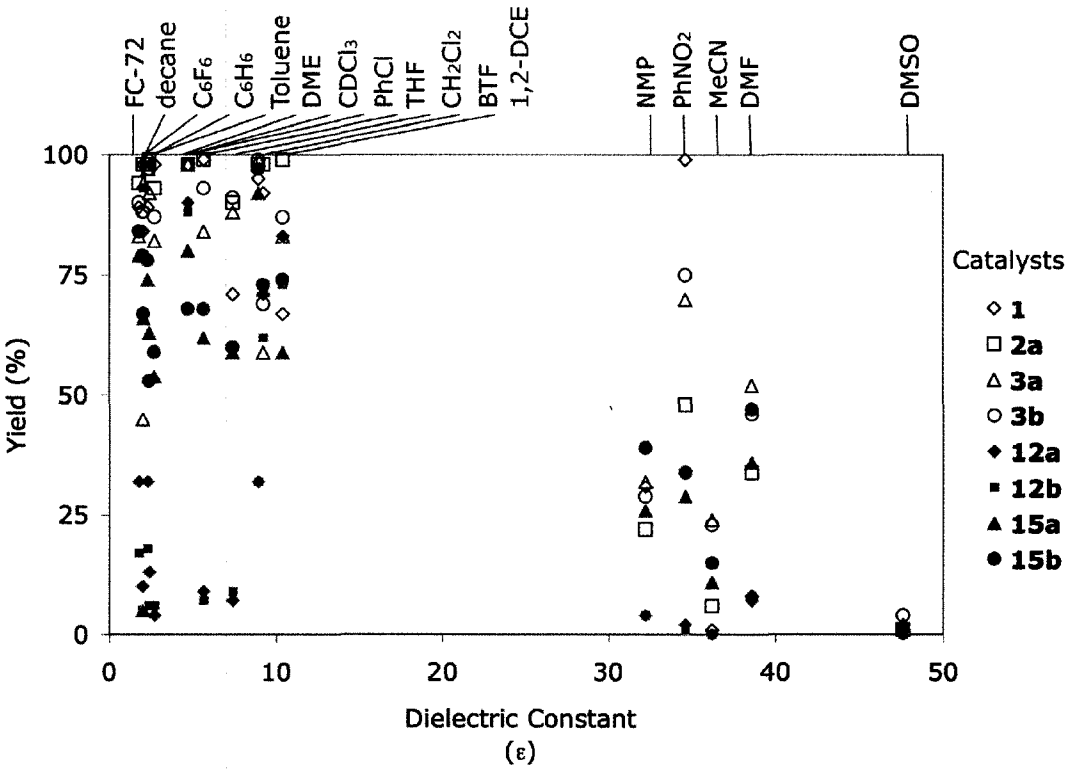

Figure 3. Scatter plot of RCM yield as a function of the solvent dielectric constant.

Pentabromoaryloxide catalysts **15a** and **15b** showed high activity in a range of solvents, reaching a maximum in CH_2Cl_2. Anticipating some correlation between solvent polarity and catalyst activity, low activity in relatively non-polar fluorinated solvents was expected low. However, the aryloxide catalysts show moderate RCM activity in BTF (α,α,α-trifluorotoluene), perfluorobenzene and (for **15a/b**) FC-72 (perfluorohexane). An inverse correlation is in fact evident from a scatter plot of RCM yield as a function of solvent dielectric constant ε (Figure 3). The aryloxide groups may thus act as solubilizing tags, opening the door to fluorous-phase chemistry (Section 4.9).

The following sections explore the behaviour of the pseudohalide catalysts in a variety of metathesis reactions. As a starting point, we chose to study the most active aryloxide catalyst, **15b**, in CH_2Cl_2 solvent.

4.3 Ring-Closing Metathesis

4.3.1 Productivity of Aryloxide Catalysts at Low Catalyst Loading

RCM of diethyldiallyl malonate (**21**) at low catalyst loadings (5000:1, or 0.02 mol % Ru) provides a benchmark for comparison to the work of other research groups. Catalyst lifetime or productivity was gauged from the maximum turnover number (TON). The RCM productivity of catalysts **12a/b**, **15a/b** is compared to that of **2a** and **3a/b** in Table 2, along with literature data for other catalysts at this loading. Some of these data should be treated with caution, owing to variations in reaction conditions. For instance, Dinger and Mol recorded an impressive TON of 200,000 for RCM in neat **21** at very low catalyst loading (1:1,160,000; neat **21**),[12] but no other catalysts have been studied under these conditions.

We find very good productivity at low catalyst loadings for the dichloride catalysts **2a** and **3a/b**, as others have reported for **1**, **2b**, and the "Hoveyda" catalyst **5a**.[13] The second-generation catalysts exhibit higher productivity than the Grubbs catalyst **1**. Of interest is the significantly higher total productivity of the PCy_3 complex **2a/b**, vs. its pyridine derivative **3a**. The pyridine catalyst initiates much more quickly,[2] but evidently has a shorter lifetime. The slowly-initiating Hoveyda catalyst **5a**[14-16] showed highest productivity at 0.05 mol % Ru, with a TON of 4550.[13] So-called "boomerang" strategies involving recapture of the active species by styrene ether groups have been proposed as a means of extending catalyst lifetime.[17] The efficiency of this approach is limited by the relative rates of both recapture

References page 147

and release. Hoveyda's group recently reported labelling studies that suggest a low efficiency of recapture in chiral systems of this type.[18] A more likely explanation for the sustained reactivity of **5a** is its very low turn-on efficiency and high thermal stability, which results in a reservoir of unreacted **5a**. This enables sustained release of the active catalyst, but diminishes the concentration of the active catalyst present at any time. Indeed, for all catalysts there is a balance between initiation efficiency and catalyst stability: at either extreme, catalyst productivity suffers.

The nature of the anionic ligands has a dramatic effect on TON. Replacing Cl with carboxylate (**23a-b**, **24**, **26**),[13,19] perfluoroaryloxide (**23c**)[13] alkoxide (**25**),[20] Schiff base (**27**),[21] tris(pyrazolyl)borate (**28**),[22] pyridine-2-carboxylate (**29**),[23] or iminopyrrole (**30**)[24] ligands reduces productivity.[13,19-24] Three factors can be identified: (1) excessive steric crowding, as in **25**; (2) the presence of four non-labile ligands in the basal plane of the square pyramid, as in **23a**, **23b**, **24** and **27-30**; and (3) the absence of a sufficiently strong donor (such as an alkylphosphine or NHC group) among the ligands retained in the active catalyst, as in **26**, **27**, **28**, and **30**.

The most striking examples of sterically restricted activity are undoubtedly presented by the four-coordinate alkylidene complexes **25a-c**.[20] Despite their nominal coordinative unsaturation, these exhibited essentially zero RCM activity, owing to the bulk of the PCy_3 and ^{t}Bu groups. Also relevant may be the π-donor ability of oxygen: the alkoxide ligand may function as both a σ and π donor, resulting in stable 18-electron species.[25] Activation of these catalysts by protonolysis with HCl reinstalls the chloride ligand(s), removing the steric constraints and restoring metathesis activity. This enables access to the highly reactive but short-lived intermediate **7**.

References page 147

The success of the perhaloaryloxide catalysts reflects a design strategy that addresses all of these points, to varying degrees. Steric constraints (issue (1)) are minimized by the planarity of the perfluoroaryloxide and pyridine donors, in conjunction with an essentially two-dimensional IMes ligand, incorporation of which addresses issue (3). Incorporation of a pyridine ligand addresses issue (2), albeit with some reduction in lability, as compared to the chloride complexes. Indeed, the extent to which pyridine lability is retained is key to the activity of this family of catalysts, and is examined in detail in Chapter 6.

In contrast to the metathesis-inactive alkoxides **25**, catalyst **12a** reached up to 41,000 turnovers for the formation of **22**, at exceptionally low catalyst loadings (5×10^{-4} mol % **12a**). High activity was observed only in $CHCl_3$ or $CDCl_3$: as noted in Section 4.2.2, activation by (e.g.) pyridine protonation could be important. Catalysts **15a** and **15b** exhibited higher activity than **12a-b**, but lower turnover numbers. The RCM and ROMP data suggest that **15b** is a fast, moderately productive catalyst, and **12a** is slow but long-lived.

References page 147

Table 2. Comparative catalyst productivity for the RCM of **21**.

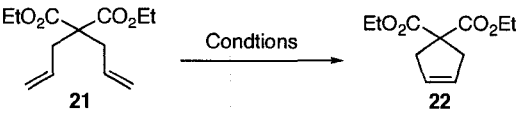

21 **22**

Entry	cat.	mol% Ru	solvent	temp.	time	% conv.	TON
1	**1**	0.02	CH_2Cl_2	40 °C	18 h	53	2650[a]
2	**2a**					89	4450
3	**2b**					85	4250[a]
4	**3a**					74	3700
5	**3b**					76	3800
6	**5a**	0.02	CH_2Cl_2	40 °C	18 h	91	4550[a]
7	**23a**					43	2150[a]
8	**23b**					67	3350[a]
9	**23c**					8	400[a]
10	**24**					9	450[a]
11	**25a**	20	C_6D_6	60 °C	96 h	5	0.25[b]
12	**25b**				96 h	70	3.5[b]
13	**25c**				12 h	40	2[b]
14		+1 equiv. HCl			1 h	100	5[b]
15	**26**	5	CH_2Cl_2	22 °C	0.5 h	30	6[c]
16	**27a**	3	C_6H_6	70 °C	1 h	32	32[d]
17	**27b**	5	C_6H_6	55 °C	4 h	20	20
18	**28**	20	CH_2Cl_2	25 °C	72 h	0	0[e]
19		+1 equiv. HCl			1 h	100	5[e]
20	**29**	5	CH_2Cl_2	20 °C	72 h	0	0[f]
21		+2 equiv. HCl			1.5 h	94	5[f]
22	**30a**	5	C_6D_6	70 °C	8 h	100	20[g]
23	**30b**				24 h	10	2[g]
24	**12a**	0.02	CH_2Cl_2	40 °C	18 h	18	900
25	**12b**					18	900
26	**15a**					33	1650
27	**15b**					47	2350
28	**12a**	0.02	C_6H_6	60 °C	18 h	6	300
29	**12b**					14	700
30	**15a**					44	2200
31	**15b**					45	2250
32	**12a**	0.02	$CHCl_3$	60 °C	18 h	58	2900
33	**12b**					47	2350
34	**15a**					46	2300
35	**15b**					37	1850
36	**12a**	0.05	$CHCl_3$	60 °C	1.5 h	91	1820
37	**15a**				2 h	45	900
38	**15a**				20 h	92	1840
39	**2a**	0.0005	$CHCl_3$	60 °C	24 h	8.5	17000
40	**3a**					2.6	5100
41	**12a**					20	40000
42	**15a**					11	21000

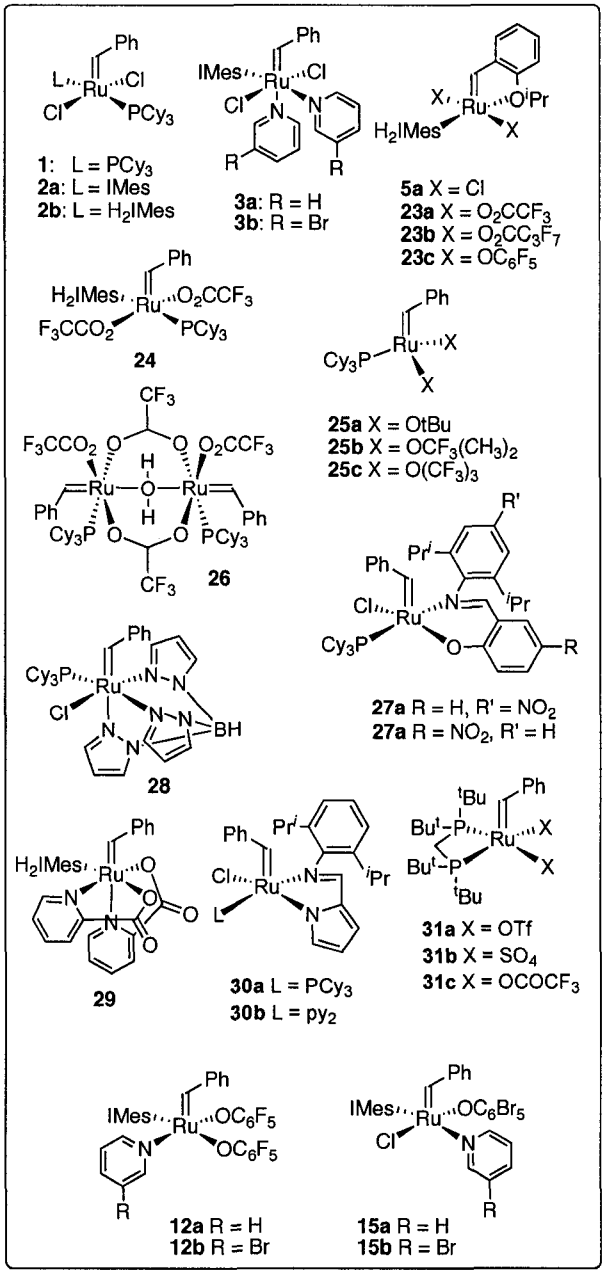

[a] Ref. 13; [b] Ref. 20; [c] Ref. 19; [d] Ref. 21; [e] Ref. 22; [f] Ref. 23; [g] Ref. 24.

References page 147

4.3.2 Substrate scope of aryloxide catalysts in RCM

Catalyst activity can often be a function of the substrate, as well as the catalyst itself. In order to gain greater insight into the behaviour of the new catalysts, the RCM of a range of substrates was undertaken, using the minimum amount of catalyst required for complete reaction by at least one catalyst in a conveniently short time. Complete conversion to product was a priority, both because this provides an ancillary test of catalyst activity (as Table 2 shows, reactions rarely go to completion at lower catalyst loadings), and because this minimizes workup costs associated with chromatographic separation of diene and ring-closed product. Short reaction times are likewise important in minimizing side-reactions,[26] while low catalyst loadings reduce workup costs as well as direct catalyst costs, as noted above.

The strong driving force for cyclization present in **21** permitted us to use this substrate to establish the minimum conditions for RCM of more demanding substrates (see Table 3 and following Sections). Complete RCM of **21** was achieved within 15 minutes at a catalyst loading of 0.5 mol %. For the most active catalysts, **15b** and **3b**, reaction in refluxing CH_2Cl_2 sufficed to effect RCM within 15 minutes. All other catalysts required use of refluxing $CDCl_3$, though reaction occurs more slowly at ambient temperatures.

While many five- or six-membered targets undergo RCM without difficulty (if without the tremendous geminal disubstitution directing force present in **21**), secondary amines such as diallylamine are almost invariably protected as the *N*-tosyl derivative, in order to prevent the deleterious effect on reactivity noted above. Indeed, RCM of diallylamine with **12a** in refluxing chloroform proceeded in only 10% yield; no other catalysts were assayed against this substrate. Of the catalysts tested for RCM of *N*-tosyl

References page 147

diallylamine **32**, only **15b**, **3a**, and **2a** effect complete cyclization within 15 minutes under the conditions used for **21**. The order of activity **15b**, **3b** > **2a**, **3a** > **14** > **15a** > **12a** was established. The cycloaddition side-reaction earlier reported for cationic allenylidenes,[27,28] $RuCl_3$, and RuCp*Cl(cod),[29,30] is observed with **12a** at a catalyst loading of 5 mol %. Catalysts **2b** and **5a** are reported to give 66% **33** at a much lower catalyst loading of 0.02 mol % Ru, vs. 3% with **23a**.[13]

Sulfides are also potential catalyst poisons, and RCM of such substrates is reported to require 5 mol % **2a**.[31] RCM of diallylsulfide **34** with 0.5 mol % **3a** or **3b** gave 60% or 90% **35**, compared to 100% conversion with **15a** or **15b** in 15 minutes. With 0.5 mol % **14** or **12a**, 31 or 40% RCM was found (100% in 15 min using 5 mol %). These data, taken together with the literature precedents noted above, suggest that sulfide is a less efficient poison than an isostructural secondary amine, despite the predictions of Pearson HSAB theory.[32] We speculate that poisoning of the ruthenium catalysts by secondary amine may reflect not so much coordinating ability, as the ability of the amine to function as a base (possibly facilitating dehydrohalogenation of the catalyst).

Linalool **36**, despite the presence of a trisubstituted olefin and a potentially problematic[33] allylic alcohol, is often readily cyclized by Ru catalysts.[34] At low catalyst loadings (0.05 mol %), only **12a** effects quantitative RCM of **36** within 1 h, a reflection of the longer lifetime of the bis(aryloxide) catalyst. This distinction is lost at higher catalyst loadings (0.5 mol % Ru), at which all of the aryloxide catalysts, as well as **2a** and **3a**, enable quantitative RCM within 15-20 minutes (refluxing $CDCl_3$). Complete RCM via **1** is reported at a catalyst loading of 5 mol %.[35] During the cyclization of linalool up to 20% isobutene is observed, but this does not appear to impede RCM. Finally, formation of dihydropyran **39**, a

References page 147

challenging trisubstituted olefin,[36] is quantitative using 0.5 mol % of **15b** or **2b**, vs. 92% for the fast-initiating but more sensitive **3b**. Formation of the five-membered carbocycle is disfavoured, as this would require reaction of two geminally-disubstituted olefins (an exceptionally challenging metathesis reaction: see Section 4.3.4). Even without this factor, however, the pyran is preferred for its higher thermodynamic stability.[37]

Table 3. RCM reactions to form five- and six-membered rings.[a]

Substrate	Product	Entry	Cat.	mol %	Sol.	Time (min)	Yield[a] (%)
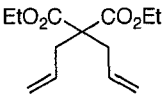	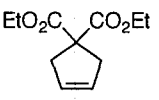	1	**15b, 3b**	0.5	CH_2Cl_2	15	100
		2	**15a, 12, 14, 2a, 3a**	0.5	$CDCl_3$	15	100
21	**22**						
		3	**2b**	0.02	CH_2Cl_2	18 h	54[13]
		4	**5a**	0.02	CH_2Cl_2	18 h	66[13]
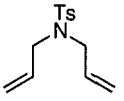		5	**23a**	0.2	CH_2Cl_2	18 h	3[13]
		6	**15b**	0.5	CH_2Cl_2	15	100
		7	**15a**	0.5	$CDCl_3$	20	79
32	**33**	8	**14**	0.5	$CDCl_3$	20	97
		9	**3b**	0.5	CH_2Cl_2	15	100
		10	**2a, 3a**	0.5	$CDCl_3$	15	100
		11	**12a**	0.05	$CDCl_3$	150	19
		12	**12a**	5	$CDCl_3$	15	91[b]
		13	**15b**	0.5	CH_2Cl_2	15	100
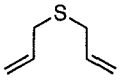		14	**15a**	0.5	$CDCl_3$	20	100
		15	**14**	0.5	$CDCl_3$	20	31
		16	**12a**	0.5	$CDCl_3$	20	40
34	**35**	17	**3a**	0.5	$CDCl_3$	20	60
		18	**3b**	0.5	CH_2Cl_2	15	90
		19	**2a**	5	C_7H_8	60	100[31]
		20	**12a, 14**	5	$CDCl_3$	15	100
		21	**15a**	0.05	$CDCl_3$	60	34
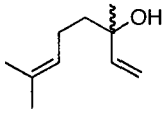	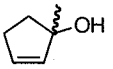	22	**14**	0.05	$CDCl_3$	60	17
		23	**12a**	0.05	$CDCl_3$	60	100
		24	**3a**	0.05	$CDCl_3$	60	29
36	**37**	25	**2a**	0.05	$CDCl_3$	60	24
		26	**15b, 3b**	0.5	CH_2Cl_2	15	100
		27	**12a, 14, 15a, 2a, 3a**	0.5	$CDCl_3$	15	100
		28	**1**	5	$CDCl_3$	60	100[38]

Table 3 continued...

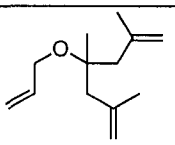	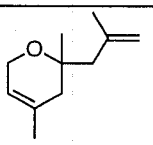	29	**15b**	0.5	CH_2Cl_2	15	100
		30	**15a**	0.5	$CDCl_3$	15	100
		31	**3b**	0.5	CH_2Cl_2	15	92
38	**39**	32	**2a**	5	CH_2Cl_2	15	100

[a] Refluxing solvent, 100 mM substrate; conversions determined by ^1H NMR ($CDCl_3$) or GC-FID (CH_2Cl_2) analysis; ±3% in replicate experiments. [b] 9% cycloaddition product formed.[39]

4.3.3 RCM of more challenging substrates

While trisubstituted olefins such as **40** undergo RCM more slowly than monosubstituted olefins,[36] high yields were attained with **1**, **2b** or **5a** after 18 h, even at low catalyst loadings. In comparison, only 3% yield was found with carboxylate **23a** under these conditions (Table 4; entries 1-4). Seeking higher conversions and much shorter reaction times, we used 5 mol % catalyst. For **15b**, RCM of **40** was complete in 2 h in refluxing CH_2Cl_2 (Entry 5), vs. 85% for **3b**. Grela's catalyst **5b** was superior for this substrate, enabling 99% RCM in 40 minutes at 20 °C (1 mol % Ru; Entry 9).[40]

Attempts to form 8-membered ring **43** from diene **42** at the normal substrate concentration of 100 mM were hampered by formation of the ADMET polymer. Likewise, at a concentration of 200 mM, only 50% conversion to **43** was reported with 20 mol % **1**.[41] At a lower substrate concentration (5 mM), RCM was complete within 1 hour using 5 mol % **15b** or **2a**, vs. 85% with **3b**. Details of the mechanism, which clarify the importance of concentration in the construction of medium-sized or macrocyclic rings by RCM, are discussed in Chapter 5.

Acrylates often undergo RCM to yield five- or six-membered rings without difficulty, providing that the initial site of metathesis is not the α,β-unsaturated olefin (substitution at which yields a Fischer carbene).[42,43] Recent reports indicate that even **1** performs well in

RCM of acrylate substrates.[44] The aryloxide catalysts show low activity toward allylacrylate **44**, however: yields were limited to ca. 75% for **15a** or **15b**, vs. 97% for **3b**, at 5 mol% Ru. Sequential ring-opening/ring-closing of **46** likewise required 5 mol % Ru. At 10 mM substrate, polymerization was suppressed, and 79% of tricyclic **47** was obtained using **15b**. Catalyst **3b** was superior to **15b** (100% in 1 h), while **1** is reportedly inferior (68% in 3 h).[45]

Schmidt and co-workers have proposed that RCM of diphenylsilane derivative **48** is challenging because the transition state for cyclization is destabilized by the steric bulk of the diphenylsilyl group.[46] RCM of **48** with 5 mol % **15b** reached a maximum of 91% in 15 minutes, while complete RCM could be effected with **15a** or **3a** in refluxing $CDCl_3$ within 20 minutes. The second-generation catalyst **2b** was the least active of the catalysts surveyed, reaching a maximum conversion of 76% within 20 minutes, although RCM proceeds to completion after 1 h. A literature report for **2b** (5 mol %) describes only 70% formation of **49** after 5 h in refluxing toluene,[46] suggesting much lower activity for the H_2IMes catalyst, at least in this solvent. RCM of dimethyldiallyl silane **50** was more challenging, and conversions achieved using catalysts **12a**, **14** or **15a** (refluxing $CDCl_3$, 15 minutes) were under 30%. During the reaction, ^{1}H NMR signals emerged between 1.5-0 ppm, possibly indicating silane redistribution.

References page 147

Table 4. RCM of more difficult substrates.[a]

Substrate	Product	Entry	Cat	mol %	Sol.	Temp. (° C)	Time (h)	Yield (%)
		1	**1**	0.2	CH_2Cl_2	40	18	83[13]
		2	**2b**	0.2	CH_2Cl_2	40	18	99[13]
EtO_2C CO_2Et	EtO_2C CO_2Et	3	**5a**	0.2	CH_2Cl_2	40	18	98[13]
		4	**23a**	0.2	CH_2Cl_2	40	18	3[13]
		5	**15b**	5	CH_2Cl_2	40	3	100
		6	**15a**	5	$CDCl_3$	60	3	100
40	**41**	7	**3b**	5	CH_2Cl_2	40	3	85
		8	**5c**	1	CH_2Cl_2	25	1	95[40]
		9	**5b**	1	CH_2Cl_2	20	0.66	99[40]
		10	**15b**	5[b]	CH_2Cl_2	40	1	100
		11	**3b**	5[b]	CH_2Cl_2	40	1	85
		12	**2a**	5[b]	CH_2Cl_2	40	1	100
42	**43**	13	**1**	20[c]	C_6H_6	55	17	50[41]
		14	**15b**	5	CH_2Cl_2	40	1	77
		15	**15a**	5	$CDCl_3$	60	1	73
44	**45**	16	**3b**	5	CH_2Cl_2	40	1	97
		17	**15b**	5[d]	CH_2Cl_2	40	1	79
		18	**3b**	5[d]	CH_2Cl_2	40	1	100
	47	19	**1**	6[e]	C_6H_6	45	3	68[45]
46								
		20	**15b**	5	CH_2Cl_2	40	0.25	91
		21	**15a**	5	$CDCl_3$	60	0.33	100
		22	**3a**	5	$CDCl_3$	60	0.33	100
		23	**2a**	5	$CDCl_3$	60	0.33	76
48	**49**	24	**2b**	5	C_6H_6	110	5	70[46]
		25	**12a**	5	$CDCl_3$	60	0.25	30
		26	**14**	5	$CDCl_3$	60	0.25	15
50	**51**	27	**15a**	5	$CDCl_3$	60	0.25	18
		28	**15b**	5	CH_2Cl_2	40	0.25	100
		29	**3a**	5	$CDCl_3$	60	0.25	100
		30	**2a**	5	$CDCl_3$	60	0.25	100
		31	**15a**	5	$CDCl_3$	60	0.25	94
52	**53**	32	**14**	5	$CDCl_3$	60	0.25	85
		33	**12a**	5	$CDCl_3$	60	0.25	24

[a] Concentration of substrate is 100 mM except as noted. Yields determined by ^1H NMR ($CDCl_3$) or GC-FID (CH_2Cl_2) analysis; ±3% in replicate experiments. [b] [S] = 5 mM. [c] 200 mM substrate. [d] 10 mM substrate. [e] 40 mM substrate.

References page 147

RCM of diallylether **52**, while superficially a problem very similar to those summarized in Table 3, presents a greater challenge to metathesis, as indicated by the tenfold higher catalyst loading required relative to (e.g.) **32** or **34**. RCM of **52** via **15b** (5 mol %) gave quantitative yields of the 2,3-dihydrofuran **53** in refluxing $CDCl_3$ within 15 minutes. In comparison, RCM via **15a** proceeded in 94% yield, but was accompanied by 6% of the cyclic enol ether (or vinyl ether) **54**, formed by isomerization. Catalyst **12a** emerged as an efficient catalyst for isomerization of **52**, providing a mixture of *E/Z* isomers **54-57**, with very little of the metathesis product **53** (Scheme 2). As the vinyl ethers are both more stable, and less reactive in metathesis, this diverts substrate from RCM pathways. While the isomerization activity of the Grubbs-class catalysts is now well known, such undesired activity tends to emerge as a problem for more challenging substrates, which require longer reaction times.[26] While we do not detect hydride signals in RCM of **52** via **12a** by in situ ^1H NMR analysis, ruthenium hydrides have long been thought to account for this common side-reaction. Work from the Sasol group suggests that such species may be generated by reductive elimination of propene from the ruthenacyclobutane intermediate.[47] Grubbs and Hong reported that prolonged thermolysis of **2b** (24 h, refluxing benzene) yields a hydride species which, like many transition-metal hydrides, functions as an olefin isomerization catalyst.[48]

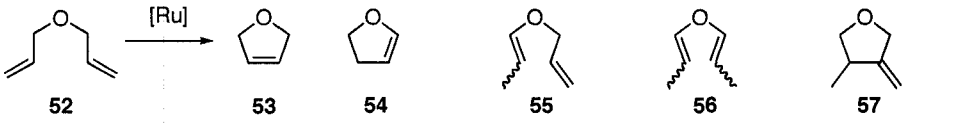

Scheme 2.

References page 147

Cossy has deliberately exploited the isomerization activity of the second-generation Grubbs catalyst to transform allylic ethers and amines into primary amines and alcohols.[49] In comparison to **12**, the bromoaryloxide catalyst **15b** is less active toward isomerization of allyl-heteroatom substrates, but we considered that this activity might be "turned on", and thus enable tandem metathesis-isomerization, if we could identify an efficient means of transforming **15** into a ruthenium hydride species. The specifics of this work will be described elsewhere.[50] In brief, however, we found that addition of K_2CO_3 after RCM acts as an efficient trigger for formation of a well-defined ruthenium hydride species, which enables RCM-isomerization with high selectivity and in high yield. After complete RCM of **52** with 5 mol % **2a** or **15b**, for example, addition of 10 mol % K_2CO_3 gave access to **54** in quantitative yields on 4 h further reaction time.[51]

Another class of challenging RCM targets are macrocycles, interest in which is spurred by the value of many such compounds. Of much interest for their desirable olfactory properties are many macrocyclic lactones, a well-known example being the saturated form of 16-membered lactone **59**, a valuable musk fragrance trademarked by Firmenich as Exaltolide.[52] Many natural products contain a macrocycle core: in epothilone A, for example, **59** can be recognized as a central structural motif,[53] while the corresponding 14-membered lactone **61** is a core structure in gloeosporone.[54]

High dilutions are normally used for the synthesis of macrocycles, in order to promote intramolecular cyclization reactions over intermolecular oligomerization of bifunctional substrates. We therefore carried out these reactions by dropwise addition of substrates and catalyst, with a maximum substrate concentration (i.e. the concentration that would result from batchwise addition of the entire substrate charge) of 5 mM. In the first

References page 147

reported example of RCM, Villemin used a tungsten catalyst to prepare 16-membered lactone **59** in 67% yield (Entry 1, Table 5).[55] Fürstner improved on this by using 5 mol % of the Grubbs catalyst, but reaction was still incomplete after 30 h (79% **59**).[56] Conversions were similarly limited to 72% on use of **2a** (2 mol %).[42] In comparison, **15a/b** effected quantitative conversion within 15 minutes at a catalyst loading of 5 mol %. RCM via **14a**, **3a** or **12a** was slower, but proceeded to completion at 0.5, 1 or 12 h, respectively. Using catalysts **15a**, **15b** or **14a**, RCM of **60** to afford 14-membered **61** was complete within 15 minutes. At the same time interval, catalysts **12a** and **3a** reached only 29 and 63% conversion respectively; a maximum conversion of 85% was obtained in both cases. The yield reported for **1b** is just 52%.[52]

Table 5. Synthesis of macrolides by RCM.[a]

58: n = 4
60: n = 2

59: n = 4
61: n = 2

Entry	Substrate	Cat.	Solvent	Temp. (°C)	Conc. (mM)	Method[b]	Time (h)	Yield (%)	*E/Z*
1	**58**	**W**[c,55]	PhCl	75	6	B	–	67	–
2	**58**	**15b**	CH_2Cl_2	40	5	Z	0.25	100	75/25
3	**58**	**15a**	CH_2Cl_2	40	5	Z	0.25	100	75/25
4	**58**	**14**	CH_2Cl_2	40	5	Z	0.25	72	
5							0.5	100	80/20
6	**58**	**12a**	CH_2Cl_2	40	5	Z	0.25	9	
7							12	100	75/25
8	**58**	**3a**	CH_2Cl_2	80	5	Z	0.25	30	
9							1	100	75/25
10	**58**	**2a**[d,42]	CH_2Cl_2	40	3	B	–	72	–
11	**58**	**1b**[e,52]	CH_2Cl_2	40	4	Z	32	79	46/54

References page 147

Table 5 continued...

12	**60**	**15b**	C_6H_6	80	5	Z	0.25	100	90/10
13	**60**	**15a**	C_6H_6	80	5	Z	0.25	100	90/10
14	**60**	**14a**	C_6H_6	80	5	Z	0.25	100	90/10
15	**60**	**12a**	C_6H_6	80	5	Z	0.25	29	80/20
16	**60**	**3a**	C_6H_6	80	5	Z	0.25	63	90/10
17	**60**	**1b**[b,52]	CH_2Cl_2	40	4	Z	–	52	–

[a] 5 mol % catalyst; Determined by GC-FID; ±3% in replicate experiments. [b] Addition method: Z, modified Ziegler conditions: high dilution, dropwise addition method; B, batchwise addition of diene and catalyst. [c] WCl_6/Me_4Sn. [d] 2 mol % catalyst. [e] **1b**: $RuCl_2(CHCHCPh_2)(PCy_3)_2$. [f] 1 mol % catalyst.

4.3.4 RCM Synthesis of Tetrasubstituted Olefins

The slow rate of metathesis of trisubstituted alkenes was noted above. Geminally disubstituted olefins are very slow to react,[36,58] owing to the steric barriers associated with olefin coordination and subsequent metathesis, and catalyst decomposition can therefore compete with metathesis. In consequence, synthesis of tetrasubstituted alkenes is very challenging. This effect is seen in Table 6 for RCM of **62**: with 5 mol % **2a**, only 47% of tetrasubstituted **63** is observed after 24 h. Even so, this catalyst out-performs **1**, **2b**, **3b** or **5a-c**, with which a maximum yield of 31% **63** was obtained,[40,59,60] although the Schrock Mo catalyst achieved nearly complete conversion.[60] Even **15b**, generally the best-performing aryloxide catalyst, gave only 16% of tetrasubstituted **63** under the reaction conditions of Table 6. Hoye has demonstrated that relay metathesis can be used to gain access to tetrasubstituted olefins,[61] though the need to synthesize a more complex substrate is a limitation of this strategy. For the catalysts in Table 6, formation of tetrasubstituted cycloalkene, even for a favoured ring size of five members, is very challenging.

References page 147

Table 6. RCM synthesis of a tetrasubstituted olefin.

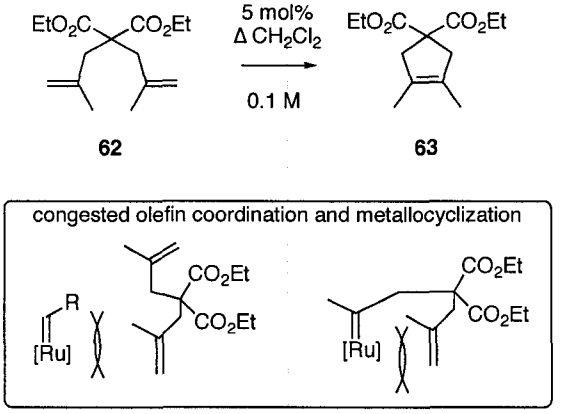

Entry	Cat.	Time (h)	Yield[a] **63** (%)
1[59]	**1**	1.5	0
2[59]	**2a**	1.5	40
3[62]	**2a**	24	47
4[60]	**2b**	8	14
5[60]	**2b**	24	31
6	**3b**	24	5
7[40]	**5a**	16	2
8[40]	**5b**	16	1
9[40]	**5c**	24	9
10	**15b**	24	16

[a]Determined by GC-FID

4.4 Tunable Selectivity in Aryloxide-Mediated RCM

In almost all of the cases shown so far, high activity was the most important catalyst feature. However, a highly reactive metathesis catalyst is not always desired. Panek has shown, for example, that the attenuated reactivity of catalyst **1** enabled higher selectivity, relative to **2b**, in RCM synthesis of 1,3,5-trienes. Catalyst **2b** reacted with the internal alkenes, truncating the molecule to a 1,3-diene.[63] As this suggests, the less reactive catalyst **12a** may be preferable to **15b** where selectivity is an issue. An example is shown in Scheme 3. Depending on the catalyst activity, metathesis of **64** may terminate at the RCM product **65a**, or may yield **65b** via a subsequent CM step. (The RCM reaction itself is selective for formation of the pyran **65a** over the five-membered carbocycle, as noted above).[37] Catalyst **12a** (1 mol %, refluxing CH_2Cl_2) produced **65a** in quantitative yield. When catalyst **15b** was used, some **65b** was invariably obtained, and complete conversion to this species was observed on heating for 2 h. The desirability of the six-membered pyran ring is highlighted by the presence of this structural motif in many natural products, especially marine

References page 147

polycyclic ethers,[64] as well as (-)-Laulimalide, one of several pyran-containing natural products currently being investigated for their pharmacological activities.[65]

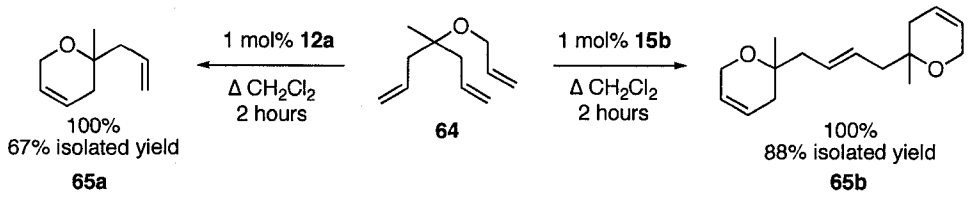

Scheme 3.

Ring-opening cross-metathesis (ROCM) provides a further example of the desirability of tunable catalyst activity. Under a narrow set of circumstances, norbornenes can be induced to undergo ROCM, in preference to ROMP (Table 7).[14,66] *Endo*-disubstituted norbornenes such as anhydride **66** are sufficiently hindered that ROMP is slow, and cross-metathesis can occur in the presence of another alkene. Using the chiral catalysts **71-72** (Figure 4), Hoveyda and co-workers demonstrated that this reaction can be used to generate four adjacent chiral centers via asymmetric ring-opening of the norbornene (**71**, **72**).[18,67] Chiral molybdenum catalysts also performed well, if a pendant ether donor was present at the C7 site; otherwise, ROMP prevailed.[68] We found that **15a** and **15b** rapidly polymerized **66**, and no cross-metathesis occurred. However, the less reactive catalyst **12a** was selective for ROCM, giving a 1.6:1 or 1:1 mixture of *E*:*Z* isomers of **68** or **70**.

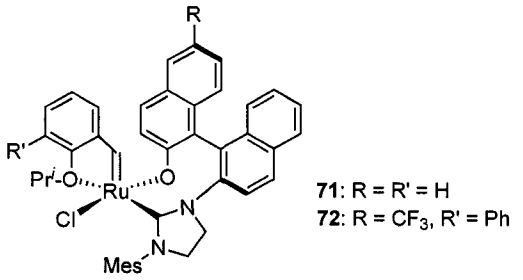

Figure 4. Hoveyda's chiral ruthenium metathesis catalysts.[18,67]

References page 147

Table 7. Ring opening cross-metathesis.

Substrate	Product	Entry	Cat.	mol %	Sol.	Temp. (°C)	Time (h)	*E*:*Z*	Yield (%)[a]
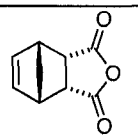 **66** + 5 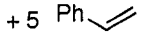 **67**	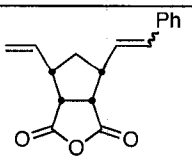 **68**	1	**5a**	5	CH_2Cl_2	40	1	1:0	100
		2[14]	**12a**	5	CH_2Cl_2	40	1	1.6:1	100
		3[67]	**72**	5	THF	50	1	1:0	100
		4[18]	**73**	5	THF	22	0.5	1:0	100
		5	**15b**	5	CH_2Cl_2	40	1	–	0[b]
		6	**15a**	5	CH_2Cl_2	40	1	–	0[b]
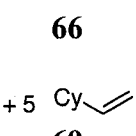 **66** + 5 **69**	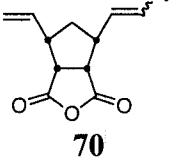 **70**	7	**12a**	5	CH_2Cl_2	40	1	1:1	100
		8[67]	**72**	5	THF	55	1	1:0	100
		9[18]	**73**	5	THF	22	0.25	1:0	100

[a] Determined by ^{1}H NMR. [b] An insoluble polymer was obtained.

4.5 Cross-metathesis (CM)

Cross-metathesis offers a means of forming acyclic carbon-carbon bonds complementary to Pd-mediated cross-coupling.[69] CM is typically much more challenging than RCM. A major problem is that of selectivity, as cross-metathesis of two olefins A and B can produce six different products, including *E* and *Z* isomers of the self-metathesis products AA and BB, as well as the desired cross-metathesis product AB. While selectivity in CM of very similar olefins remains problematic, Grubbs and Chatterjee have proposed a method of coupling terminal olefins of very dissimilar reactivity with high selectivity, by combining highly reactive (Type I) olefins with less reactive (Type II) olefins.[70] The already low reactivity of Type II olefins is further diminished by homo-coupling to give an internal olefin, and their self-metathesis is therefore essentially irreversible. Type I olefins are likewise susceptible to self-metathesis: however, if this is a fast, reversible process, an

equilibrium concentration of the terminal olefin is present, which on CM with a Type II olefin yields an product of intermediate activity. Pairing Type II olefins with an excess of a Type I olefin is thus aimed at minimizing self-metathesis of the former, while trapping out the CM product. Excellent results have been reported in some cases: using 5 mol % **2b**, for example, CM of various (Type 2) acrylates with a twofold excess of the Type 1 olefin styrene gave 80-90% of the CM product.[70]

We find that this approach works less well with CM via **15**. In these reactions, we used a five-fold excess of the Type 1 substrate, as initial experiments indicated inefficient trapping of the CM product. Thus, CM of five equivalents of styrene **72** and *t*-butyl acrylate **78** in refluxing CH_2Cl_2, using 5 mol % **15a** or **15b**, yielded 73 or 86%, respectively, of **74** (Scheme 4, Table 8). In comparison, **3b** (itself an efficient[2] CM catalyst) gave **74** in 94% yield. This difference may indicate that self-metathesis of stilbene is less reversible for **15**, possibly owing to the greater bulk of **15**, relative to **2** or **3**.

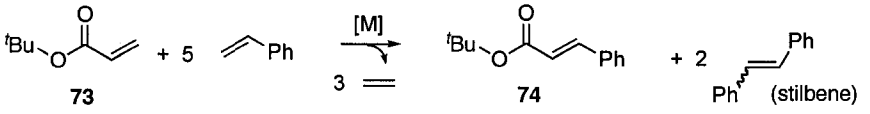

73 74

Scheme 4.

Table 8. Cross-metathesis of styrene and *t*-butylacrylate, and self-metathesis of methyl oleate.[a]

Entry	Catalyst	Sub	$[S_{C1}]:[S_{C2}]:[Ru]$	[S] (mM)	Solvent	Temp. (°C)	Time (h)	Yield (%)	TON
1	**15b**	**73**	100:20:1	100	CH_2Cl_2	40	12	86	17
2	**15a**	**73**	100:20:1	100	$CHCl_3$	60	12	73	15
3	**3b**	**73**	100:20:1	100	CH_2Cl_2	40	12	94	19
4	**15b**	**73**	2,000,000:1	neat	–	60	12	43	860,000
5	**15b**	**75**	1,000,000:1	neat	–	60	12	48	480,000
6	**2b**[71]	**75**	990,000:1	neat	–	55	4	45	440,000
7	**15b**	**75**	100,000:1	neat	–	60	12	47	47,000
8	**2a**	**75**	40,000:1	neat	–	60	4	49	19,000
9	**15b**	**75**	40,000:1	neat	–	60	12	46	18,200
10	**1**[71]	**75**	25,000:1	neat	–	55	4	10	2,500
11	**26**[19]	**75**	550:1	300	CH_2Cl_2	20	4	36	220

[a]CM yield determined by ^{1}H NMR analysis, based on *t*-butylacrylate **73**. Self-metathesis yield, by calibrated GC-FID; *E/Z* isomers obtained. $[S_{C1}]:[S_{C2}]:[Ru]$ = relative concentrations of Class 1, Class 2 substrates, catalyst.

This behaviour highlights the potential of **15b** in self-metathesis. The target chosen for examination was methyl oleate **75** (Scheme 5). Methyl oleate, a soybean derivative, has potential as a biodiesel,[72] and yields useful products on self-metathesis. Octadec-9-ene **76** is a high-octane fuel additive,[73] while **77** can be cyclized to form a macrocycle,[74] or used as an additive in polyolefin production.[75] To make the reaction economically viable on commodity scale, a very high catalyst TON is required. Substrate **75** is pseudosymmetrical, given the seven-carbon separation between the olefin and the ester functionality, and a 2:1:1 ratio of **75**:**76**:**77** is obtained at equilibrium, with a maximum yield of 50%.

Scheme 5.

A Ru-methylidene intermediate is not involved in CM of this internal olefin, which may contribute to the high lifetimes attainable.[47,76] Mol and Dinger achieved an impressive TON of 440,000 using **2b** at a substrate:catalyst ratio of 990,000.[12] We find that CM of 1,000,000 equivalents of neat **75** with **15b** reached 48% conversion, with a TON of 480,000 (Table 8). On halving the catalyst loading (2,000,000 equiv **75**), the reaction does not reach equilibrium, but a TON of 860,000 was obtained. Use of a lower substrate charge (100,000 or 40,000 equiv **75**) causes the maximum TON to drop to 47,000 or 18,200. In comparison, **1** reaches just 10% conversion, with a TON of 2,500.[77] For the carboxylate catalyst **26**, a modest TON of 220 was recorded, albeit under unoptimized conditions.[19] Catalyst **15b**, in contrast, performs well: at very low loadings, turnovers are comparable to or better than the second-generation Grubbs catalyst **2b**.

4.6 Enyne metathesis

Enyne metathesis, a process closely related to RCM, has emerged as a useful synthetic route to linear and cyclic 1,3-dienes, via reaction of an alkene with an alkyne.[78] The diene products are very useful precursors for cycloaddition reactions. Also attractive is the atom economy of the reaction[79] in comparison to RCM reactions, in which ethylene is ejected. Because related metal-mediated cyclizations of enynes are known to involve Lewis acidic, late-transition-metal catalysts,[80] we speculated that enyne metathesis might be more efficient for the aryloxide catalysts, which (as discussed in Chapter 6) are more electrophilic than the Grubbs-class, dichloride catalysts.

The productivity of catalysts **15a/b** in enyne metathesis was assayed against that of **2a/b** and **3b** (Table 9). High conversions, under the mildest conditions yet reported, are

characteristic of the aryloxide catalysts. At 0.5 mol % **15b**, enyne **78** was converted into carbocycle **79** within 15 minutes. In comparison, the second-generation catalyst **2b** was reported to reach only 15% conversion to **79**, though this increased to 99% under ethylene atmosphere.[81] Furan **81** was formed with equal ease by **15a/b** or **3b**, at 0.5 mol % Ru. Using double the loading of **5c** and low temperatures (1 mol % Ru, 0 °C), Grela and co-workers also obtained **81** in high yield.[40] In contrast, 5 mol % of **2a/b** was required to reach similar conversions. Sequential enyne-RCM reactions can give efficient access to fused cyclic products, if the catalyst is long-lived enough to support the metathesis cascade. Reaction of **82** with 3 mol % **1** was reported to generate **83** in 95% yield (refluxing CH_2Cl_2, 8 hours).[82] At 0.5 mol % Ru, **15b** outperformed **3b**, yielding ca. 80% **83**, while yields were quantitative within 20 minutes on use of 5 mol % **15b**.

Table 9. Examples of enyne metathesis.

Substrate	Product	Entry	Cat.	mol %	solv.	T (°C)	Time (min)	Yield (%)
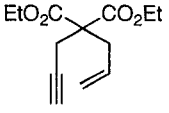	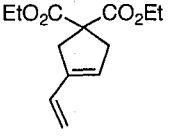	1	**15b**	0.5	CH_2Cl_2	40	15	100
		2[40]	**2b**	5	CH_2Cl_2	40	15	15
78	**79**							
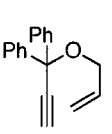	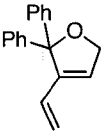	3	**15b**	0.5	CH_2Cl_2	40	15	100
		4	**15a**	0.5	$CHCl_3$	60	15	100
		5[82]	**5c**	1	CH_2Cl_2	0	60	98
		6	**3b**	0.5	CH_2Cl_2	40	15	100
		7[62]	**2b**	5	C_7H_8	80	60	98
80	**81**	8	**2a**	5	CH_2Cl_2	40	60	85
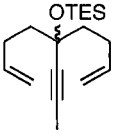	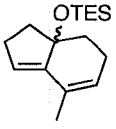	9	**15b**	0.5	CH_2Cl_2	40	15	79
		10	**3b**	0.5	CH_2Cl_2	40	15	68
		11	**15b**	5	CH_2Cl_2	40	20	100
82	**83**	12[82]	**1**	1	CH_2Cl_2	40	8 h	95

[a] [S] = 100 mM, determined by GC-FID (CH_2Cl_2) or ^1H NMR ($CDCl_3$).

References page 147

4.7 Synthesis of Tetrasubstituted Olefins via Enyne Metathesis

4.7.1 Enyne Metathesis Formation of Tetrasubstituted Olefin

The low yield found in the RCM synthesis of tetrasubstituted olefins, in conjunction with the strong performance of **15b** in enyne metathesis, led us to explore the potential of the latter methodology for gaining access to these challenging targets. The less sterically hindered alkyne functionality is potentially a better, smaller, synthon for the target alkene. As well, formation of the conjugated diene product is very exothermic (ΔE = -29.5 kcal/mol for formation of **85**), propelling the reaction forward.

Reaction of enyne **85** with 5 mol % **15a** in refluxing $CDCl_3$ for 6 hours furnished the desired alkene in 70% yield (Table 10). The yield for **15b** was even higher, reaching 85% in refluxing CH_2Cl_2 after 6 hours. Under these conditions, **3b** afforded only 43% of **86**, this figure increasing to 76% after 24 hours. Catalyst **2b** was reported to reach 20% conversion in CH_2Cl_2,[40] or 74% conversion in toluene.[62] The Hoveyda catalysts **5a-c** reach a maximum yield of 17% in CH_2Cl_2. Variants of **2a** containing different NHC ligands (**86-88**) give yields ranging from 5-74%: consistent with the hypothesis that catalyst electrophilicity favours enyne metathesis, the best performance was found for the weakest NHC donor (**88**).[62] However, catalyst **15b** gives access to tetrasubstituted dihydropyran **85** in the highest yield so far reported. Encouraged by this success, we undertook further optimization by high-throughput methods, with quantitative conversion to tetrasubstituted olefin as the primary goal.

Table 10. Formation of a tetrasubstituted alkene from an enyne substrate (5 mol% Ru).

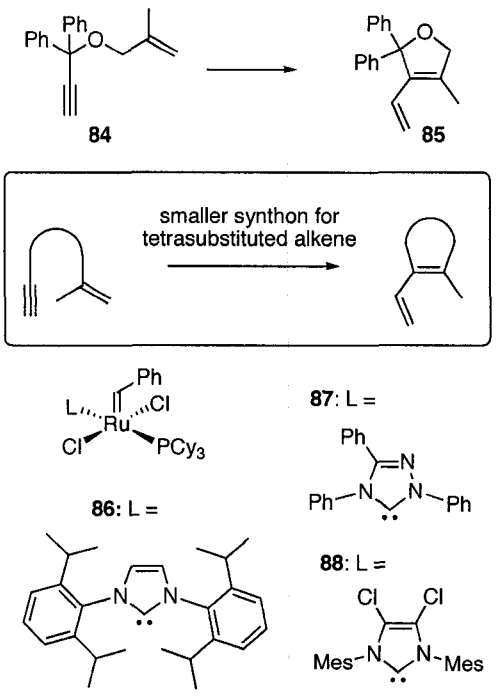

Entry	Cat.	Solvent	Temp. (°C)	Time (h)	Yield[a] (%)
1[40]	**2b**	CH_2Cl_2	40	20	20
2	**3b**	CH_2Cl_2	40	24	76
3[40]	**5a**	CH_2Cl_2	40	20	7
4[40]	**5b**	CH_2Cl_2	40	20	17
5[40]	**5c**	CH_2Cl_2	40	20	0
6[62]	**2b**	Toluene	80	18	75
7[62]	**91**	Toluene	80	18	58
8[62]	**92**	Toluene	80	18	5
9[62]	**93**	Toluene	80	18	74
10	**15a**	$CDCl_3$	60	2	70
11	**15b**	CH_2Cl_2	40	6	85

[a]Determined by ^{1}H NMR or GC-FID.

4.7.2 High-Throughput Catalysis

High-throughput (HT) catalysis involves screening many catalytic reactions in parallel.[83-91] The application of combinatorial chemistry techniques to homogeneous catalysis was born out of necessity, given that the variables governing catalytic behaviour are so many, and the differences that determine success or failure so small. Breakthroughs in enantioselective hydrogenation[90] and olefin polymerization[92] have resulted from this approach. Variables considered may include metal, counter-ion, ligand, ancillary ligand, metal:ligand stoichiometry, catalyst preparation (in situ or otherwise), catalyst loading, reactant or activator, solvent, temperature, pressure, concentration, order and rate of addition, pH, and additives such as acids or bases.[89] These variables are changed systematically to find the solution to a particular problem. For reaction-by-reaction screening, several passes are

required to find optimal conditions (Figure 5). Parallel HT screening methods cover a much greater diversity in experimental conditions than would otherwise be feasible, and can therefore capture unexpected findings.

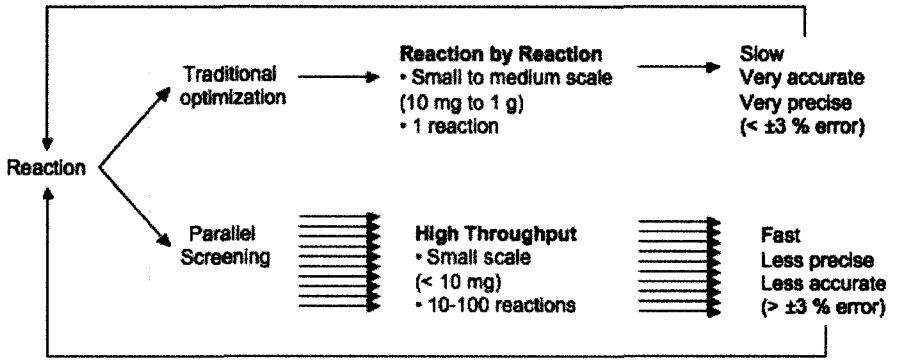

Figure 5. Conventional reaction optimization. vs. high-throughput screening.[84]

In HT catalysis, hardware adapted from the biotechnology sector includes 12×8 well-plates now routine in combinatorial screening, and computer-controlled robotics, which maximize reproducibility in reaction assembly and analysis. The increased costs associated with the large number of reactions is offset by a reduction in reaction volume. Great care is essential to avoid propagation of systematic errors. For instance, the speed of solvent dispensing must be adjusted to minimize splattering, and the minimum volume that can be reproducibly dispensed determined (20 μL in our Symyx system, using the Cavro liquid dispensing robots). Validation of data in "real" benchtop reactions is essential to assure the accuracy of the data, as is replication of experimental data in any reaction.

4.7.3 Screening Strategy for Tetrasubstituted Olefin Formation

Our goal for synthesis of tetrasubstituted **85** from enyne **84** was 100% conversion in less than 10 hours using 5 mol % Ru. A summary of our campaign is shown in Figure 6.

Initial reactions were run at low concentration with a wide set of variables. Control reactions were used to set a bar for yields of **85**, above which variables that increased the yield were passed to the next stage of screening. As the study progressed, precision increased, the number of reactions declined, and reaction scale increased. This screening process culminated in an optimized reaction which was then validated on bench scale. Catalyst **15b** and CH_2Cl_2 solvent were chosen as starting points.

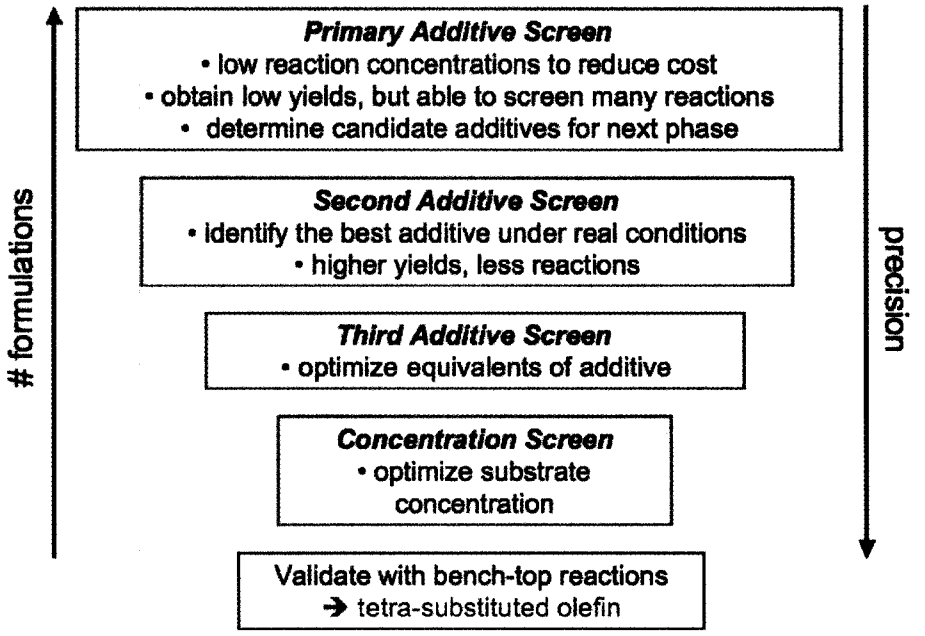

Figure 6. Plan for optimization of the enyne reaction.

Earlier work from our group showing the susceptibility of phenoxide ligands to hydrogen-bonding with added phenols,[93] buttressed by a report from the Sasol group of increased productivity on use of phenol additives in metathesis via **1**,[77] led us to consider using phenol additives to boost the productivity of **15b**. An increase in the electrophilic character of the metal center associated with hydrogen-bonding could increase the reactivity

toward enyne substrate, though diminished initiation efficiency may result (Chapter 6). We chose to screen a range of phenols and other weak acids (Figure 7).

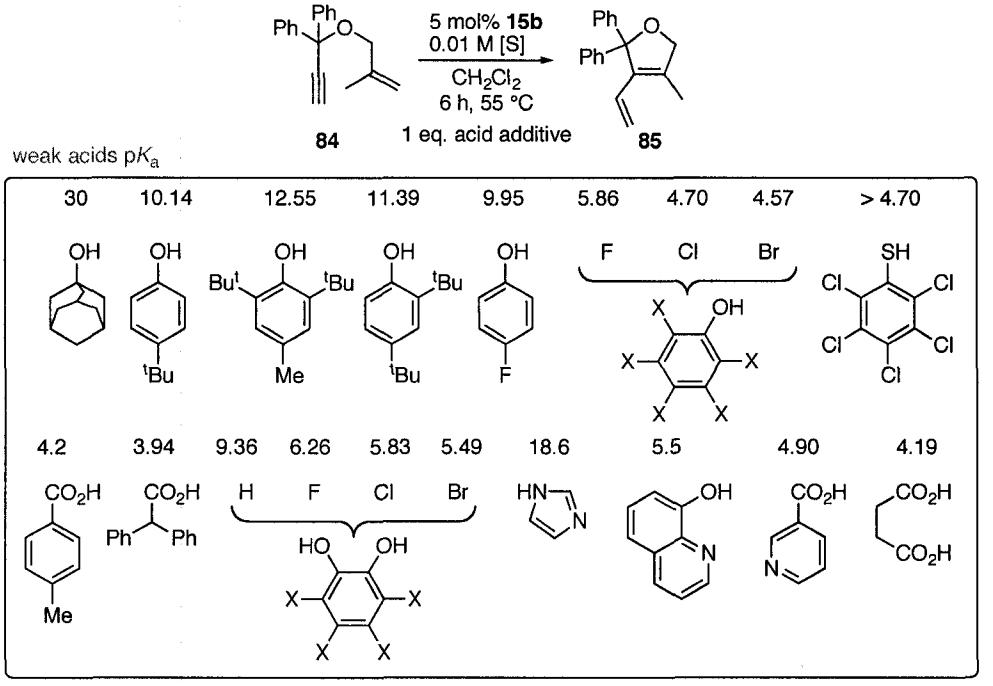

Figure 7. Acid additives screened, with pK_a values.

To minimize the amount of substrate required, screening reactions were carried out at 10 mM **84** (~1 mg per reaction), using a minimum volume of 200 μL to ensure adequate mixing. Yields were limited to <40% in order to evaluate the impact of additives on yield (Figure 8a; average error ±3%). The pass/fail line was set to 36%, the yield of the reaction without additive. Most additives had a negative impact. No correlation between pK_a and yield emerged, indicating that steric factors were also important. Five candidates emerged at this stage, which were then tested at a more realistic substrate concentration of 100 mM. Yields ranged from 25-80%, with 71% for the control reaction (Figure 8b). (The "real"

References page 147

reaction achieves 85% yield, suggesting that the small-scale screening may represent a lower limit).

In the next stage, the proportion of additive was optimized by using a gradient of BHT from 0-100 mol %. The optimal amount of BHT was identified as 80 mol % (0.8 equivalents, relative to substrate, Figure 8c). Finally, we screened for optimum reaction concentration, using larger amounts of substrate in individual screw-top vials. The optimal reaction concentration was 500 mM (Figure 8d). The results were then validated on bench scale (~200 mg) to establish whether the formulation worked, and whether it was superior to the reaction without additive under otherwise identical conditions. The GC yield was 100%, and the isolated yield 93%, vs. values of 87% and 83% for the reaction without BHT. This screening process enabled, for the first time using olefin metathesis, the quantitative formation of a five-membered furan containing a tetrasubstituted olefin. The related methyl/phenyl tetrasubstituted enyne **90**, previously obtained with a maximum conversion of 67% using **2a**,[62] was likewise obtained in 100% yield (84% isolated) by use of BHT as additive (Scheme 6).

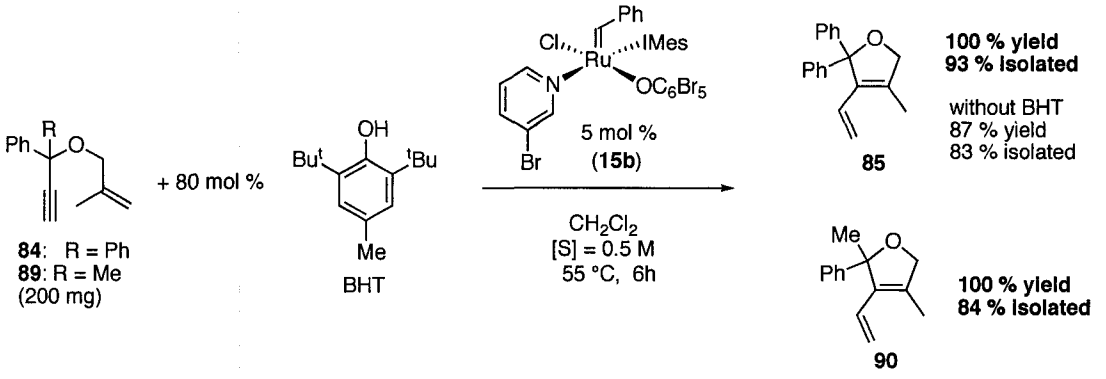

84: R = Ph
89: R = Me
(200 mg)

Scheme 6.

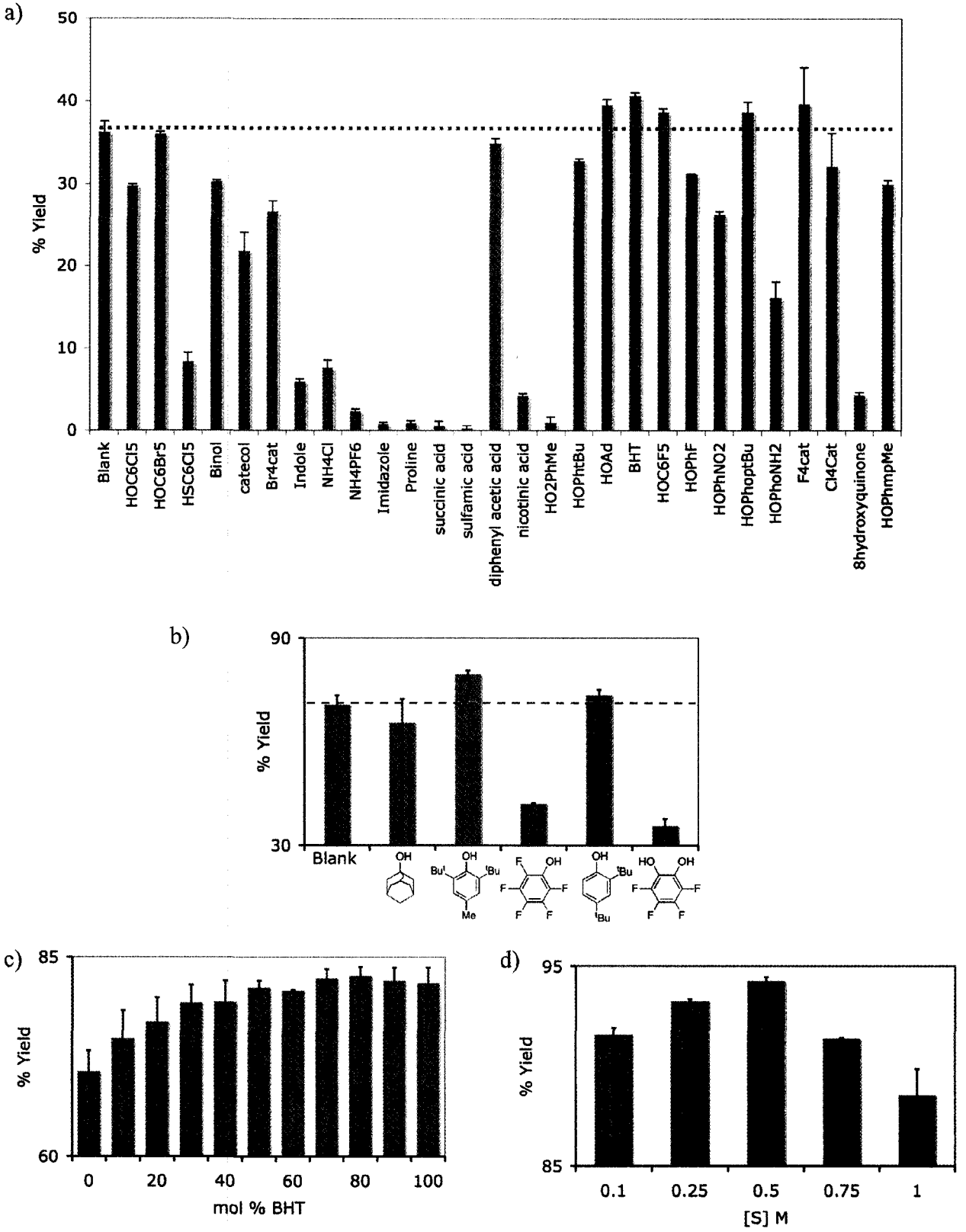

Figure 8. High-throughput optimization results for the production of tetrasubstituted **85**.

4.7.4 The Role of BHT Additive

^{1}H NMR analysis reveals a downfield shift of the benzylidene signal (Scheme 7) on addition of 10 equivalents of BHT to **15b** in C_6D_6. This may indicate an increase in the positive charge on the alkylidene ligand. This would be expected to increase the rate of reaction with olefin, but to decrease initiation (i.e. loss of the pyridine donor ligand). The Sasol study showed that hydrogen-bonding between phenol and **2b** increased the bond dissociation energy of PCy_3 by 5 kcal/mol.[77] BHT may also play a role in trapping the dissociated pyridine, as hydrogen bonding of pyridine to phenol has an enthalpy of -6.8 kcal/mol.[94] While the initiated catalyst can potentially be stabilized by hemi-labile coordination of phenol, the bulk of the ortho *t*-Bu groups would likely inhibit such an interaction for BHT. As a net effect, BHT could create a reservoir of highly active catalyst. The sensitive balance of the various factors involved is illustrated by the failure of the other weak acid additives, all of which were less bulky than BHT, and stronger H-bond donors (BHT, pK_a 12.55; other phenols studied, pK_a <11).

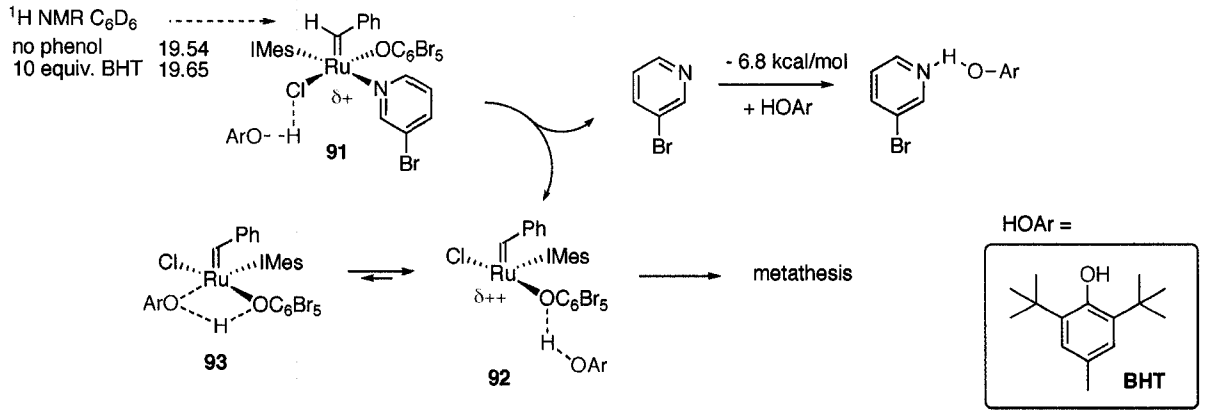

Scheme 7. Proposed mechanisms for effect of phenol on **15b**.

4.8 Removal of Ruthenium Residues from Catalytic Reactions

The advantages of homogenous catalysis, vs. heterogeneous catalysis, are offset by the difficulty in separating the catalysts from the organic products of reaction. This is particularly important where the proportion of trace metals in pharmaceutical products is concerned. A limit of 5 ppm of Pt, Pd, Ir, Rh, Ru or Os residues is set for pharmaceuticals, based on a (high) daily dose of 10 g and a 60 kg body mass. This amount decreases to 0.5 ppm for pregnant women.[95]

The majority of the Ru metathesis catalysts in current use decompose into highly colored byproducts that are difficult to separate from the organic products. Attempts to remove the organic fraction by distillation can trigger olefin isomerization[42,49,96,97] and other undesirable side-reactions catalyzed by the ruthenium species present.[26] Column chromatography is difficult for Grubbs-class catalysts, as described below. In the hope of removing trace Ru, and recycling the expensive catalysts, "flow-through", supported metathesis methodologies have been sought.[17,98-105] Catalyst leaching remains problematic, however, and Blaser notes that supported catalysts are not yet used in fine chemicals production. Further, this leading industrial researcher has commented: "Pharmaceutical users especially do not want to reuse catalysts, because even slight changes in performance can change the profile or stability of a process. We try to optimize for once-through catalyst use... removing trace metals will probably be an issue no matter what catalyst is used."[95] Because we were already able to reduce the amount of catalyst needed for RCM, we focused on post-metathesis removal of a one-use catalyst.

A common protocol used to evaluate purification processes in metathesis involves removal of Ru residues following RCM of **21** with 5 mol % **1**. The maximum amount of

References page 147

ruthenium remaining is 21,000 ppm, or 0.21 wt.%, though crude reaction mixtures are reported to contain 16,900-14,300 ppm (Entries 1-3, Table 11). Silica gel chromatography reduces this to 11,900 or 2,400 ppm, depending on the solvent polarity. Additives used to modify or sequester the spent ruthenium (including lead tetraacetate,[106] triphenylphosphine oxide,[107] polymer-bound diarylphosphines,[108] or water-soluble phosphines)[109] reduce the ruthenium content to 200-1200 ppm (0.2-1.2 μg/mg), while extraction with modified mesoporous silica leaves 776 ppm.[110] By using a relatively polar, methoxy-functionalized Hoveyda-class catalyst **94**, and an appropriate solvent system for chromatography, the Grela group was able to reduce the Ru content to 110 ppm and recycle most of the catalyst.[111] Finally, Cho and Kim decreased the Ru content to ca. 60 ppm by incubating the RCM products with activated charcoal for 12 hours, followed by two cycles of chromatography.[112]

In comparison to the Grubbs catalysts, the Ru-aryloxide complexes have a high affinity for silica gel, which facilitates their separation from non-polar organic compounds. Unlike **1** or **2**, they show minimal "streaking" on the column (Figure 9).[113] A single cycle of flash chromatography[114] afforded colorless oils in which the residual Ru content was below the detection limit in inductively coupled plasma atomic emission spectroscopy (<100 ppm, or 0.1 μg/mg **12a**; <10 ppm with **15b**). This compares favourably to the literature methods for removal of catalyst residues, an advantage for both purification of the organic products and also for solvent recycling.

References page 147

Table 11. Protocols designed to remove spent Ru residues after metathesis.[a]

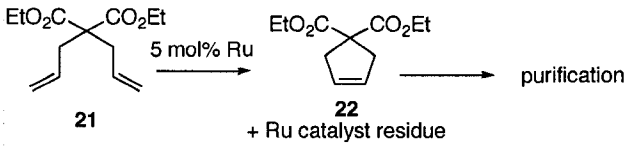

Entry	Cat.	Purification protocol	Yield (%)	Ru ppm (μg/g)
1	**1**[112]	none	95	14,300
2	**1**[109]	none	–	14,900
3	**1**[106]	none	–	16,900
4	**1**[107]	1 cycle chromatography (12% EtOAc /hexanes); filter	95	11,900
5	**1**	1 cycle flash chromatography (12% EtOAc /hexanes)	92	11,900
6	**1**	1 cycle flash chromatography (15% EtOAc /hexanes)	93	2,450
7	**1**[107]	50 equiv PPh_3O, 12 h; 1 cycle chromatography (12% EtOAc /hexanes)	90	240
8	**1**[107]	100 equiv DMSO, 12 h; 1 cycle chromatography (12% EtOAc /hexanes)	90	268
9	**1**[109]	86 equiv $P(CH_2OH)_3$ Triple extraction with water / CH_2Cl_2	–	670
10	**1**[109]	86 equiv $P(CH_2OH)_3$; stir with silica gel, filter	–	206
11	**1**[112]	Activated carbon 24 h;1 cycle chromatography (12% EtOAc / hexanes)	91	60
12	**1**[106]	1.5 equiv $Pb(OAc)_4$ 1 cycle chromatography (CH_2Cl_2)	90	310
13	**1**[110]	modified mesoporous silica	–	776
14	**94**[111]	1 cycle chromatography (CH_2Cl_2, then EtOAc)	96	110
15	**12a**	1 cycle chromatography (5% EtOAc / hexanes)	92	<100
16	**15a**	1 cycle flash chromatography (5% EtOAc / hexanes)	97	<100
17	**15b**	1 cycle flash chromatography (5% EtOAc / hexanes)	90	<10

[a] Standard conditions: 5 mol % catalyst, [**21**] = 100 mM, CH_2Cl_2, 40 °C, 15 minutes. Chromatography on silica gel. Entries 4-12 converted from reported units to ppm (μg/g).

References page 147

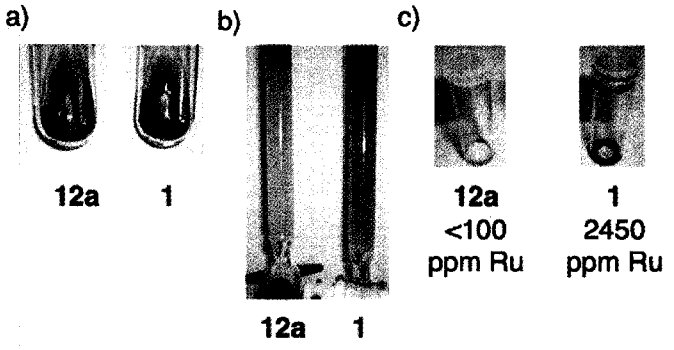

Figure 9. a) Solution of **21** and 5 mol % catalyst. b) Silica gel columns after elution of **22** with 5% EtOAc/hexanes. c) Oils of **22**, post-chromatography, with residual catalyst.

4.9 Alternative Reaction Media: Metathesis in Fluorous Solvent

Section 2 of this chapter described the high activity of the aryloxide catalysts in fluorinated solvents. Fluorous solvents,[115] ionic liquids[116-118] and supercritical CO_2[119,120] can all facilitate product purification and catalyst recycling, providing "green" alternatives to normal organic solvents.[121] Horváth has noted that a key advantage of fluorous solvents is their miscibility with organic solvents at higher temperature, but not at room temperature, enabling extraction of organic-soluble species. Fluorous tags developed to promote catalyst solubility in fluorous media, facilitating separation and recycling,[122] offer transfer of one of the core advantages of heterogeneous catalysts into the homogeneous context.

For aryloxide catalyst **15b**, retention of activity in refluxing FC-72 (perfluorohexane) was interesting, because **15b** is insoluble in FC-72 at 21 °C. This offers a potential means of separating the catalyst by filtration from both the (expensive) solvent and from organic product, prior to extraction of the latter with organic solvent. The perbromoaryloxide ligand thus appears to mimic a fluorous tag with temperature-tunable solubility. The first fluorous-tagged Ru metathesis catalyst, reported by the Yao group,[123] is shown in Scheme 4. A polyfluoroacrylate-bound version of the Hoveyda catalyst (fluorous-**5a**) was heated with

References page 147

substrate **32** in BTF/CH_2Cl_2 until RCM was complete. On cooling to room temperature, the CH_2Cl_2 layer containing **33** separated, leaving the catalyst in the fluorous phase.

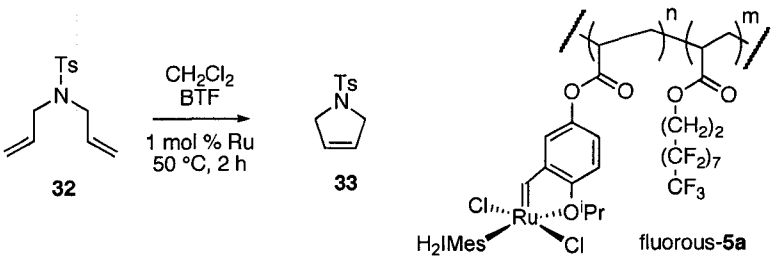

Scheme 8.

In a test reaction, we carried out RCM of substrate **21** with 1 mol % **15b** in FC-72 (Figure 10). Even at 60 °C, the catalyst was only partially dissolved, and RCM required 5 h to complete. The organic product **22** was extracted by adding pentane and cooling to -78 °C to trigger phase separation (Appendix D). The biphasic solution, with its precipitate of **15b**, was then allowed to warm to room temperature, and the upper pentane layer was separated. The coloration of the organic phase indicated the presence of some Ru residues, which were reduced to 205 ppm by filtering through a plug of silica. The fluorous solvent was recovered and purified similarly. Addition of further substrate could potentially have enabled reuse of the catalyst at the bottom of the FC-72 layer, but this aspect was not pursued.

References page 147

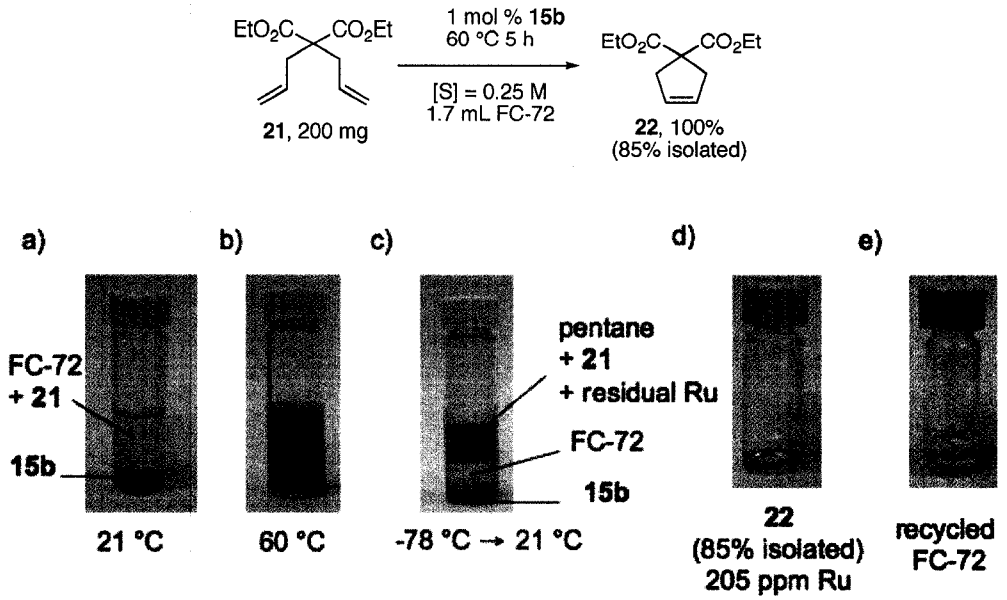

Figure 10. RCM in fluorous solvent: a) 21 °C; b) 60 °C; c) after addition of pentane and cooling; d) isolated **22**; e) recycled FC-72 solution.

4.10 Conclusions.

No catalyst is a magic bullet. For each application, any given catalyst will have advantages or disadvantages that also depend on the substrate. Catalyst screening rapidly identified **15b** as a very good catalyst for olefin metathesis. Although less active (lower TOF) than the "third-generation" Grubbs catalyst **3a** for synthesis of readily cyclized five- or six-membered rings, it proved to be more productive, and more reactive toward challenging substrates (higher TON). The less reactive fluoroaryloxide catalyst **12b** offers longer lifetime and higher selectivity, highlighting the value of the modularity of this catalyst class. A potential bias toward self-metathesis was exploited in the self-metathesis of methyl oleate, where a TON of 860,000 was recorded. Using state-of-the-art catalyst screening equipment, a protocol was developed for quantitative formation of a tetrasubstituted alkene from an enyne substrate. Finally, the aryloxide catalysts are readily separated from organic products

by chromatography. These advantages make the aryloxides highly attractive alternatives to the Grubbs-class catalysts.

4.11 References

(1) Sanford, M.S.; Love, J.A.; Grubbs, R.H. *Organometallics* **2001**, *20*, 5314-5318.
(2) Love, J.A.; Morgan, J.P.; Trnka, T.M.; Grubbs, R.H. *Angew. Chem., Int. Ed.* **2002**, *41*, 4035-4037.
(3) Buncel, E.; Stairs, R.; Wilson, H., *The Role of Solvent in Chemical Reactions*. Oxford University Press: New York, 2003.
(4) Teng, X.; Cefalo, D.R.; Schrock, R.R.; Hoveyda, A.H. *J. Am. Chem. Soc.* **2002**, *124*, 10779-10784.
(5) James, B.; Markham, L. *Inorg. Chem.* **1974**, *13*, 97-100.
(6) Aullon, G.; Bellamy, D.; Orpen, A.G.; Brammer, L.; Bruton, E.A. *Chem. Commun.* **1998**, 653-654.
(7) Slugovc, C.; Demel, S.; Stelzer, F. *Chem. Commun.* **2002**, 2572-2573.
(8) Kirkland, T.A.; Lynn, D.M.; Grubbs, R.H. *J. Org. Chem.* **1998**, *63*, 9904-9909.
(9) Banti, D.; Mol, J.C. *J. Organomet. Chem.* **2004**, *689*, 3113-3116.
(10) Dinger, M.B.; Mol, J.C. *Organometallics* **2003**, *22*, 1089-1095.
(11) Dinger, M.B.; Mol, J.C. *Eur. J. Inorg. Chem.* **2003**, 2827-2833.
(12) Dinger, M.B.; Mol, J.C. *Adv. Synth. Catal.* **2002**, *344*, 671-677.
(13) Halbach, T.S.; Mix, S.; Fischer, D.; Maechling, S.; Krause, J.O.; Sievers, C.; Blechert, S.; Nuyken, O.; Buchmeiser, M.R. *J. Org. Chem.* **2005**, *70*, 4687-4694.
(14) Kingsbury, J.S.; Harrity, J.P.A.; Bonitatebus, P.J.; Hoveyda, A.H. *J. Am. Chem. Soc.* **1999**, *121*, 791-799.
(15) Garber, S.B.; Kingsbury, J.S.; Gray, B.L.; Hoveyda, A.H. *J. Am. Chem. Soc.* **2000**, *122*, 8168-8179.
(16) Hoveyda, A.H.; Gillingham, D.G.; Van Veldhuizen, J.J.; Kataoka, O.; Garber, S.B.; Kingsbury, J.S.; Harrity, J.P.A. *Org. Biomol. Chem.* **2004**, *2*, 8-23.
(17) Jafarpour, L.; Nolan, S.P. *Org. Lett.* **2000**, *2*, 4075-4078.
(18) Van Veldhuizen, J.J.; Gillingham, D.G.; Garber, S.B.; Kataoka, O.; Hoveyda, A.H. *J. Am. Chem. Soc.* **2003**, *125*, 12502-12508.
(19) Buchowicz, W.; Ingold, F.; Mol, J.C.; Lutz, M.; Spek, A.L. *Chem. Eur. J.* **2001**, *7*, 2842-2847.
(20) Sanford, M.S.; Henling, L.M.; Day, M.W.; Grubbs, R.H. *Angew. Chem., Int. Ed.* **2000**, *39*, 3451-3453.
(21) Chang, S.; Jones, L., II; Wang, C.; Henling, L.M.; Grubbs, R.H. *Organometallics* **1998**, *17*, 3460-3465.
(22) Sanford, M.S.; Henling, L.M.; Grubbs, R.H. *Organometallics* **1998**, *17*, 5384-5389.
(23) Hahn, F.E.; Paas, M.; Froehlich, R. *J. Organomet. Chem.* **2005**, *690*, 5816-5821.
(24) Drouin, S.D.; Foucault, H.M.; Yap, G.P.A.; Fogg, D.E. *Can. J. Chem.* **2005**, *83*, 748-754.

(25) Caulton, K.G. *New J. Chem.* **1994**, *18*, 25-41.
(26) Alcaide, B.; Almendros, P. *Chem. Eur. J.* **2003**, *9*, 1259-1262.
(27) Fürstner, A.; Liebl, M.; Lehmann, C.W.; Picquet, M.; Kunz, R.; Bruneau, C.; Touchard, D.; Dixneuf, P.H. *Chem. Eur. J.* **2000**, *6*, 1847-1857.
(28) Fürstner, A.; Picquet, M.; Bruneau, C.; Dixneuf, P.H. *Chem. Commun.* **1998**, 1315-1316.
(29) Yamamoto, Y.; Ohkoshi, N.; Kameda, M.; Itoh, K. *J. Org. Chem.* **1999**, *64*, 2178-2179.
(30) Yamamoto, Y.; Nakagai, Y.-i.; Ohkoshi, N.; Itoh, K. *J. Am. Chem. Soc* **2001**, *123*, 6372-6380.
(31) Spagnol, G.; Heck, M.-P.; Nolan, S.P.; Mioskowski, C. *Org. Lett.* **2002**, *4*, 1767-1770.
(32) Huheey, J.E.; Keiter, E.A.; Keiter, R.L., *Inorganic Chemistry*. 4th ed.; HarperCollins: New York, 1993.
(33) Werner, H.; Grunwald, C.; Stuer, W.; Wolf, J. *Organometallics* **2003**, *22*, 1558-1560.
(34) Hoye, T.R.; Zhao, H. *Org. Lett.* **1999**, *1*, 1123-1125.
(35) Braddock, D.C.; Matsuno, A. *Tetrahedron Lett.* **2002**, *43*, 3305-3308.
(36) Ulman, M.; Grubbs, R.H. *Organometallics* **1998**, *17*, 2484-2489.
(37) Cefalo, D.R.; Kiely, A.F.; Wuchrer, M.; Jamieson, J.Y.; Schrock, R.R.; Hoveyda, A.H. *J. Am. Chem. Soc.* **2001**, *123*, 3139-3140.
(38) Braddock, D.C.; Wildsmith, A.J. *Tetrahedron Lett.* **2001**, *42*, 3239-3242.
(39) Fürstner, A.; Ackermann, L. *Chem. Commun.* **1999**, 95-96.
(40) Michrowska, A.; Bujok, R.; Harutyunyan, S.; Sashuk, V.; Dolgonos, G.; Grela, K. *J. Am. Chem. Soc.* **2004**, *126*, 9318-9325.
(41) Miller, S.J.; Kim, S.-H.; Chen, Z.-R.; Grubbs, R.H. *J. Am. Chem. Soc.* **1995**, *117*, 2108-2109.
(42) Fürstner, A.; Thiel, O.R.; Ackermann, L.; Schanz, H.-J.; Nolan, S.P. *J. Org. Chem.* **2000**, *65*, 2204-2207.
(43) Chatterjee, A.K.; Morgan, J.P.; Scholl, M.; Grubbs, R.H. *J. Am. Chem. Soc.* **2000**, *122*, 3783-3784.
(44) Bassetti, M.; D'Annibale, A.; Fanfoni, A.; Minissi, F. *Org. Lett.* **2005**, *7*, 1805-1808.
(45) Zuercher, W.J.; Hashimoto, M.; Grubbs, R.H. *J. Am. Chem. Soc.* **1996**, *118*, 6634-6640.
(46) Schmidt, B.; Pohler, M.; Costisella, B. *J. Org. Chem.* **2004**, *69*, 1421-1424.
(47) van Rensburg, W.J.; Steynberg, P.J.; Meyer, W.H.; Kirk, M.M.; Forman, G.S. *J. Am. Chem. Soc.* **2004**, *126*, 14332-14333.
(48) Hong, S.H.; Day, M.W.; Grubbs, R.H. *J. Am. Chem. Soc.* **2004**, *126*, 7414-7415.
(49) Cadot, C.; Dalko, P.I.; Cossy, J. *Tetrahedron Lett.* **2002**, *43*, 1839-1841.
(50) Conrad, J.C.; Blacquiere, J.M.; Fogg, D.E. manuscript in preparation.
(51) Conrad, J.C.; Blacquiere, J.; Fogg, D.E. *Organometalics* **2006**, submitted.
(52) Fürstner, A.; Langemann, K. *Synthesis* **1997**, 792-803.
(53) Rivkin, A.; Yoshimura, F.; Gabarda, A.E.; Cho, Y.S.; Chou, T.C.; Dong, H.J.; Danishefsky, S.J. *J. Am. Chem. Soc.* **2004**, *126*, 10913-10922.
(54) Rivkin, A.; Cho, Y.S.; Gabarda, A.E.; Yoshimura, F.; Danishefsky, S.J. *J. Nat. Prod.* **2004**, *67*, 139-143.
(55) Villemin, D. *Tetrahedron Lett.* **1980**, *21*, 1715-18.
(56) Fürstner, A.; Langemann, K. *J. Org. Chem.* **1996**, *61*, 3942-3943.
(57) Lee, C.W.; Grubbs, R.H. *Org. Lett.* **2000**, *2*, 2145-2147 see erratum p 2558.
(58) Kirkland, T.A.; Grubbs, R.H. *J. Org. Chem.* **1997**, *62*, 7310-7318.

(59) Scholl, M.; Ding, S.; Lee, C.W.; Grubbs, R.H. *Org. Lett.* **1999**, *1*, 953-956.
(60) Scholl, M.; Trnka, T.M.; Morgan, J.P.; Grubbs, R.H. *Tetrahedron Lett.* **1999**, *40*, 2247-2250.
(61) Hoye, T.R.; Jeffrey, C.S.; Tennakoon, M.A.; Wang, J.Z.; Zhao, H.Y. *J. Am. Chem. Soc.* **2004**, *126*, 10210-10211.
(62) Furstner, A.; Ackermann, L.; Gabor, B.; Goddard, R.; Lehmann, C.W.; Mynott, R.; Stelzer, F.; Thiel, O.R. *Chem. Eur. J.* **2001**, *7*, 3236-3253.
(63) Langille, N.F.; Panek, J.S. *Org. Lett.* **2004**, *6*, 3203-3206.
(64) Kadota, I.; Yamamoto, Y. *Acc. Chem. Res.* **2005**, *38*, 423-432.
(65) Nelson, S.G.; Cheung, W.S.; Kassick, A.J.; Hilfiker, M.A. *J. Am. Chem. Soc.* **2002**, *124*, 13654-13655.
(66) Weatherhead, G.S.; Ford, J.G.; Alexanian, E.J.; Schrock, R.R.; Hoveyda, A.H. *J. Am. Chem. Soc.* **2000**, *122*, 1828-1829.
(67) Van Veldhuizen, J.J.; Garber, S.B.; Kingsbury, J.S.; Hoveyda, A.H. *J. Am. Chem. Soc.* **2002**, *124*, 4954-4955.
(68) La, D.S.; Sattely, E.S.; Ford, J.G.; Schrock, R.R.; Hoveyda, A.H. *J. Am. Chem. Soc.* **2001**, *123*, 7767.
(69) Chatterjee, A.K.; Toste, F.D.; Choi, T.-L.; Grubbs, R.H. *Adv. Synth. Catal.* **2002**, *344*, 634-637.
(70) Chatterjee, A.K.; Choi, T.-L.; Sanders, D.P.; Grubbs, R.H. *J. Am. Chem. Soc.* **2003**, *125*, 11360-11370.
(71) Forman, G.S.; McConnell, A.E.; Hanton, M.J.; Slawin, A.M.Z.; Tooze, R.P.; van Rensburg, W.J.; Meyer, W.H.; Dwyer, C.; Kirk, M.M.; Serfontein, D.W. *Organometallics* **2004**, *23*, 4824-4827.
(72) Bowman, M.; Hilligoss, D.; Rasmussen, S.; Thomas, R. *Hydrocarbon Processing* **2006**, 103-106.
(73) Grubbs, R.H., *Handbook of Metathesis*. Wiley-VCH: Weinheim, Germany, 2003.
(74) Tsuji, J.; Hashiguchi, S. *Tetrahedron Lett.* **1980**, *21*, 2955-8.
(75) Mol, J.C. *J. Mol. Catal. A* **2004**, *213*, 39-45.
(76) Ulman, M.; Grubbs, R.H. *J. Org. Chem.* **1999**, *64*, 7202-7207.
(77) Forman, G.S.; McConnell, A.E.; Tooze, R.P.; Van Rensburg, W.J.; Meyer, W.H.; Kirk, M.M.; Dwyer, C.L.; Serfontein, D.W. *Organometallics* **2005**, *24*, 4528-4542.
(78) Diver, S.T.; Giessert, A.J. *Chem. Rev.* **2004**, *104*, 1317-1382.
(79) Trost, B.M. *Science* **1991**, *254*, 1471-7.
(80) Trost, B.M.; Toste, F.D.; Pinkerton, A.B. *Chem. Rev.* **2001**, *101*, 2067-2096.
(81) Mori, M.; Sakakibara, N.; Kinoshita, A. *J. Org. Chem.* **1998**, *63*, 6082-6083.
(82) Kim, S.-H.; Zuercher, W.J.; Bowden, N.B.; Grubbs, R.H. *J. Org. Chem.* **1996**, *61*, 1073-81.
(83) Ding, K.; Du, H.; Yuan, Y.; Long, J. *Chem. Eur. J.* **2004**, *10*, 2872-2884.
(84) Hagemeyer, A.; Jandeleit, B.; Liu, Y.; Poojary, D.M.; Turner, H.W.; Volpe, A.F.; Henry Weinberg, W. *Applied Catalysis, A: General* **2001**, *221*, 23-43.
(85) Weinberg, W.H.; Turner, H.W., Impact of High-Throughput Screening Technologies On Chemical Catalysis. In *High Throughput Screening in Chemical Catalysis: Technologies, Strategies and Applications,*, Hagemeyer, A.; Strasser, P.; Volpe, A., Eds. Wiley VCH Verlag GmbH: Weinheim, 2004.
(86) Dahmen, S.; Brase, S. *Synthesis* **2001**, 1431-1449.

(87) Reetz, M. *Angew. Chem., Int. Ed.* **2001**, *40*, 284.
(88) Hoveyda, A.H. *Chem. Biol.* **1998**, *5*, R187-R191.
(89) de Vries, J.G.; de Vries, A.H.M. *Eur. J. Org. Chem.* **2003**, 799.
(90) Jaekel, C.; Paciello, R. *Chem. Rev.* **2006**, *106*, 2912-2942.
(91) Boussie, T.R.; Diamond, G.M.; Goh, C.; Hall, K.A.; LaPointe, A.M.; Leclerc, M.; Lund, C.; Murphy, V.; Shoemaker, J.A.W.; Tracht, U.; Turner, H.; Zhang, J.; Uno, T.; Rosen, R.K.; Stevens, J.C. *J. Am. Chem. Soc.* **2003**, *125*, 4306-4317.
(92) Boussie, T.R.; Diamond, G.M.; Goh, C.; Hall, K.A.; LaPointe, A.M.; Leclerc, M.K.; Murphy, V.; Shoemaker, J.A.W.; Turner, H.; Rosen, R.K.; Stevens, J.C.; Alfano, F.; Busico, V.; Cipullo, R.; Talarico, G. *Angew. Chem., Int. Ed.* **2006**, *45*, 3278-3283.
(93) Snelgrove, J.L. Ph. D. thesis, University of Ottawa, 2004.
(94) Spencer, J.N.; Andrefsky, J.C.; Grushow, A.; Naghdi, J.; Patti, L.M.; Trader, J.F. *J. Phys. Chem.* **1987**, *91*, 1673-1674.
(95) Taylor, A. *Chem. Eng. News* **2005**, *83*, 55-58.
(96) Lehman, S.E.; Schwendeman, J.E.; O'Donnell, P.M.; Wagener, K.B. *Inorg. Chim. Acta* **2003**, *345*, 190-198.
(97) Grasa, G.A.; Moore, Z.; Martin, K.L.; Stevens, E.D.; Nolan, S.P.; Paquet, V.; Lebel, H. *J. Organomet. Chem.* **2002**, *658*, 126-131.
(98) Buchmeiser, M.R. *New J. Chem.* **2004**, *28*, 549-557.
(99) Krause, J.O.; Nuyken, O.; Wurst, K.; Buchmeiser, M.R. *Chem. Eur. J.* **2004**, *10*, 777-784.
(100) Jafarpour, L.; Heck, M.-P.; Baylon, C.; Lee, H.M.; Mioskowski, C.; Nolan, S.P. *Organometallics* **2002**, *21*, 671-679.
(101) Varray, S.; Lazaro, R.; Martinez, J.; Lamaty, F. *Organometallics* **2003**, *22*, 2426-2435.
(102) Grela, K.; Tryznowski, M.; Bieniek, M. *Tetrahedron Lett.* **2002**, *43*, 9055.
(103) Yao, Q.W.; Motta, A.R. *Tetrahedron Lett.* **2004**, *45*, 2447-2451.
(104) Nguyen, S.T.; Grubbs, R.H. *J. Organomet. Chem.* **1995**, *497*, 195-200.
(105) Cetinkaya, B.; Gurbuz, N.; Seckin, T.; Ozdemir, I. *J. Mol. Catal. A* **2002**, *184*, 31-38.
(106) Paquette, L.A.; Schloss, J.D.; Efremov, I.; Fabris, F.; Gallou, F.; Mendez-Andino, J.; Yang, J. *Org. Lett.* **2000**, *2*, 1259-1261.
(107) Ahn, Y.M.; Yang, K.; Georg, G.I. *Org. Lett.* **2001**, *3*, 1411-1413.
(108) Westhus, M.; Gonthier, E.; Brohm, D.; Breinbauer, R. *Tetrahedron Lett.* **2004**, *45*, 3141-3142.
(109) Maynard, H.D.; Grubbs, R.H. *Tetrahedron Lett.* **1999**, *40*, 4137-4140.
(110) McEleney, K.; Allen, D.P.; Holliday, A.E.; Crudden, C.M. *Org. Lett.* **2006**, *8*, 2663-2666.
(111) Michrowska, A.; Gulajski, L.; Grela, K. *Chem. Commun.* **2006**, 841-843.
(112) Cho, J.H.; Kim, B.M. *Org. Lett.* **2003**, *5*, 531-533.
(113) Effiette Sauer, who first remarked upon the ease of separation of **12a** from organic species in studies of the precursor to Weidemannic acid, is gratefully acknowledged for useful conversations on this topic. See Sauer, E. L. O.; Barriault, L. *Org. Lett.* **2004**, *6*, 3329-3332.
(114) Still, W.C.; Kahn, M.; Mitra, A. *J. Org. Chem.* **1978**, *43*, 2923-5.
(115) Horvath, I.T.; Rabai, J. *Science* **1994**, *266*, 72-5.
(116) Audic, N.; Clavier, H.; Mauduit, M.; Guillemin, J.C. *J. Am. Chem. Soc.* **2003**, *125*, 9248-9249.

References page 147

(117) Clavier, H.; Audic, N.; Mauduit, M.; Guillemin, J.C. *Chem. Commun.* **2004**, 2282-2283.
(118) Csihony, S.; Fischmeister, C.; Bruneau, C.; Horvath, I.T.; Dixneuf, P.H. *New J. Chem.* **2002**, *26*, 1667-1670.
(119) Fürstner, A.; Ackermann, L.; Beck, K.; Hori, H.; Koch, D.; Langemann, K.; Liebl, M.; Six, C.; Leitner, W. *J. Am. Chem. Soc.* **2001**, *123*, 9000-9006.
(120) Fürstner, A.; Koch, D.; Langemann, K.; Leitner, W.; Six, C. *Angew. Chem., Int. Ed. Engl.* **1997**, *36*, 2466-2469.
(121) Gladysz, J.A.; Curran, D.P.; Horvath, I.T.; Editors, *Handbook of Flurorous Chemistry*. 2004; p 594.
(122) Horvath, I.T.; Kiss, G.; Cook, R.A.; Bond, J.E.; Stevens, P.A.; Rabai, J.; Mozeleski, E.J. *J. Am. Chem. Soc.* **1998**, *120*, 3133-3143.
(123) Yao, Q.W.; Zhang, Y.L. *J. Am. Chem. Soc.* **2004**, *126*, 74-75.

References page 147

5 Oligomers as Intermediates in Ring Closing Metathesis

5.1 Introduction

In their now-classic text *Olefin Metathesis and Metathesis Polymerization*, Ivin and Mol describe olefin metathesis as a series of equilibria relating diene, cycloolefin, and polyolefin species (Figure 1a).[1] In ring-closing metathesis, however, non-equilibrium processes are routinely invoked, and RCM products are represented as arising solely from diene (Figure 1b).[2-4] In this Chapter we show that neither of these models adequately describes RCM of α,ω-dienes, the dominant class of substrates. A more appropriate representation of these reaction manifolds is that shown in Figure 1c, in which loss of ethylene is essentially irreversible, and RCM products are formed from oligomeric intermediates. Limitations in the methods normally used to monitor RCM reactions are partially responsible for this oversight. This chapter (re)examines in depth the mechanism of RCM, using information from a variety of quantitative and qualitative analytical methods, and places RCM within the context of classic cyclization and polymerization chemistry.

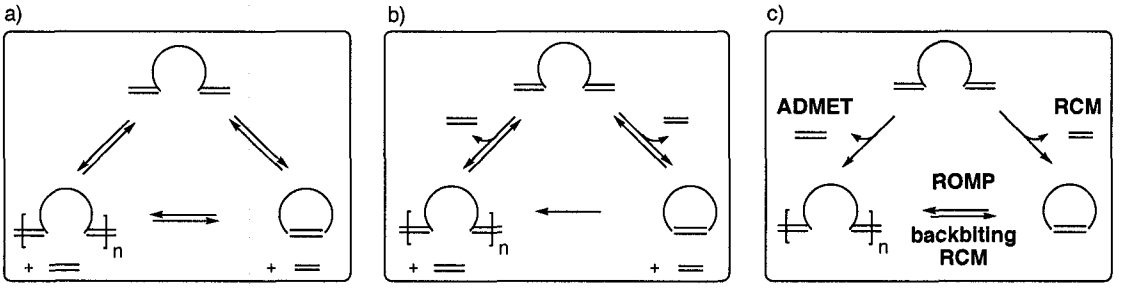

Figure 1. (a) Conventional olefin metathesis manifold, (b) Commonly used manifold,[2-4] (c) More appropriate metathesis manifold for RCM of α,ω-olefins.

5.1.1 Comparison of Classical and Catalytic Cyclization Reactions

Work by Illuminati and Mandolini,[5] among others, has shaped modern understanding of ring closure reactions.[6] The rate of cyclization for uncatalyzed reactions is determined largely by strain in the nascent ring system, and the probability of end-to-end encounter.[5] Both contribute to activation energy, the latter owing to the entropic cost of freezing the disordered open chain into the ring-shaped transition state. Strain results principally from imperfect staggering and transannular strain between atoms forced into proximity from opposite sides of the ring, though early force-field calculations on cycloalkanes suggest that bond angle deformation makes a further, smaller contribution.[7] As a cumulative effect of these factors, the activation enthalpy is high for very small carbocycles (3-4 members), drops sharply for small rings (5-7 members), and increases again for medium-sized rings (8-11 members), in which transannular interactions emerge. Further increases in ring size decrease ring strain, and $\Delta H^{\ddagger}$. While the presence of heteroatoms or unsaturation modulates total strain (as will the presence of a transition metal), these general trends apply to a wide range of ring systems.[5]

For cyclization of small chains, the high probability of end-to-end encounter offsets the loss of rotational freedom in the molecular backbone. As chain lengths increase, however, the probability of intramolecular chain-end encounter drops, while entropic costs associated with loss of rotational freedom in the disordered chain upon ring-closing decrease. $\Delta S^{\ddagger}$ for ring-closing thus decreases with increasing chain size (though this decline ultimately levels off, probably owing to an increase in out-of-plane bending, which can compensate for constraints on internal rotation). At constant concentration, intermolecular reactions become more favourable with increasing chain length, both because of encounter probabilities, and

References page 174

because the loss in translational entropy associated with polymerization becomes less acute with increasing (monomer) chain length, to the point where it may be outweighed by the positive torsional and vibrational entropy resulting from the conformational mobility of the polymer chain. The activation enthalpy and entropy required for uncatalyzed cyclizations to form lactones of three to 18 members were quantified by Illuminati and Mandolini (Figure 2).[5]

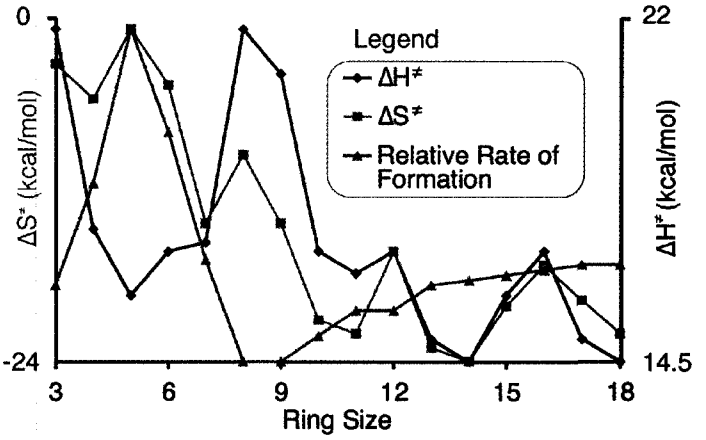

Figure 2. Activation energy parameters and relative rates of (uncatalyzed) ring closing for saturated macrolactones.[5]

For other substrates, a bias toward cyclization can be introduced by incorporating geminal disubstitution. This bias is exerted by means of the gem-dialkyl[8] and Thorpe-Ingold effects (Figure 3).[9] In an impressive demonstration of the power of these effects, Forbes et al. showed that formation of five- and seven-membered rings is favoured over polymerization by acyclic diene metathesis (ADMET) polymers, even in neat substrate. The effect is not invariable, however, and exceptions were also noted, even for five-membered rings.[10]

References page 174

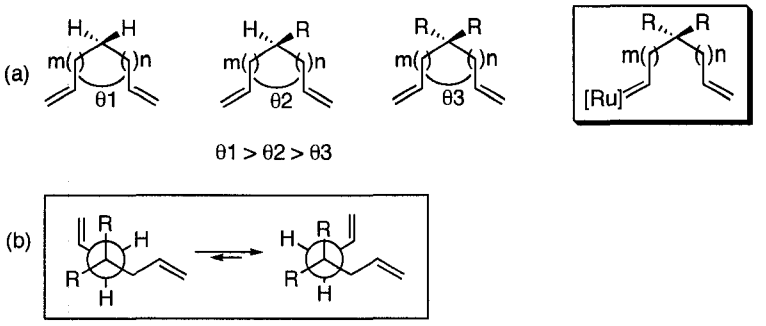

Figure 3. Conformational constraints in acyclic substrates: (a) the Thorpe-Ingold effect; (b) the gem-dialkyl effect.

While the balance between ring strain and the probability of encounter (discussed in terms of effective molarity in Section 5.5) is fundamental to determining the rate of cyclization, the reaction rates and product selectivity are dependent on the nature of the catalyst used, and on reaction concentrations. In his 1980 report on macrolactonization via tungsten-catalyzed RCM, Villemin commented that polymerization was dominant at high diene concentrations (>15 mM), and that cyclization was successful only at ca. 6 mM.[11] In synthesis of large rings, irrespective of the reaction mechanism involved, high dilutions are commonly employed in order to promote cyclization over intermolecular coupling. Most rigorous are the "infinite dilution" conditions developed for macrocyclizations by Ziegler,[12] in which the substrate is infused at a rate equal to or less than the rate of cyclization. This approach is suitable for non-catalytic (e.g. SN2) reactions, because the rate of cyclization exhibits a first-order dependence on diene, where the rate of oligomerization exhibits a second-order dependence. In RCM, however, the reaction of substrate with catalyst is necessarily bimolecular, and the reaction rate will therefore be adversely affected by use of high dilutions. As well, the order of the reaction with respect to substrate is less clear-cut for oligomerization via ADMET processes.

Low yields in RCM are often ascribed to competing intermolecular reactions.[13-15] Although the ADMET products have sometimes been converted to RCM products by use of a more reactive catalyst, or by heating,[16-18] they are generally regarded as a synthetic "dead end". Reaction protocols are therefore designed to minimize oligomerization, albeit at the cost of experimental convenience. In a recent review, Gradilas and Perez-Castells tabulated the conditions used for assembly of macrocycles via RCM.[19] Moderate to low (< 10 mM) concentrations of diene are typical, with catalyst loadings of 5-10 mol % relative to substrate. While true Ziegler conditions are rarely employed, low diene concentration are maintained, either by batch addition of catalyst to substrate in large volumes of solvent, or by slow, dropwise addition of substrate. Reaction times can be very long at room temperature. Elevated temperatures are commonly used to overcome the unfavorable effect of dilution on the reaction rates,[20,21] and to maximize thermal weighting of the entropic parameter. Because catalyst lifetime is short at elevated temperatures, dropwise addition of catalyst is then also advisable.[22] A range of solvents can be employed, among which chlorocarbon and aromatic solvents dominate.

5.2 Identification of Oligomer Intermediates in Ring Closing Metathesis

Our attention was drawn to the potential intermediacy of oligomers in RCM during experiments involving metathesis of diene **58** under modified Ziegler conditions (slow, dropwise addition of substrate and catalyst). While $RuCl(OC_6Br_5)(IMes)(py)(CHPh)$ **15a** effected complete formation of 16-membered **59** by the end of the 15 minute addition period, **1** and **2a** yield <40% **59** at this stage, despite near-complete consumption of **58**. The rapidity of oligomerization is notable, as this indicates a significant kinetic bias toward oligomerization even at diene concentrations significantly below 5 mM (this being an upper

limit that would be achieved by batch addition of **58**). Importantly, however, ring-closing is near-quantitative on longer reaction (**1**: 1 h; **2a**: 9 h). The mechanistic implications of this observation are discussed in detail below. First, however, the details of the analytical methodologies on which the observation rests will be examined, both to validate the claim that oligomers are formed as the initial reaction products, and to understand why this behaviour has not been more generally recognized.

5.2.1 Monitoring RCM

At the initial stages of this investigation, RCM reactions were monitored by 1H NMR analysis. A discrepancy, however, emerged between NMR and subsequent TLC and GC analyses, which we ultimately traced to formation of oligomeric species (Section 5.2.2). The utility of NMR methods is limited by the resemblance between spectra of the oligomers, and those of a mixture of diene and RCM product. A representative series of spectra is shown in Figure 4 for **58**: similar results were found for other substrates described in this chapter. The resemblance between the component spectra complicates attempts to measure reaction rates from either the rate of disappearance of diene, or that of appearance of product. This behaviour is of considerable concern, as NMR analysis is one of the most common and convenient methods of monitoring RCM reactions, and yet its limitations appear to have gone unrecognized. Literature reports in which the extent of reaction is quantified by ^{1}H NMR analysis alone should therefore be treated with caution.

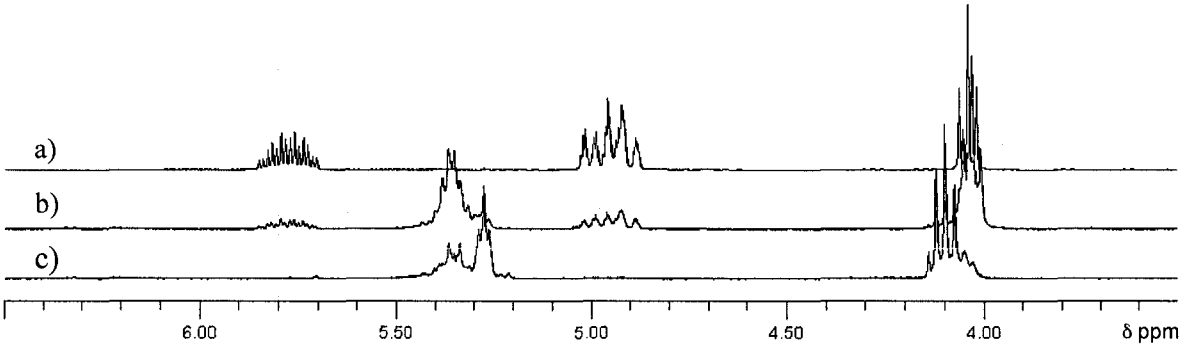

Figure 4. Olefinic region of the ^{1}H NMR spectrum of (a) diene **58**, (b) oligomer **poly-58** (c) RCM product **59** ($CDCl_3$, 300 MHz).

Given the unreliability of NMR analysis, we turned to GC analysis. Quantification of reaction rates (i.e. the proportions of the diene starting material and RCM product) requires the construction of calibration curves from which response factors can be extracted. Tetrahydronaphthalene was used as an internal standard, at a concentration approximately half to that of diene, to correct for small variations in operational conditions (non-systematic errors). A typical GC trace for the RCM reaction of **58** (5 mol % **2a**, refluxing CH_2Cl_2, dropwise addition of catalyst and substrate; final concentration 5 mM), is shown in Figure 5a. The initial peak areas for the diene **58** and tetrahydronaphthalene were approximately equal. After 15 minutes, the signal for **58** had nearly disappeared, and small peaks for the product (**59**) began to emerge. After 5 h the reaction was complete. The peak area for **59** (two peaks; mixture of *E* and *Z* isomers) is equal to that of starting **58**, weighted by the ratio of the response factors for these two species (1.39 for **58**/**59**). Noteworthy in Figure 5b is the discrepancy between the amounts of diene consumed and cycloolefin produced at intermediate reaction times, indicating formation of species too involatile to be observed under our analytical conditions (maximum oven temperature 225 °C). Evidence for the oligomeric nature of these intermediates is discussed below. All RCM reactions discussed

were analyzed as described above, with direct measurement of the proportion of diene and RCM product, and the proportion of oligomers being inferred by difference. The data are tabulated in Appendix A.

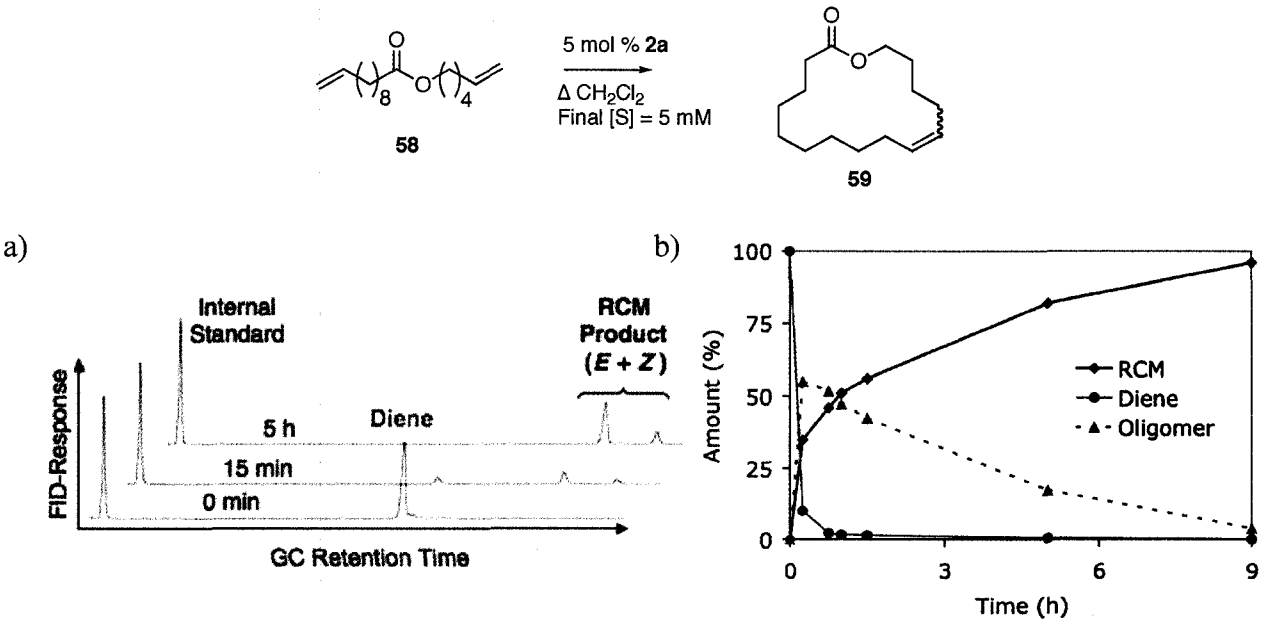

Figure 5. a) GC-FID traces showing the progress of RCM of **58** to yield **59**. b) Plot of calibrated amounts of **58** and **59** over time.

5.2.2 Characterization of Oligomers

Qualitative evidence for oligomeric intermediates was provided by TLC analysis of reaction mixtures at intermediate stages of reaction. For RCM reactions using 5 mM of substrate **58** and 5 mol % **2a** in CH_2Cl_2, faint spots were observed below those due to diene and product (retention factors R_f of 95–75; 10% EtOAc/hexanes; Appendix B). On reaction at 100 mM diene, these spots became much more intense (Figure 6). Multiple spots were observed, consistent with the presence of chains of different lengths (R_f 53–0, Figure 6). Chromatographic isolation yielded greasy solids which were subjected to mass spectrometric analysis.

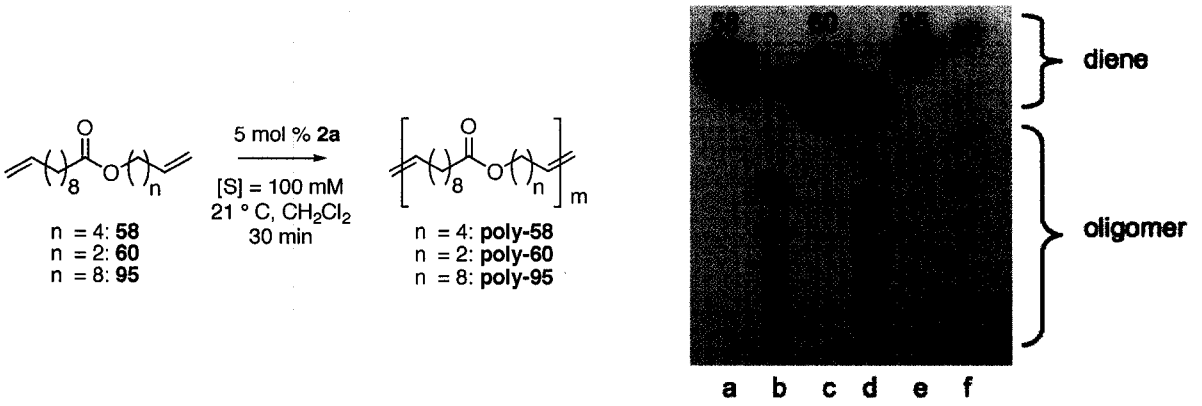

Figure 6. TLC analysis of RCM reactions, using a 10% EtOAc/hexanes mixture. (a) **58**, (b) **poly-58**, (c) **60**, (d) **poly-60**, (e) **95**, (f) **poly-95**. Developed with anisaldehyde stain.

MALDI-TOF mass spectrometric analysis was carried out on a sample in which the involatile component was maximized by use of high diene concentrations (i.e. 100 mM **58**; CH_2Cl_2, 5 mol % **2a**). Dithranol was used as matrix. The spectrum showed strong signals for dimer and a cyclotrimer, and weak signals corresponding to intact pentamer, hexamer, etc. Many fragments containing 2-6 repeat units are also evident (Figure 7; the fully assigned spectrum is shown in Appendix B). A second spectrum was obtained by carrying out metathesis at the standard dilutions of 5 mM, under the conditions indicated in Figure 5, and arresting the reaction at 15 minutes. A greasy solid was obtained by stripping off the solvent. A sample of this material, co-crystallized with pyrene as the MALDI matrix, gave a mass spectrum showing signals for a trimer, and a tetramer that had undergone a McLafferty rearrangement (Appendix B).

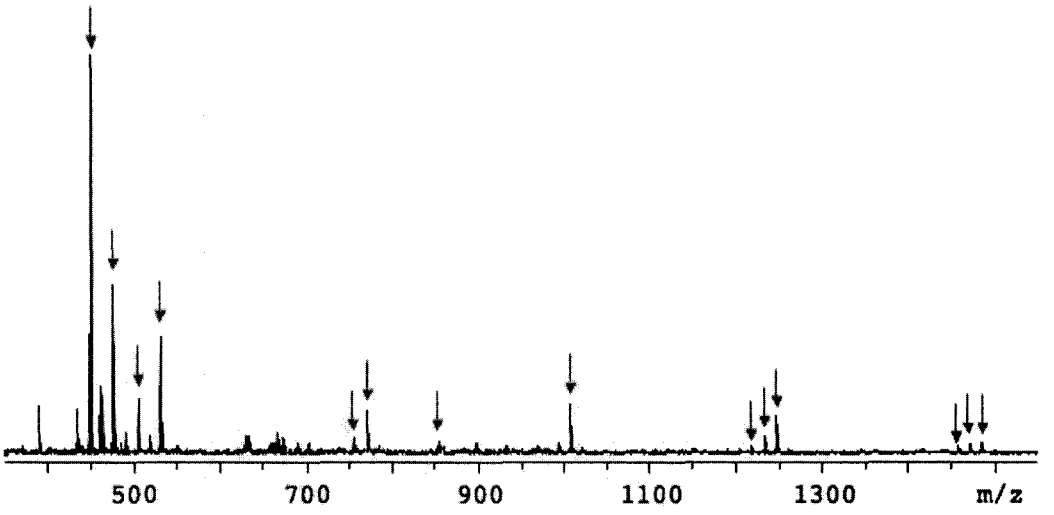

Figure 7. MALDI-TOF MS spectrum of poly-**58**. The arrows indicate signals assigned to oligomers.

While mass spectrometry confirms the formation of oligomeric intermediates, attempts to confirm molecular weights by gel permeation chromatography (GPC) were fruitless, as the GPC columns available in our laboratories and others nearby are optimized for significantly higher molecular weight polymers (10,000-1,000,000 Da). The average chain length of the isolated oligomers (prepared from **58**, **60** and **95**; 5 mM, CH_2Cl_2; 5 mol % **2a**, 21 °C) was estimated by ^1H NMR endgroup analysis, by measuring the relative integrated intensities of the signals for the terminal and internal alkenes. These values are summarized in Appendix B. The discussion in Section 5.1.1 suggests that the chain length of the oligomer should increase in tandem with increasing length of the diene "monomer". Consistent with this, the longest chain (estimated at 18 repeat units) is found for the largest substrate, **95**. While qualitatively useful, these data should be treated with some caution, as cyclooligomers may also be present, in which no endgroups are present.

5.3 Mechanism

5.3.1 Loss of Ethylene

A major driving force for both RCM and CM of terminal olefins is the loss of ethylene. While the ethylene evolved can in principle reenter the catalytic cycle, its low solubility in organic solvents, particularly at elevated temperatures (<1 mM in toluene at 45 °C, even under 1 atm C_2H_4),[23] favours volatilization. RCM in refluxing solutions under Ar or N_2 further improves the efficiency of degassing, and evolution of ethylene can be presumed to be essentially irreversible. This precludes operation of the classic, equilibrium manifold for diene metathesis. Efficient volatilization of ethylene biases metathesis of diene in favour of CM or RCM. Because the low concentration of ethylene prevents quantitative, or indeed significant, depolymerization of ADMET products, an alternative explanation is required for the near-quantitative formation of RCM products from ADMET oligomers.

5.3.2 RCM via an Oligomerization-Backbiting Mechanism

The formation of significant amounts of involatile materials during diene metathesis, the identification of the involatile materials as ADMET products, and the literature evidence for irreversible loss of ethylene under RCM conditions, can be summed up as evidence that near-quantitative macrocycle formation is *preceded* by significant and irreversible ADMET oligomerization. The inescapable conclusion is that the ADMET oligomers can be efficiently degraded into the macrolactones. A mechanism enabling formation of RCM products from the oligomers, via reinstallation of the ruthenium endgroup and backbiting extrusion of cyclic species, is shown in Scheme 1.

References page 174

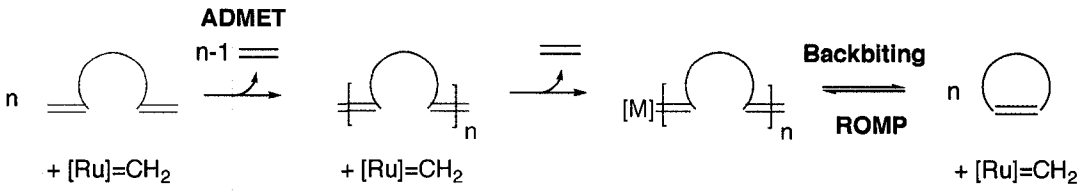

Scheme 1.

Degradation of oligomers to cyclic products via concentration-dependent oligomerization-cyclodepolymerization reactions form the basis of ring-chain equilibria long recognized in polymer chemistry, and discussed extensively in the ROMP literature.[24,25] In cyclodepolymerization of polybutadiene, for example, polymer chains dominate at high concentrations (1.8 M), but extrusion of trimeric rings is thermodynamically favoured at 0.13 M, with smaller cyclooligomers emerging at lower concentrations. This behavior is described by Jacobson-Stockmayer theory and its descendants,[25-27] among which a recent modification by Kornfield and co-workers takes into account the effect of ring strain.[28,29] Reaction of the ADMET oligomers with the [Ru]=CH_2 catalyst installs the ruthenium endgroup on the oligomer chain, and enables the backbiting essential to establish the equilibrium between the oligomers and cyclic species. Where ring strain is present in the RCM product (or indeed in the cyclooligomers formed by backbiting at a remote site), ROMP can occur as the reverse reaction. The position of equilibrium is thus determined by the ring strain, vs. entropic factors (including translational entropy). In the extreme of high concentration (0.7 M and higher), Hodge and Kamau reported entropically *driven* ROMP of macrocycles with 21-84 ring atoms.[30]

The relevance of ring-chain equilibria to RCM has been surprisingly little discussed. In a rare exception, the Grubbs group employed alkali metal ions as templates to aid in metathesis cyclodepolymerization of linear polyethers.[31] Solely ADMET oligomers were

References page 174

observed at a diene concentration of 1.2 M, but crown ethers were produced at 20 mM and 50 °C in the presence of Li^+. This example is revisited in Section 5.5.

5.3.3 Optimum Reaction Conditions for RCM

As the foregoing suggests, concentration is critically important to the success of RCM reactions, where the products are characterized by any significant degree of ring strain. At high concentrations of conformationally flexible dienes, unsurprisingly, intermolecular reactions dominate, while at very low concentrations intramolecular cyclization is favoured. These effects are illustrated in Figure 8. At 100 mM, the reaction of **2a** with **58** produced 95% oligomers. Reaction at 5 mM, gave oligomers as the kinetic products, which disappear to give the ring-closed product.

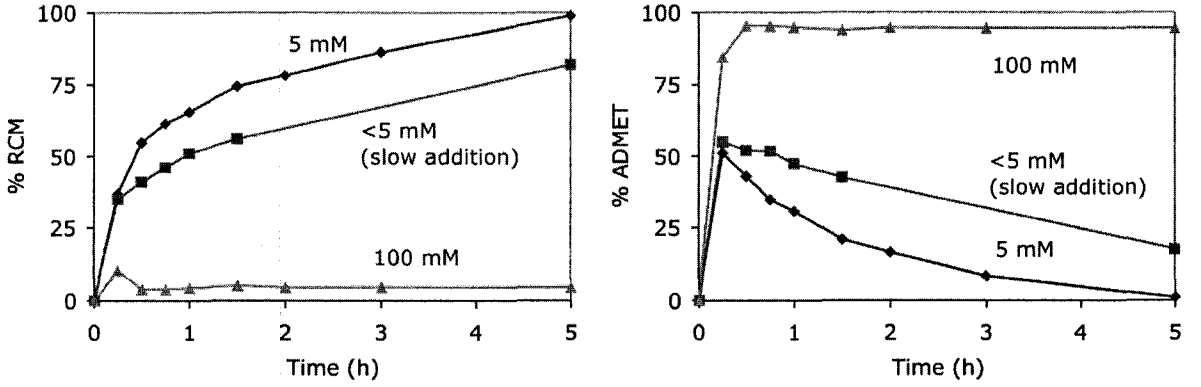

Figure 8. Progress of the reaction of **58** with catalyst **2a** using different substrate concentrations.

The obvious question, if oligomerization is the dominant route to RCM products, is if the cumbersome reaction protocols designed to limit oligomerization are needed. Indeed, simply mixing substrate **58** and catalyst **2a** at 100 mM to enable oligomerization (>80%),

then diluting to 5 mM at 15 minutes, reduces the reaction time dramatically. Essentially quantitative yields of the RCM product **59** were obtained within 1 h (Appendix A), as compared to 9 h under the standard conditions. Clearly, maximizing the initial oligomerization can offer an exceptionally efficient route to RCM products. Limitations can be envisaged, however, where oligomer solubility is an issue.

5.4 Generality of the Oligomerization-Backbiting Mechanism: Substrate Scope

The generality of this mechanism was explored using a substrate concentration of 5 mM in CH_2Cl_2 with 5 mol % **2a** at 21 °C for 15 minutes, then heating to reflux until the maximum amount of RCM product is obtained. The concentration was then changed as required.

5.4.1 Macrolactones

Macrolactones larger and smaller than **59** likewise form via the oligomerization-backbiting mechanism. During RCM synthesis of 14-membered lactone **61** (5 mM CH_2Cl_2, 5 mol % **2a**, refluxing CH_2Cl_2), up to 39% oligomer was formed at 15 minutes, which over a further 3 h yielded 94% **61**. Under the same conditions, substrate **95** gave 55% oligomers at 15 minutes, and 91% of the 20-membered macrolactone **96** after 3 h (Appendix A). For precursors **58**, **60**, and **95**, the degree of oligomerization at 15 minutes (32, 51 and 55%) mirrors the order of increasing diene chain length.

5.4.2 Medium Sized Rings (7-10 members)

Medium ring sizes are much more difficult to form, as discussed above (Section 5.1.1). Surprisingly, despite the well-documented importance of concentration in classical syntheses

of medium-ring systems, recent reviews of RCM approaches to such targets focus only on conformational and stereoelectronic means of biasing reactions toward cyclization.[32,33] We find that control over diene concentration offers a much more general means of access, albeit with limits (Table 1). Even at 0.05 mM **99**, RCM to form eight-membered lactone **100** (5 mol % **2a**, refluxing CH_2Cl_2) proved impossible, the relatively high ring strain inhibiting backbiting. Only oligomers and unreacted diene were observed. The presence of the latter indicates that the rate of reaction between catalyst and diene at this concentration has declined below the rate of unimolecular decomposition of the [Ru]=CH_2 catalyst.[34] At a concentration of 0.5 mM, all of the diene was consumed, but only oligomers were formed.

Decreasing the ring size of the target RCM product to seven members enabled cyclization, as expected from Figure 2. Formation of lactone **102** was limited to 22% at a diene concentration of 5 mM, with the balance of the material being oligomers; at 2.5 mM, 49% of the RCM product was obtained, increasing to nearly 80% at 0.5 mM. For ten-membered lactone **98**, 95% RCM was attained at this concentration, vs. a maximum of ca. 40% at 5 mM. Similar behaviour is found for the seven-membered malonate **104**, for ten-membered catecholate **106**, and for crown ether **112**. In each case, oligomerization was evident even at 5 mM (Table 1). The tenfold higher dilution required for the medium-sized rings, relative to the macrolactones, as well as the greater bias toward cyclization of diethyl diallylmalonate **21** and catechol ether **43**, are consistent with the theory of effective molarity advanced by Mandolini and Illuminati, and described in the next section.

References page 174

Table 1. Yields of RCM and ADMET products as a function of concentration.[a]

Diene Substrate	RCM Target	Target: ring size (EM_k) (EM_k in mM)	[S] (mM)	T_{max} (h)	% oligomers[b] / T_{max} (15 min)	% RCM at T_{max}
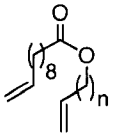	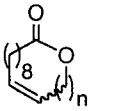	**59**: 16 (29)	100	0.25	85 (85)	10
			100-5[c]	1	0 (82)	97
			5	5	0 (51)	99
			Z–5[d]	9	4 (55)	96
n = 4, **58**	n = 4, **59**	**61**: 14 (24)	5	3	3 (32)	94
n = 2, **60**	n = 2, **61**	**96**: 20 (–)	5	3	5 (55)	91
n = 8, **95**	n = 8, **96**					
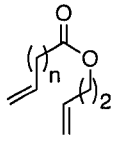	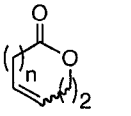	**98**: 10 (1.9)	5	0.5	52 (10)	41
			0.5	0.75	5 (6)	95
		100: 8 (0.57)	5	0.75	99 (12)	0
			0.05	3	66 (25)	0
		102: 7 (55)	5	0.75	56 (20)	29
			0.5	3	22 (7)	78
n = 4, **97**	n = 4, **98**					
n = 2, **99**	n = 2, **100**					
n = 1, **101**	n = 1, **102**					
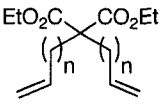	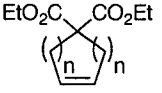	**104**: 7 (23)	5	0.5	52 (49)	48
			0.5	0.75	50 (45)	49
		21: 5 (2.1 x 10^6)	100	0.25	0 (0)	100
n = 1, **20**	n = 1, **21**					
n = 2, **103**	n = 2, **104**					
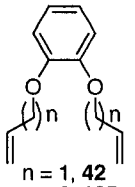	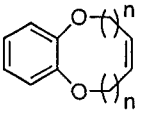	**106**: 10 (28)	5	1	58 (44)	41
			2.5	0.5	53 (21)	43
			0.5	0.5	14 (7)	85
		43: 8 (750)	100	0.75	21 (18)	61
			5	0.5	0 (0)	99
n = 1, **42**	n = 1, **43**					
n = 2, **105**	n = 2, **106**					
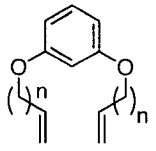	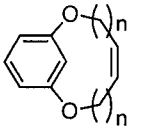	**110**: 13 (2)	5	0.5	98 (78)	0
			0.5	3	93 (42)	0
		108: 11 (<2)	5	0.75	97 (95)	0
			0.5	3	93 (29)	0
n = 1, **107**	n = 1, **108**					
n = 2, **109**	n = 2, **110**					
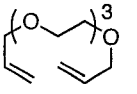	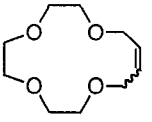	**112**: 14 (–)	5	0.5	96 (100)	4
			2.5	0.5	29 (39)	68
			0.5	0.5	8 (24)	92
		(+ 5 eq. $LiClO_4$)	20	1	0	>95[e]
111	**112**					

[a] Conditions: 21 °C for 15 min then Δ CH_2Cl_2. Entries for substrates **106-112** recorded by Sebastien Monfette or Jõao Duarte Silva of this lab. Substrate conversion, % RCM measured by externally calibrated GC-FID. Identity of RCM products confirmed by GC-MS. *Trans/cis* ratios of product at highest conversion: **59**, **96**, 72:28; **61**, 89:11; **98**, 41:59; **106**, **21**, **102**, **43**, 0:100; **112**, 53:47. EM_k values see Ref. 5. [b] Calculated by difference. [c] Initial concentration 100 mM, diluted to 5 mM after 15 min. [d] Z = Ziegler conditions. [e] see Ref. 31.

5.5 Effective Molarity

The kinetic preference for diene oligomerization, even at millimolar concentrations, is a key factor biasing RCM toward the oligomerization-backbiting mechanism. The trend in the initial proportion of oligomerization for different substrates is consistent with trends observed by Mandolini and Illuminati in a classic series of papers describing the competition between cyclization and oligomerization of bifunctional substrates.[5] The competition was analyzed in terms of the kinetic effective molarity (EM_k) of the substrates examined. The EM_k value represents the concentration at which the rates of intermolecular and intramolecular reaction are equal (Scheme 2), higher values reflecting a lower susceptibility to oligomerization. EM_k values are generally insensitive to the nature of the reacting groups, reaction medium, or mechanism: to a good approximation, they are determined by the number and nature of skeletal bonds in the transition state for cyclization.[5]

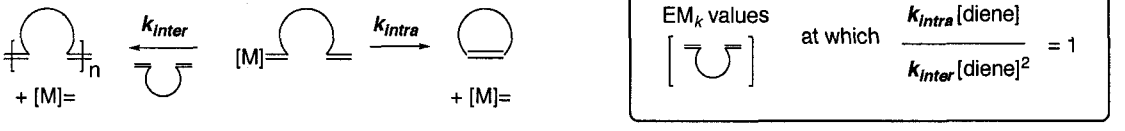

Scheme 2. Illustration of the concept of effective molarity in context of metathesis.

The data discussed in the previous section are consistent with the trends in the EM_k values, which suggest the generality of the oligomerization-backbiting pathway. Thus, EM_k values for macrolactones (14-20 members; 24–29 mM)[35] are *higher* than those for medium-sized lactones (8-13 members, 0.57–2 mM)[35] or diethyl malonates (8-10 members, 0.39 mM–3.6 nM).[36] Values for 7-membered malonate (23 mM)[36] and lactone (55 mM)[35] rings are similar, or only slightly greater. The data in Table 1 show that oligomerization occurs,

even at 5 mM, for all systems studied in which the EM_k values were 55 mM or less. Subtrates with a high conformational bias, such as diethyl diallylmalonate **20** (EM_k 2100 M)[36] or 8-membered catechol polyether **43** (EM_k 750 mM),[37] undergo RCM without apparent formation of ADMET products at 5 mM. These high EM_k values reflect the low ring strain, resulting from the presence of the sp^2 carbons and the oxygen atoms in the 8-membered ring for **43**,[38] and by the Thorpe-Ingold and gem-dimethyl effects (Section 5.1) for **20**. Indeed, **20** is readily cyclized to 5-membered **21** even at 100 mM, though **42** yields ADMET oligomers at this concentration. ADMET has been reported to occur on metathesis of neat *dimethyl* diallylmalonate.[10] At "normal" concentrations, however, the combination of low ring strain and a high probability of end-group encounter favors direct RCM. *Conversely, the oligomerizaton-backbiting pathway can be expected to apply to any conformationally flexible substrates leading to ring sizes greater than six.*

Finally, where EM values are 1.9 mM or below (Table 1), no RCM was observed. Thus, ansa-bridged **107** (EM_k 2 mM)[39] and **109** did not cyclize to **108** or **110** at 0.5 mM, owing to excessive ring strain. Attempts to form lactone **100** (EM_k 0.57)[35] also failed, as noted above. This underscores the point that use of substrate concentrations substantially below the EM_k values to enforce direct RCM is not feasible, because the resulting reduction in the rate of the bimolecular reaction between substrate and catalyst means that the rate of metathesis can no longer compete with that of catalyst decomposition.

It will be noted from Table 1 that the substrate concentrations required to shift the ring-chain equilibrium in favor of RCM products was lower for the medium-ring products than large rings. While consistent with the trends in EM_k values for most substrates, the need for higher dilutions to induce cyclization to 7-membered **102** (EM_k 55 mM) vs.14-16-membered **58-60** (EM_k 24-30 mM), was initially puzzling. The explanation lies in the fact

that EM_k values are kinetic in origin, while the product distribution at equilibrium is not. It will be noted that the initial proportion of ADMET species is lower for **102** at constant concentration, consistent with the trends in EM_k values. To account for the unexpectedly high concentration-dependence in the yield of **102**, the thermodynamic effective molarity (Scheme 3) must be considered.[40]

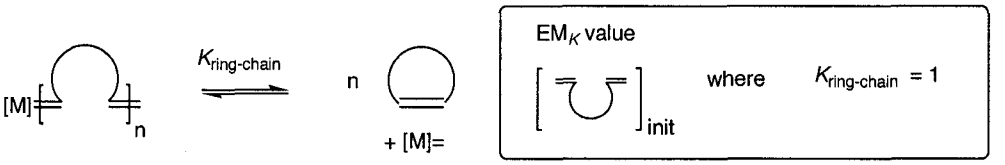

Scheme 3. Representation of the concept of thermodynamic effective molarity (EM_K) in context of metathesis.

While EM_K values are less extensively documented than EM_k values, saturated lactones have been comprehensively examined.[40] Trends in EM_K values generally track with trends in EM_k, but the values for the 7-membered lactone are an exception. Despite its higher EM_k value, relative to (e.g.) the 14-membered lactone, its EM_K value is ca. 15 times lower. Accordingly, efficient formation of 7-membered **102** requires dilution to 0.5 mM, where 14-membered **61** is fully formed at 5 mM.

These findings are summarized in Figure 9. The trend in the proportion of RCM product formed under kinetic control (15 minutes, 21 °C; 5 mM diene) corresponds closely with the trend in EM_k values for SN2 lactonization of ω–bromo acids.[5] The agreement suggests minimal perturbation by the presence of unsaturation in the metathesis intermediates, and the presence of the metal in the transition state for cyclization (though the impact of these factors can be expected to increase at smaller ring sizes). The amount of oligomer formed initially is determined by kinetic parameters inherent in the substrate and, presumably, the catalyst structure, which dictate the balance between ring strain and the

probability of encounter. Where ring strain does not prohibit cyclization, backbiting yields RCM products as the reaction evolves toward equilibrium (40 °C).

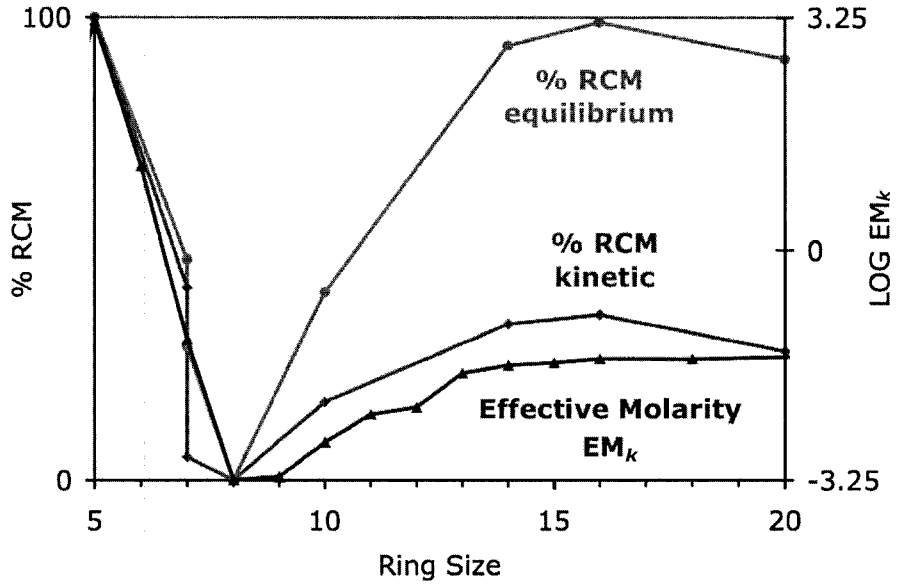

Figure 9. Yields for RCM products, and log EM_k values for SN2 lactonization of ω–bromo acids,[5] as a function of ring size.

5.6 Revised RCM Mechanism

A revised mechanism for ring-closing metathesis is shown in Figure 10. Selectivity for direct RCM or for oligomerization occurs following initial formation of intermediate **A**, and reflects the kinetic preference of this species for intramolecular cyclization, vs. intermolecular reaction. Direct RCM is favoured for unstrained rings where a strong conformational driving force is present, but – as the foregoing indicates – the strain otherwise present in the transition state for cyclization biases the reaction toward oligomerization. Reinstallation of a ruthenium endgroup on the ADMET oligomer enables either propagation, via reaction with further diene, or backbiting reaction with a pendant alkene, resulting in extrusion of a cycloolefin. Provided that the lifetime of the catalyst is sufficient (a factor that can be strongly affected by concentration, and hence reaction rate, as

well as temperature), the ADMET and/or RCM reactions continue until the diene is completely consumed. The backbiting reaction can extrude either the desired RCM product, or larger cyclooligomers, with the former being favoured at higher dilutions. Finally, the cycloolefins can themselves undergo ROMP, and the ROMP-backbiting equilibrium is likewise a sensitive function of thermodynamic parameters that can be manipulated by altering the reaction concentration.

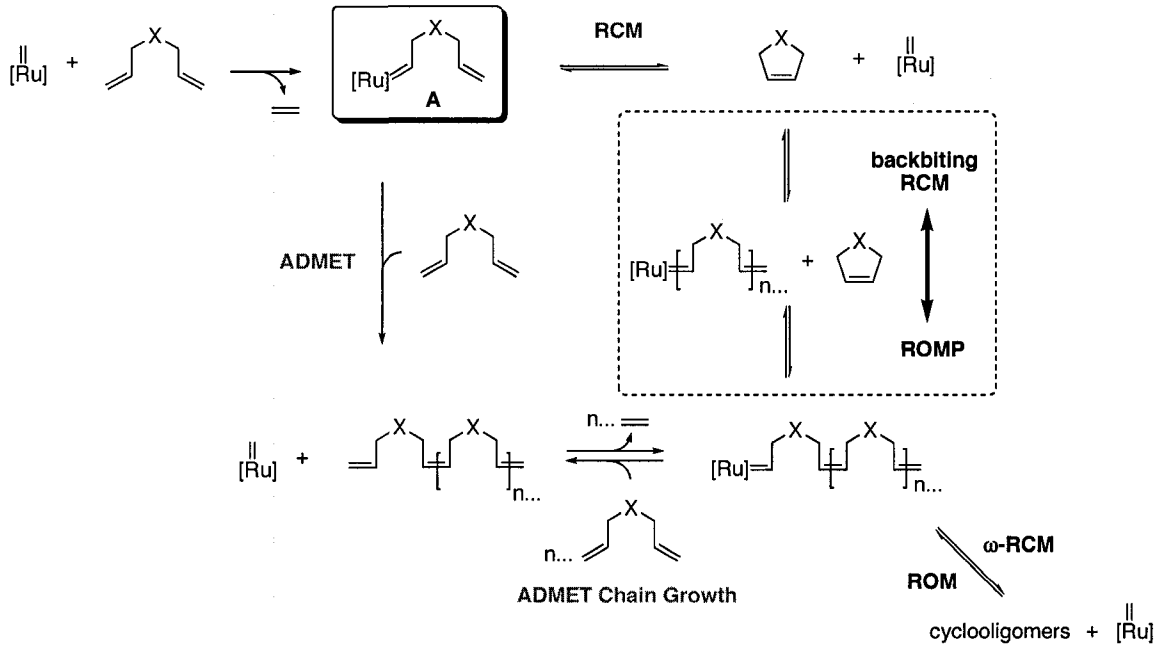

Figure 10. RCM manifold illustrated with the model diene.

5.7 Conclusion

Oligomers are widely recognized as side-products in "challenging" RCM reactions, and although examples have been reported in which oligomeric species have been induced to ring-close, ADMET products are overwhelmingly regarded as inimical, rather than intrinsic, to formation of ring-closed products. As the foregoing demonstrates, this is a false premise. The dominant route to medium and large rings via **2a**, under dilutions compatible with

efficient metathesis, typically involves not direct ring-closing, but an oligomerization-backbiting pathway.

The key factor in maximizing RCM yields is simply the concentration-dependence of the ring-chain equilibrium. Macrocyclic lactones, or cyclic catechol polymethylene ethers, are efficiently obtained at 5 mM. Consistent with the trends predicted by thermodynamic EM_k values, medium-sized rings required dilutions tenfold higher. High dilutions are essential not only to favour the cyclic products, but also to maximize selectivity for the smallest ring sizes.

An intriguing inference from these results is the possibility that some RCM reactions reported in the literature may be more promising than they originally seemed. When all of the starting material is consumed, the natural response, on observing oligomerization, is to terminate reaction. The work in this chapter shows that this can limit the potentially high-yield formation of RCM products, by hindering backbiting. Where RCM cyclizations halt prior to complete product formation, and starting diene is still present, catalyst decomposition may be implicated. Where diene is fully consumed, however, we are now able to suggest that the concentration regime was too high, and that diluting the reaction may improve RCM yields by shifting the ring-chain equilibrium to favour the cyclic product.

References page 174

5.8 References

(1) Ivin, K.J.; Mol, J.C., *Olefin Metathesis and Metathesis Polymerization.* Academic Press: New York, 1997.
(2) Nicolaou, K.C.; Bulger, P.G.; Sarlah, D. *Angew. Chem., Int. Ed.* **2005**, *44*, 4490-4527.
(3) Fürstner, A. *Angew. Chem., Int. Ed.* **2000**, *39*, 3012-3043.
(4) Trnka, T.M.; Grubbs, R.H. *Acc. Chem. Res.* **2001**, *34*, 18-29.
(5) Illuminati, G.; Mandolini, L. *Acc. Chem. Res.* **1981**, *14*, 95-102.
(6) Mandolini, L. *Adv. Phys. Org. Chem.* **1986**, *22*, 1-111.
(7) Allinger, N.L.; Tribble, M.T.; Miller, M.A.; Wertz, D.H. *J. Am. Chem. Soc.* **1971**, *93*, 1637-48.
(8) (a) Bruice, T. C.; Pandit, U. K., *J. Am. Chem. Soc.*, **1960**, *82*, 5858-5865. (b) Schleyer, P. V. R., *J. Am. Chem. Soc.*, **1961**, *83*, 1368-1373.
(9) Jung, M.E.; Piizzi, G. *Chem. Rev.* **2005**, *105*, 1735-1766.
(10) Forbes, M.D.E.; Patton, J.T.; Myers, T.L.; Maynard, H.D.; Smith Jr., D.W.; Schulz, G.R.; Wagener, K.B. *J. Am. Chem. Soc.* **1992**, *114*, 10978-10980.
(11) Villemin, D. *Tetrahedron Lett.* **1980**, *21*, 1715-18.
(12) Ziegler, K.; Eberle, H.; Ohlinger, H. *Liebigs Ann. Chem.* **1933**, *504*, 94.
(13) Yamamoto, K.; Biswas, K.; Gaul, C.; Danishefsky, S.J. *Tetrahedron Lett.* **2003**, *44*, 3297-3299.
(14) Lee, C.W.; Grubbs, R.H. *J. Org. Chem.* **2001**, *66*, 7155-7158.
(15) Lemarchand, A.; Bach, T. *Tetrahedron* **2004**, *60*, 9659-9673.
(16) Fürstner, A.; Thiel, O.R.; Ackermann, L. *Org. Lett.* **2001**, *3*, 449-451.
(17) Xu, Z.; Johannes, C.W.; Houri, A.F.; La, D.S.; Cogan, D.A.; Hofilena, G.E.; Hoveyda, A.H. *J. Am. Chem. Soc.* **1997**, *119*, 10302-10316.
(18) Kirkland, T.A.; Grubbs, R.H. *J. Org. Chem.* **1997**, *62*, 7310-7318.
(19) Gradillas, A.; Perez-Castells, J. *Angew. Chem., Int. Ed.* **2006**, *45*, 6086-6101.
(20) Lee, C.W.; Grubbs, R.H. *Org. Lett.* **2000**, *2*, 2145-2147 see erratum p 2558.
(21) Michrowska, A.; Wawrzyniak, P.; Grela, K. *Eur. J. Org. Chem.* **2004**, 2053-2056.
(22) Fürstner, A.; Langemann, K. *Synthesis* **1997**, 792-803.
(23) Lee, L.O., H.; Hsu, H. Fluid-phase Equilibria 2005, 231, 221. *Fluid-phase Equilibria* **2005**, *231*, 221.
(24) (a) H. Höcker, W. Reimann, K. Riebel, Z. Szentivanyi, *Makromol. Chem.* **1976**, *177*, 1707-1715. (b) H. Höcker, W. Reimann, L. Reif, K. Riebel, *J. Mol. Catal.* **1980**, *8*, 191-202. (c) L. Reif, H. Höcker, *Macromolecules* **1984**, *17*, 952-956.
(25) (a) Thorn-Csanyi, E. *NATO ASI Series C* **1998**, *506*, 117. (b) Thorn-Csanyi, E.; Ruhland, K. *Macromol. Symp.* **2000**, *153*, 145. (c) Thorn-Csanyi, E.; Ruhland, K. *Macromol. Chem. Phys.* **1999**, *200*, 1662.
(26) Jacobson, H.; Stockmayer, W.H. *J. Chem. Phys.* **1958**, *18*, 1600-1606.
(27) Ercolani, G.; Mandolini, L.; Mencareli, P.; Roelens, S. *J. Am. Chem. Soc.* **1993**, *115*, 3901-3908.
(28) Chen, Z.; Kornfield, J.A.; Claverie, J.P.; Grubbs, R.H. *Polymer Prepr.* **1994**, *35*, 692-693.
(29) Chen, Z.-R.; Claverie, J.P.; Grubbs, R.H.; Kornfield, J.A. *Macromolecules* **1995**, *28*, 2147-2154.
(30) Hodge, P.; Kamau, S.D. *Angew. Chem., Int. Ed.* **2003**, *42*, 2412-2414.

(31) Marsella, M.J.; Maynard, H.D.; Grubbs, R.H. *Angew. Chem., Int. Ed.* **1997**, *36*, 1101-1103.
(32) Yet, L. *Chem. Rev.* **2000**, *100*, 2963-3007.
(33) Maier, M.E. *Angew. Chem., Int. Ed.* **2000**, *39*, 2073-2077.
(34) (a) Sanford, M. S.; Love, J. A.; Grubbs, R. H., *J. Am. Chem. Soc.*, **2001**, *123*, 6543-6544. (b) Ulman, M.; Grubbs, R. H., *J. Org. Chem.*, **1999**, *64*, 7202-7207.
(35) Galli, C.; Illuminati, G.; Mandolini, L.; Tamborra, P. *J. Am. Chem. Soc.* **1977**, *99*, 2591-2597.
(36) Casadei, M.A.; Galli, C.; Mandolini, L. *J. Am. Chem. Soc.* **1984**, *106*, 1051-1056.
(37) Dalla Cort, A.; Illuminati, G.; Mandolini, L.; Masci, B. *J. Chem. Soc., Dalton Trans. 2* **1980**, 1774-1777.
(38) Illuminati, G.; Mandolini, L.; Masci, B. *J. Am. Chem. Soc.* **1977**, *99*, 6308-6312.
(39) Dalla Cort, A.; Mandolini, L.; Masci, B. *J. Org. Chem.* **1980**, *45*, 3923-3925.
(40) Galli, C.; Mandolini, L. *Eur. J. Org. Chem.* **2000**, 3117-3125.

6 Probing the Electronic Nature of the Ru-X Bond

6.1 Background

Emerging as a key issue in the general area of Ru-promoted olefin metathesis is the efficiency of catalyst utilization: that is, the extent to which the turnover numbers (TON) observed for a given pre-catalyst reflect the activity of the ensemble of catalyst molecules, versus the activity of a smaller portion of "initiated" species. For complexes of type **2**, for example, the low lability of the PCy_3 ligand means that a very small proportion of the added complex is responsible for the observed activity.[1,2] For complex **1**, initiation can be considerably more homogeneous (that is, initiation is fast relative to propagation),[3] depending on the monomer employed.[4] However, slow initiation of **1** via loss of PCy_3, as well as preferential reaction with the dissociated PCy_3, rather than olefin,[5] contribute to low rates of metathesis. In comparison, **3** exhibits much faster reaction: factors in its high initiation efficiency are the rapid loss of pyridine, and the minimal re-uptake of the dissociated ligand.[5,6] In the case of catalysts **12a** and **15a**, the need for elevated temperatures (40-60 °C) to induce efficient ring-closing metathesis (RCM) suggested that the pyridine ligand is unexpectedly non-labile at room temperature.

While theoretical and kinetic studies have yielded much insight into the behaviour and requirements of the neutral donors in catalysts **1-3**, the essential properties of the anionic ligands have gone largely unexamined. To date, the only anionic ligands studied in any detail are the halides, for which steric and electronic effects cannot be deconvoluted.[5,7,8] This Chapter examines the efficiency of initiation and propagation of catalysts **12** and **15**, relative to **1**, **2a**, and **3a** (Figure 1), and relates it to the fundamental nature of the Ru-X bond.

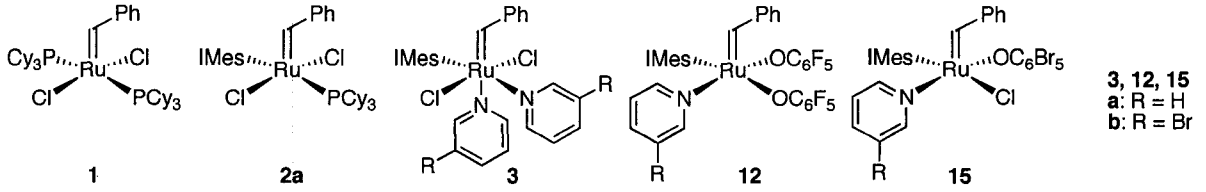

Figure 1. Ruthenium metathesis catalysts investigated.

6.2 Characterization of Catalyst Properties by ROMP

6.2.1 ROMP Activities of Cyclooctene and Norbornene Monomers

For **1** and **2a/b**, loss of PCy_3 is rate-limiting, and the rate of exchange of free and bound phosphine can thus give valuable insight into the kinetics of initiation. These rates have been evaluated for **1** and **2** by ^{31}P NMR spin saturation transfer experiments.[5] The extremely low absolute sensitivity of the ^{15}N nucleus, coupled with the high cost of pyridine-^{15}N, hampers analysis of pyridine derivatives such as **3**, **12a**, and **15a** by this method.[9] Initiation and propagation rates can also be measured by direct observation of metathesis reactions by NMR analysis, although accurate determination of initiation rates is difficult where these rates are very low, or polymerization is very fast.[6] Use of ROMP to assess the reactivity of **12a** and **15a**, vs. the Grubbs catalysts, has a number of advantages. In contrast with RCM, ROMP can be carried out for all catalysts at ambient temperatures; more fundamentally, catalysis is carried by an alkylidene intermediate, rather than a methylidene species (decomposition of which could complicate the kinetics).[10] Finally, and most importantly, the polymerization experiments provide additional insight into the efficiency and homogeneity of initiation, via measurement of absolute molecular weights and polymer polydispersity (PDI).

We chose to examine cyclooctene (COE, **20**) and (±)-5-norbornene-2-methylacetate (NBE-CH_2OAc; 5:1 mixture of *endo* and *exo* isomers, **113**) as representative low- and high-strain cycloolefins that enable efficient screening for initiator activity, while maintaining a level of discrimination that can be harder to gauge using highly reactive monomers. NBE-CH_2OAc is attractive for the lower susceptibility to chain transfer reactions anticipated for its ROMP polymer, relative to polyoctene.[11] Also a potential advantage is the damping effect on ROMP reactivity associated with the *endo*-orientation of the acetate group in the majority isomer. Rates of polymerization of COE and NBE-CH_2OAc were measured *in situ* by arrayed ^1H NMR experiments (22 °C, 100 mM [monomer]; $CDCl_3$) from the decrease in integrated intensity for the olefinic signals for the monomer, and the increase in integrated intensity for the olefinic signals for the polymer (Figure 2).

Good first-order kinetics are found in all cases, except for ROMP of COE by **15b**, for which the rapidity of reaction may compromise the accuracy of the data, and ROMP of NBE-CH_2OAc by **12b**, for which an induction period is evident. The rate curves show strikingly similar reaction rates for the two monomers, despite the higher reactivity typical of high-strain norbornene substrates. In fact, NBE-CH_2OAc undergoes ROMP more slowly than COE, almost certainly due to chelation of the acetate carbonyl to form a favoured seven-membered ring, which can be expected to depress rates of propagation, relative to initiation. Consistent with this, the ^1H NMR chemical shifts for the propagating alkylidene species are comparable with values reported for chelate complexes formed on ROMP of other carbonyl-functionalized substrates.[12-15]

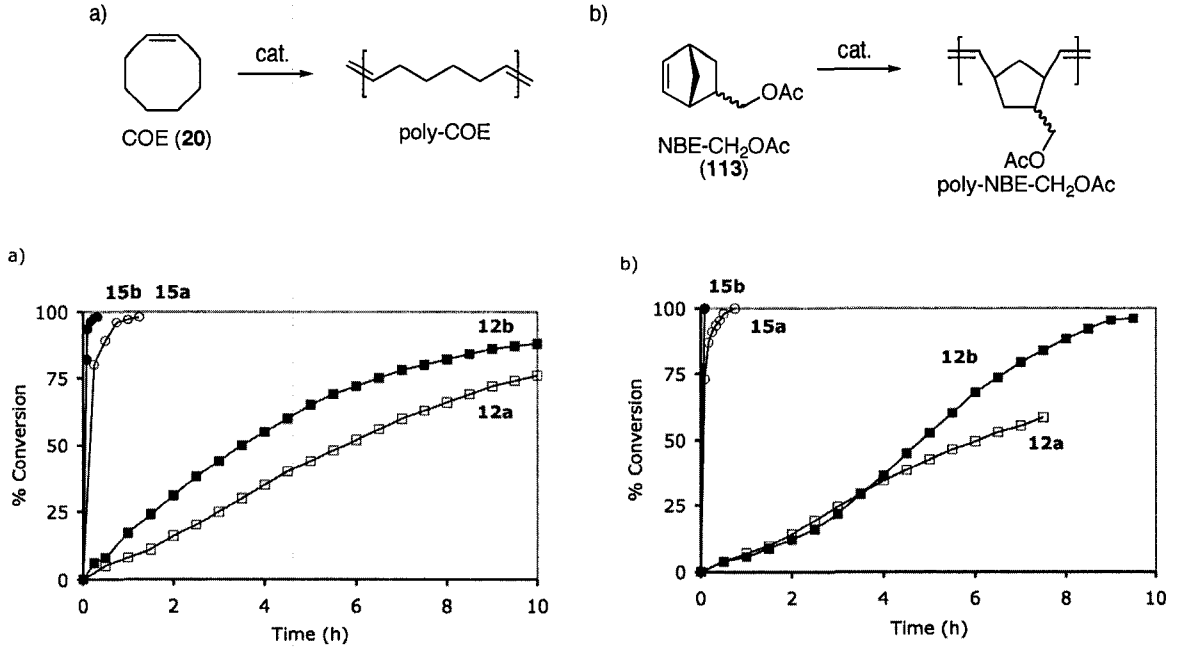

Figure 2. Time profiles (^{1}H NMR, $CDCl_3$, 0.1 M, 21 °C) for ROMP of: a) cyclooctene; b) NBE-CH_2OAc. Lines are intended as visual aids, rather than curve fits.

The trend in activity for ROMP of both monomers follows the order **15b** > **15a** >> **12b** > **12a**. Within each pair, **12a/b** or **15a/b**, the bromopyridine derivative effects faster metathesis, as expected,[6,16] but the pentabromoaryloxide series exhibits much higher activity. A more quantitative comparison comes from the turnover frequencies for these initiators at 50% conversion (Table 1), which suggest that the most reactive initiator, **15b**, effects ROMP of COE ca. 60 times faster than the least, **12a**. This difference is amplified for NBE-CH_2OAc, for which **15b** is 150 times more reactive than **12a**. For these two monomers, incorporation of bromopyridine, vs. pyridine, increases initiator activity by 1.5 to 3 times.

References page 201

Table 1. Relative ROMP reactivity of initiators **12a/b** and **15a/b**.[a]

Initiator	COE (200 equiv)		NBE-CH_2OAc (100 equiv)	
	k_{rel}	TOF (h^{-1})	k_{rel}	TOF (h^{-1})
12a	1	34	1	8
12b	1.7	58	1.3	11
15a	19	640	108	876
15b	58	1980	148	1200

[a] k_{rel} = polymerization rates normalized to that of initiator **12a**. TOF = turnover frequency at 50% conversion.

6.2.2 Initiation and Propagation

Initiators **12a/b** and **15a/b** were used to polymerize 200 equivalents of COE or 100 equivalents of NBE-CH_2OAc at room temperature (22 °C), at a monomer concentration of 100 mM in CH_2Cl_2 solvent. ROMP of the norbornene monomer was also undertaken. Data for the polymers obtained are summarized in Table 2. Even after ten hours, **12a** and **12b** effect only 10-25% conversion of COE. In comparison, the bromoaryloxide complexes **15a/b** enable near-complete consumption of COE or NBE-CH_2OAc within 30 minutes. For all four initiators, propagation is faster than initiation, as indicated by the high molecular weights and broad PDI values for the resulting polymer (particularly for ROMP of COE, as expected). As the ease of backbiting and chain transfer reactions in polyoctene can limit the relevance of molecular weight and PDI values to initiator efficiency, subsequent studies were limited to NBE-CH_2OAc. The high chain lengths and polydispersities found even for the highly reactive Grubbs system **3b** indicate that this monomer provides a rather stringent test of initiation efficiency, possibly owing to simultaneous chelation of the *endo*-carbonyl and olefin functionalities by the ruthenium pre-catalyst. The superior performance of **1** may indicate that recoordination of PCy_3 occurs preferentially to chelation, and that the phosphine

ligand dissociates more readily than the carbonyl donor. The potential of added phosphine to improve PDIs was previously described.[15]

Table 2. Polymer properties.[a]

Monomer	Initiator	Time	% Conv.	% Yield	$M_w \times 10^3$	PDI
COE (**20**)	**12a**	10 h	76	71	141	1.60
	12b	10 h	88	71	74.0	1.36
	15a	30 min	89	79	160	1.48
	15b	30 min	100	92	141	1.46
NBE-CH_2OAc (**113**)	**1**	30 min	100	89	23.7	1.05
	2a	30 min	100	89	280	1.35
	3a	30 min	100	97	31.2	1.13
	3b	30 min	100	98	40.8	1.12
	12a	24 h	100	84	104	1.40
	12b	10 h	100	80	143	1.70
	15a	30 min	98	85	186	1.20
	15b	5 min	100	87	180	1.38

[a]Conditions as in Table 1. [Monomer]:[initiator] = 200:1 (COE); 100:1 (NBE-CH_2OAc); calculated molecular weights: 22,040 g·mol^{-1} (polyoctene); 26,239 g·mol^{-1} (poly(NBE-CH_2OAc)). % Conv = conversion to polymer at time specified (^{1}H NMR). Yield = isolated yield. M_w determined by light-scattering GPC.

6.2.3 Determining Rate of Initiation and Propagation

Slugovc, Stelzer and co-workers have pointed out that direct measurement of initiation rate constants (k_i) by NMR methods is hampered where initiation rates are low (as suspected for **12a/b**), or where ROMP is fast (as shown for **15a/b** in Figure 2).[2,6] As an alternative means of gaining insight into initiation efficiency, relative rates of initiation and propagation (k_p/k_i) can be evaluated for any given monomer-initiator pair according to Equation 1.[17]

$$\frac{k_p}{k_i} = \frac{-M_o / I_o}{\ln\left(\frac{I_t}{I_o}\right) + (I_t)\left(\frac{I_t}{I_o} - 1\right)} \qquad (1)$$

M_0 = monomer concentration at time 0
I_0 = initiator concentration at time 0
I_t = initiator concentration at time t

The NMR signals for the alkylidene proton in the propagating species (that is, the ruthenium species bearing a subtended polymer chain) appear ca. 1 ppm upfield from the singlet for the benzylidene group in the initiators. Ratios of k_p/k_i were evaluated from the integrated intensities of these signals for the initiating and propagating alkylidenes formed in ROMP of COE and NBE-CH_2OAc by **1-3** and **15a/b**, under conditions analogous to those shown for **15b** in Scheme 1. An initiator concentration of 10 mM was used, to achieve a balance between the signal-to-noise ratio attainable with a 1 minute experiment time (16 scans), and the integrated intensity of the signals for the propagating species. Moderate ratios of monomer to initiator (ca. 10:1) are also necessary, to minimize changes in viscosity that can impede resolution or alter reaction rates, and to limit secondary metathesis. Finally, short reaction times (30 minutes) were chosen, in order to inhibit chain transfer processes and catalyst decomposition.

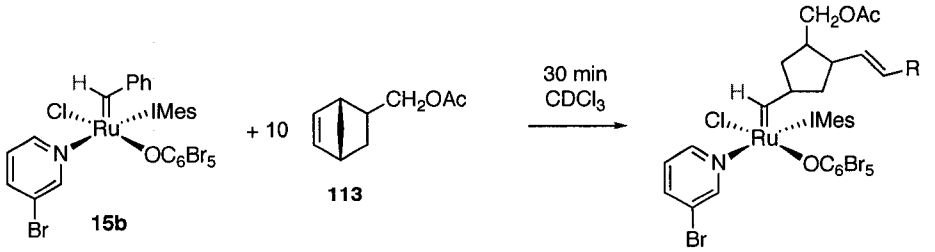

Scheme 1.

Values of k_p/k_i obtained from these experiments for all catalyst-substrate combinations (Table 3) follow the trend **3b** < **3a** < **1** < **15b** < **15a** < **2a**. Values for the pentafluorophenoxide catalysts **12a/b** could not be obtained, owing to the very low integrated intensity of the signal for the propagating alkylidene for these initiators. This is due in part to the low reactivity evident from the rate plots in Figure 2. A high rate of propagation can also be inferred, however, from the fact that the signal for the propagating species remains undetectable even where monomer consumption nears 30%. Of the remaining systems, the Grubbs initiators **3b** and **2a** exhibit the lowest and highest k_p/k_i ratios, respectively, consistent with the PDI values for the polymers prepared using these initiators (see Table 2 above). Rates of propagation relative to initiation are exaggerated for the NBE-CH_2OAc system, as indicated by the unexpectedly poor performance of the normally fast-initiating complexes **3**. The faster reaction of alkylidene, relative to benzylidene,[18] will exacerbate these differences. Initiators **15a/b** give rise to k_p/k_i ratios lower than those for **2a**, but much higher than for **3**. The increase is smallest for the bromoaryloxide complexes, consistent with the lower PDI values for polymers prepared using **15b**, but the composite picture indicates significantly slower loss of pyridine from all of the aryloxide complexes, relative to the chlororuthenium analogues **3**.

Table 3. Calculated k_p/k_i ratios for initiators **1-3** and **15a/b**, for ROMP of COE and NBE-CH_2OAc.[a]

Initiator	COE (**20**)	NBE-CH_2OAc (**113**)
1	2.9	35
2a	760	340
3a	2.4	4.7
3b	1.6	4.1
15a	431	240
15b	84	66

This behaviour was presumed to reflect the inductive effects associated with the strongly electron-withdrawing character of the perhaloaryloxide ligands. If use of an electron-deficient aromatic ring is essential to prevent σ–π isomerization of the aryloxide ligand (Chapter 3), high rates of propagation relative to initiation may be an inherent limitation of this family of catalysts. Given the higher reactivity of these complexes in ROMP, vs. RCM, it may be inferred that their impressive RCM performance reflects the operation of an even smaller number of initiated species. This suggests that the *inherent* reactivity of these systems is extremely high. In order to improve our understanding the impact of the aryloxide ligand on metathesis reactivity, we undertook a DFT analysis of catalyst **15a**.

6.3 DFT Studies[a]

The degenerate cross-metathesis of ethylene with a model Ru-methylidene catalyst containing a truncated IMe ligand (IMe = 1,3-dimethylimidazol-2-ylidene) was examined. The difference in electronic energies (ΔE) between isomers of **15b** is compared to reported values for **1** and **3**.[19] Metathesis via the established dissociative pathway for square-pyramidal $RuX_2L_2(=CHR)$ species is invoked, in which the Chauvin [2+2] cycloaddition represents a key step.[19-22]

6.3.1 Catalyst Structure

As the starting point for inquiry, we undertook a DFT assessment of the structure for $RuCl(OC_6Br_5)(CH_2)(IMes)(py)$, **15a**. While the apical site preference of the alkylidene ligand

[a] Calculations carried out in collaboration with Dr. Claudio Carra of the Scaiano research group, Univ. Ottawa.

in such square pyramidal complexes is well established, the evidence for the relative positioning of the basal ligands in the mono-aryloxide derivatives **15** (and, by extension, the perchloroaryloxide analogues **14**) is more equivocal. We originally proposed a *cis*-anionic structure, by analogy to established by X-ray analysis for $Ru(OC_6F_5)_2$(IMes)(py)(=CHPh) **12a**, positing a push-pull interaction between *trans*-disposed pyridine and aryloxide ligands. More detailed DFT analysis of the IMe model system (using the 6-31G* basis set) indicated that a five-coordinate structure in which the aryloxide and NHC ligands lie mutually *trans* were lower in energy than one in which these ligands are mutually *cis*. Isomers in which the alkylidene ligand is sited in the basal plane are much higher in energy (>30 kcal/mol), and were excluded from further consideration. The strong apical site preference of this strong *trans*-influence ligand has been noted previously.[23] Lower in energy by 4 kcal, however, is pseudo-octahedral structure **116**, in which the anionic ligands are *trans*-disposed, and the aryloxide ligand forms a five-membered, pseudo-chelate ring with a dative Br···Ru interaction. While the internuclear Br···Ru distance is considerably elongated (calculated distance 2.91 Å, vs. a value of 2.39 Å for the sum of the covalent radii), the interaction substantially reduces the energy of the complex, by ca. 3.7 kcal/mol relative to **114**.

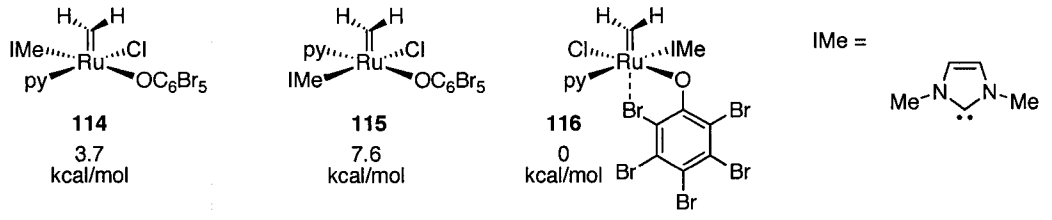

Figure 3. Calculated relative energies of isomers of **15a**, $RuCl(OC_6Br_5)(CH_2)$(IMes)(py).

Precedent for the κ^2-coordination of aryloxide ligands bearing an *ortho*-halo functionality is found in several coordination complexes, including $CpRu(\kappa^2\text{-}O,Cl\text{-}OC_6Cl_5)$[24] and the crystallographically characterized $Ru(\kappa^2\text{-}S,F\text{-}SC_6F_5)(SC_6F_5)(PMe_2Ph)_2$,[25] $Ru_3(CO)_8(\kappa^2\text{-}O,Cl\text{-}OC_6H_4Cl)_2$,[26] $Ru(\kappa^2\text{-}O,Cl\text{-}OC_8I_5)_2(\kappa^2\text{-}P,P\text{-}Ph_2PCH_2CH_2PPCy_2)$,[27] and $Ru(\kappa^2\text{-}O,Br\text{-}2,4,6\text{-}OC_6H_2Br_3)(PPh_3)_2$ (Ru-Br 2.63 Å).[28] A survey of 420 crystal structures in the Cambridge Crystallographic Database containing a Ru-Br bond indicate a mean bond length of 2.55 Å. While the calculated bond length of 2.91 Å is longer than those reported, the importance of this limited interaction is suggested by attempts to impose a κ^2-chelating interaction on **114** or **115**, while maintaining the *cis*-disposition of the anionic ligands, which regenerates the starting conformers on energy minimization. Despite their higher energy relative to **116**, we did not rule out the potential participation of **114** and/or **115** in the catalytic cycle, in view of the number of examples of *cis*-anionic structures reported in other $RuX_2L_2(=CHR)$ systems.[29-31]

6.3.2 The Dissociative Chauvin Mechanism

Scheme 2 illustrates the key steps involved in olefin metathesis promoted by five-coordinate $[Ru]=CH_2$ precatalysts such as **114** and **115**. A detailed cycle for **116** is shown in Scheme 3. We chose to study the degenerate metathesis of ethylene, in order to reduce the computational demands arising from the relatively large number of atoms present. Structures shown as **I-IV** and as (**I**)-(**IV**) in the resulting catalytic cycle are enantiomers, and are thus energetically equivalent. Given the low barriers associated with methylidene rotation, these processes are not shown: we assumed that initiation is dominated by dissociation of a neutral donor ligand L (**I**→**II**). Methylidene rotation is dealt with in the following section.

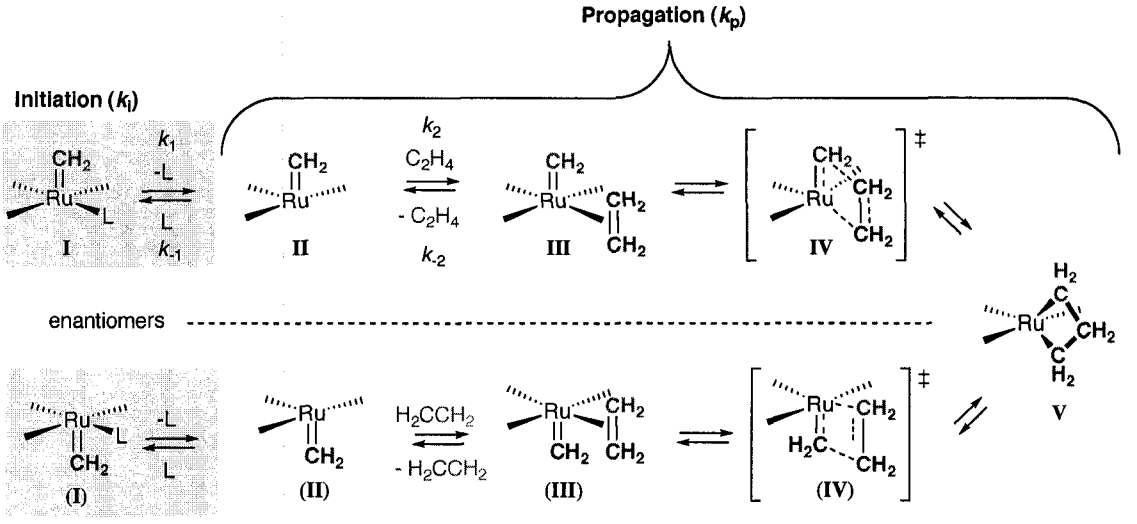

Scheme 2. Ethylene metathesis promoted by a five-coordinate [Ru]=CH_2 catalyst.

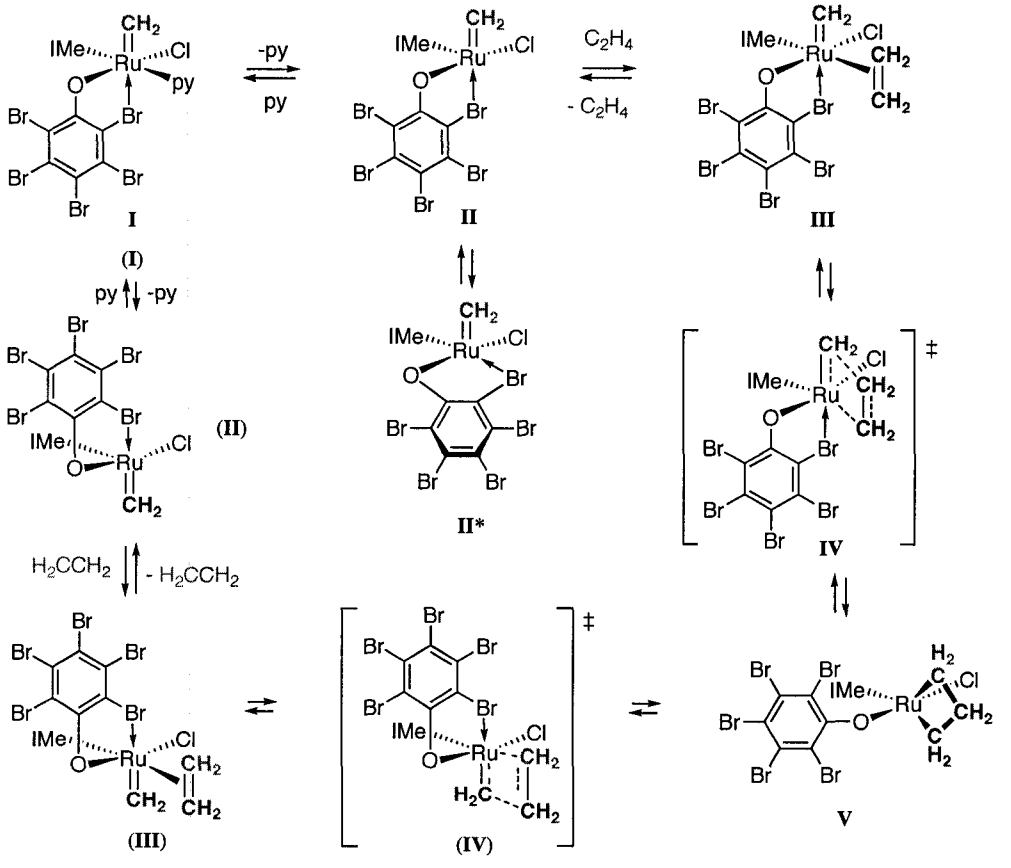

Scheme 3. Mechanism of ethylene metathesis promoted by **116**. Geometries **I-IV** and **(I)-(IV)** are related by a mirror plane, and are energetically equivalent. The numbering scheme corresponds to that shown in Scheme 2.

6.3.3 Initiation (Step I→II)

Ru-methylidene complexes are commonly used to determine bond dissociation energy (BDE) values for ruthenium benzylidene precatalysts (Figure 4). Loss of the pyridine ligand requires more energy for **114** and **115** (21.5 and 25 kcal/mol, respectively), than for **116** (15.3 kcal/mol). Given the high energy required for loss of pyridine from **115**, its significantly higher ground-state energy relative to **114** or **116**, and the spontaneous rearrangement of complex **115(II)** to **116(II)**, geometry **115** was eliminated from further consideration. Consistent with the ROMP data, dissociation of the pyridine ligand from $[RuCl_2(IMe)(=CH_2)(py)]$ **119** is considerably lower in energy than from **114** or **115** (12.7 kcal/mol). In comparison, phosphine loss from complexes **1** or **2b** (models **117** and **118**) requires 21.1 and 26.1 kcal/mol, respectively.

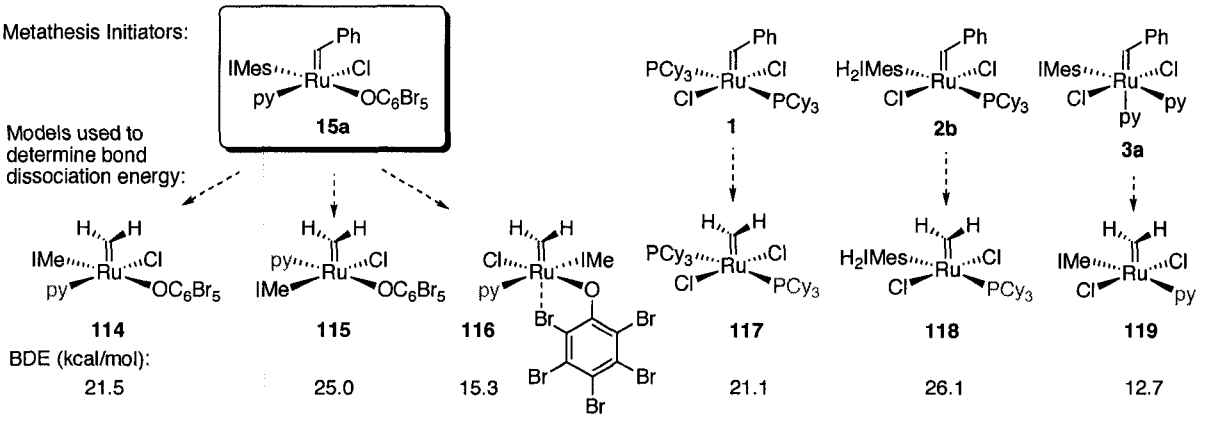

Figure 4. Model complexes used to calculate ligand dissociation of **1**,[19] **2b**,[19] **3a** and **15a**. Dissociating ligand shown in red, with dissociation energy in kcal/mol.

Ligand dissociation from **114** gives a four-coordinate, 14-electron structure of type **II**, analogous to the intermediates proposed in metathesis via the chloride catalysts **1-3** (Scheme 2). In contrast, loss of pyridine from **116** gives five-coordinate, 16-electron

structure **116(II)** (Scheme 3). Rotation of the Ru-Br bond into the basal plane of the square pyramid, and of the methylidene into an orientation parallel with the anionic ligands **116(II*)**, may contribute a small additional stabilization of ca. 1 kcal/mol. More significant is the increase in rotational and translational freedom associated with the free ligand, which reduces the total energy of the system. This effect is greater for loss of PCy_3 than pyridine, as indicated by the drop by 3.6 or 3.8 kcal/mol for loss of PCy_3 from **1b** or **2b**, respectively, vs. a drop of only 0.5 kcal/mol for loss of pyridine from **116**.

6.3.4 Olefin Binding (Step II→III)

The energy required for olefin binding was calculated from the bond dissociation energy for the microscopic reverse, loss of ethylene from 16-electron **114(III)** to yield **114(II)**, or from 18-electron **116(III)** to yield **116(II)**. The **114(III)**-**114(II)** transformation is much more endothermic (14.5 kcal/mol, vs. 2.9 kcal/mol). These values bracket the bond dissociation energy of 7.3 kcal/mol reported for the dichloride catalyst **2b** (model reaction: **118(II)→118(III)**).[19] (Note: after ligand dissociation, all dichloride catalysts **2-5** have the same structure).

6.3.5 Alkylidene Orientation

A central issue in olefin metathesis, highlighted more than two decades ago by Eisenstein, Hoffmann, and coworkers, is the geometry of the alkylidene ligand relative to bound olefin.[32,33] Where the initial orientation of the alkylidene π system is orthogonal to bound olefin, as shown for the perbromoaryloxide system in Figure 5 (structure (iii)), rotation to place these bond vectors parallel (see (iv)) is an essential first step.[34] This *syn*-

coplanar arrangement of the Ru-alkylidene and C=C π systems is a prerequisite to formation of the metallacyclobutane intermediate. Rotamers (i) and (ii), lie only 0.1 or 0.3 kcal/mol higher in energy, with a barrier of 1.1 kcal/mol. While orientation (iii) is the lowest-energy geometry for our model system, the barrier to ethylene rotation to yield the productive conformer (ii) is small (see transition state (iv); +0.6 kcal/mol). Subsequent formation of metallacyclobutane proceeds spontaneously. The fast rate of propagation observed experimentally for **15a/b** may thus reflect a strong bias toward an adoption of a productive alkylidene conformation.

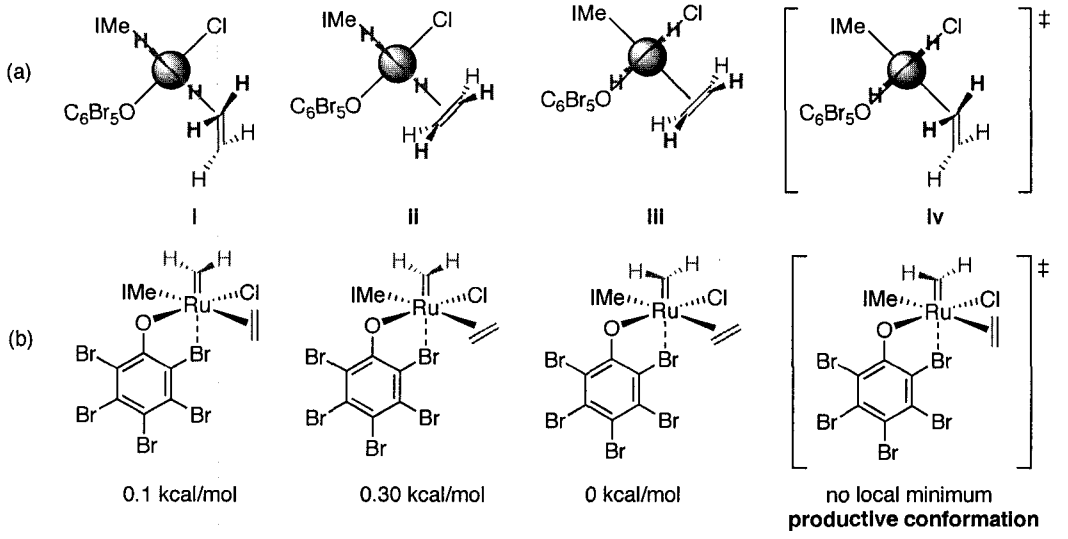

Figure 5. Conformational possibilities for $RuCl(OC_6Br_5)(IMe)(C_2H_4)(=CH_2)$ **116(III)**: ΔE kcal/mol. (a) Structures drawn looking down the axis of the $Ru=CH_2$ bond. (b) Corresponding structures, as conventionally depicted.

Related NHC complexes are likewise characterized by low barriers to alkylidene rotation, a factor that has been identified as contributing to the enhanced activity of the "second-generation" Grubbs catalysts.[19-21] Straub has proposed that the high rate of propagation found for **2** versus **1** is also due to the ease with which the former adopts the "productive conformation" (Figure 6). For both **1** and **2b**, intermediate (i) is more stable, and

the alkylidene must rotate in order for metathesis to occur. This step is most endothermic for **1**, for which rotamer iii is 5.7 kcal/mol higher in energy, whereas it requires only 0.3 kcal/mol for **2b**. The reorganization energy required to approach the transition state is thus considerably lower for **15** or **2b** , vs. **1**.

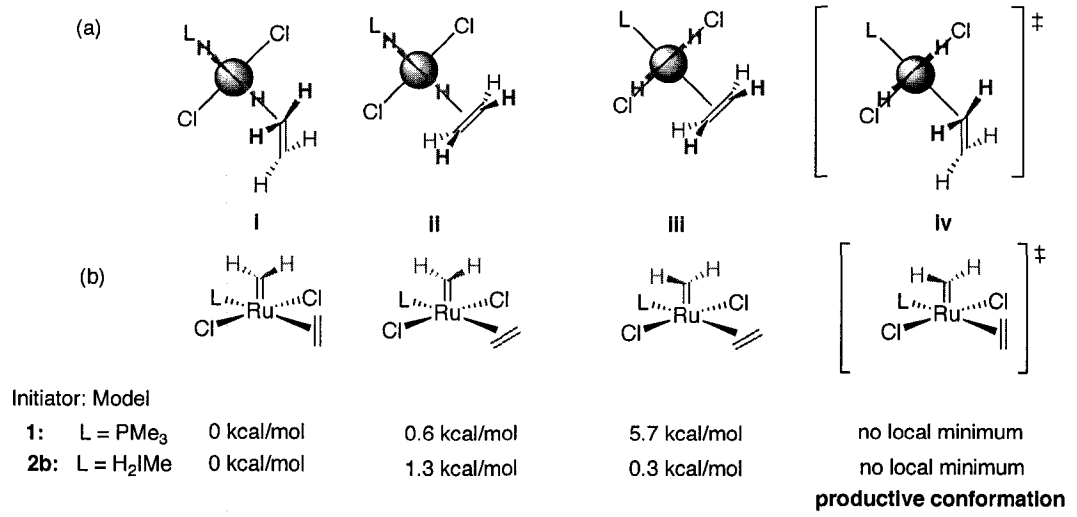

Figure 6. Conformational energies calculated for **1(III)** and **2(III)**: ΔG kcal/mol. [20] (a) Structures drawn looking down the axis of the Ru=CH_2 bond. (b) Corresponding structures, as conventionally depicted.

The ease of rotation of the alkylidene ligand in the *precatalyst* can provide a clue to the accessibility of orientations that favour cycloaddition in subsequent steps. Diagnostic for a low-energy rotation of the alkylidene ligand in type **2**[35,36] and **15a** is the breadth of the signals for the benzylidene phenyl protons in room-temperature ^{1}H NMR spectra. In contrast, **1** is characterized by well-defined benzylidene resonances,[37] and a higher barrier to rotation (2.7 kcal/mol).[21] NMR features at 298K can thus be used as a qualitative predictor for the barrier to benzylidene rotation, and hence cycloaddition (providing that the latter transition state is dominated by rotation). The benzylidene signals for **15a** do not resolve even at low

temperatures (202 K), consistent with a very low barrier to metallacyclobutane formation. (Satisfactory spectra could not be obtained at lower temperatures in either CD_2Cl_2 or $C_6D_5CD_3$, owing to precipitation of the complex).

6.3.6 Formation of Metallacyclobutane (III-[IV]-V)

The approach to transition state **[IV]** involves alignment of the methylidene and ethylene π orbitals, thus permitting [2+2] cycloaddition, and elongation of the Ru=C and C=C bonds as the double bonds begin to break. The transition state **114([IV])** has a high energy barrier, relative to **117([IV])** or **118([IV])** (7.2 kcal/mol, vs. 3.4 and 2.3 kcal/mol, respectively).[19] (Interestingly, benzylidene is reported to have a lower barrier to metallacycle formation relative to methylidene: the energy for transformation **III-[IV]** for **2a** and **3a** is 1.9 kcal/mol).[21] In contrast, **116(III)** passes through transition state **[IV]** to yield metallacyclobutane **116(V)** in a near-barrierless process (0.6 kcal/mol). Noteworthy is the ease with which the Ru···Br interaction is lost to accommodate metallacycle formation.

The most stable metallacyclobutane structure is **118(V)**,[19] at -9.7 kcal/mol. The energies of the corresponding metallacyclobutane **114(V)** and **116(V)** are higher (-4.9 and -7.5 kcal/mol, respectively). A recent experimental study provides precedent for a trigonal bipyramidal intermediate, in which the NHC and metallacyclobutane moieties occupy the trigonal plane.[38] The ΔE values for structures **II-V** in complexes **114-118** are shown in Table 4 and Figure 7.

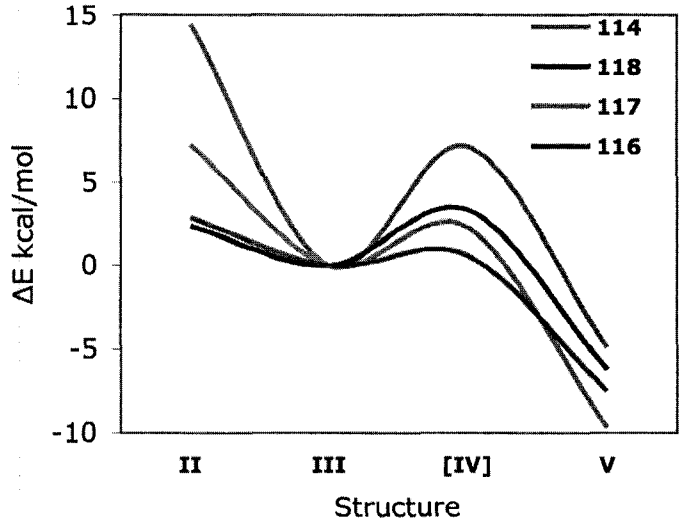

Figure 7. Plot of ΔE for structures **II-V** corresponding to the model systems shown Table 4.

Table 4. ΔE values (kcal/mol) for the transformations illustrated in Scheme 2 and 3. Values are normalized to that of the ethylene-bound structure **III** at 0 kcal/mol.

Entry	Initiator	Model	**II**	**III**	**[IV]**	**V**
1[19]	**1**	**117**	2.4	0	3.4	-6.2
2[39]	**2b**	**118**	7.3	0	2.3	-9.7
3	**15b**	**114**	14.5	0	7.2	-4.9
4	**15b**	**116**	2.9	0	0.6	-7.5

6.3.7 Electronic Effects

Several features can contribute to a distinction between the electronic characteristics of the aryloxide and the chloride complexes. While the Brønsted acidity of pentabromophenol, vs. HCl (pK_a 4.57[40] vs. -8), suggests that the former should be the stronger σ-donor, the electron-withdrawing capacity of the aryloxide ligand is enhanced by the greater electronegativity of the oxygen atom (3.44 vs. 3.16),[41] and the potential to delocalize electron density away from the metal center onto the aryl ring. Also relevant may

be the greater π-donor capability of oxygen, relative to chlorine, although this may be limited by the occupancy of the Ru dπ (t_2g) orbitals.[42,43] To gain greater insight into the electronic impact of the OC_6Br_5 ligand, we calculated the atomic charges for Ru and the atoms directly bound to it, using natural bond orbital (NBO)[44] analysis (Table 5). The positive charge on the metal center is considerably larger for the aryloxide complex (**114**, 0.521; **115**, 0.448; **116**, 0.437) than the dichloride catalysts (**120**, 0.115; **121**, 0.235). The very high charge on ruthenium in **114** may be a function of the *cis* arrangement of the anionic ligands in this isomer. The increased charge on Ru in these structures would disfavour loss of the Lewis basic pyridine ligand, providing a partial explanation for the higher activation energy for **15a**. Also relevant may be the three-orbital, four-electron binding interaction described in Chapter 3.

Table 5. Calculated charge (NBO analysis) present on the central metal and atoms bound directly to it for models and conformers relevant to **1**, **2**, and **15a**.

Initiator	Model system	C (CH_2)	Ru	Cl	C (NHC)	N (py)	o-Br	O
1	**120(I)**	-0.267	0.115	-0.493	-	-	-	-
2	**121(I)**	-0.254	0.235	-0.510	0.245	-	-	-
15a	**114(I)**	-0.284	0.521	-0.556	0.276	-0.388	0.096	-0.721
15a	**115(I)**	-0.223	0.448	-0.552	0.261	-0.431	0.115	-0.691
15a	**116(I)**	-0.217	0.437	-0.525	0.301	-0.471	0.152	-0.687
15a	**114(II)**	-0.348	0.622	-0.433	0.242	-	0.110	-0.719
15a	**116(II)**	-0.272	0.508	-0.518	0.358	-	0.151	-0.693
15a	**114(III)**	-0.251	0.463	-0.516	0.305	-	0.082	-0.710
15a	**116(III)**	-0.219	0.417	-0.508	0.316	-	0.151	-0.683

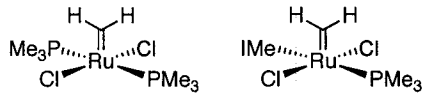

Figure 8. Models of **1** and **2** used to calculate NBO charges in Table 6.

A related DFT study[45] indicated that the energy barrier to loss of pyridine from *cis*-anionic **122** was ca. 7 kcal/mol higher than from the *trans*-Cl_2 isomer **123** (Scheme 4). The *cis*-dichloride arrangement leads to a higher dipole moment (e.g. 12.4 D vs. 1.5 D for *cis* **122** and *trans* **123**, respectively), thus linking catalyst polarity to initiation efficiency. Loss of pyridine from **114** is likewise 6 kcal/mol higher in energy than from **116**.

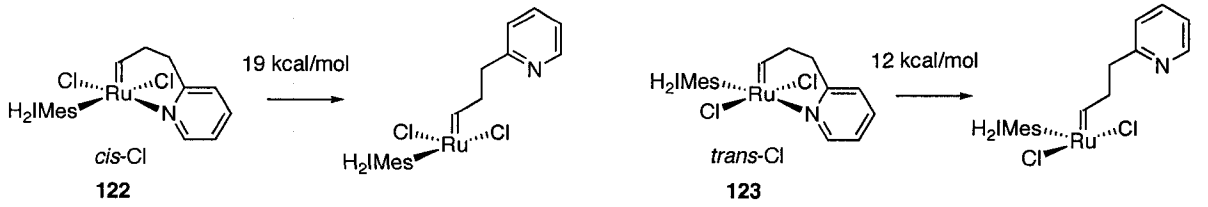

Scheme 4.[45]

Relative rates of ligand dissociation have been established for **1** and **2b**, and their bromide and iodide derivatives. A combination of electronic and steric effects can contribute to observed trend, I > Br > Cl.[5] In a study of the effects of phenol additives on the reactivity of **1** and **2b**, Forman and coworkers sought to modulate electronic properties without perturbing steric parameters.[46] Hydrogen-bonding of phenol to a chloride ligand in **1** or **2b** siphons off electron density from the halide ligand, increasing the positive charge on the metal center. A ca. 5 kcal/mol increase in the energy for ligand dissociation from **1**·PhOH and **2b**·PhOH was noted, again suggesting that increases in the electropositive character of Ru increases the energy required for ligand dissociation. The presence of a sixth metal-ligand interaction in **116**, which can be expected to lower the barrier to ligand loss, can compensate to some extent for the positive charge on ruthenium. In a very recent, related report (Scheme

5b), a weak Ru···F interaction *trans* to the alkylidene was found to enhance the rate of initiation of **124** relative to **2b**.[47]

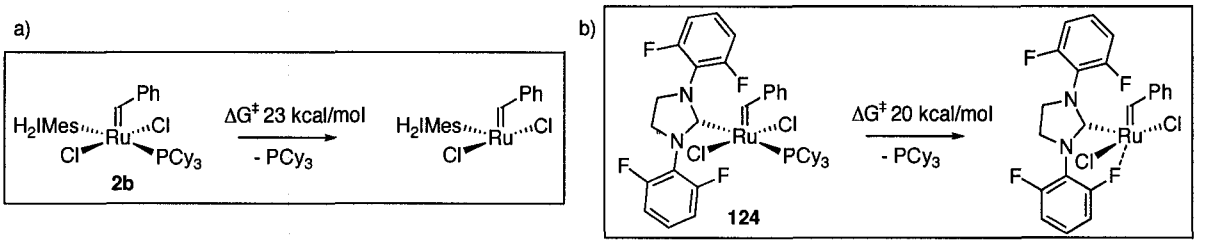

Scheme 5.

A possible explanation of the low barrier to cyclometallation may be found in the raised the energy of the Ru dπ orbitals, making Ru easier to ionize, and countering the negative effect expected for a more electron deficient metal (Figure 9).[43]

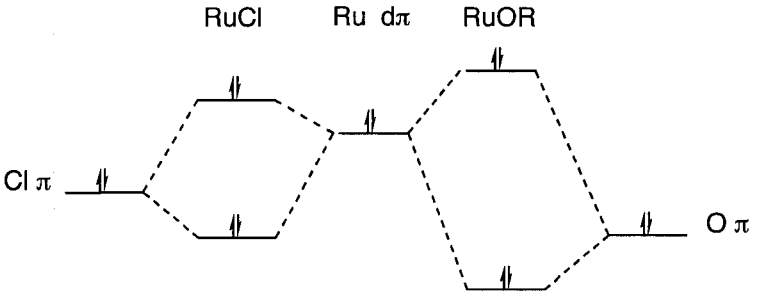

Figure 9. Comparison of Cl and O X ligand filled-filled repulsions with Ru d^6 filled dπ orbitals. The Ru-OR complex has a smaller ionization potential.[43]

6.3.8 X-Ray Absorption Spectroscopy

The NBO calculations agree with experimental trends suggested by X-ray absorption studies. The electron density on ruthenium, and the covalency of the Ru-Cl bond, can be gauged from the chloride κ-edge spectra by measuring the Iψ*←Cl1s signal. Values for the

covalency of the Ru-Cl bond in **1**, **2b**, and **15a** were 1.34, 1.35 and 1.15 respectively.[48] This parallels the trend in the NBO partial charge analysis. A more ionic Ru-Cl bond is present in the aryloxide complex, for which the highest positive charge on Ru is found.

6.3.9 Comparison with Reported Catalytic Data

Figure 7 showed a plot of the relative energies for ethylene metathesis by **117**, **118**, **114**, and **116**. The difference in behaviour between **117** and the second-generation catalyst **118** is well understood.[19,21] For **116**, the secondary donor interaction with a bromide group, and the electron-withdrawing effect of the aryloxide ligand, lowers the barriers to initiation *and* propagation. The transition state for metallacyclobutane formation is lowest for **116**, and very fast propagation can therefore be expected. This presumably accounts for the exceptional RCM performance of **15a** described in Chapter 4.

RCM reactions do not permit discrimination between a highly active catalyst with low initiation efficiency,[49] and a moderately active catalyst with a higher initiation rate. ROMP methodologies (see Section 6.2.1) offer greater insight, as the polymer chain lengths report on the relative rates of initiation, vs. propagation.[2] High molecular weights result where barriers to initiation are significantly greater than barriers to propagation. Such catalysts are characterized by low turn-on efficiency, but higher "commitment"; that is, the barrier to back-reaction is also high, so reaction proceeds in the forward direction.[50] Catalyst **2b** exemplifies this behaviour. It has a high activation energy for ligand dissociation, but following loss of phosphine, olefin binding and cycloaddition is favoured ($k_2 < k_{-1}$, experimental value for $k_{-1}/k_2 = 1.25$). For **1**, in contrast, back-reaction with PCy_3 is favoured over olefin binding and cycloaddition ($k_2 << k_{-1}$; experimental value k_{-1}/k_2 1.3×10^4).[5] The

consequence is immediately evident in ROMP reactions: **2b** is highly reactive, but gives poor control over chain lengths, resulting in high molecular weight polymers, while **1** is slower, but gives polymers in which the number of repeat units corresponds closely to the monomer: catalyst ratio. In comparison, we have shown that ROMP via aryloxide catalyst **15a** leads to high-molecular weight polymers, consistent with "committed" kinetics, as found for **2a** and **2b**. Its turn-on efficiency is higher than **2b**, but much lower than **1**. The k_p/k_i ratio for **15a** also indicated fast propagation, relative to initiation.

The difference in the barriers to ligand dissociation and metallacyclobutane formation can also be used to define a reaction as committed (positive ΔΔE values) or not committed (negative ΔΔE values). The trend in calculated ΔΔE values, **2a > 15a > 1** (Table 6: the trend for the model complexes is **118 > 116 > 117**), corresponds to the experimental trends in k_p/k_i, and ROMP efficiency, tending to validate our computational approach.

Table 6. Comparison of reported kinetic and ROMP data with the calculated difference in reaction barriers, ΔΔE (**II** vs. [**IV**]).

Initiator	Model	k_{-1}/k_2 [a]	k_p/k_i	Eff.[b]	Initiation ΔE	Commitment ΔΔE[c]
1	**117**	13000	35	91	21.1[19]	-1
2a	**118**	1.25	340	8	26.1[19]	5
3a	**119**	–	5	71	12.7	5
15a	**116**	–	240	11	15.3	2.3[d]

[a] Measured for reaction of **1a** and **2a** with ethyl vinyl ether. [b] Efficiency = M_n(theor)/ M_n(exptl) x 100; reported for ROMP of norbornene-2-methylacetate, [c]ΔΔE = (ΔE[**III**→**II**] – ΔE[**III**→**IV**]) [d] Value for **115**: 7.3 kcal/mol.

6.4 $RhX(CO)(PPh_3)_2$ Complexes as a Probe for the Donor Power of Anionic Ligands

A classic means of assessing the electronic nature of anionic ligands involves measuring the change in the IR stretching frequency of carbonyl ligand in complexes of the Vaska type, $RhX(CO)(PPh_3)_2$.[51] Vaska's work offered a simple probe of ligand donor power long before cyclic voltammetry[52] or DFT studies became routinely accessible.[53] While iridium complexes have also been used for this purpose, we chose to examine the rhodium derivatives, as a potentially better comparison to Ru systems.[b] The effects are well established.[51] π–Donating, σ-withdrawing X-ligands cause a decrease in the Rh-CO bond distance, and increase donation from the metal into the C-O π* antibonding orbital. The decrease in bond order for the carbonyl ligand results in a decrease in ν(CO). Where back-bonding onto the anionic ligand can compete, a higher-frequency ν(CO) band results. For strong σ-donors, the *trans* effect causes elongation of the Rh-CO bond, again decreasing back-bonding, and increasing the frequency of the ν(CO) band. While ambiguous results may therefore be found where the anionic donor can function as both a σ- and a π–donor, this is unlikely to be the case for oxygen-bound anionic ligands, as the high electronegativity of oxygen contributes to a relative σ-withdrawing effect.

Reaction of *trans*-$RhCl(CO)(PPh_3)_2$ with one equivalent of MX in THF resulted in clean formation of a series of *trans*-$RhX(CO)(PPh_3)_2$ complexes, the ν(CO) data for which are summarized in Table 7. Of the approximately two dozen derivatives prepared, the stretching frequency for the ν(CO) vibration is lowest for the OC_6Br_5 derivative. This suggests a strong σ-withdrawing/π-donating "push-pull" effect, as depicted in the bonding scheme of Figure 10. This effect may be important in offsetting the electron-withdrawing

[b] Some of the Vaska type complexes were prepared by Sebastien Monfette of this research group.

effect of the O ligand. However, this data must be approached with some caution, the vibration may be effected by the significantly larger OC_6Br_5 group.

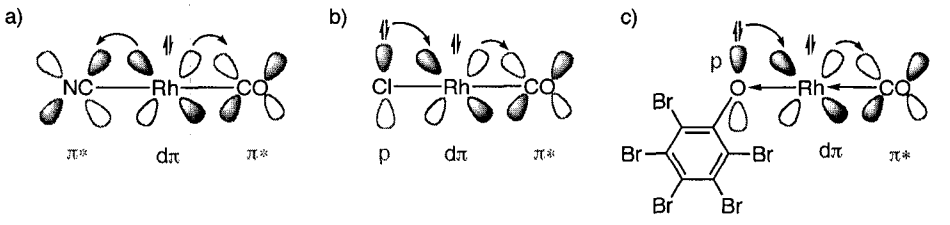

Figure 10. Interactions between the carbonyl and the anionic ligands in $RhX(CO)(PPh_3)_2$. a) π-acid, CN; b) π-base, Cl; c) π-base and σ-withdrawing OC_6Br_5.

Table 7. Comparison of X-ligand effect on IR CO stretch in [*trans*-$Rh(X)CO(PPh_3)_2$] **125**.

125	**X**	IR ν(CO) (cm^{-1}) Nujol	IR ν(CO) (cm^{-1}) CH_2Cl_2[51]
a	CN	2002	2003
b	NCS	1995	1990
c	NO_2		1996
d	SC_6F_5	1988	
e	NCO	1986	1982
f	I	1983	1981
g	$OC_6F_4C_6F_5$	1981	
h	Br		1980
i	OC_6F_4-4-CF_3	1079	
j	SC_6Cl_5	1972	
k	OC_6F_5	1971	
l	OC_6H_3-3,5-$(CF_3)_2$	1966	
m	Cl	1964	1980
n	SC_6H_5	1965	1980
o	O_2CPh		1973
p	O_2CMe		1972
q	F		1971
r	OC_6H_4-4-NO_2	1962	
s	OC_6H_5	1962	1970
t	OC_6H_4-3-CF_3	1962	
u	OH		1961
v	OC_6H_4-4-F	1956	
w	OC_6Cl_5	1956	
x	OC_6H_2-2,6-Br_2-4-NO_2	1954	
y	OC_6Br_5	1950	

[a] IR resolution 4 cm^{-1}.

6.5 Conclusion

The DFT studies summarized in this Chapter suggest that metathesis via catalysts of type **15** proceeds through a 18-16-electron pathway fundamentally different from the 16-14-electron mechanism operative for the Grubbs systems. Grubbs and co-workers have proposed that an effective ruthenium metathesis catalyst must contain both electron-donating and electron-withdrawing ligands: that the metal should be electron-rich to facilitate ligand dissociation, but electron-deficient, to favour olefin binding.[8] The strongly electron-withdrawing character of the Ru-OAr σ-bond contributes toward the latter, but impedes initiation by decreasing the lability of the pyridine ligand in **15**, relative to its chloride analogues. The π-donor capacity of the aryloxide ligand, and the dative Br···Ru interaction, presumably offset the high positive charge at the metal to some extent. Nevertheless, the metathesis activity of initiators **15** is impeded by their low initiation efficiency. Their impressive RCM performance is the more remarkable, given that it reflects the operation of a relatively small proportion of catalyst. Catalyst productivity comes at the expense of initiation efficiency.

6.6 References

(1) Bielawski, C. W.; Grubbs, R. H. *Angew. Chem., Int. Ed.*, **2000**, *39*, 2903-2906.
(2) Demel, S.; Schoefberger, W.; Slugovc, C.; Stelzer, F. *J. Mol. Catal.*, **2003**, *200*, 11-19.
(3) Slugovc, C.; Demel, S.; Stelzer, F. *Chem. Commun.*, **2002**, 2572-2573.
(4) Six, C.; Beck, K.; Wegner, A.; Leitner, W. *Organometallics,* **2000**, *19*, 4639-4642.
(5) Sanford, M. S.; Love, J. A.; Grubbs, R. H. *J. Am. Chem. Soc.*, **2001**, *123*, 6543-6554.
(6) Slugovc, C.; Riegler, S.; Hayn, G.; Saf, R.; Stelzer, F. *Macromol. Rapid Commun.*, **2003**, *24*, 435-439.
(7) Sanford, M. S.; Ulman, M.; Grubbs, R. H. *J. Am. Chem. Soc.*, **2001**, *123*, 749-750.
(8) Dias, E. L.; Nguyen, S. T.; Grubbs, R. H. *J. Am. Chem. Soc.*, **1997**, *119*, 3887-3897.
(9) Poor absolute sensitivity is a function of the low natural abundance (0.37%) and low sensitivity (1.04 x 10^{-3} vs. ^{1}H) of the ^{15}N isotope. The spin 1 nucleus ^{14}N, while more abundant (>99%) has a comparably low sensitivity and broad line, owing to quadrupolar relaxation effects.
(10) Ulman, M.; Grubbs, R. H. *J. Org. Chem.*, **1999**, *64*, 7202-7207.

(11) Ivin, K. J.; Mol, J. C., *Olefin Metathesis and Metathesis Polymerization.* Academic Press: New York, 1997.
(12) Slugovc, C.; Demel, S.; Riegler, S.; Hobisch, J.; Stelzer, F. *Macromol. Rapid Commun.,* **2004**, *25*, 475-480.
(13) Haigh, D. M.; Kenwright, A. M.; Khosravi, E. *Tetrahedron,* **2004**, *60*, 7217-7224.
(14) Haigh, D. M.; Kenwright, A. M.; Khosravi, E. *Macromolecules,* **2005**, *38*, 7571-7579.
(15) Bielawski, C. W.; Grubbs, R. H. *Macromolecules,* **2001**, *34*, 8838-8840.
(16) Choi, T.-L.; Grubbs, R. H. *Angew. Chem., Int. Ed.,* **2003**, *42*, 1743-1746.
(17) (a) Gold, L., *J. Chem. Phys.,* **1958**, *28*, 91. (b) Rempp, R.; Merrill, E. W., *Polymer Synthesis*; Huethig and Wepf : New York, 1986. (c) Bazan, G. C.; Khosravi, T.; Schrock, R. R.; Feast, W. J.; Gibson, V. C.; O'Regan, M. B.; Thomas, J. K.; Davis, W. M., *J. Am. Chem. Soc.,* **1990**, *112*, 8378-8379.
(18) Williams, J. E.; Harner, M. J.; Sponsler, M. B. *Organometallics,* **2005**, *24*, 2013-2015.
(19) Adlhart, C.; Chen, P. *J. Am. Chem. Soc.,* **2004**, *126*, 3496-3510.
(20) Straub, B. F. *Angew. Chem., Int. Ed.,* **2005**, *44*, 5974-5978.
(21) Cavallo, L. *J. Am. Chem. Soc.,* **2002**, *124*, 8965-8973.
(22) Vyboishchikov, S. E.; Buhl, M.; Thiel, W. *Chem. Eur. J.,* **2002**, *8*, 3962-3975.
(23) Amoroso, D.; Fogg, D. E. *Macromolecules,* **2000**, *33*, 2815-2818.
(24) Werner, H.; Braun, T.; Daniel, T.; Gevert, O.; Schulz, M. *J. Organomet. Chem.,* **1997**, *541*, 127-141.
(25) Catala, R. M.; Cruz-Garritz, D.; Hills, A.; Hughes, D. L.; Richards, R. L.; Sosa, P.; Torrens, H. *Chem. Commun.,* **1987**, 261-262.
(26) Darensbourg, D. J.; Fontal, B.; Chojnacki, S. S.; Klausmeyer, K. K.; Reibenspies, J. H. *Inorg. Chem.,* **1994**, *33*, 3526-3532.
(27) Fries, G.; Ilg, K.; Pfeiffer, M.; Stalke, D.; Werner, H. *Eur. J. Inorg. Chem.,* **2000**, 2597-2601.
(28) Sinha, P. K.; Falvello, L. R.; Peng, S. M.; Bhattacharya, S. *Polyhedron,* **2000**, *19*, 1673-1680.
(29) Ung, T.; Hejl, A.; Grubbs, R. H.; Schrodi, Y. *Organometallics,* **2004**, *23*, 5399-5401.
(30) Pruehs, S.; Lehmann, C. W.; Fuerstner, A. *Organometallics,* **2004**, *23*, 280-287.
(31) Slugovc, C.; Perner, B.; Stelzer, F.; Mereiter, K. *Organometallics,* **2004**, *23*, 3622-3626.
(32) Volatron, F.; Eisenstein, O. *J. Am. Chem. Soc.,* **1986**, *108*, 2173-2179.
(33) Eisenstein, O.; Hoffmann, R.; Rossi, A. R. *J. Am. Chem. Soc.,* **1981**, *103*, 5582-5584.
(34) Aagaard, O. M.; Meier, R. J.; Buda, F. *J. Am. Chem. Soc.,* **1998**, *120*, 7174-7182.
(35) Weskamp, T.; Schattenmann, W. C.; Spiegler, M.; Herrmann, W. A. *Angew. Chem., Int. Ed.,* **1998**, *37*, 2490-2493.
(36) Huang, J.; Stevens, E. D.; Nolan, S. P.; Petersen, J. L. *J. Am. Chem. Soc.,* **1999**, *121*, 2674-2678.
(37) Schwab, P.; Grubbs, R. H.; Ziller, J. W. *J. Am. Chem. Soc.,* **1996**, *118*, 100-110.
(38) Romero, P. E.; Piers, W. E. *J. Am. Chem. Soc.,* **2005**, *127*, 5032-5033.
(39) Adlhart, C.; Chen, P. *J. Am. Chem. Soc.,* **2004**, *126*, 3496-3510.
(40) Aptula, A. O.; Netzeva, T. I.; Valkova, I. V.; Cronin, M. T. D.; Schultz, T. W.; Kuhne, R.; Schuurmann, G. *QSAR,* **2002**, *21*, 12-22.
(41) Pauling, L., *The Nature of the Chemical Bond, 3rd ed.* Cornell Univ.: Ithaca, U.S., 1960.
(42) Schrock, R. R. *Polyhedron,* **1995**, *14*, 3177-3195.
(43) Caulton, K. G. *New J. Chem.,* **1994**, *18*, 25-41.

(44) Carpenter, J. E.; Weinhold, F. *Theochem,* **1988**, *46*, 41-62.
(45) Benitez, D.; Goddard, W. A., III *J. Am. Chem. Soc.,* **2005**, *127*, 12218-12219.
(46) Forman, G. S.; McConnell, A. E.; Tooze, R. P.; Van Rensburg, W. J.; Meyer, W. H.; Kirk, M. M.; Dwyer, C. L.; Serfontein, D. W. *Organometallics,* **2005**, *24*, 4528-4542.
(47) Ritter, T.; Day, M. W.; Grubbs, R. H. *J. Am. Chem. Soc.,* **2006**, *128*, 11768-11769.
(48) Delgado-Jaime, M. U.; Conrad, J. C.; Fogg, D. E.; Kennepohl, P. *Inorg. Chim. Acta,* **2006**, *359*, 3042-3047.
(49) Halpern, J. *Science,* **1982**, *217*, 401-407.
(50) Adlhart, C.; Chen, P. *Helv. Chim. Acta,* **2003**, *86*, 941-949.
(51) Vaska, L.; Rhodes, R. E. *J. Am. Chem. Soc.,* **1965**, *87*, 4970-4971.
(52) Lever, A. B. P. *Inorg. Chem,* **1990**, *29*, 1271-1285.
(53) Perrin, L.; Clot, E.; Eisenstein, O.; Loch, J.; Crabtree, R. H. *Inorg. Chem.,* **2001**, *40*, 5806-5811.

References page 201

7 Conclusions and Future Directions

This work described in this thesis began with fundamental studies directed at synthesis of stable ruthenium-aryloxide complexes. Consideration of both steric and electronic parameters enabled the construction of a family of "pseudohalide" catalysts with the general formula RuXX'(CHPh)(IMes)(py). Key issues in gaining access to these complexes were: (a) minimizing the steric demand present in both the Ru alkylidene precursor and the incoming anionic ligand, which allowed us to circumvent formation of Ru-carbynes via α-elimination, and (b) preventing isomerization of the Ru(σ-OAr) moiety into π-bound arene complexes by use of electron-deficient aryloxide ligands. Notable as an inference from point (a) is the possibility of exploiting the α-elimination chemistry to develop general routes to coordinatively unsaturated ruthenium carbynes, long-sought species that could enable alkyne metathesis chemistry.

Unique to these catalysts, among the Ru metathesis catalysts so far developed, is their modular structure, which permits control over selectivity via matching of catalyst and substrate reactivity. The extreme of selectivity is found in asymmetric catalysis, and incorporation of suitably adapted, chiral aryloxides within this catalyst platform holds great promise for stereoselective transformations relying on matching of catalyst and substrate sterics, as well as reactivity.

Also unique are some aspects of their reactivity. The initiation efficiency of these catalysts is reduced by their electron-deficiency (though this is attenuated in the case of **15**, containing one perbromoaryloxide and one chloride, by an *ortho*-Br···Ru interaction), and they fall somewhere between the second- and third-generation Grubbs catalysts in terms of activity in such undemanding reactions as ROMP of cyclooctene or RCM of diethyldiallyl

malonate. This can be an asset, however, in delivering a sustained infusion of active catalyst from a reservoir of uninitiated species, and their longer lifetimes (or, perhaps, the longer duration of release) enables higher productivity in RCM of more demanding substrates. Their tolerance for sulfide donors, and their activity in enyne metathesis, is particularly notable, as indeed is their performance in CM (in, e.g., self-metathesis of methyl oleate) at very low catalyst loadings. In RCM of a range of other five- or six-membered substrates, their performance relative to the most active of the Grubbs systems is sometimes better, sometimes less good, with the optimum catalyst being a matter of trial and error (though the sustained activity of the aryloxide catalysts means that they often perform better in reactions that require long lifetimes). With the help of additives, the reactivity of **15b** could be optimized for quantitative formation of tetrasubstituted olefin, a first in Ru-catalyzed metathesis.

Where the aryloxide catalysts are set apart from any of the pre-existing catalyst systems, however, is in their ability to effect RCM of conformationally flexible substrates – dienes that form rings larger than six members, for which cyclization is not driven by a strong conformational bias. In the course of this work, we discovered that RCM of such rings via the Grubbs-NHC catalysts does not proceed by direct ring-closing, as had previously been believed, but instead via oligomerization and backbiting. The mono-aryloxide catalysts are astonishingly more efficient than their chloride analogues in this reaction, and therefore for RCM of medium-sized and macrocyclic ring systems. A question of keen interest is whether their rapid formation of cyclic products reflects an inherent bias toward direct RCM, or simply faster backbiting.

DFT studies indicated that the slow initiation of **15** (i.e. slow ligand loss) is countered by a decrease in the energy barrier to cyclometallation. Again, this suggests as a cumulative effect the creation of a reservoir of uninitiated catalyst that can slowly release the active species. As with most of these catalysts, a trade-off exists between initiation efficiency and productivity. The RCM performance of **15** is the more impressive, if this reflects operation of a small amount of the active species, and a more detailed evaluation of this point (by MALDI-MS studies, NMR analysis, and ROMP of additional monomers is warranted).

Further investigation into the properties of the OC_6Br_5 ligand would also be valuable in gaining deeper insight. Determination of Dq (Δ_{OCT}) and the Lever electronic parameter (LEP) will help to place the ligand within the spectrochemical or electrochemical series. As well, a more detailed theoretical investigation mapping the orbital between the anionic donors and Ru, especially for the transition state leading to the key metallacyclobutane intermediate, may be useful in pinpointing the factors responsible for the low barrier to metathesis found in **15a/b**. This may have predictive value for identification of new anionic ligands that confer performance superior to perbromoaryloxide. The steric and electronic effects of anionic ligands are beginning to be understood: work on Ru-catecholate catalysts by Sebastien Monfette of this research group holds much promise for its potential to deconvolute the effect of electronic and steric parameters in Ru-catalyzed olefin metathesis.

A further catalyst formulation can be obtained by altering the neutral ligands to afford structures with the general formulation $[RuX(OC_6Br_5)(CHR)LL']$. Factors worth exploring include alternative NHC ligands (such as H_2IMes, iPr, etc.), as well as replacement of the potentially π-accepting pyridine ligand with a more labile ligand, changing chloride for a different anionic ligand (or removing it altogether making a cationic complex), changing

alkylidene for styrene ether or phosphonium alkylidene may be worthwhile. Modification of the aryloxide ligands to create a link to a solid support would enable easy catalyst separation and potentially flow through metathesis reactors to be developed. Furthermore, exciting new chiral derivatives (not included here) already show promising results.

Issues of catalyst design aside, the most important discovery of this thesis was the uncovering of a previously unrecognized mechanism for RCM, now one of the one of the most widely used reactions in chemical synthesis. As alluded to above, this involves the kinetically driven oligomerization of α,ω-dienes, followed by a concentration-dependent cyclodepolymerization–ROMP equilibrium which yields the intended RCM products. Of fundamental (and indeed practical) importance is the implication that the optimal reaction concentration for RCM is determined not by the kinetic parameters, but by thermodynamic parameters such as ring strain and translational entropy, which govern the equilibrium between cyclic product and oligomer. It also means that the observation of oligomers at the initial stages of a reaction – often taken as a sign that RCM has failed – has been completely misinterpreted in this research area. Many negative results in the literature may in fact be an artifact of not allowing the reaction to reach equilibrium at an appropriate concentration, which prevents the yield from reaching a maximum. Because RCM is used so widely in industry and academia, the impact of these results is expected to be far-reaching.

The oligomer-backbiting story has just been opened, and many very important questions remain to be answered. What role does catalyst and catalyst concentration play? Can metathesis catalysts be described as having an effective molarity (as enzymes do)? What is the rate of backbiting compared to RCM for different catalysts? Once catalyst is installed on the oligomer, is the rate zero order in oligomer, as our proposed mechanism would

suggest? What is the impact of this mechanism on asymmetric catalysis? A detailed kinetic analysis of the backbiting mechanism will likely provide some important answers, and most interesting will be how this information might be used to access difficult ring sizes and chiral targets.

Table 1. ROMP of 200 equivalents of cyclooctene followed by NMR with various catalysts, [S] = 0.1 M $CDCl_3$, 21 °C

Time (h)	**2a**	**3a**	**12a**	**12a**[1]	**12b**	**13**	**14a**	**15a**	**15b**	**16a**	**16b**	**17**	**18a**	**19b**
0	0	0	0	0	0	0	0	0	0	0	0	0	0	0
0.08	90	98							82	4	4	23	1	24
0.17	98			90					93	7	7	37	1	46
0.25	98			98	6		49	80	96	9	11	45	1	56
0.50			5	98	8	4	63	89	98	27	15	52	1	65
0.75						4	87	96	98	36	19	58	2	71
1.00			8		17	4	93	97		45	23	61	2	76
1.25						5	95	98		60	28	72	2	84
1.50			11		24	6	96	97		71	31	81	2	87
1.75						7	96	98		79	34	84	2	92
2.00			16		31	8	96			86	38	87	3	93
2.25						9	97			90	41	89	3	95
2.50			20		38	10	97			93	44	93	3	96
2.75						11	98			95	47	95	4	97
3.00			25		44	12	98			97	53	95	4	97
3.50			30		50	15	98			98	58		5	97
4.00			35		55	17	98			99	62		5	97
4.50			40		60	20				99	65		6	98
5.00			44		65	21					68		6	
5.50			48		69	25					71		7	
6.00			52		72	28					74		8	
6.50			56		75	30					76		9	
7.00			60		78	33					78		9	
7.50			63		80	37					80		10	
8.00			66		82	39					81		11	
8.50			69		84	43					82		11	
9.00			72		86								12	
9.50			74		87								12	
10.00			76		88								13	

[1] 60 °C

Table 2. Solvent screen for formation of **22** from **21** using 0.5 mol% Ru, [**21**] = 0.1 M, 75 °C, 3 h.

Catalyst	CH_2Cl_2	$CDCl_3$	1,2-DCE	PhCl	FC-72	C_6F_6	BTF	benzene	toluene	decane	THF	DME	DMF	NMP	$PhNO_2$	MeCN	DMSO
1	95	98	67	99	89	98	92	89	99	98	71	98	8	31	99	1	1
2a	98	98	99	99	94	98	98	98	99	98	90	93	34	22	48	6	1
3a	99	98	83	84	83	94	59	97	92	45	88	82	52	32	70	24	2
3b	99	98	87	93	90	88	69	98	97	88	91	87	46	29	75	23	4
12a	32	90	83	9	32	84	71	32	13	10	7	4	7	4	2	0	0
12b	32	88	73	7	17	93	62	18	6	5	9	6	8	4	1	0	0
15a	92	80	59	62	79	66	72	74	63	81	59	54	36	26	29	11	1
15b	97	68	74	68	84	67	73	78	53	79	60	59	47	39	34	15	1

± % error on replicate runs (below)

1	1.3	0.3	7.1	0.1	1.3	0.0	1.4	0.4	0.1	0.0	0.4	0.0	0.1	0.5	0.0	0.1	0.1
2a	0.0	0.1	0.1	0.1	0.8	0.2	0.1	0.0	0.3	0.4	1.0	0.6	0.0	0.1	0.8	0.2	0.1
3a	0.9	0.1	0.9	1.6	2.7	0.6	1.1	0.2	1.0	0.8	0.4	0.3	0.1	0.3	2.5	0.6	0.1
3b	0.9	0.0	1.0	0.7	2.7	0.8	9.1	0.1	0.4	2.8	0.7	1.4	0.2	0.1	0.3	0.6	0.1
12a	1.0	0.6	4.0	0.0	1.8	2.8	0.3	1.0	5.7	3.1	2.5	0.6	0.2	0.1	1.0	0.1	0.0
12b	15.8	0.6	1.2	0.2	0.7	2.1	1.4	0.0	0.3	0.3	0.3	0.1	0.2	0.4	0.0	0.0	0.0
15a	0.7	0.3	1.6	2.5	7.4	0.0	0.6	0.1	4.2	6.4	1.3	1.8	0.5	0.7	0.5	0.2	0.1
15b	0.6	0.3	2.8	5.9	0.6	1.1	1.3	0.5	6.2	3.3	1.3	4.1	1.0	0.1	0.0	0.7	0.1

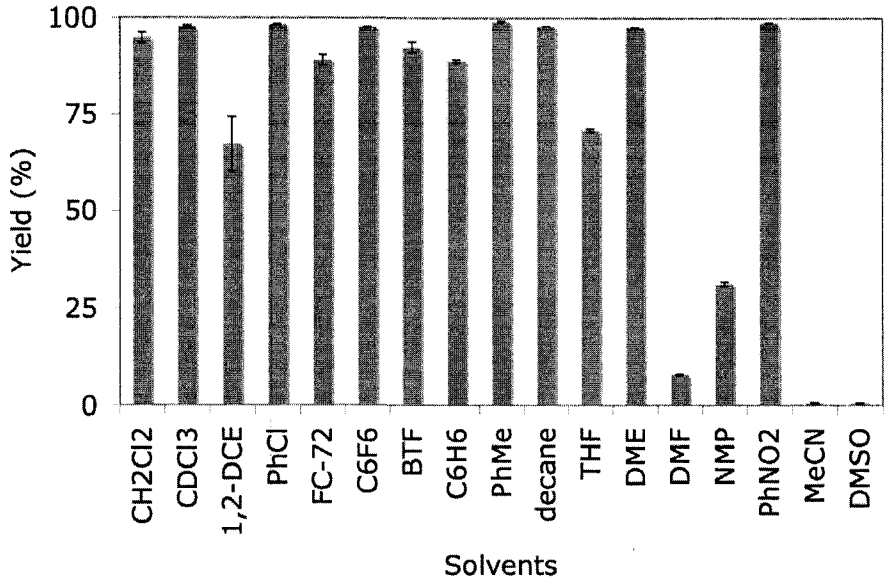

Figure 1. Solvent screen yield for catalyst **1**, conditions as in Table 2 above.

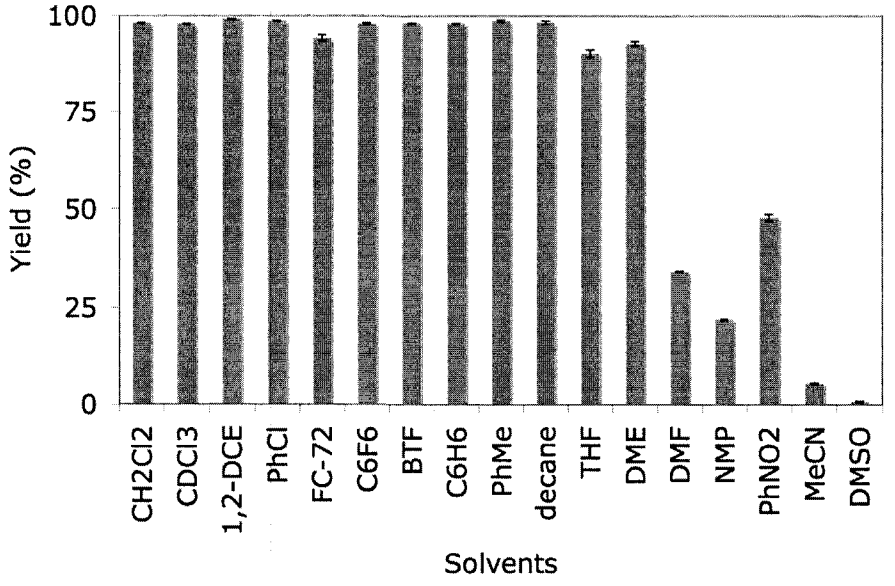

Figure 2. Solvent screen yield for catalyst **2a**, conditions as in Table 2 above.

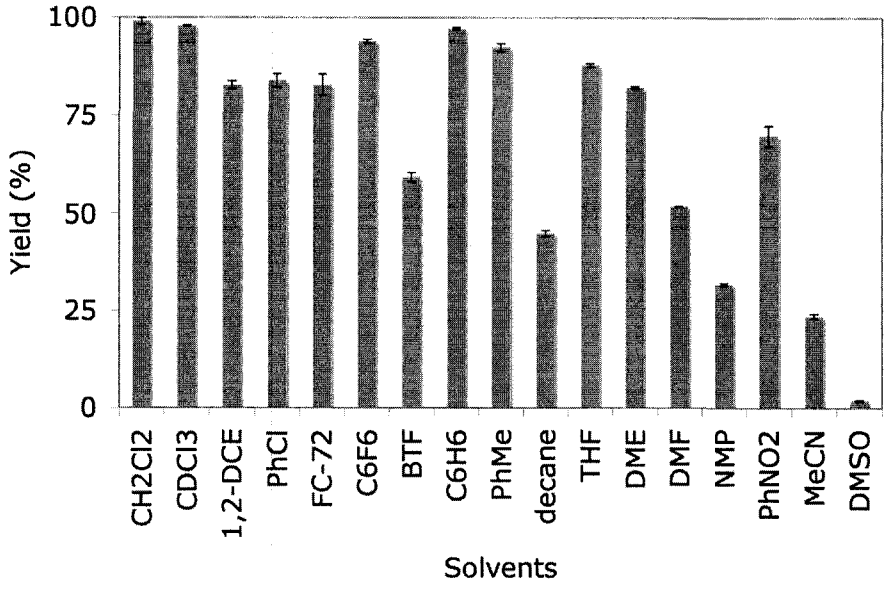

Figure 3. Solvent screen yield for catalyst **3a**, conditions as in Table 2 above.

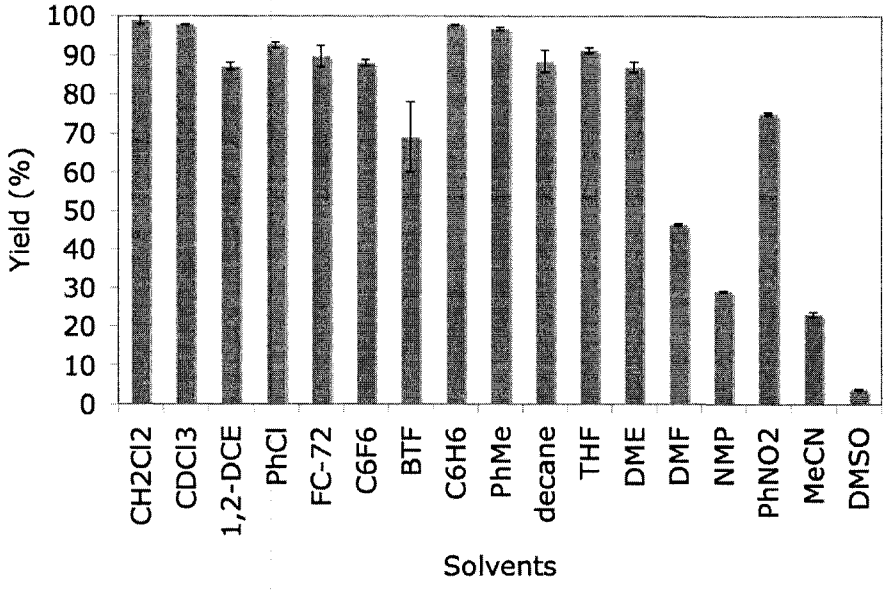

Figure 4. Solvent screen yield for catalyst **3b**, conditions as in Table 2 above.

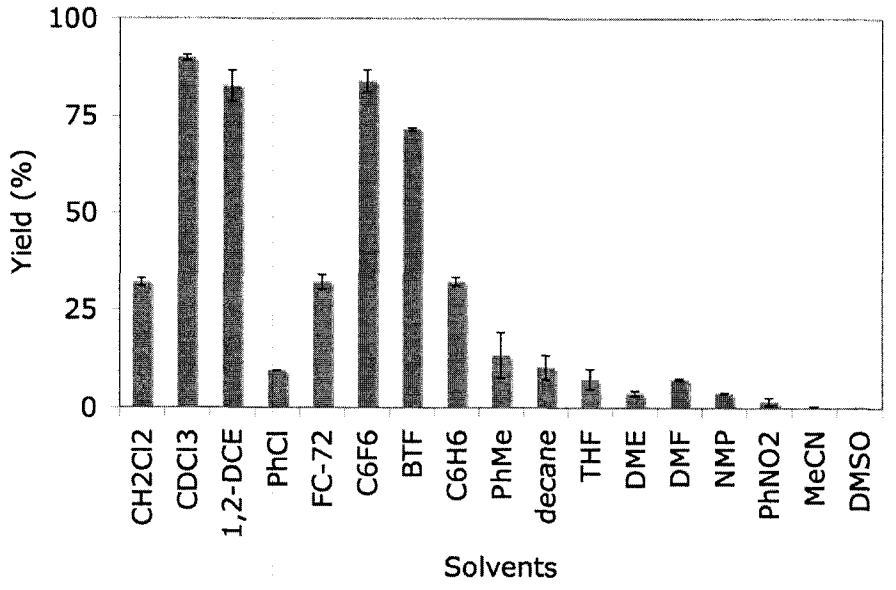

Figure 5. Solvent screen yield for catalyst **12a**, conditions as in Table 2 above.

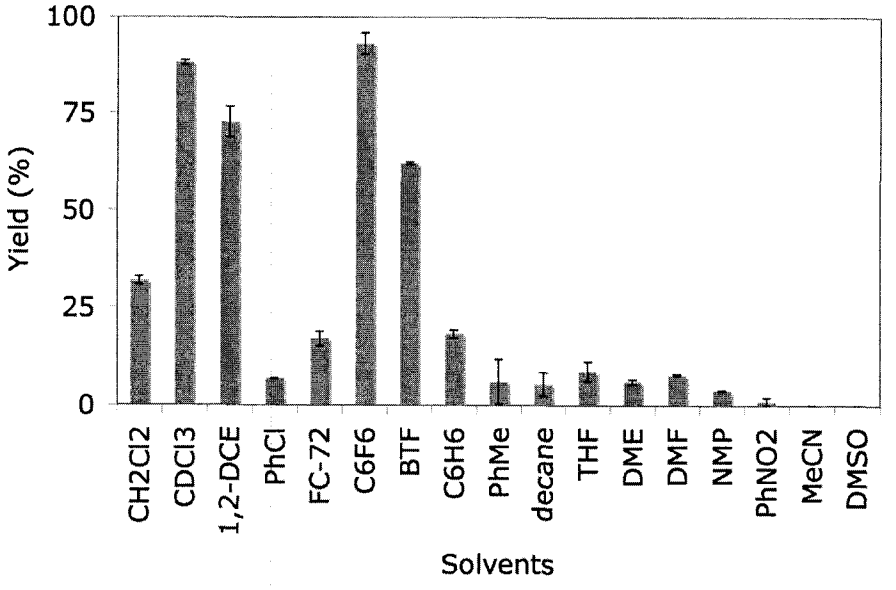

Figure 6. Solvent screen yield for catalyst **12b**, conditions as in Table 2 above.

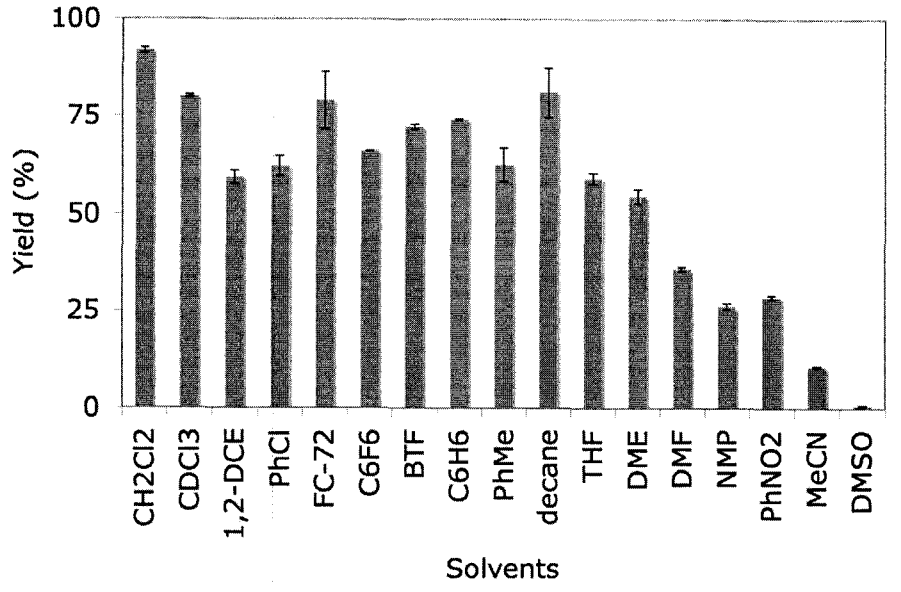

Figure 7. Solvent screen yield for catalyst **15a**, conditions as in Table 2 above.

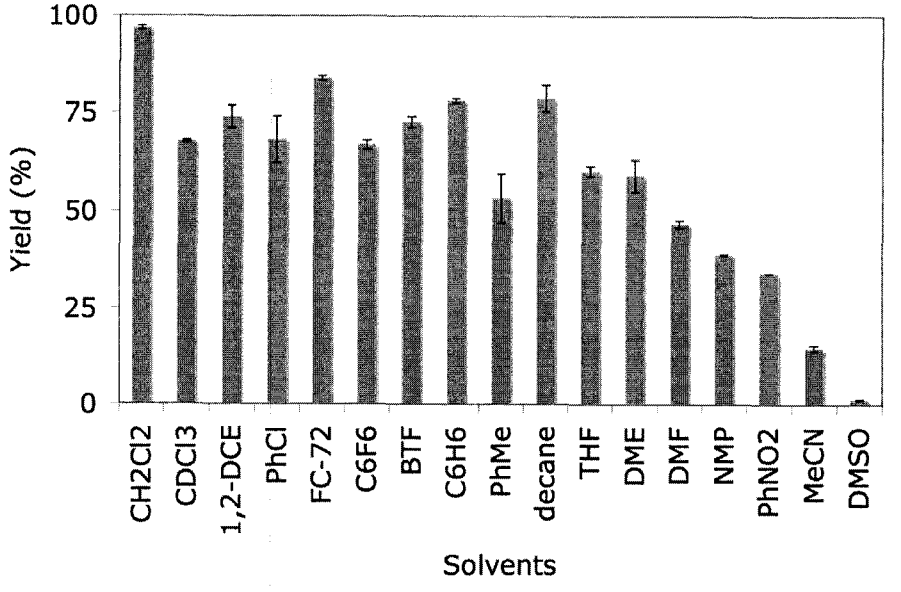

Figure 8. Solvent screen yield for catalyst **15b**, conditions as in Table 2 above.

Table 3. Yield and error of enyne metathesis additive screen.

Additive	Yield (%)	± error
Blank	36.31	1.23
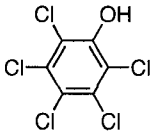	29.77	0.20
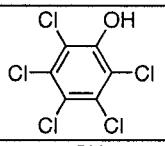	36.06	0.28
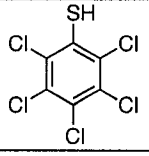	8.36	1.08
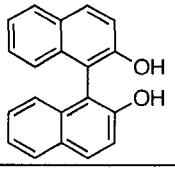	30.31	0.16
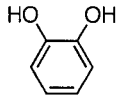	21.84	2.26
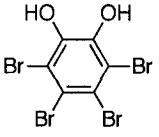	26.69	1.26
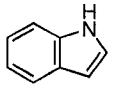	5.97	0.26
NH_4Cl	7.71	0.81
NH_4PF_6	2.37	0.24
	0.79	0.20

Additive	Yield (%)	± error
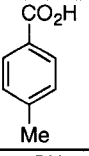	0.94	0.66
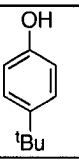	32.86	0.24
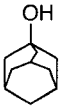	39.54	0.69
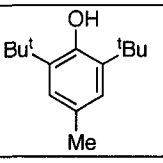	40.65	0.40
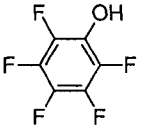	38.75	0.35
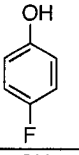	31.24	0.02
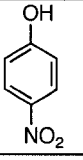	26.36	0.36
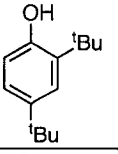	38.72	1.18
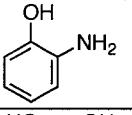	16.21	1.88
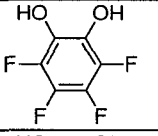	39.71	4.39
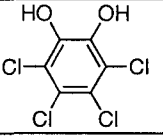	32.16	4.02

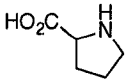	0.94	0.24
	0.57	0.57
NH_3SO_3H	0.31	0.31

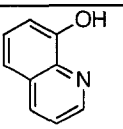	4.34	0.32
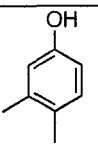	30.00	0.46
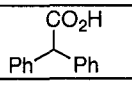	35.04	0.54

Table 4. Narrowed Additive Screen results and error.

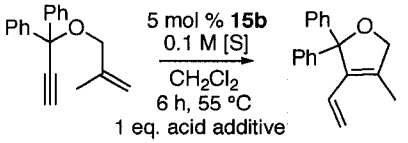

Additive	Yield (%)	(+/-)
Blank	73.4	2.6
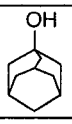	65.6	6.7
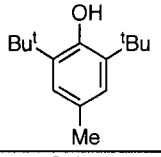	79.6	1.0
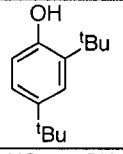	73.5	1.5
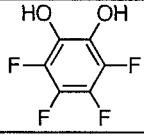	35.6	2.1

Table 5. Equivalents of BHT screen results and error.

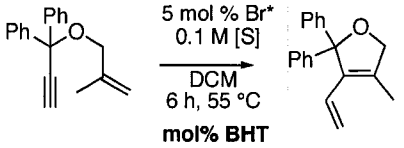

BHT mol%	Yield (%)	(+/-)
0	70.8	2.6
10	74.9	3.5
20	77.0	3.0
30	79.4	2.2
40	79.5	2.6
50	81.3	0.8
60	80.9	0.1
70	82.4	1.1
80	82.7	1.1
90	82.1	1.6
100	81.8	1.9

Table 6. Concentration of substrate screen results and error.

[S] M	Yield (%)	(+/-)
0.1	91.6	0.3
0.25	93.3	0.1
0.5	94.3	0.2
0.75	91.4	0.1
1	88.6	1.3

Table 7. RCM of **58** with 5 mol% **2a**, slow addition protocol, refluxing CH_2Cl_2 (<<5 mM).

Time (h)	Diene (%)	RCM (%)	Oligomers (%)	(± %) Diene	(± %) RCM
0	100	0	0	0	0
0.25	10	35	55	3	4
0.5	7	41	52	5	3
0.75	2	46	52	0	2
1	2	51	47	0	2
1.5	2	56	42	0	0
5	1	82	18	1	0
9	0	96	4	0	0

Table 8. RCM of **58** via 5 mol% **2a**, 21 °C 15 min, then refluxing CH_2Cl_2 (5 mM).

Time (h)	Diene (%)	RCM (%)	Oligomers (%)	(± %) Diene	(± %) RCM
0	100	0	0	0	0
0.25	12	37	51	0	1
0.5	2	55	43	0	2
0.75	4	61	35	0	0
1	4	66	31	0	0
1.5	5	75	21	0	1
2	5	78	17	0	0
3	5	86	8	1	1
5	1	100	0	0	4

Table 9. RCM of **58** with 5 mol% **2a**, 21 °C 15 min, refluxing CH_2Cl_2 (0.1 M).

Time (h)	Diene (%)	RCM (%)	Oligomers (%)	(± %) Diene	(± %) RCM
0	100	0	0	0	0
0.25	5	10	85	1	2
0.5	1	4	95	0	1
0.75	1	4	95	0	1
1	1	4	95	0	1
1.5	1	5	94	0	0
2	1	5	95	0	1
3	1	5	95	0	1
5	1	5	95	0	1

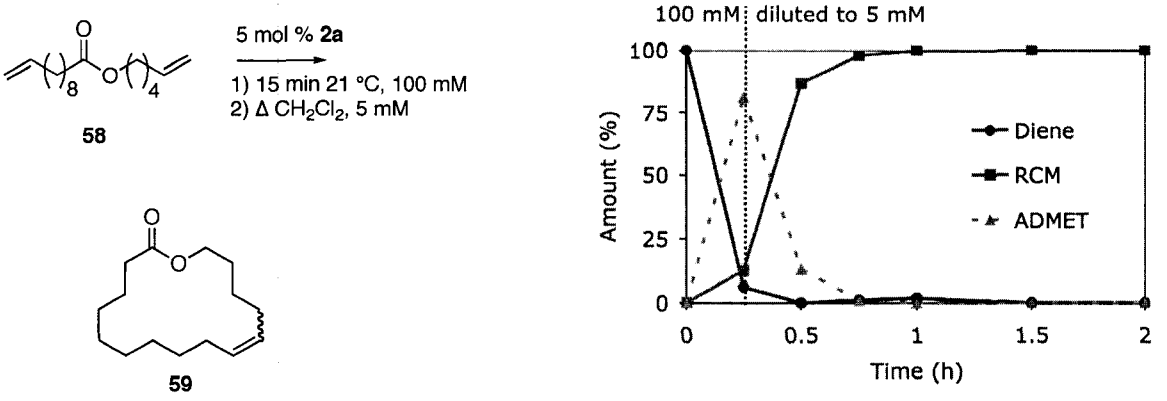

Figure 9. ADMET polymerization of **58** at 100 M, then depolymerization via backbiting RCM at 5 mM to yield RCM product **59**.

Table 10. RCM of **58** with 5 mol% **2a**, 0.1 M, 21 °C then after 15 min diluted to 5 mM and heated to reflux.

Time (h)	Diene (%)	RCM (%)	Oligomers (%)	(± %) Diene	(± %) RCM
0	100	0	0	0	0
0.25	6	13	81	1	3
0.5	0	87	13	0	3
0.75	1	98	1	1	0
1	2	100	0	1	4
1.5	0	100	0	0	1

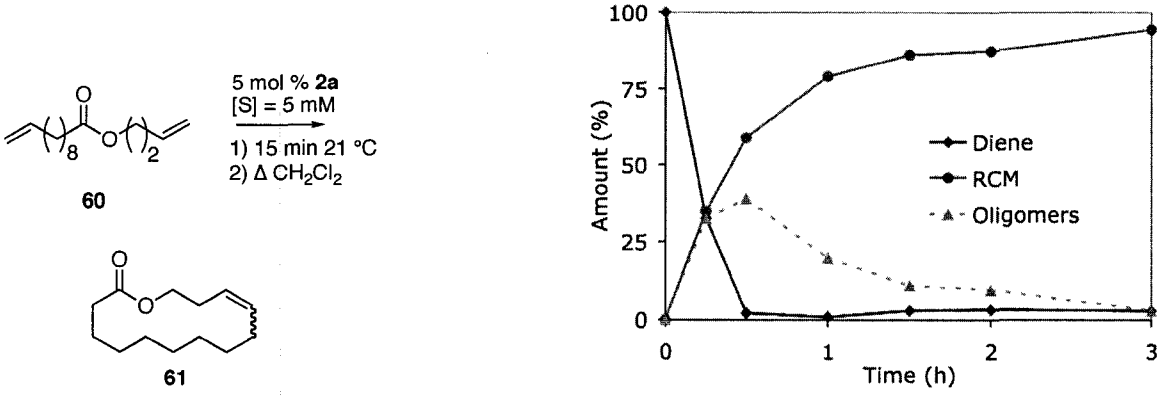

Figure 10. RCM of **60** to form 14-membered lactone **61** using 5 mol % **2a**, 21 °C 15 minutes then refluxing dichloromethane (5 mM).

Table 11. RCM of **61** with 5 mol% **2a**, 21 °C 15 min, then refluxing CH_2Cl_2 (5 mM).

Time (h)	Diene (%)	RCM (%)	Oligomers (%)	(± %) Diene	(± %) RCM
0	100	0	0	0	0
0.25	37	35	28	2	1
0.5	2	69	29	0	3
0.75	2	76	21	0	1
1	2	79	19	0	3
1.5	3	86	12	0	0
2	3	87	10	0	0
3	3	94	3	1	2

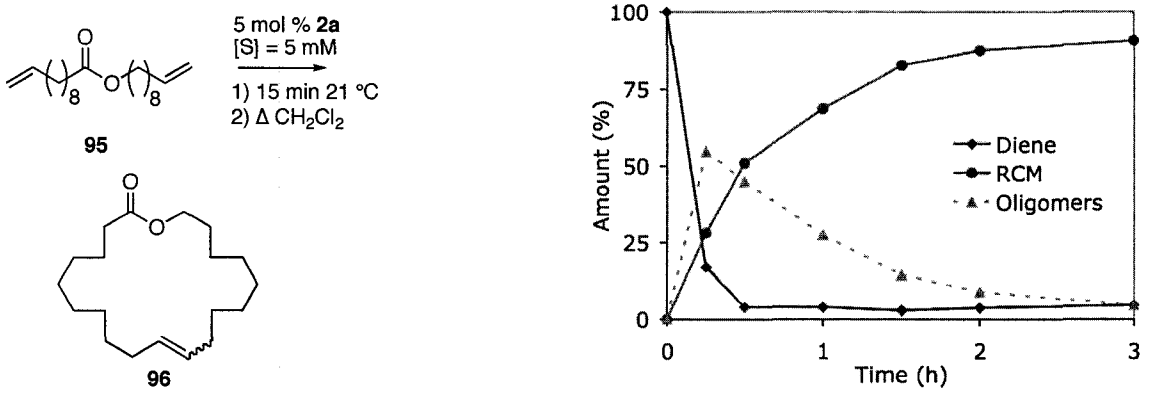

Figure 11. RCM of **95** to form 20-membered lactone **96** using 5 mol % **2a**, 21 °C 15 minutes then refluxing dichloromethane (5 mM).

Table 12. RCM of **95** with 5 mol% **2a**, 21 °C 15 min, refluxing CH_2Cl_2 (5 mM).

Time (h)	Diene (%)	RCM (%)	Oligomers (%)	(± %) Diene	(± %) RCM
0	100	0	0	0	0
0.25	17	28	55	5	1
0.5	4	51	45	0	2
0.75	6	54	40	2	0
1	4	69	27	1	1
1.5	3	83	14	0	5
2	4	87	9	1	4
3	5	91	5	1	1

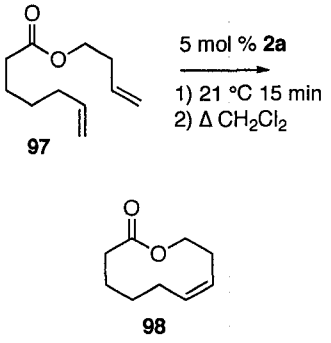

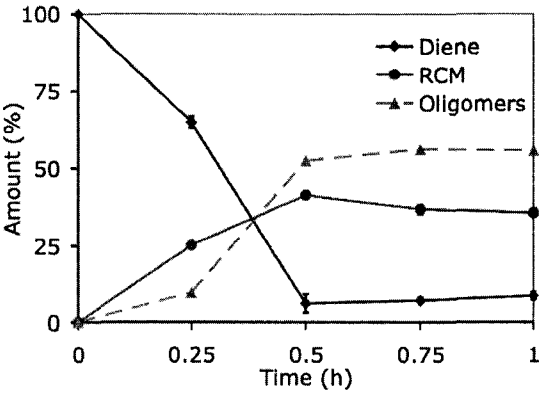

Figure 12. . RCM of **97** to form 10-membered lactone **98** using 5 mol % **2a**, 21 °C 15 minutes then refluxing dichloromethane (5 mM).

Table 13. RCM of **97** with 5 mol% **2a**, 21 °C 15 min, refluxing CH_2Cl_2 (5 mM).

Time (h)	Diene (%)	RCM (%)	Oligomers (%)	(± %) Diene	(± %) RCM
0	100	0	0	0	0
0.25	65	25	10	2	0
0.5	6	41	52	3	0
0.75	7	37	56	1	1
1	9	36	56	1	1

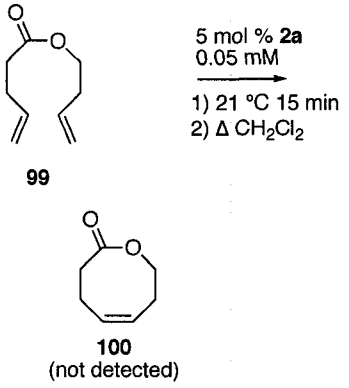

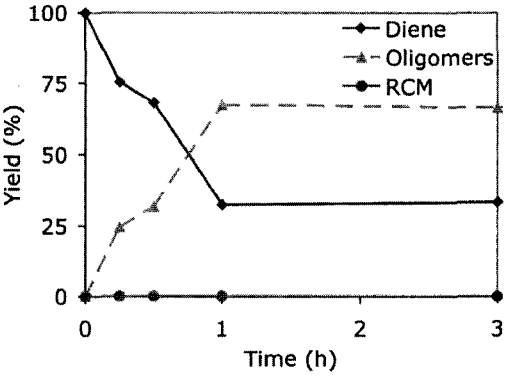

Figure 13. Attempted RCM of **99** to form 8-membered lactone **100** using 5 mol % **2a**, 21 °C 15 minutes then refluxing dichloromethane (0.05 mM).

Table 14. RCM of **99** with 5 mol% **2a**, , 21 °C 15 min, then refluxing CH_2Cl_2 (0.05 mM).

Time (h)	Diene (%)	RCM (%)	Oligomers (%)
0	100	0	0
0.25	75	0	25
0.5	68	0	32
1	33	0	67
3	33	0	67

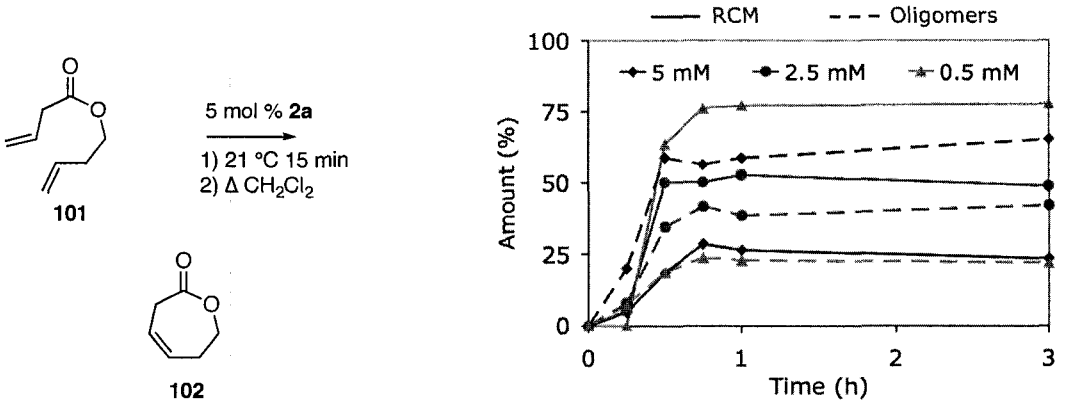

Figure 14. RCM of **101** with 5 mol % **2a** to form 7 membered lactone **102** at different concentrations. The RCM yield is shown as a solid line and the oligomer yield is shown as a dotted line.

Table 15. RCM of **101** with 5 mol% **2a**, , 21 °C 15 min, then refluxing CH_2Cl_2 (5 mM).

Time (h)	Diene (%)	RCM (%)	Oligomers (%)	(± %) Diene	(± %) RCM
0	100	0	0	0	0
0.25	75	5	20	0	1
0.5	23	19	59	2	12
0.75	15	29	56	1	6
1	15	26	59	1	3
3	11	23	65	1	3

Table 16. RCM of **101** with 5 mol% **2a**, , 21 °C 15 min, then refluxing CH_2Cl_2 (0.5 mM).

Time (h)	Diene (%)	RCM (%)	Oligomers (%)	(± %) Diene	(± %) RCM
0	100	0	0	0	0
0.25	93	0	7	7	0
0.5	18	64	19	1	1
0.75	0	76	24	0	0
1	0	77	23	0	1
3	0	78	22	0	1

Table 17. RCM of **101** with 5 mol% **2a**, , 21 °C 15 min, then refluxing CH_2Cl_2 (2.5 mM).

Time (h)	Diene (%)	RCM (%)	Oligomers (%)	(± %) Diene	(± %) RCM
0	100	0	0	0	0
0.25	87	5	8	0	0
0.5	15	50	34	1	3
0.75	8	50	42	4	2
1	9	53	38	3	5
3	9	49	42	0	1

Table 18. ROMP (%) of NBE- CH_2OAc using various catalysts followed by ^1H NMR in $CDCl_3$, [NBE-CH_2OAc] = 0.1 M, 21 °C.

Time (h)	**12a**	**12b**	**15a**	**15b**	**15b** + 80 mol% BHT
0	0		0	0	0
0.08			73	100	77
0.17			87		89
0.25			91		95
0.33			93		98
0.42			95		99
0.50	4	4	98		100
0.58					
0.67					
0.75			100		
1	7	6			
1.5	10	9			
2	14	12			
2.5	19	16			
3	24	22			
3.5	29	29			
4	34	36			
4.5	38	45			
5	42	53			
5.5	46	60			
6	49	68			
6.5	53	73			
7	55	79			
7.5	59	84			
8		88			
8.5		92			
9		95			
9.5		96			

Table 19. Self-metathesis of methyl oleate, neat, 60 °C 24 h.

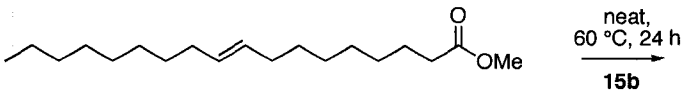

75

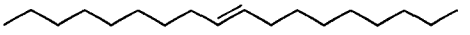

76

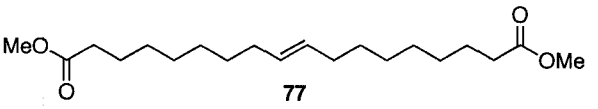

77

Entry	Catalyst	Equiv. **75**	Conv. of **75** (%)	Error (± %)	TON
1	**15b**	40,000	46	3	18,200
2	**15b**	100,000	47	3	47,000
3	**15b**	1,000,000	48	3	480,000
4	**15b**	2,000,000	43	2	860,000

[a]Determined by calibrated GC-FID, HP-1 column.

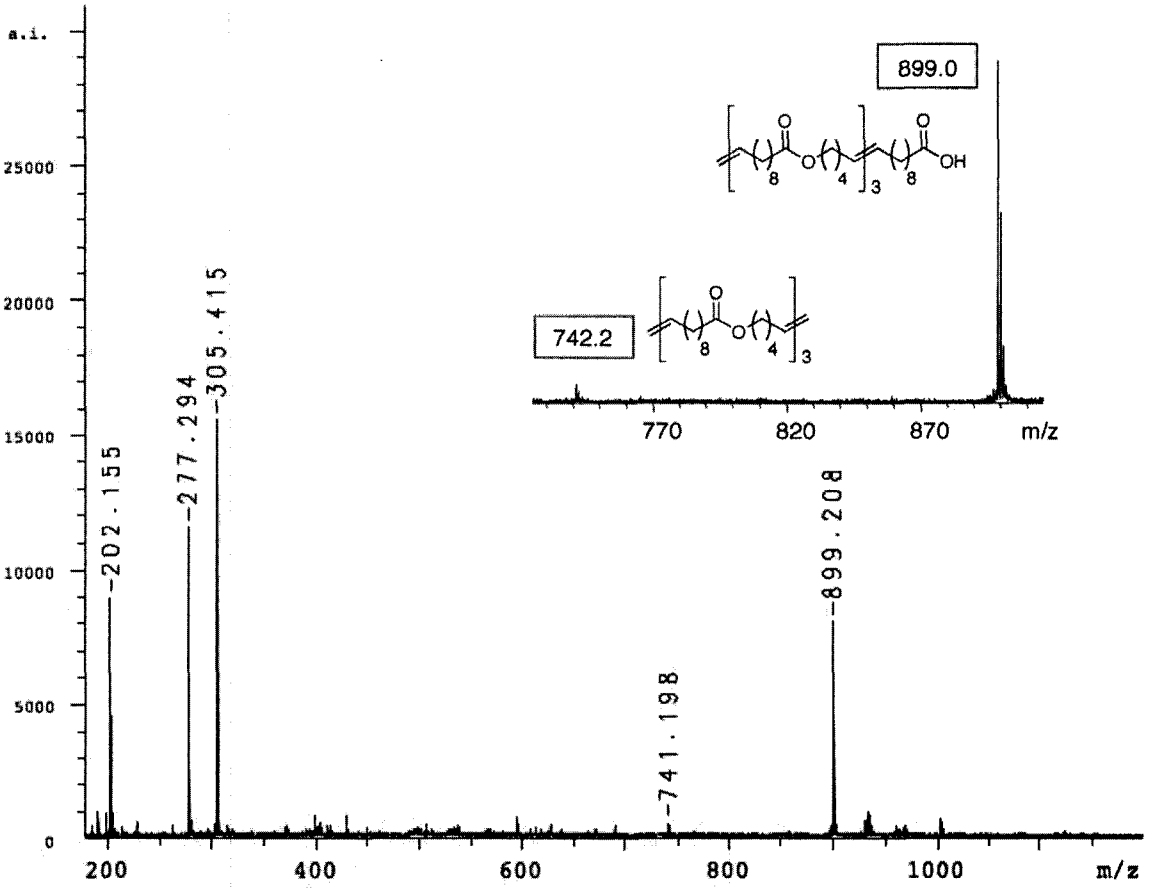

Figure 1. Full MALDI-TOF spectrum of the ADMET oligomer poly-**58** obtained from **58** using 5 mol% **2a**, Ziegler high dilution conditions, [S] = 5 mM, 15 minutes in refluxing CH_2Cl_2.

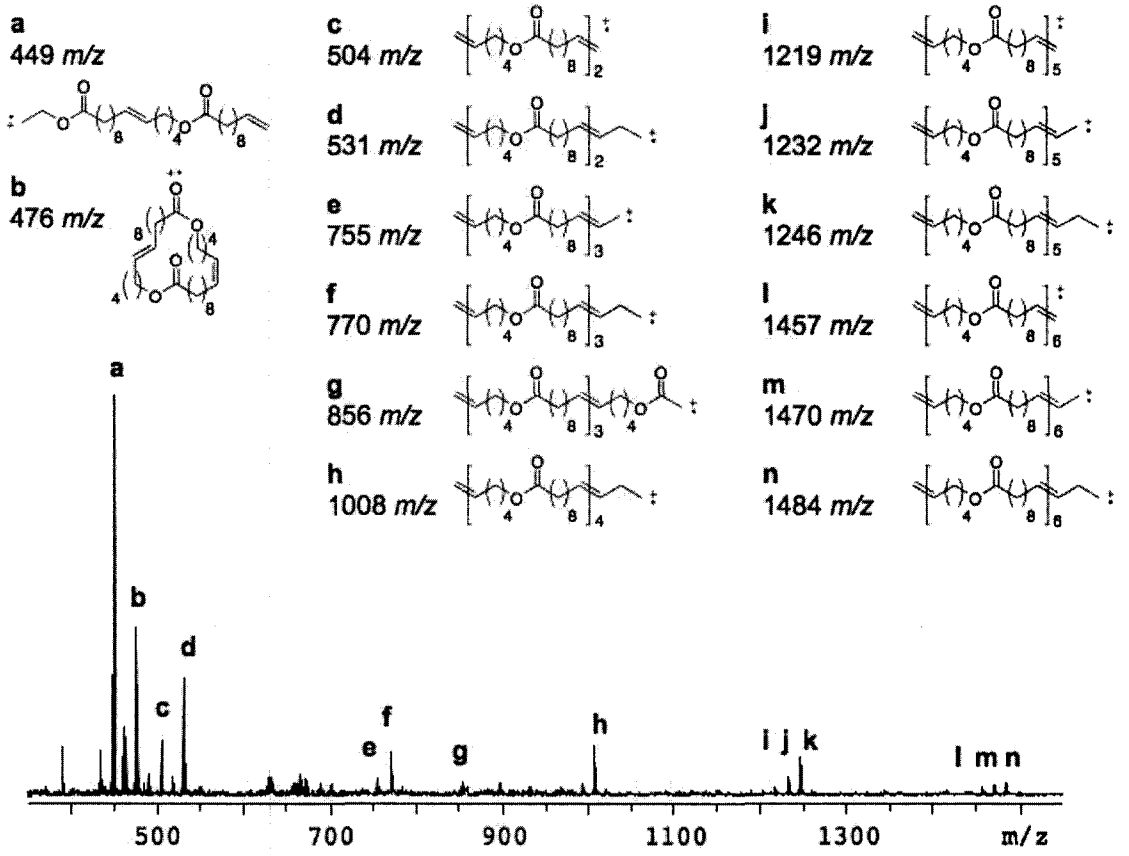

Figure 2. Full MALDI-TOF spectrum of the ADMET oligomer poly-**58** obtained from **58** using 5 mol% **2a**, [S] = 100 mM, 30 minutes in refluxing CH_2Cl_2.

Table 1. ^{1}H NMR end group analysis of average chain length of oligomers.[a]

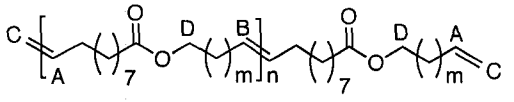

m = 3, **poly-58**
m = 1, **poly-60**
m = 7, **poly-95**

(δ ppm)
A: 5.7 - 6.0
B: 5.2 - 5.5
C: 5.3 - 4.7
D: 4.3 - 4.0

Oligomer	Ring size of RCM Product	A	B	C	D	Average Chain Length
poly-58	16	1	5	2	7	5
poly-60	14	1	2	3	5	2
poly-95	20	1	18	2	20	18

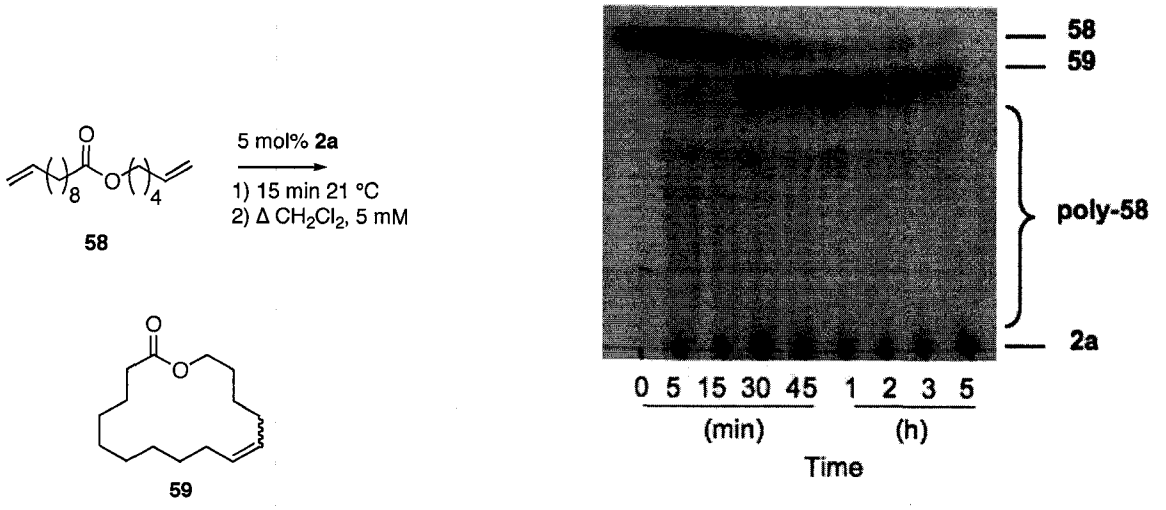

Figure 3. Progress of the reaction of substrate **58** (5 mM) and 5 mol % **2a**, 0-5h as followed by TLC; eluted with 10%EtOAc/hexanes and developed with anisaldehyde stain. Oligomers form initially and then disappear to yield the RCM product.

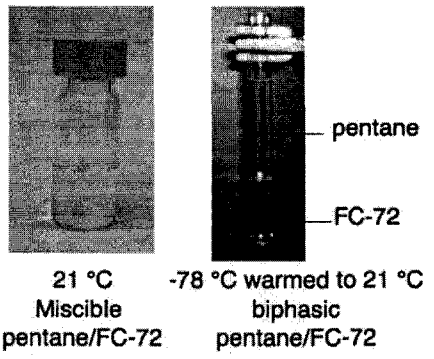

Figure 1. Pentane and FC-72 are miscible at 21 °C. If the solution is cooled to -78 °C and allowed to warm to 21 °C the solvents separate and pentane can be extracted from the top.

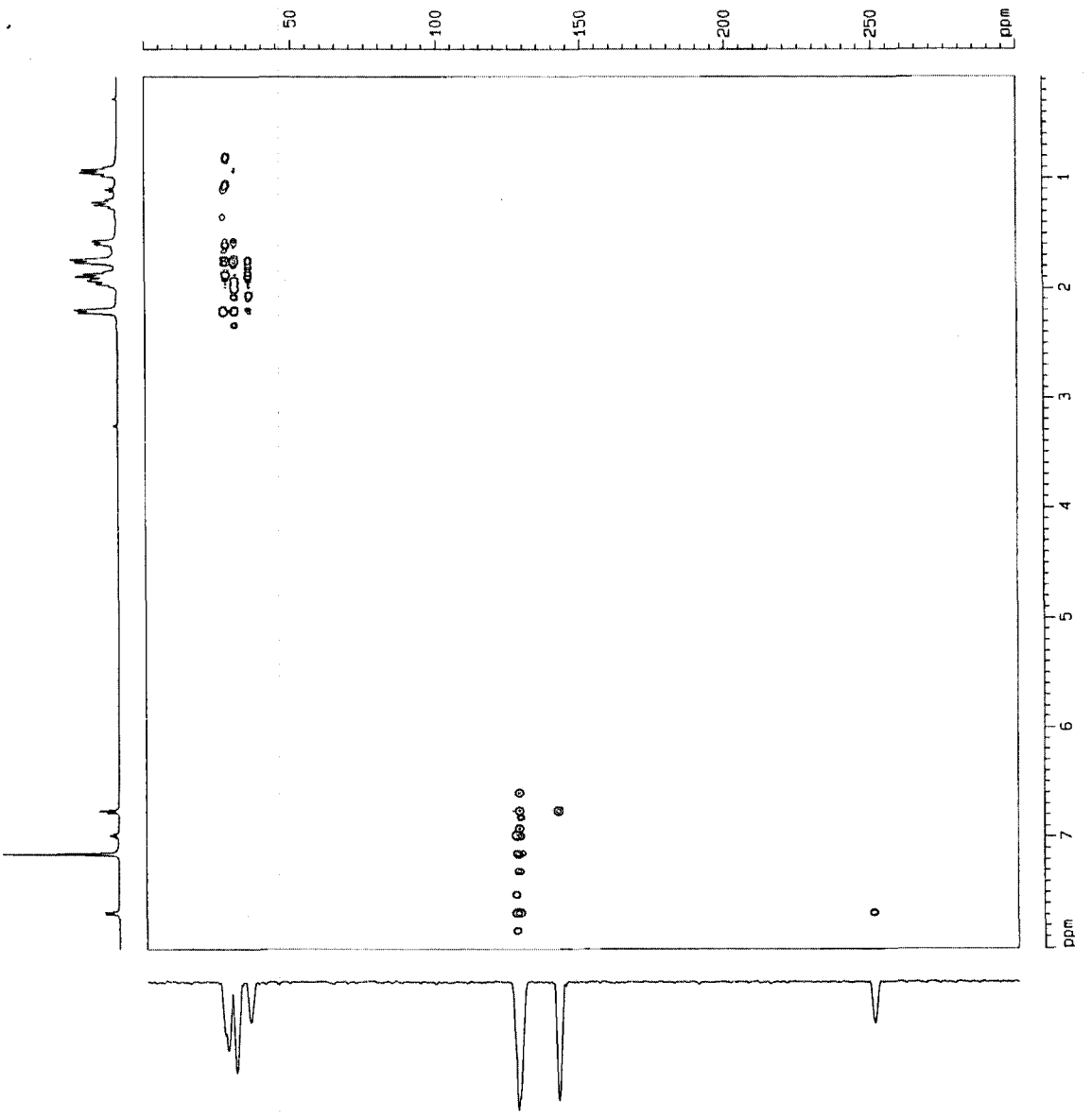

Figure 1. ^{1}H-^{13}C HMBC spectrum of **11** (500 MHz; C_6D_6) showing the ^{13}C signals that, due to rapid decomposition of this complex in solution, were otherwise unattainable from 1-D ^{13}C NMR spectra. The carbyne ^{13}C signal is located at δ 250.2 ppm.

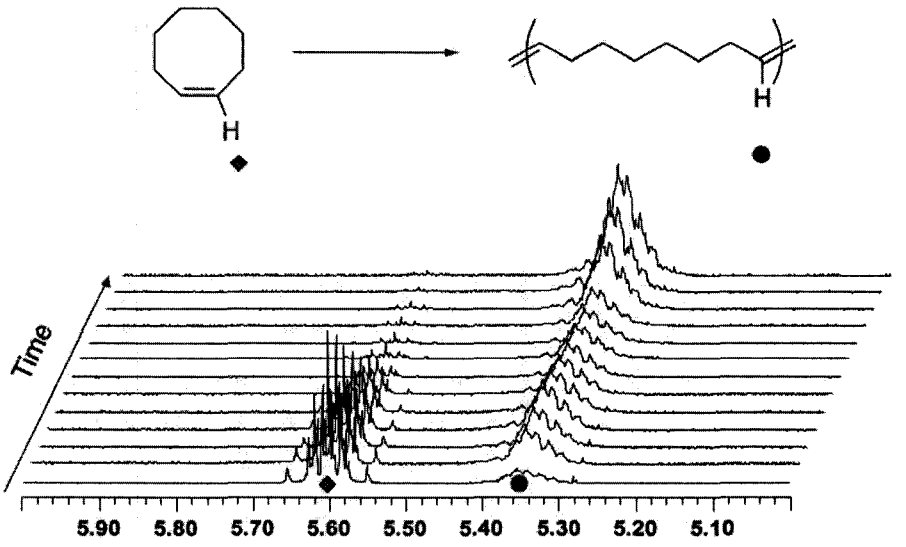

Figure 2. ROMP of cyclooctene followed by ^{1}H NMR, shown are the signals for olefinic peaks. The reaction is in $CDCl_3$ using 200:1, cyclooctene:catalyst, with concentration of cyclooctene of 0.1 M. The NMR probe spin rate was 20 Hz and the temperature was 21°C.

CIF files for published crystal structures have been deposited with Cambridge Crystallographic Data Centre (CCDC). The data can be obtained free of charge on application to the CCDC at 12 Union Road, Cambridge CB2 1EZ, UK; fax: (+44) 1223-336-033; email deposit@ccdc.cam.ac.uk.

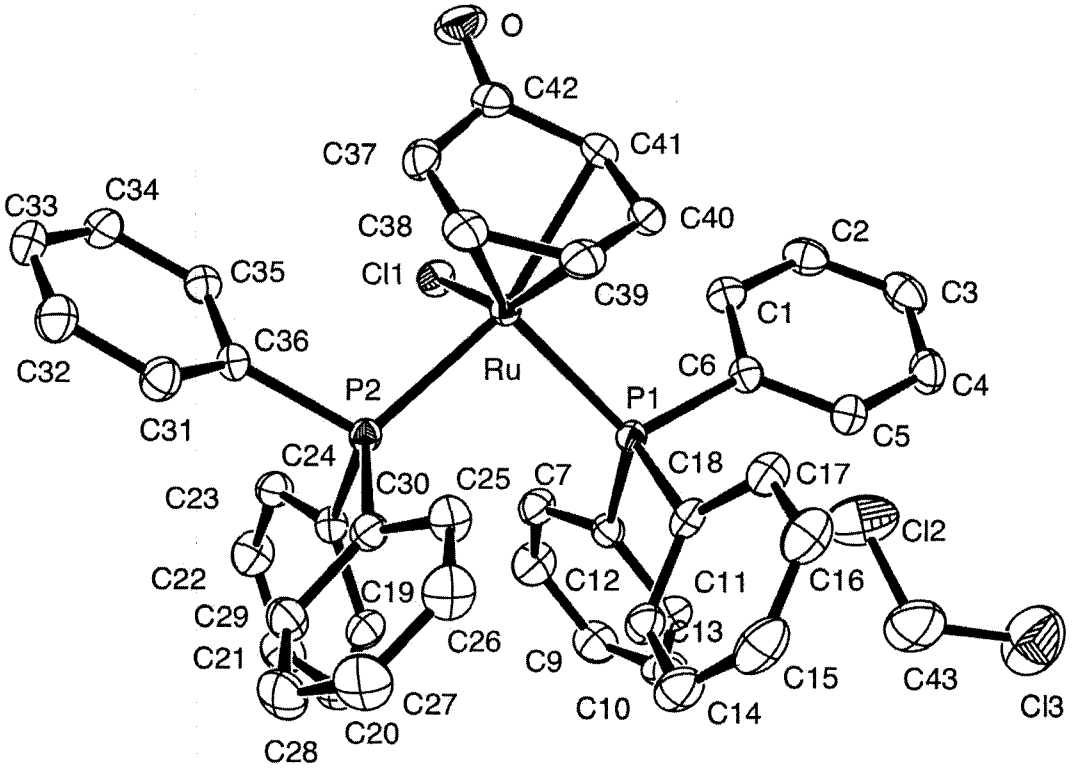

Figure 1. ORTEP representations of $RuCl(OC_6H_5)(PPh_3)_2$, **9**. Thermal ellipsoids are shown at 50% probability level, hydrogen atoms are omitted for clarity.

Table 1. Crystal data and structure refinement for $RuCl(OC_6H_5)(PPh_3)_2$, **9**.

Crystallographer	Dr. Glenn Yap	DF2011
Publication	*Inorg.Chim. Acta, 345*, 268.	
Empirical formula	$C_{43}\ H_{37}\ Cl_3\ O\ P_2\ Ru$	
Formula weight	839.09	
Temperature	203(2) K	
Wavelength	0.71073 Å	
Crystal system, space group	Triclinic, P-1	
Unit cell dimensions	a = 9.9280(10) Å	α = 76.697(2)°
	b = 10.3483(10) Å	β = 82.978(2)°
	c = 19.3175(19) Å	γ = 74.918(2)°
Volume	1860.7(3)Å^3	
Z, Calculated density	2, 1.498 Mg/m^3	
Absorption coefficient	0.757 mm^{-1}	
F(000)	856	
Crystal size	0.20 x 0.10 x 0.05 mm	
Theta range for data collection	2.33 to 28.70 deg.	
Limiting indices	-16<=h<=16, 0<=k<=32, 0<=l<=32	
Reflections collected / unique	13621 / 8024 [R(int) = 0.0237]	
Completeness to theta	83.0 %	
Absorption correction	Semi-empirical from equivalents	
Refinement method	Full-matrix least-squares on F^2	
Data / restraints / parameters	8024 / 0 / 451	
Goodness-of-fit on F^2	1.007	
Final R indices [I>2sigma(I)]	R1 = 0.0403, wR2 = 0.0729	
R indices (all data)	R1 = 0.0321, wR2 = 0.0687	
Largest diff. peak and hole	0.706 and -0.689 e.Å^{-3}	

Table 2. Bond lengths (Å) for $RuCl(OC_6H_5)(PPh_3)_2$, **9**.

Ru	C38	2.208(2)	Ru	C39	2.215(2)
Ru	C40	2.240(2)	Ru	C37	2.306(2)
Ru	C41	2.306(2)	Ru	P2	2.3422(7)
Ru	P1	2.3633(6)	Ru	Cl1	2.4393(6)
P1	C6	1.841(2)	P1	C18	1.847(2)
P1	C12	1.848(2)	P2	C30	1.840(2)
P2	C24	1.848(2)	P2	C36	1.860(2)
Cl2	C43	1.735(4)	Cl3	C43	1.762(4)
O	C42	1.238(3)	C1	C2	1.394(3)
C1	C6	1.403(3)	C2	C3	1.386(4)
C3	C4	1.382(4)	C4	C5	1.394(3)
C5	C6	1.404(3)	C7	C12	1.399(3)
C7	C8	1.400(3)	C8	C9	1.387(4)
C9	C10	1.387(4)	C10	C11	1.391(3)
C11	C12	1.402(3)	C13	C14	1.399(3)
C13	C18	1.400(4)	C14	C15	1.392(4)
C15	C16	1.385(4)	C16	C17	1.398(4)
C17	C18	1.405(3)	C19	C20	1.394(3)
C19	C24	1.399(3)	C20	C21	1.392(4)
C21	C22	1.379(4)	C22	C23	1.395(3)
C23	C24	1.404(3)	C25	C30	1.396(3)
C25	C26	1.395(3)	C26	C27	1.379(4)
C27	C28	1.394(4)	C28	C29	1.394(4)
C29	C30	1.406(4)	C31	C36	1.400(3)
C31	C32	1.401(3)	C32	C33	1.391(4)
C33	C34	1.390(4)	C34	C35	1.394(3)
C35	C36	1.406(3)	C37	C38	1.411(4)
C37	C42	1.452(4)	C38	C39	1.422(3)
C39	C40	1.424(4)	C40	C41	1.401(3)
C41	C42	1.476(3)			

Table 3. Bond angles (°)for $RuCl(OC_6H_5)(PPh_3)_2$, **9**.

C38	Ru	C39	37.50(9)	C38	Ru	C40	66.29(9)
C39	Ru	C40	37.27(9)	C38	Ru	C37	36.34(9)
C39	Ru	C37	66.08(9)	C40	Ru	C37	76.24(9)
C38	Ru	C41	76.93(9)	C39	Ru	C41	65.98(9)
C40	Ru	C41	35.85(9)	C37	Ru	C41	63.59(9)
C38	Ru	P2	88.48(7)	C39	Ru	P2	109.22(7)
C40	Ru	P2	145.87(7)	C37	Ru	P2	97.30(7)
C41	Ru	P2	160.82(6)	C38	Ru	P1	133.85(7)
C39	Ru	P1	99.41(7)	C40	Ru	P1	86.83(6)
C37	Ru	P1	163.01(6)	C41	Ru	P1	103.18(6)
P2	Ru	P1	95.90(2)	C38	Ru	Cl1	130.41(7)
C39	Ru	Cl1	154.00(7)	C40	Ru	Cl1	123.61(7)
C37	Ru	Cl1	95.04(6)	C41	Ru	Cl1	90.02(6)
P2	Ru	Cl1	90.08(2)	P1	Ru	Cl1	95.58(2)
C6	P1	C18	105.21(11)	C6	P1	C12	96.44(10)
C18	P1	C12	104.25(11)	C6	P1	Ru	112.84(8)
C18	P1	Ru	110.07(7)	C12	P1	Ru	125.76(7)
C30	P2	C24	101.45(11)	C30	P2	C36	101.30(10)
C24	P2	C36	102.24(10)	C30	P2	Ru	119.50(8)
C24	P2	Ru	119.91(8)	C36	P2	Ru	109.69(8)
C2	C1	C6	120.1(2)	C3	C2	C1	120.5(2)
C4	C3	C2	119.8(2)	C3	C4	C5	120.7(2)
C4	C5	C6	119.9(2)	C5	C6	C1	119.1(2)
C5	C6	P1	122.27(19)	C1	C6	P1	118.28(17)
C12	C7	C8	119.9(2)	C9	C8	C7	120.5(2)
C10	C9	C8	119.7(2)	C9	C10	C11	120.3(2)
C10	C11	C12	120.5(2)	C7	C12	C11	118.9(2)
C7	C12	P1	119.53(18)	C11	C12	P1	120.59(17)
C14	C13	C18	121.1(2)	C15	C14	C13	119.9(3)
C16	C15	C14	119.6(2)	C15	C16	C17	120.8(3)
C16	C17	C18	120.3(3)	C17	C18	C13	118.2(2)
C17	C18	P1	120.8(2)	C13	C18	P1	120.56(18)
C20	C19	C24	121.1(2)	C21	C20	C19	119.9(3)
C22	C21	C20	119.7(2)	C21	C22	C23	120.6(2)
C22	C23	C24	120.6(2)	C23	C24	C19	118.0(2)
C23	C24	P2	121.46(18)	C19	C24	P2	120.56(17)
C30	C25	C26	120.6(2)	C27	C26	C25	120.5(2)
C26	C27	C28	120.0(2)	C27	C28	C29	119.8(3)
C28	C29	C30	120.8(2)	C25	C30	C29	118.4(2)
C25	C30	P2	120.16(19)	C29	C30	P2	121.33(18)
C36	C31	C32	120.7(2)	C33	C32	C31	120.4(2)
C32	C33	C34	119.5(2)	C33	C34	C35	120.4(2)
C34	C35	C36	120.9(2)	C31	C36	C35	118.1(2)
C31	C36	P2	122.59(18)	C35	C36	P2	119.26(17)
C38	C37	C42	122.0(2)	C38	C37	Ru	68.06(13)
C42	C37	Ru	84.55(14)	C37	C38	C39	121.1(2)

C37	C38	Ru	75.60(13)	C39	C38	Ru	71.51(13)
C40	C39	C38	117.4(2)	C40	C39	Ru	72.29(13)
C38	C39	Ru	70.99(13)	C41	C40	C39	121.4(2)
C41	C40	Ru	74.68(14)	C39	C40	Ru	70.44(13)
C40	C41	C42	121.1(2)	C40	C41	Ru	69.47(14)
C42	C41	Ru	84.02(15)	O	C42	C37	124.4(2)
O	C42	C41	122.9(2)	C37	C42	C41	112.2(2)
Cl2	C43	Cl3	112.2(2)				

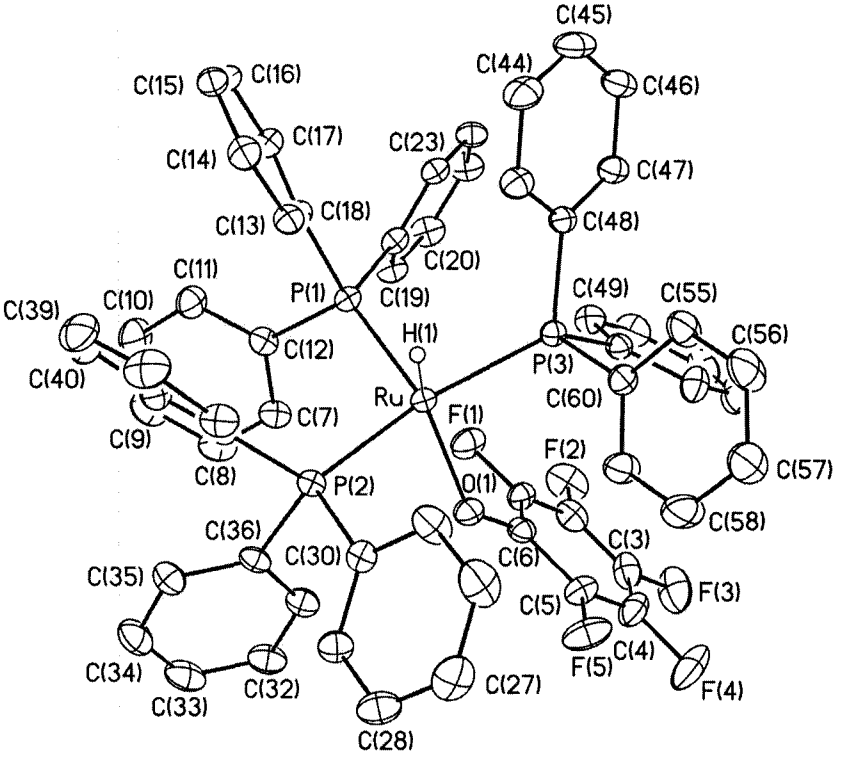

Figure 2. ORTEP representations of $RuH(OC_6F_5)(PPh_3)_3$, **10**. Thermal ellipsoids are shown at 50% probability level, hydrogen atoms (except for hydride) and solvates are omitted for clarity.

Table 4. Crystal data and structure refinement for $RuH(OC_6F_5)(PPh_3)_3$, **10**.

Crystallographer	Dr. Glenn Yap	
CCDC #	246452	
Publication	*Organometallics*, *24*, 103	
Empirical formula	$C_{64}\ H_{56}\ F_5\ O_2\ P_3\ Ru$	
Formula weight	1146.07	
Temperature	203(2) K	
Wavelength	0.71073 Å	
Crystal system, space group	Monoclinic, P2 (1) / n	
Unit cell dimensions	a = 12.773(2) Å	α = 90°
	b = 25.338(5) Å	β = 105.381(3)°
	c = 17.282(3) Å	γ = 90°
Volume	5392.9(17)Å^3	
Z, Calculated density	4, 1.411 Mg/m^3	
Absorption coefficient	0.44 mm^{-1}	
F(000)	2360	
Crystal size	0.20 x 0.10 x 0.05 mm	
Theta range for data collection	1.46 to 28.65 deg.	
Limiting indices	-16<=h<=16, 0<=k<=32, 0<=l<=32	
Reflections collected / unique	37344 / 12027 [R(int) = 0.0441]	
Completeness to theta	28.65 86.7 %	
Absorption correction	Semi-empirical from equivalents	
Max. and min. transmission	1.000000 and 0.626317	
Refinement method	Full-matrix least-squares on F^2	
Data / restraints / parameters	12027 / 0 / 635	
Goodness-of-fit on F^2	1.033	
Final R indices [I>2sigma(I)]	R1 = 0. 0561, wR2 = 0.1075	
R indices (all data)	R1 = 0.403, wR2 = 0.1003	
Largest diff. peak and hole	0.584 and -0.963 e.Å^{-3}	

Definition of R indices: $R_1 = \Sigma(F_o - F_c)/\Sigma(F_o)$; $wR_2 = [\Sigma[w(F_o^2 - F_c^2)^2]/\Sigma[w(F_o^2)^2]]^{1/2}$

Table 5. Bond distances (Å) for $RuH(OC_6F_5)(PPh_3)_3$, **10**.

Ru O(1)	2.1350(17)	Ru P(1)	2.2242(6)
Ru P(3)	2.3389(7)	Ru P(2)	2.3911(7)
Ru H(1)	1.49(3)	P(1) C(18)	1.852(2)
P(1) C(12)	1.860(2)	P(1) C(24)	1.863(2)
P(2) C(42)	1.841(3)	P(2) C(30)	1.848(3)
P(2) C(36)	1.851(2)	P(3) C(48)	1.841(2)
P(3) C(60)	1.845(2)	P(3) C(54)	1.845(3)
O(1) C(6)	1.311(3)	F(1) C(1)	1.356(3)
F(2) C(2)	1.353(3)	F(3) C(3)	1.359(3)
F(4) C(4)	1.350(3)	F(5) C(5)	1.355(3)
C(1) C(2)	1.374(4)	C(1) C(6)	1.403(4)
C(2) C(3)	1.375(4)	C(3) C(4)	1.375(5)
C(4) C(5)	1.387(4)	C(5) C(6)	1.405(4)
C(7) C(12)	1.396(4)	C(7) C(8)	1.400(4)
C(8) C(9)	1.377(5)	C(9) C(10)	1.378(5)
C(10) C(11)	1.403(4)	C(11) C(12)	1.397(4)
C(13) C(18)	1.395(3)	C(13) C(14)	1.398(3)
C(14) C(15)	1.382(4)	C(15) C(16)	1.387(4)
C(16) C(17)	1.395(4)	C(17) C(18)	1.402(3)
C(19) C(20)	1.396(4)	C(19) C(24)	1.407(3)
C(20) C(21)	1.388(4)	C(21) C(22)	1.385(4)
C(22) C(23)	1.397(4)	C(23) C(24)	1.392(3)
C(25) C(26)	1.393(4)	C(25) C(30)	1.395(4)
C(26) C(27)	1.389(5)	C(27) C(28)	1.379(5)
C(28) C(29)	1.396(4)	C(29) C(30)	1.394(3)
C(31) C(32)	1.390(4)	C(31) C(36)	1.399(4)
C(32) C(33)	1.387(5)	C(33) C(34)	1.374(5)
C(34) C(35)	1.398(4)	C(35) C(36)	1.398(4)
C(37) C(42)	1.391(4)	C(37) C(38)	1.398(4)
C(38) C(39)	1.384(5)	C(39) C(40)	1.380(5)
C(40) C(41)	1.395(4)	C(41) C(42)	1.408(4)
C(43) C(44)	1.397(4)	C(43) C(48)	1.402(4)
C(44) C(45)	1.383(5)	C(45) C(46)	1.374(4)
C(46) C(47)	1.400(4)	C(47) C(48)	1.394(4)
C(49) C(50)	1.389(4)	C(49) C(54)	1.394(4)
C(50) C(51)	1.394(5)	C(51) C(52)	1.375(5)
C(52) C(53)	1.395(4)	C(53) C(54)	1.393(4)
C(55) C(56)	1.389(4)	C(55) C(60)	1.405(4)
C(56) C(57)	1.383(5)	C(57) C(58)	1.378(5)
C(58) C(59)	1.382(4)	C(59) C(60)	1.392(4)

Table 6. Bond angles (°)for $RuH(OC_6F_5)(PPh_3)_3$, **10**.

O(1) Ru P(1)	135.23(6)	O(1) Ru P(3)	94.91(5)
P(1) Ru P(3)	99.22(3)	O(1) Ru P(2)	85.40(5)
P(1) Ru P(2)	98.42(3)	P(3) Ru P(2)	154.40(2)
H(1) Ru P(1)	86(1)	H(1) Ru P(2)	82(1)
H(1) Ru P(3)	81(1)	H(1) Ru O(1)	138(1)
C(18) P(1) C(12)	103.77(11)	C(18) P(1) C(24)	100.99(11)
C(12) P(1) C(24)	98.95(11)	C(18) P(1) Ru	122.50(8)
C(12) P(1) Ru	110.62(8)	C(24) P(1) Ru	116.81(8)
C(42) P(2) C(30)	102.77(11)	C(42) P(2) C(36)	102.71(11)
C(30) P(2) C(36)	101.20(11)	C(42) P(2) Ru	118.59(8)
C(30) P(2) Ru	105.21(8)	C(36) P(2) Ru	123.26(8)
C(48) P(3) C(60)	100.62(11)	C(48) P(3) C(54)	102.72(11)
C(60) P(3) C(54)	100.56(12)	C(48) P(3) Ru	120.62(8)
C(60) P(3) Ru	107.54(8)	C(54) P(3) Ru	121.19(8)
C(6) O(1) Ru	135.80(15)	F(1) C(1) C(2)	118.1(3)
F(1) C(1) C(6)	118.5(2)	C(2) C(1) C(6)	123.4(2)
F(2) C(2) C(1)	120.0(3)	F(2) C(2) C(3)	119.7(3)
C(1) C(2) C(3)	120.3(3)	F(3) C(3) C(4)	120.1(3)
F(3) C(3) C(2)	120.9(3)	C(4) C(3) C(2)	119.0(3)
F(4) C(4) C(3)	119.9(3)	F(4) C(4) C(5)	119.9(3)
C(3) C(4) C(5)	120.2(3)	F(5) C(5) C(4)	118.4(3)
F(5) C(5) C(6)	118.8(2)	C(4) C(5) C(6)	122.9(3)
O(1) C(6) C(1)	123.4(2)	O(1) C(6) C(5)	122.4(2)
C(1) C(6) C(5)	114.2(2)	C(12) C(7) C(8)	120.9(3)
C(9) C(8) C(7)	119.8(3)	C(8) C(9) C(10)	120.3(3)
C(9) C(10) C(11)	120.2(3)	C(12) C(11) C(10)	120.3(3)
C(7) C(12) C(11)	118.4(2)	C(7) C(12) P(1)	117.65(19)
C(11) C(12) P(1)	123.9(2)	C(18) C(13) C(14)	121.2(2)
C(15) C(14) C(13)	120.0(3)	C(14) C(15) C(16)	119.8(2)
C(15) C(16) C(17)	120.3(3)	C(16) C(17) C(18)	120.8(3)
C(13) C(18) C(17)	117.9(2)	C(13) C(18) P(1)	119.95(18)
C(17) C(18) P(1)	122.13(19)	C(20) C(19) C(24)	120.4(2)
C(21) C(20) C(19)	120.3(3)	C(22) C(21) C(20)	119.8(3)
C(21) C(22) C(23)	120.1(3)	C(24) C(23) C(22)	120.9(2)
C(23) C(24) C(19)	118.4(2)	C(23) C(24) P(1)	121.23(18)
C(19) C(24) P(1)	120.28(19)	C(26) C(25) C(30)	120.8(3)
C(27) C(26) C(25)	120.0(3)	C(28) C(27) C(26)	120.0(3)
C(27) C(28) C(29)	119.8(3)	C(30) C(29) C(28)	121.1(3)
C(29) C(30) C(25)	118.2(2)	C(29) C(30) P(2)	122.5(2)
C(25) C(30) P(2)	119.3(2)	C(32) C(31) C(36)	120.9(3)
C(33) C(32) C(31)	120.1(3)	C(34) C(33) C(32)	120.0(3)
C(33) C(34) C(35)	120.4(3)	C(34) C(35) C(36)	120.5(3)
C(35) C(36) C(31)	118.2(2)	C(35) C(36) P(2)	124.4(2)
C(31) C(36) P(2)	117.33(19)	C(42) C(37) C(38)	120.3(3)

C(39) C(38) C(37)	120.3(3)	C(40) C(39) C(38)	120.1(3)
C(39) C(40) C(41)	120.2(3)	C(40) C(41) C(42)	120.3(3)
C(37) C(42) C(41)	118.8(3)	C(37) C(42) P(2)	122.4(2)
C(41) C(42) P(2)	118.7(2)	C(44) C(43) C(48)	120.4(3)
C(45) C(44) C(43)	119.8(3)	C(46) C(45) C(44)	120.7(3)
C(45) C(46) C(47)	120.1(3)	C(48) C(47) C(46)	120.3(3)
C(47) C(48) C(43)	118.8(2)	C(47) C(48) P(3)	123.0(2)
C(43) C(48) P(3)	118.20(19)	C(50) C(49) C(54)	120.7(3)
C(49) C(50) C(51)	120.3(3)	C(52) C(51) C(50)	119.1(3)
C(51) C(52) C(53)	121.0(3)	C(54) C(53) C(52)	120.1(3)
C(53) C(54) C(49)	118.7(2)	C(53) C(54) P(3)	122.7(2)
C(49) C(54) P(3)	118.58(19)	C(56) C(55) C(60)	120.1(3)
C(57) C(56) C(55)	120.6(3)	C(58) C(57) C(56)	119.6(3)
C(57) C(58) C(59)	120.2(3)	C(58) C(59) C(60)	121.2(3)
C(59) C(60) C(55)	118.1(2)	C(59) C(60) P(3)	119.0(2)
C(55) C(60) P(3)	122.8(2)		

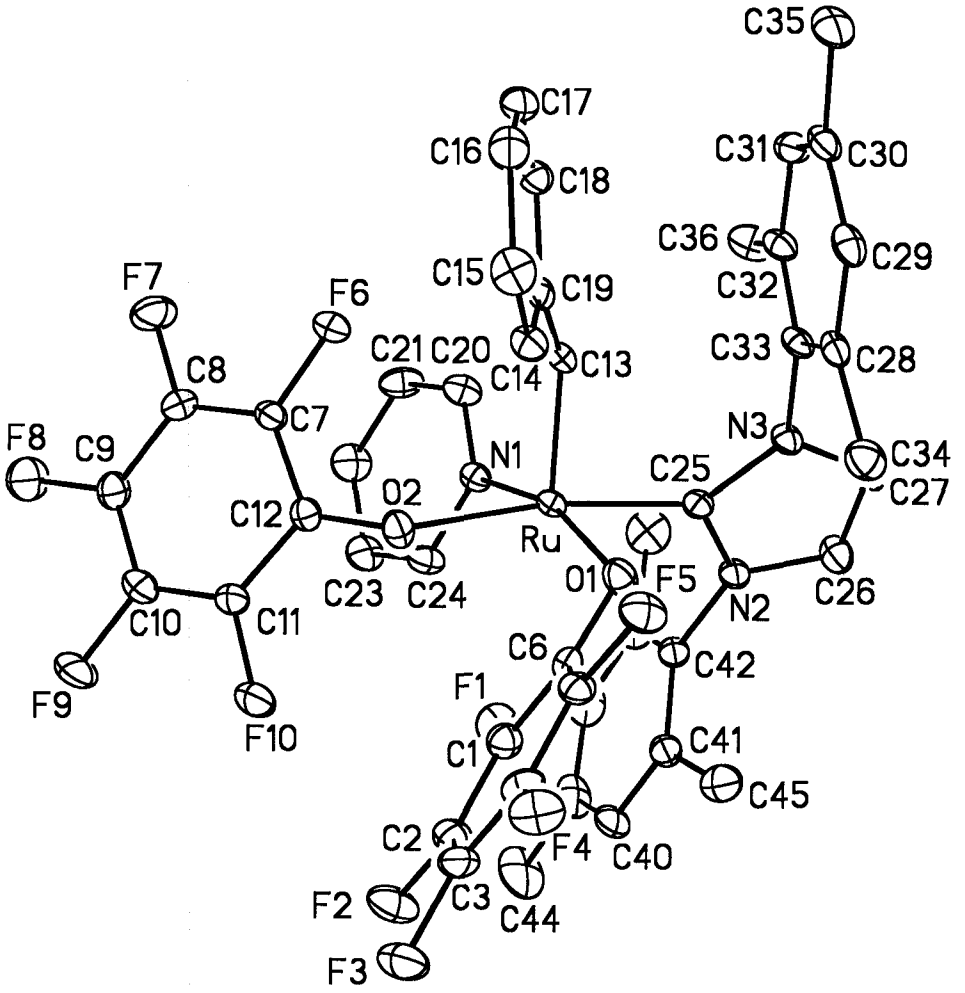

Figure 3. ORTEP representation of $Ru(OC_6F_5)_2(CHPh)(IMes)(py)$, **12a**. Thermal ellipsoids are shown at 50% probability level; hydrogen atoms and toluene solvate omitted for clarity.

Table 7. Crystal data and structure refinement for $Ru(OC_6F_5)_2(CHPh)(IMes)(py)$, **12a**.

Crystallographer	Dr. Glenn Yap	
CCDC #	208989	
Publication	*Organometallics*, **2003**, *22*, 3634.	
Identification code	**12a**, $Ru(OC_6F_5)_2(CHPh)(IMes)(py)$	
Empirical formula	C48 H38 F10 N3 O2 Ru	
Formula weight	979.88	
Temperature	203(2) K	
Wavelength	0.71073 A	
Crystal system	Triclinic	
Space group	P-1	
Unit cell dimensions	a = 10.3425(13) Å	α = 81.473(2)°
	b = 13.0063(17) Å	β = 72.540(2)°
	c = 16.638(2) Å	γ = 85.148(2)°
Volume	2109.4(5) $Å^3$	
Z	2	
Density (calculated)	1.543 Mg/m^3	
Absorption coefficient	0.460 mm^{-1}	
F(000)	994	
Crystal size	0.10 x 0.05 x 0.05 mm^3	
Theta range for data collection	1.58 to 28.87 °.	
Index ranges	-9<=h<=13, -17<=k<=16, -21<=l<=22	
Reflections collected	11312	
Independent reflections	8648 [R(int) = 0.0287]	
Completeness to theta = 28.87°	78.0 %	
Absorption correction	Semi-empirical from equivalents	
Max. and min. transmission	0.9774 and 0.9554	
Refinement method	Full-matrix least-squares on F^2	
Data / restraints / parameters	8648 / 0 / 577	
Goodness-of-fit on F^2	1.003	
Final R indices [I>2sigma(I)]	R1 = 0.0487, wR2 = 0.0973	
R indices (all data)	R1 = 0.0826, wR2 = 0.1097	
Largest diff. peak and hole	0.496 and -0.765 $e.Å^{-3}$	

Table 8. Bond distances (Å) for $Ru(OC_6F_5)_2(CHPh)(IMes)(py)$, **12a**.

Ru	C13	1.843(3)	Ru	C25	2.040(4)
Ru	O1	2.076(3)	Ru	N1	2.085(3)
Ru	O2	2.110(3)	F1	C1	1.350(4)
F2	C2	1.358(4)	F3	C3	1.354(4)
F4	C4	1.355(4)	F5	C5	1.361(4)
F6	C7	1.354(4)	F7	C8	1.338(4)
F8	C9	1.349(4)	F9	C10	1.352(4)
F10	C11	1.350(4)	N1	C20	1.346(5)
N1	C24	1.352(4)	N2	C25	1.376(4)
N2	C26	1.379(5)	N2	C42	1.451(4)
N3	C27	1.375(5)	N3	C25	1.383(4)
N3	C33	1.456(4)	O1	C6	1.323(4)
O2	C12	1.305(4)	C1	C2	1.387(5)
C1	C6	1.404(5)	C2	C3	1.366(6)
C3	C4	1.372(5)	C4	C5	1.377(5)
C5	C6	1.393(5)	C7	C8	1.377(5)
C7	C12	1.406(5)	C8	C9	1.384(5)
C9	C10	1.372(6)	C10	C11	1.367(6)
C11	C12	1.408(5)	C13	C19	1.472(5)
C14	C15	1.384(5)	C14	C19	1.401(5)
C15	C16	1.386(6)	C16	C17	1.373(6)
C17	C18	1.387(5)	C18	C19	1.393(5)
C20	C21	1.362(6)	C21	C22	1.374(5)
C22	C23	1.387(6)	C23	C24	1.376(5)
C26	C27	1.337(5)	C28	C33	1.380(5)
C28	C29	1.401(5)	C28	C34	1.502(5)
C29	C30	1.386(6)	C30	C31	1.386(6)
C30	C35	1.515(5)	C31	C32	1.401(5)
C32	C33	1.405(5)	C32	C36	1.491(6)
C37	C42	1.387(6)	C37	C38	1.393(5)
C37	C43	1.504(6)	C38	C39	1.375(7)
C39	C40	1.375(7)	C39	C44	1.534(5)
C40	C41	1.400(5)	C41	C42	1.412(5)
C41	C45	1.486(6)	C47	C48	1.371(7)
C47	C49	1.362(7)	C48	C49	1.362(7)

Table 9. Bond angles (°) $Ru(OC_6F_5)_2(CHPh)(IMes)(py)$, **12a**.

C13	Ru	C25	91.22(14)	C13	Ru	O1	103.12(13)
C25	Ru	O1	88.91(13)	C13	Ru	N1	92.58(13)
C25	Ru	N1	93.78(13)	O1	Ru	N1	164.02(10)
C13	Ru	O2	96.72(13)	C25	Ru	O2	171.18(12)
O1	Ru	O2	85.57(10)	N1	Ru	O2	89.70(11)
C20	N1	C24	116.2(3)	C20	N1	Ru	129.0(2)
C24	N1	Ru	114.2(3)	C25	N2	C26	112.5(3)
C25	N2	C42	126.4(3)	C26	N2	C42	121.1(3)
C27	N3	C25	111.9(3)	C27	N3	C33	120.4(3)
C25	N3	C33	127.6(3)	C6	O1	Ru	120.4(2)
C12	O2	Ru	125.4(2)	F1	C1	C2	119.3(3)
F1	C1	C6	118.9(3)	C2	C1	C6	121.9(4)
F2	C2	C3	119.4(3)	F2	C2	C1	119.7(4)
C3	C2	C1	120.9(3)	F3	C3	C2	120.5(3)
F3	C3	C4	120.8(4)	C2	C3	C4	118.7(4)
F4	C4	C3	119.8(3)	F4	C4	C5	119.6(3)
C3	C4	C5	120.6(4)	F5	C5	C4	118.4(3)
F5	C5	C6	118.8(3)	C4	C5	C6	122.8(3)
O1	C6	C5	121.9(3)	O1	C6	C1	122.9(4)
C5	C6	C1	115.1(3)	F6	C7	C8	116.9(3)
F6	C7	C12	119.3(3)	C8	C7	C12	123.7(3)
F7	C8	C7	121.0(3)	F7	C8	C9	118.9(4)
C7	C8	C9	120.1(4)	F8	C9	C10	121.8(4)
F8	C9	C8	120.3(4)	C10	C9	C8	118.0(4)
F9	C10	C9	118.7(4)	F9	C10	C11	119.7(4)
C9	C10	C11	121.6(4)	F10	C11	C10	118.4(3)
F10	C11	C12	118.5(4)	C10	C11	C12	123.1(4)
O2	C12	C7	124.6(3)	O2	C12	C11	121.9(3)
C7	C12	C11	113.5(3)	C19	C13	Ru	128.4(3)
C15	C14	C19	119.9(4)	C14	C15	C16	120.4(4)
C17	C16	C15	120.2(4)	C16	C17	C18	120.0(4)
C17	C18	C19	120.7(4)	C18	C19	C14	118.8(3)
C18	C19	C13	117.4(3)	C14	C19	C13	123.7(3)
N1	C20	C21	123.8(3)	C20	C21	C22	119.5(4)
C21	C22	C23	118.1(4)	C24	C23	C22	119.1(4)
N1	C24	C23	123.1(4)	N2	C25	N3	101.7(3)
N2	C25	Ru	127.6(2)	N3	C25	Ru	130.5(2)
C27	C26	N2	106.6(3)	C26	C27	N3	107.3(3)
C33	C28	C29	117.1(4)	C33	C28	C34	122.7(3)
C29	C28	C34	120.2(4)	C30	C29	C28	122.4(4)
C31	C30	C29	118.3(3)	C31	C30	C35	120.4(4)
C29	C30	C35	121.3(4)	C30	C31	C32	122.0(4)
C31	C32	C33	116.9(4)	C31	C32	C36	120.5(4)
C33	C32	C36	122.6(3)	C28	C33	C32	123.1(3)
C28	C33	N3	119.4(3)	C32	C33	N3	117.3(3)

C42	C37	C38	117.8(4)	C42	C37	C43	122.4(4)
C38	C37	C43	119.8(4)	C39	C38	C37	121.8(5)
C40	C39	C38	119.2(4)	C40	C39	C44	120.5(5)
C38	C39	C44	120.3(5)	C39	C40	C41	122.4(4)
C40	C41	C42	116.3(4)	C40	C41	C45	120.9(4)
C42	C41	C45	122.6(3)	C37	C42	C41	122.5(3)
C37	C42	N2	118.9(3)	C41	C42	N2	118.4(4)
C48	C47	C49	121.0(5)	C47	C49	C48	120.0(5)
C47	C48	C49	119.0(5)				

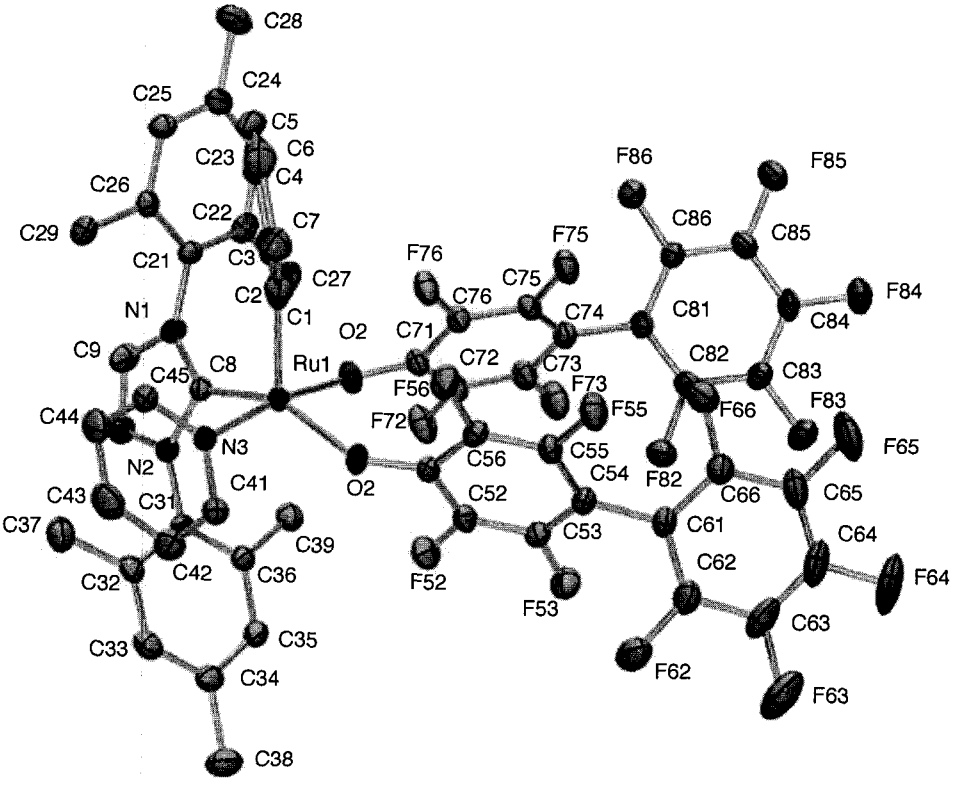

Figure 4. ORTEP representation of $Ru(OC_6F_4C_6F_5)_2(CHPh)(IMes)(py)$, **13**. Thermal ellipsoids shown at 30% probability level; hydrogen atoms and THF solvate omitted for clarity.

Table 10. Crystal data and structure refinement for, $Ru(OC_6F_4C_6F_5)_2(CHPh)(IMes)(py)$, **13**.

Crystallographer	Dr. Hillary Jenkins	
Identification code	df0209m	
Formula	$C_{57}H_{35}F_{18}N_3O_2Ru$	
Formula weight	1236.95	
Size	0.12 x 0.4 x 0.45 mm	
Crystal morphology	Green Plate	
Temperature	291(2) K	
Wavelength	0.71073 Å	
Crystal system	Monoclinic	
Space group	P2(1)/n	
Unit cell dimensions	a = 13.1429(8) Å	$\alpha = 90.00°$
	b = 19.0908(12) Å	$\beta = 105.2390(10)°$
	c = 22.0303(13) Å	$\gamma = 90.00°$
Volume	5333.2(6) $Å^3$	
Z	4	
Density (calculated)	1.541Mg/m^3	
Absorption coefficient	0.403 mm^{-1}	
$F(000)$	2480	
Data collection range	$1.43 \leq \theta \leq 25.00°$	
Index ranges	$-15 \leq h \leq 15$, $-22 \leq k \leq 22$,	
	$-26 \leq l \leq 26$	
Reflections collected	38959	
Independent reflections	9399 [R(int) = 0.043]	
Observed reflections	5473 [$I > 2\sigma(I)$]	
Absorption correction	multi-scan	
Refinement method	Full	
Data / restraints / parameters	9399 / 0 / 730	
Goodness of fit	0.920	
Final R indices [$I > 2\sigma(I)$]	R_1 = 0.0736, wR_2 = 0.0596	
R indices (all data)	R_1 = 0.0324, wR_2 = 0.0560	
Largest diff. peak and hole	0.379and -0.315e.$Å^{-3}$	

Table 11. Bond distances (Å) for $Ru(OC_6F_4C_6F_5)_2(CHPh)(IMes)(py)$, **13**.

Ru1	C1	1.823(2)	Ru1	C8	2.024(2)
Ru1	O1	2.0530(16)	Ru1	N3	2.071(2)
Ru1	O2	2.0766(17)	O1	C51	1.303(3)
O2	C71	1.296(3)	N1	C8	1.364(3)
N1	C9	1.386(3)	N1	C21	1.438(3)
N2	C8	1.371(3)	N2	C10	1.379(3)
N2	C31	1.435(3)	N3	C41	1.346(3)
N3	C45	1.343(3)	C1	C2	1.465(3)
C2	C3	1.385(3)	C2	C7	1.402(3)
C3	C4	1.369(3)	C4	C5	1.379(4)
C5	C6	1.357(4)	C6	C7	1.377(4)
C9	C10	1.326(3)	C21	C26	1.387(3)
C21	C22	1.390(3)	C22	C23	1.392(4)
C22	C27	1.518(3)	C23	C24	1.374(4)
C24	C25	1.366(3)	C24	C28	1.515(3)
C25	C26	1.392(3)	C26	C29	1.504(3)
C31	C32	1.390(3)	C31	C36	1.399(3)
C32	C33	1.378(3)	C32	C37	1.516(3)
C33	C34	1.386(3)	C34	C35	1.370(3)
C34	C38	1.515(3)	C35	C36	1.392(3)
C36	C39	1.494(3)	C41	C42	1.362(4)
C42	C43	1.362(4)	C43	C44	1.367(4)
C44	C45	1.374(4)	C51	C56	1.400(3)
C51	C52	1.391(3)	C52	F52	1.355(3)
C52	C53	1.365(3)	C53	F53	1.344(3)
C53	C54	1.383(3)	C54	C55	1.375(3)
C54	C61	1.481(3)	C55	F55	1.356(3)
C55	C56	1.363(3)	C56	F56	1.355(3)
C61	C62	1.372(4)	C61	C66	1.366(4)
C62	F62	1.345(3)	C62	C63	1.372(4)
C63	C64	1.347(5)	C63	F63	1.350(4)
C64	F64	1.336(3)	C64	C65	1.350(5)
C65	F65	1.341(4)	C65	C66	1.367(4)
C66	F66	1.341(3)	C71	C76	1.400(3)
C71	C72	1.403(3)	C72	F72	1.350(3)
C72	C73	1.358(3)	C73	F73	1.354(3)
C73	C74	1.378(3)	C74	C75	1.377(3)
C74	C81	1.479(3)	C75	F75	1.350(3)
C75	C76	1.364(3)	C76	F76	1.353(3)
C81	C86	1.369(3)	C81	C82	1.378(3)
C82	F82	1.343(3)	C82	C83	1.366(4)
C83	F83	1.344(3)	C83	C84	1.361(4)
C84	F84	1.346(3)	C84	C85	1.360(4)
C85	F85	1.349(3)	C85	C86	1.362(4)
C86	F86	1.345(3)			

Table 12. Bond angles (°) for $Ru(OC_6F_4C_6F_5)_2(CHPh)(IMes)(py)$, **13**.

C1	Ru1	C8	94.59(10)	C1	Ru1	O1	111.58(9)
C8	Ru1	O1	153.79(8)	C1	Ru1	N3	97.56(10)
C8	Ru1	N3	92.74(9)	O1	Ru1	N3	85.47(8)
C1	Ru1	O2	90.87(9)	C8	Ru1	O2	87.37(8)
O1	Ru1	O2	90.68(7)	N3	Ru1	O2	171.53(7)
C51	O1	Ru1	141.25(17)	C71	O2	Ru1	134.36(16)
C8	N1	C9	110.9(2)	C8	N1	C21	128.6(2)
C9	N1	C21	120.4(2)	C8	N2	C10	111.2(2)
C8	N2	C31	125.7(2)	C10	N2	C31	122.9(2)
C41	N3	C45	115.3(2)	C41	N3	Ru1	118.91(18)
C45	N3	Ru1	125.69(19)	C2	C1	Ru1	132.85(19)
C3	C2	C7	117.5(2)	C3	C2	C1	122.8(2)
C7	C2	C1	119.5(3)	C4	C3	C2	121.1(3)
C3	C4	C5	120.3(3)	C6	C5	C4	119.9(3)
C5	C6	C7	120.4(3)	C6	C7	C2	120.7(3)
N1	C8	N2	103.4(2)	N1	C8	Ru1	135.35(18)
N2	C8	Ru1	121.18(19)	C10	C9	N1	107.4(2)
C9	C10	N2	107.1(2)	C26	C21	C22	122.1(2)
C26	C21	N1	118.9(2)	C22	C21	N1	118.8(2)
C21	C22	C23	117.4(3)	C21	C22	C27	120.9(3)
C23	C22	C27	121.7(3)	C24	C23	C22	122.0(3)
C25	C24	C23	118.9(3)	C25	C24	C28	120.7(3)
C23	C24	C28	120.4(3)	C24	C25	C26	122.1(3)
C21	C26	C25	117.5(2)	C21	C26	C29	122.2(2)
C25	C26	C29	120.3(2)	C32	C31	C36	122.2(3)
C32	C31	N2	119.5(2)	C36	C31	N2	118.1(3)
C33	C32	C31	117.4(3)	C33	C32	C37	120.5(3)
C31	C32	C37	122.0(3)	C32	C33	C34	122.6(3)
C35	C34	C33	118.0(3)	C35	C34	C38	121.2(3)
C33	C34	C38	120.8(3)	C34	C35	C36	122.6(3)
C35	C36	C31	116.9(3)	C35	C36	C39	119.9(3)
C31	C36	C39	123.1(3)	N3	C41	C42	123.6(3)
C41	C42	C43	120.0(3)	C42	C43	C44	117.9(3)
C43	C44	C45	119.3(3)	N3	C45	C44	123.8(3)
O1	C51	C56	122.4(3)	O1	C51	C52	124.0(3)
C56	C51	C52	113.5(2)	F52	C52	C53	118.8(3)
F52	C52	C51	117.9(2)	C53	C52	C51	123.3(3)
F53	C53	C52	118.9(3)	F53	C53	C54	118.8(2)
C52	C53	C54	122.3(3)	C55	C54	C53	115.0(2)
C55	C54	C61	121.6(3)	C53	C54	C61	123.2(2)
F55	C55	C56	118.5(2)	F55	C55	C54	118.7(2)
C56	C55	C54	122.9(3)	F56	C56	C55	118.5(3)
F56	C56	C51	118.6(2)	C55	C56	C51	122.9(3)
C62	C61	C66	115.7(3)	C62	C61	C54	121.3(3)

C66	C61	C54	122.9(3)	F62	C62	C61	119.1(3)
F62	C62	C63	119.0(3)	C61	C62	C63	121.9(3)
C64	C63	F63	120.7(4)	C64	C63	C62	120.5(4)
F63	C63	C62	118.8(4)	C63	C64	F64	120.4(5)
C63	C64	C65	119.2(3)	F64	C64	C65	120.3(4)
F65	C65	C64	119.5(4)	F65	C65	C66	120.5(4)
C64	C65	C66	119.9(4)	F66	C66	C65	118.1(3)
F66	C66	C61	119.2(3)	C65	C66	C61	122.8(3)
O2	C71	C76	126.6(2)	O2	C71	C72	120.3(2)
C76	C71	C72	113.1(2)	F72	C72	C73	118.4(3)
F72	C72	C71	118.3(2)	C73	C72	C71	123.3(3)
F73	C73	C72	118.8(3)	F73	C73	C74	118.6(3)
C72	C73	C74	122.5(3)	C73	C74	C75	115.3(2)
C73	C74	C81	123.7(3)	C75	C74	C81	120.9(3)
F75	C75	C76	118.1(2)	F75	C75	C74	119.3(2)
C76	C75	C74	122.6(3)	F76	C76	C75	117.6(2)
F76	C76	C71	119.3(2)	C75	C76	C71	123.1(3)
C86	C81	C82	115.5(3)	C86	C81	C74	122.8(3)
C82	C81	C74	121.5(3)	F82	C82	C83	117.8(3)
F82	C82	C81	119.8(3)	C83	C82	C81	122.3(3)
F83	C83	C84	119.8(3)	F83	C83	C82	120.2(3)
C84	C83	C82	119.9(3)	F84	C84	C85	119.9(3)
F84	C84	C83	120.6(3)	C85	C84	C83	119.5(3)
F85	C85	C84	119.6(3)	F85	C85	C86	120.9(3)
C84	C85	C86	119.4(3)	F86	C86	C85	117.2(3)
F86	C86	C81	119.5(3)	C85	C86	C81	123.2(3)

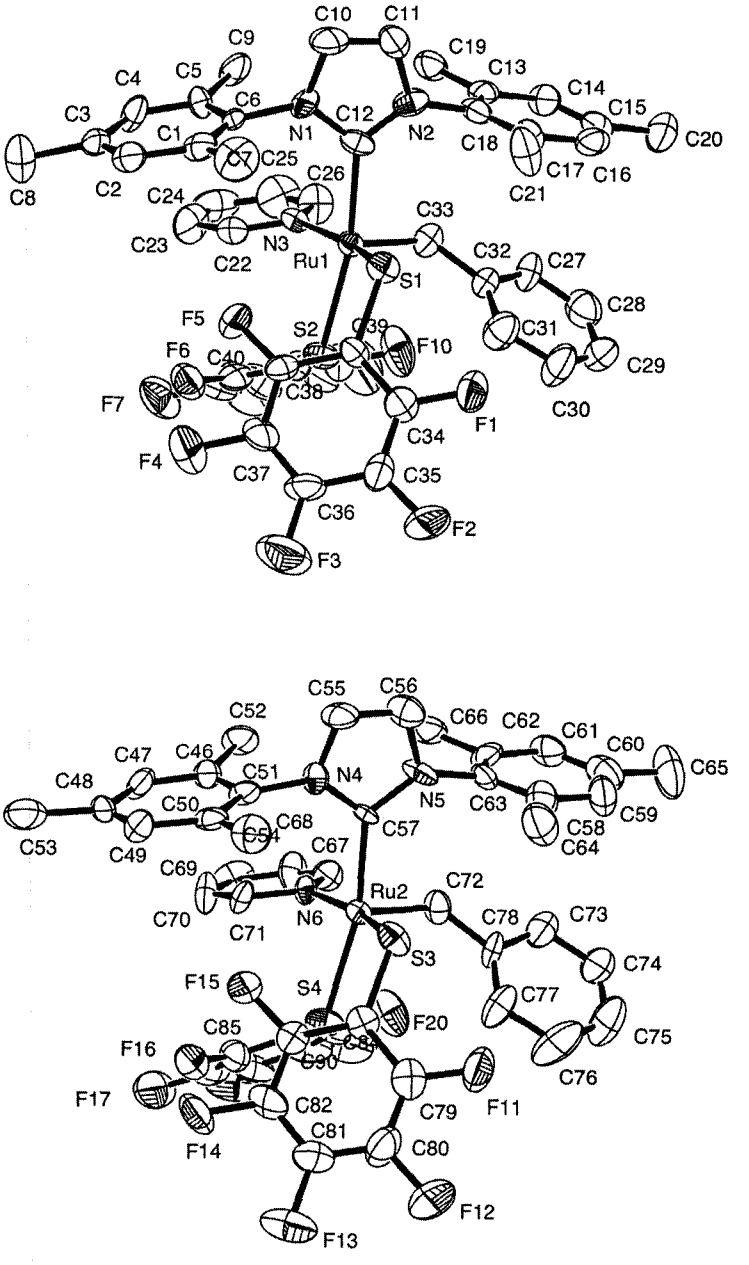

Figure 5. ORTEP representation of the two unique Ru centers found in the crystal structure of $Ru(SC_6F_5)_2(CHPh)(IMes)(py)$, **16b**. Thermal ellipsoids are shown at 50% probability level, hydrogen atoms and decane solvate omitted for clarity.

Table 13. Crystal data and structure refinement for $Ru(SC_6F_5)_2(CHPh)(IMes)(py)$, **16b**.

Crystallographer	Patrick Crewdson	
Identification code	**16b**, $Ru(SC_6F_5)_2(CHPh)(IMes)(py)$	
Empirical formula	C52 H50 F10 N3 S2 Ru	
Formula weight	1083.25	
Temperature	208(2) K	
Wavelength	0.71073 A	
Crystal system	Triclinic	
Space group	P-1	
Unit cell dimensions	a = 12.071(6) Å	α = 94.554(9)°
	b = 20.602(9) Å	β = 105.730(9)°
	c = 21.248(10) Å	γ = 93.469(10)°
Volume	5052(4) $Å^3$	
Z	49	
Density (calculated)	1.396 Mg/m^3	
Absorption coefficient	0.467 mm^{-1}	
F(000)	2172	
Crystal size	0.30 x 0.20 x 0.10 mm^3	
Theta range for data collection	1.76 to 21.26 °.	
Index ranges	-12<=h<=12, -21<=k<=21, -21<=l<=21	
Reflections collected	11101	
Independent reflections	7635 [R(int) = 0.0287]	
Completeness to theta = 28.87°		
Absorption correction	Semi-empirical from equivalents	
Max. and min. transmission	0.8726 and 0.9548	
Refinement method	Full-matrix least-squares on F^2	
Data / restraints / parameters	11101 / 9 / 1159	
Goodness-of-fit on F^2	1.093	
Final R indices [I>2sigma(I)]	R1 = 0.0974, wR2 = 0.2355	
R indices (all data)	R1 = 0.1423, wR2 = 0.2155	
Largest diff. peak and hole	1.639 and -0.540 $e.Å^{-3}$	

Table 14. Bond distances (Å) $Ru(SC_6F_5)_2(CHPh)(IMes)(py)$, **16b**.

Ru1	C33	1 .824(14)	Ru1	C12	2 .062(11)
Ru1	N3	2 .123(10)	Ru1	S1	2 .364(4)
Ru1	S2	2 .369(4)	Ru2	C78	1 .872(13)
Ru2	C57	2 .097(13)	Ru2	N6	2 .148(11)
Ru2	S3	2 .370(4)	Ru2	S4	2 .385(3)
S1	C39	1 .787(13)	S2	C45	1 .748(13)
S3	C84	1 .776(13)	S4	C90	1 .780(13)
N1	C12	1 .390(14)	N1	C10	1 .413(16)
N1	C6	1 .465(16)	N2	C12	1 .383(14)
N2	C11	1 .393(16)	N2	C18	1 .417(15)
N3	C22	1 .336(15)	N3	C26	1 .355(15)
N4	C55	1 .388(16)	N4	C57	1 .391(16)
N4	C51	1 .439(15)	N5	C57	1 .367(16)
N5	C56	1 .382(17)	N5	C63	1 .438(16)
N6	C67	1 .346(17)	N6	C71	1 .356(16)
F1	C34	1 .359(14)	F2	C35	1 .372(15)
F3	C36	1 .365(15)	F4	C37	1 .328(16)
F5	C38	1 .329(16)	F6	C40	1 .329(16)
F7	C41	1 .337(18)	F8	C42	1 .340(17)
F9	C43	1 .319(18)	F10	C44	1 .347(16)
F11	C79	1 .336(14)	F12	C80	1 .342(15)
F13	C81	1 .352(15)	F14	C82	1 .365(15)
F15	C83	1 .328(15)	F16	C85	1 .319(15)
F17	C86	1 .372(18)	F18	C87	1 .330(17)
F19	C88	1 .313(17)	F20	C89	1 .349(16)
C1	C6	1 .386(19)	C1	C2	1 .39(2)
C1	C7	1 .50(2)	C2	C3	1 .40(2)
C3	C4	1 .34(2)	C3	C8	1 .56(2)
C4	C5	1 .381(18)	C5	C6	1 .395(19)
C5	C9	1 .547(19)	C10	C11	1 .319(18)
C13	C14	1 .391(18)	C13	C18	1 .405(18)
C13	C19	1 .502(17)	C14	C15	1 .394(18)
C15	C16	1 .354(19)	C15	C20	1 .512(19)
C16	C17	1 .386(18)	C17	C18	1 .436(17)
C17	C21	1 .462(18)	C22	C23	1 .342(18)
C23	C24	1 .37(2)	C24	C25	1 .40(2)
C25	C26	1 .365(19)	C27	C32	1 .367(19)
C27	C28	1 .39(2)	C28	C29	1 .37(2)
C29	C30	1 .36(2)	C30	C31	1 .36(2)
C31	C32	1 .373(18)	C32	C33	1 .479(17)
C34	C35	1 .361(18)	C34	C39	1 .388(17)
C35	C36	1 .326(19)	C36	C37	1 .34(2)
C37	C38	1 .39(2)	C38	C39	1 .408(18)
C40	C45	1 .384(18)	C40	C41	1 .42(2)

C41	C42	1 .39(2)	C42	C43	1 .37(2)
C43	C44	1 .44(2)	C44	C45	1 .349(19)
C46	C47	1 .392(18)	C46	C51	1 .410(17)
C46	C52	1 .507(19)	C47	C48	1 .379(18)
C48	C49	1 .396(18)	C48	C53	1 .520(18)
C49	C50	1 .355(17)	C50	C51	1 .390(17)
C50	C54	1 .510(17)	C55	C56	1 .309(19)
C58	C59	1 .374(18)	C58	C63	1 .412(18)
C58	C64	1 .490(18)	C59	C60	1 .35(2)
C60	C61	1 .381(19)	C60	C65	1 .529(19)
C61	C62	1 .397(18)	C62	C63	1 .385(19)
C62	C66	1 .508(19)	C67	C68	1 .39(2)
C68	C69	1 .38(2)	C69	C70	1 .35(2)
C70	C71	1 .36(2)	C72	C73	1 .38(2)
C72	C77	1 .409(18)	C73	C74	1 .37(2)
C74	C75	1 .36(2)	C75	C76	1 .36(2)
C76	C77	1 .380(18)	C77	C78	1 .466(17)
C79	C84	1 .383(17)	C79	C80	1 .399(19)
C80	C81	1 .348(19)	C81	C82	1 .358(19)
C82	C83	1 .368(18)	C83	C84	1 .406(18)
C85	C90	1 .386(18)	C85	C86	1 .39(2)
C86	C87	1 .33(2)	C87	C88	1 .39(2)
C88	C89	1 .37(2)	C89	C90	1 .398(18)

Table 15. Bond angles (°) $Ru(SC_6F_5)_2(CHPh)(IMes)(py)$, **16b**.

C33	Ru1	C12	93.2(5)	C33	Ru1	N3	91.8(5)
C12	Ru1	N3	94.7(4)	C33	Ru1	S1	103.1(4)
C12	Ru1	S1	83.8(3)	N3	Ru1	S1	165.1(3)
C33	Ru1	S2	104.3(4)	C12	Ru1	S2	162.1(3)
N3	Ru1	S2	88.4(3)	S1	Ru1	S2	88.66(12)
C78	Ru2	C57	93.1(5)	C78	Ru2	N6	92.4(5)
C57	Ru2	N6	92.9(4)	C78	Ru2	S3	105.3(4)
C57	Ru2	S3	83.4(4)	N6	Ru2	S3	162.1(3)
C78	Ru2	S4	101.9(4)	C57	Ru2	S4	164.7(4)
N6	Ru2	S4	89.7(3)	S3	Ru2	S4	89.46(12)
C39	S1	Ru1	111.6(4)	C45	S2	Ru1	113.0(4)
C84	S3	Ru2	110.4(4)	C90	S4	Ru2	109.7(4)
C12	N1	C10	112.9(10)	C12	N1	C6	129.8(10)
C10	N1	C6	116.6(10)	C12	N2	C11	111.4(10)
C12	N2	C18	127.1(11)	C11	N2	C18	120.6(11)
C22	N3	C26	114.6(11)	C22	N3	Ru1	128.8(8)
C26	N3	Ru1	116.2(8)	C55	N4	C57	110.4(11)
C55	N4	C51	122.3(11)	C57	N4	C51	126.7(10)
C57	N5	C56	110.4(11)	C57	N5	C63	128.9(11)
C56	N5	C63	120.4(12)	C67	N6	C71	116.8(12)
C67	N6	Ru2	114.0(9)	C71	N6	Ru2	128.7(9)

C6	C1	C2	117.2(14)	C6	C1	C7	123.0(13)
C2	C1	C7	119.6(15)	C1	C2	C3	120.1(15)
C4	C3	C2	120.5(14)	C4	C3	C8	120.4(17)
C2	C3	C8	119.0(17)	C3	C4	C5	121.6(14)
C4	C5	C6	117.3(13)	C4	C5	C9	120.9(13)
C6	C5	C9	121.2(12)	C1	C6	C5	122.8(12)
C1	C6	N1	118.8(13)	C5	C6	N1	118.3(13)
C11	C10	N1	104.8(12)	C10	C11	N2	109.5(12)
N2	C12	N1	101.4(9)	N2	C12	Ru1	125.5(8)
N1	C12	Ru1	131.5(8)	C14	C13	C18	118.3(12)
C14	C13	C19	119.9(13)	C18	C13	C19	121.6(12)
C13	C14	C15	122.0(14)	C16	C15	C14	117.8(13)
C16	C15	C20	122.7(13)	C14	C15	C20	119.4(14)
C15	C16	C17	125.1(13)	C16	C17	C18	115.8(13)
C16	C17	C21	122.5(12)	C18	C17	C21	121.6(12)
C13	C18	N2	119.2(11)	C13	C18	C17	120.9(11)
N2	C18	C17	119.4(12)	N3	C22	C23	124.8(13)
C22	C23	C24	120.8(15)	C23	C24	C25	116.6(13)
C26	C25	C24	118.6(14)	N3	C26	C25	124.5(13)
C32	C27	C28	118.6(16)	C29	C28	C27	122.1(18)
C30	C29	C28	117.9(17)	C29	C30	C31	121.0(17)
C30	C31	C32	121.0(15)	C27	C32	C31	119.2(12)
C27	C32	C33	122.5(13)	C31	C32	C33	118.3(13)
C32	C33	Ru1	133.0(10)	F1	C34	C35	118.9(13)
F1	C34	C39	119.3(12)	C35	C34	C39	121.7(13)
C36	C35	C34	121.8(14)	C36	C35	F2	120.5(13)
C34	C35	F2	117.7(13)	C35	C36	C37	119.6(14)
C35	C36	F3	119.9(15)	C37	C36	F3	120.3(14)
F4	C37	C36	121.5(15)	F4	C37	C38	117.3(14)
C36	C37	C38	121.1(14)	F5	C38	C37	120.4(13)
F5	C38	C39	119.3(13)	C37	C38	C39	120.3(14)
C34	C39	C38	115.4(13)	C34	C39	S1	122.7(11)
C38	C39	S1	121.8(11)	F6	C40	C45	119.8(13)
F6	C40	C41	117.0(14)	C45	C40	C41	123.2(15)
F7	C41	C42	121.5(16)	F7	C41	C40	120.2(18)
C42	C41	C40	118.3(16)	F8	C42	C43	120.3(18)
F8	C42	C41	118.7(18)	C43	C42	C41	121.0(15)
F9	C43	C42	120.6(18)	F9	C43	C44	122.7(18)
C42	C43	C44	116.6(16)	F10	C44	C45	121.7(14)
F10	C44	C43	112.8(15)	C45	C44	C43	125.5(15)
C44	C45	C40	115.2(13)	C44	C45	S2	120.6(11)
C40	C45	S2	123.8(11)	C47	C46	C51	116.9(13)
C47	C46	C52	120.8(13)	C51	C46	C52	122.0(13)
C48	C47	C46	122.2(12)	C47	C48	C49	117.8(12)
C47	C48	C53	120.6(13)	C49	C48	C53	121.6(14)
C50	C49	C48	122.9(13)	C49	C50	C51	118.0(12)
C49	C50	C54	120.4(12)	C51	C50	C54	121.5(11)

C50	C51	C46	122.1(11)	C50	C51	N4	118.1(11)
C46	C51	N4	119.6(12)	C56	C55	N4	107.0(13)
C55	C56	N5	108.9(13)	N5	C57	N4	103.3(11)
N5	C57	Ru2	130.2(10)	N4	C57	Ru2	125.9(9)
C59	C58	C63	116.5(13)	C59	C58	C64	121.9(13)
C63	C58	C64	121.6(13)	C60	C59	C58	123.8(14)
C59	C60	C61	118.9(14)	C59	C60	C65	122.0(15)
C61	C60	C65	119.0(14)	C60	C61	C62	121.1(13)
C63	C62	C61	117.8(13)	C63	C62	C66	122.0(12)
C61	C62	C66	120.1(13)	C62	C63	C58	121.7(12)
C62	C63	N5	120.4(12)	C58	C63	N5	117.7(12)
N6	C67	C68	123.6(16)	C69	C68	C67	118.3(17)
C70	C69	C68	117.9(17)	C69	C70	C71	122.4(18)
N6	C71	C70	121.0(16)	C73	C72	C77	118.3(15)
C74	C73	C72	122.6(16)	C75	C74	C73	117.6(16)
C76	C75	C74	122.2(17)	C75	C76	C77	120.7(14)
C76	C77	C72	118.5(12)	C76	C77	C78	126.7(13)
C72	C77	C78	114.8(12)	C77	C78	Ru2	129.6(10)
F11	C79	C84	120.9(12)	F11	C79	C80	118.5(12)
C84	C79	C80	120.5(12)	F12	C80	C81	121.3(14)
F12	C80	C79	117.8(13)	C81	C80	C79	120.7(13)
C80	C81	F13	119.9(14)	C80	C81	C82	119.4(13)
F13	C81	C82	120.6(14)	C81	C82	F14	119.4(13)
C81	C82	C83	121.7(13)	F14	C82	C83	118.8(14)
F15	C83	C82	118.8(13)	F15	C83	C84	121.1(12)
C82	C83	C84	120.1(13)	C79	C84	C83	117.3(12)
C79	C84	S3	121.6(10)	C83	C84	S3	120.7(10)
F16	C85	C90	119.9(13)	F16	C85	C86	120.7(14)
C90	C85	C86	119.4(14)	C87	C86	F17	120.9(17)
C87	C86	C85	123.5(16)	F17	C86	C85	115.6(17)
C86	C87	F18	120.4(18)	C86	C87	C88	119.1(16)
F18	C87	C88	120.4(16)	F19	C88	C89	122.3(16)
F19	C88	C87	119.6(16)	C89	C88	C87	118.0(16)
F20	C89	C88	115.7(13)	F20	C89	C90	120.0(12)
C88	C89	C90	124.3(15)	C85	C90	C89	115.7(13)
C85	C90	S4	123.2(11)	C89	C90	S4	121.1(10)
C93	C92	C91	113(3)	C92	C93	C94	117(2)
C95	C94	C93	117.7(19)	C94	C95	C96	119(2)
C95	C96	C97	111(2)	C98	C97	C96	114(3)
C97	C98	C99	110(3)	C100	C99	C98	115(3)
C101	C101	C102	130(3)	C101	C102	C103	110(2)
C103	C104	C105	111(3)	C104	C103	C102	120(3)

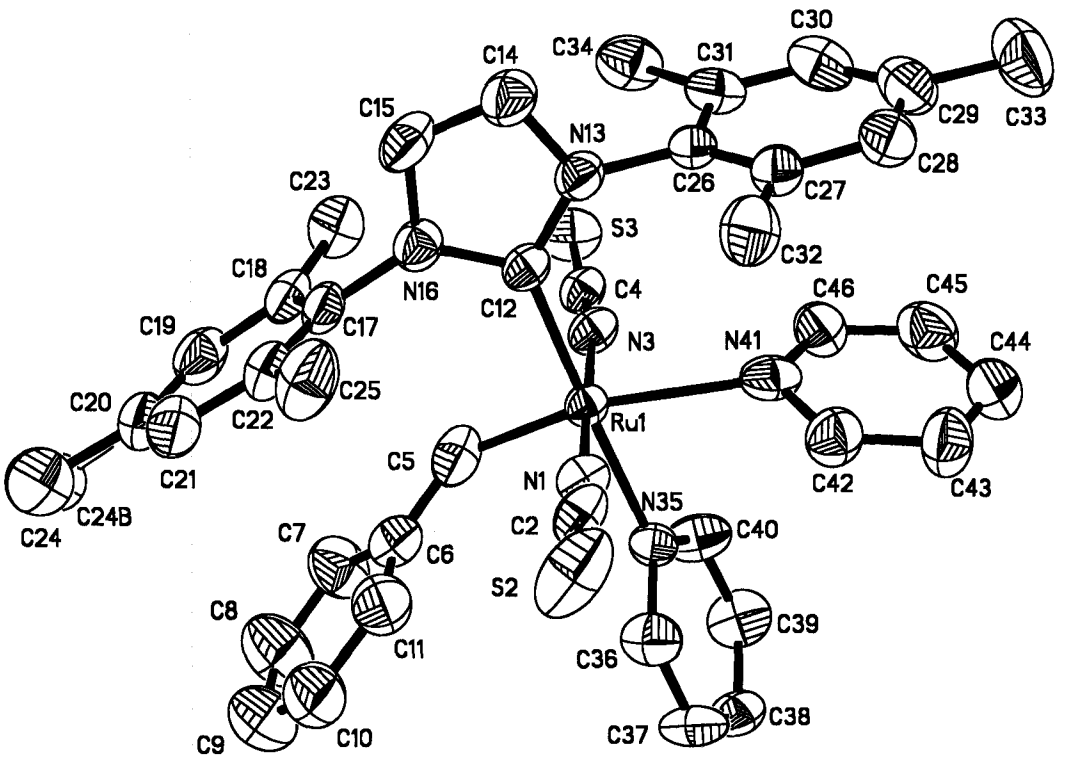

Figure 6. ORTEP representation of $Ru(NCS)_2(CHPh)(IMes)(py)_2$, **18a**. Thermal ellipsoids are shown at 50% probability level; hydrogen atoms, THF solvate omitted for clarity.

Table 16. Crystal data and structure refinement for $Ru(NCS)_2(CHPh)(IMes)(py)_2$, **18a**.

Crystallographer	Prof. Hillary Jenkins	
Empirical formula	C42 H44 N6 O0.50 Ru S2	
Formula weight	806.02	
Temperature	208(2) K	
Wavelength	0.71073 Å	
Crystal system	Monoclinic	
Space group	C2/c	
Unit cell dimensions	a = 35.989(4) Å	α = 90°.
	b = 10.5410(10) Å	β = 118.082(2)°
	c = 24.085(3) Å	γ = 90°
Volume	8061.2(15) $Å^3$	
Z	8	
Density (calculated)	1.328 Mg/m^3	
Absorption coefficient	0.531 mm^{-1}	
F(000)	3344	
Crystal size	0.40 x 0.20 x 0.08 mm^3	
Theta range for data collection	1.28 to 26.37°.	
Index ranges	-44<=h<=44, -13<=k<=13,	
	-19<=l<=29	
Reflections collected	18700	
Independent reflections	8200 [R(int) = 0.0729]	
Completeness to theta = 26.37°	99.5 %	
Absorption correction	Semi-empirical from equivalents	
Max. and min. transmission	1.0 and 0.76	
Refinement method	Full-matrix least-squares on F^2	
Data / restraints / parameters	8200 / 9 / 467	
Goodness-of-fit on F^2	1.029	
Final R indices [I>2sigma(I)]	R1 = 0.0633, wR2 = 0.1268	
R indices (all data)	R1 = 0.1175, wR2 = 0.1437	
Largest diff. peak and hole	0.689 and -0.653 $e.Å^{-3}$	

Table 17. Bond distances (Å) for $Ru(NCS)_2(CHPh)(IMes)(py)_2$, **18a**.

Ru1	C5	1.901(6)	Ru1	N1	2.042(4)
Ru1	N3	2.050(4)	Ru1	C12	2.068(4)
Ru1	N35	2.191(4)	Ru1	N41	2.331(4)
N1	C2	1.161(6)	C2	S2	1.631(5)
N3	C4	1.156(6)	C4	S3	1.627(5)
C5	C6	1.357(8)	C6	C11	1.357(8)
C6	C7	1.463(8)	C7	C8	1.342(9)
C8	C9	1.351(9)	C9	C10	1.379(9)
C10	C11	1.388(8)	C12	N13	1.362(6)
C12	N16	1.390(6)	N13	C14	1.375(6)
N13	C26	1.440(6)	C14	C15	1.324(7)
C15	N16	1.376(6)	N16	C17	1.444(6)
C17	C22	1.368(7)	C17	C18	1.420(6)
C18	C19	1.391(7)	C18	C23	1.483(7)
C19	C20	1.391(8)	C20	C21	1.385(8)
C20	C24	1.502(9)	C20	C24B	1.562(14)
C21	C22	1.383(8)	C22	C25	1.508(7)
C26	C31	1.388(7)	C26	C27	1.409(7)
C27	C28	1.391(7)	C27	C32	1.487(7)
C28	C29	1.381(8)	C29	C30	1.385(8)
C29	C33	1.520(8)	C30	C31	1.389(7)
C31	C34	1.516(7)	N35	C36	1.323(6)
N35	C40	1.328(6)	C36	C37	1.388(7)
C37	C38	1.341(7)	C38	C39	1.376(7)
C39	C40	1.398(7)	N41	C46	1.334(6)
N41	C42	1.339(6)	C42	C43	1.371(7)
C43	C44	1.365(8)	C44	C45	1.392(8)
C45	C46	1.378(7)			

Table 18. Bond angles (°) for $Ru(NCS)_2(CHPh)(IMes)(py)_2$, **18a**.

C5	Ru1	N1	97.1(2)	C5	Ru1	N3	85.7(2)
N1	Ru1	N3	176.55(16)	C5	Ru1	C12	96.3(2)
N1	Ru1	C12	87.32(16)	N3	Ru1	C12	90.38(17)
C5	Ru1	N35	86.15(19)	N1	Ru1	N35	90.18(15)
N3	Ru1	N35	92.02(15)	C12	Ru1	N35	176.67(16)
C5	Ru1	N41	161.54(18)	N1	Ru1	N41	89.96(15)
N3	Ru1	N41	87.97(15)	C12	Ru1	N41	101.03(16)
N35	Ru1	N41	76.75(14)	C2	N1	Ru1	173.2(4)
N1	C2	S2	178.1(5)	C4	N3	Ru1	170.2(4)
N3	C4	S3	178.4(5)	C6	C5	Ru1	138.2(5)
C5	C6	C11	125.3(6)	C5	C6	C7	117.0(6)
C11	C6	C7	117.8(6)	C8	C7	C6	117.8(6)
C7	C8	C9	125.3(7)	C8	C9	C10	116.4(7)
C9	C10	C11	122.2(7)	C6	C11	C10	120.5(6)
N13	C12	N16	102.4(4)	N13	C12	Ru1	129.7(3)
N16	C12	Ru1	127.6(3)	C12	N13	C14	112.0(4)
C12	N13	C26	127.9(4)	C14	N13	C26	119.7(4)
C15	C14	N13	107.2(5)	C14	C15	N16	107.5(5)
C15	N16	C12	110.8(4)	C15	N16	C17	120.8(4)
C12	N16	C17	128.2(4)	C22	C17	C18	123.3(5)
C22	C17	N16	119.2(4)	C18	C17	N16	117.3(5)
C19	C18	C17	114.9(5)	C19	C18	C23	121.2(5)
C17	C18	C23	123.9(5)	C18	C19	C20	123.8(6)
C21	C20	C19	117.4(6)	C21	C20	C24	110.3(14)
C19	C20	C24	132.0(14)	C21	C20	C24B	131.6(13)
C19	C20	C24B	110.9(13)	C24	C20	C24B	23.38(16)
C22	C21	C20	122.1(6)	C17	C22	C21	118.3(5)
C17	C22	C25	121.5(5)	C21	C22	C25	120.2(5)
C31	C26	C27	122.3(5)	C31	C26	N13	118.7(5)
C27	C26	N13	118.7(5)	C28	C27	C26	117.1(5)
C28	C27	C32	121.6(5)	C26	C27	C32	121.2(5)
C29	C28	C27	121.9(5)	C28	C29	C30	119.1(6)
C28	C29	C33	120.3(6)	C30	C29	C33	120.7(6)
C29	C30	C31	121.8(6)	C30	C31	C26	117.7(5)
C30	C31	C34	120.8(5)	C26	C31	C34	121.6(5)
C36	N35	C40	116.9(4)	C36	N35	Ru1	122.2(3)
C40	N35	Ru1	120.9(3)	N35	C36	C37	123.1(5)
C38	C37	C36	120.2(5)	C37	C38	C39	118.1(5)
C38	C39	C40	118.7(5)	N35	C40	C39	123.1(5)
C46	N41	C42	116.2(5)	C46	N41	Ru1	121.5(3)
C42	N41	Ru1	120.0(4)	N41	C42	C43	123.5(5)
C44	C43	C42	120.3(6)	C43	C44	C45	117.1(6)
C46	C45	C44	119.2(6)	N41	C46	C45	123.7(5)

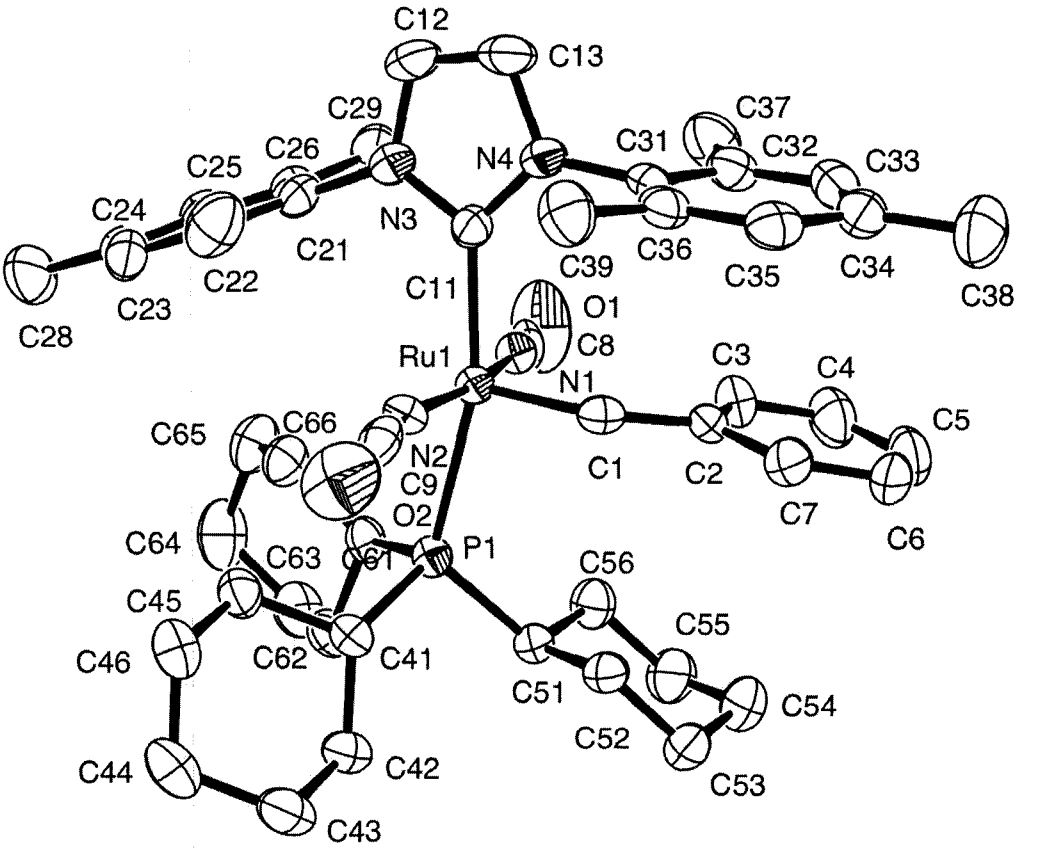

Figure 7. ORTEP representation of $Ru(NCO)_2(CHPh)(IMes)(PCy_3)$, **19b**. Thermal ellipsoids are shown at 50% probability level; hydrogen atoms omitted for clarity.

Table 19. Crystal data and structure refinement for $Ru(NCO)_2(CHPh)(IMes)(PCy_3)$, **19b**.

Crystallographer	Dr. Hilary Jenkins	
Empirical formula	C48 H63 N4 O2 P Ru	
Formula weight	860.06	
Temperature	223(2) K	
Wavelength	0.71073 A	
Crystal system	Monoclinic	
Unit cell dimensions	a = 18.9622(13)Å	α = 90.00°
	b = 15.2158(10) Å	β = 104.7590(10)°
	c = 15.9493(11) Å	γ = 90.00°
Volume	4449.9(5) $Å^3$	
Z	4	
Density (calculated)	1.284 Mg/m^3	
Absorption coefficient	0.460 mm^{-1}	
F(000)	1864	
Crystal size		
Theta range for data collection	1.11 to 25.00	
Index ranges	-22<=h<=22, -18<=k<=18, -18<=l<=18	
Reflections collected	32350	
Independent reflections	32350 [R(int) = 0.0496]	
Completeness to theta =		
Absorption correction	Semi-empirical from equivalents	
Max. and min. transmission		
Refinement method	Full-matrix least-squares on F^2	
Data / restraints / parameters	7829 / 0 / 505	
Goodness-of-fit on F^2	1.007	
Final R indices [I>2sigma(I)]	R1 = 0.0745, wR2 = 0.0753	
R indices (all data)	R1 = 0.0370, wR2 = 0.0709	
Largest diff. peak and hole	0.364 and -0.438 $e.Å^{-3}$	

Table 20. Bond distances (Å) for $Ru(NCO)_2(CHPh)(IMes)(PCy_3)$, **19b**.

Ru1	C1	1.834(3)	Ru1	C11	2.087(3)
Ru1	N2	2.092(3)	Ru1	N1	2.101(3)
Ru1	P1	2.4506(8)	P1	C61	1.845(3)
P1	C51	1.857(3)	P1	C41	1.864(3)
N1	C8	0.906(4)	N2	C9	1.006(4)
O1	C8	1.344(4)	O2	C9	1.293(4)
N3	C11	1.361(3)	N3	C12	1.387(4)
N3	C21	1.443(4)	N4	C11	1.360(3)
N4	C13	1.390(4)	N4	C31	1.450(3)
C1	C2	1.464(4)	C2	C3	1.387(4)
C2	C7	1.397(4)	C3	C4	1.373(4)
C4	C5	1.381(5)	C5	C6	1.377(5)
C6	C7	1.391(4)	C12	C13	1.322(4)
C21	C22	1.390(4)	C21	C26	1.393(4)
C22	C23	1.390(4)	C22	C27	1.503(4)
C23	C24	1.384(4)	C24	C25	1.387(4)
C24	C28	1.508(4)	C25	C26	1.385(4)
C26	C29	1.511(4)	C31	C36	1.381(4)
C31	C32	1.389(4)	C32	C33	1.379(4)
C32	C37	1.508(4)	C33	C34	1.379(4)
C34	C35	1.396(4)	C34	C38	1.502(4)
C35	C36	1.383(4)	C36	C39	1.515(4)
C41	C45	1.531(4)	C41	C42	1.541(4)
C42	C43	1.524(4)	C43	C44	1.514(4)
C44	C46	1.520(4)	C45	C46	1.525(4)
C51	C52	1.531(4)	C51	C56	1.535(4)
C52	C53	1.530(4)	C53	C54	1.509(4)
C54	C55	1.522(4)	C55	C56	1.530(4)
C61	C62	1.537(4)	C61	C66	1.537(4)
C62	C63	1.530(4)	C63	C64	1.513(4)
C64	C65	1.524(5)	C65	C66	1.530(4)

Table 21. Bond angles (°) for $Ru(NCO)_2(CHPh)(IMes)(PCy_3)$, **19b**.

C1	Ru1	C11	98.62(11)	C1	Ru1	N2	87.01(12)
C11	Ru1	N2	90.73(10)	C1	Ru1	N1	102.00(12)
C11	Ru1	N1	87.63(11)	N2	Ru1	N1	170.98(11)
C1	Ru1	P1	97.99(8)	C11	Ru1	P1	163.39(8)
N2	Ru1	P1	90.55(7)	N1	Ru1	P1	88.53(8)
C61	P1	C51	102.20(13)	C61	P1	C41	109.81(13)
C51	P1	C41	103.66(13)	C61	P1	Ru1	107.88(9)
C51	P1	Ru1	119.34(9)	C41	P1	Ru1	113.23(9)
C8	N1	Ru1	173.9(4)	C9	N2	Ru1	168.9(3)
C11	N3	C12	111.2(3)	C11	N3	C21	126.7(2)

C12	N3	C21	122.0(3)	C11	N4	C13	111.2(3)
C11	N4	C31	127.9(2)	C13	N4	C31	120.9(3)
C2	C1	Ru1	137.1(2)	C3	C2	C7	117.7(3)
C3	C2	C1	124.5(3)	C7	C2	C1	117.8(3)
C4	C3	C2	121.7(3)	C3	C4	C5	119.7(3)
C6	C5	C4	120.6(3)	C5	C6	C7	119.2(3)
C6	C7	C2	121.1(3)	N1	C8	O1	176.1(5)
N2	C9	O2	178.3(4)	N3	C11	N4	103.5(2)
N3	C11	Ru1	124.7(2)	N4	C11	Ru1	131.8(2)
C13	C12	N3	107.1(3)	C12	C13	N4	107.0(3)
C22	C21	C26	122.3(3)	C22	C21	N3	118.9(3)
C26	C21	N3	118.6(3)	C21	C22	C23	117.2(3)
C21	C22	C27	122.0(3)	C23	C22	C27	120.8(3)
C24	C23	C22	122.7(3)	C23	C24	C25	117.8(3)
C23	C24	C28	121.3(3)	C25	C24	C28	120.9(3)
C26	C25	C24	122.1(3)	C25	C26	C21	117.8(3)
C25	C26	C29	119.6(3)	C21	C26	C29	122.6(3)
C36	C31	C32	122.6(3)	C36	C31	N4	118.8(3)
C32	C31	N4	118.3(3)	C33	C32	C31	117.5(3)
C33	C32	C37	121.0(3)	C31	C32	C37	121.5(3)
C32	C33	C34	122.6(3)	C33	C34	C35	117.6(3)
C33	C34	C38	121.8(3)	C35	C34	C38	120.6(3)
C36	C35	C34	122.1(3)	C31	C36	C35	117.5(3)
C31	C36	C39	121.9(3)	C35	C36	C39	120.6(3)
C45	C41	C42	109.2(2)	C45	C41	P1	113.1(2)
C42	C41	P1	117.5(2)	C43	C42	C41	110.5(2)
C44	C43	C42	112.0(3)	C43	C44	C46	110.8(3)
C46	C45	C41	110.9(2)	C44	C46	C45	110.9(3)
C52	C51	C56	110.4(2)	C52	C51	P1	111.57(19)
C56	C51	P1	113.5(2)	C53	C52	C51	111.6(2)
C54	C53	C52	111.3(3)	C53	C54	C55	110.9(3)
C54	C55	C56	111.8(3)	C55	C56	C51	111.0(2)
C62	C61	C66	110.6(2)	C62	C61	P1	116.1(2)
C66	C61	P1	114.6(2)	C63	C62	C61	110.5(3)
C64	C63	C62	111.1(3)	C63	C64	C65	111.3(3)
C64	C65	C66	111.4(3)	C65	C66	C61	109.7(2)

13) J. C. Conrad, M. D. Eelman, J. A. Duarte Silva, S. Monfette, H. H. Parnas, J. L. Snelgrove, D. E. Fogg,* "Oligomers as Intermediates in Ring-Closing Metathesis." *J. Am. Chem. Soc.*, **2006**, 1024-1025.

12) S. Monfette, J. C. Conrad, J. M. Blacquiere, N. Beach, D. E. Fogg "Ru-Aryloxide Catalysts for Olefin Metathesis" *NATO ASI series*, accepted.

11) M.U. Delgado-Jaime, J.C. Conrad, D.E. Fogg, P. Kennepohl*, "Electronic Structure of Ru Catalysts using X-ray Absorption." *Inorg. Chim. Acta,* **2006**, *359*, 3042-3047.

10) J. C. Conrad, J. L. Snelgrove, M. D. Eeelman, S. Hall, D. E. Fogg*, "Ruthenium Aryloxide Catalysts: Synthesis and Applications in Ring-Closing Metathesis" *J. Mol. Catal. A*, **2006**, *254*, 105-110.

9) J. C. Conrad, D.E. Fogg,* "Ring-Closing Metathesis: Advances, Limitations, and Opportunities." *Current Organic Chemistry*, **2006**, *10*, 185-202

8) J. C. Conrad, K. D. Camm, D. E. Fogg*, "Ru-Aryloxide Metathesis Catalysts with Enhanced Lability." *Inorg. Chim. Acta*, **2006**, *359*, 1967–1973.

7) J. C. Conrad, H. Parnas, J. S. Snelgrove, D. E. Fogg,* "Ruthenium-Pseudohalide Complexes: Efficient Catalysts for Olefin Metathesis." *J. Am. Chem. Soc.*, **2005**, *127*, 11882-11883.

6) J.L. Snelgrove, J.C. Conrad, M.D. Eelman, M.M. Moriarty, G.P.A. Yap, D.E. Fogg*, "Inhibiting σ–π Isomerization of Aryloxide in Late Transition Metal Complexes." *Organometallics*, **2005**, *24*, 103.

5) J.C. Conrad, D. Amoroso, P. Czechura, G.P.A. Yap, D.E. Fogg*, "The First Highly Active, Halide-Free Ruthenium Catalyst for Olefin Metathesis", *Organometallics*, **2003**, *22*, 3634.

4) J.L. Snelgrove, J.C. Conrad, G.P.A. Yap, D. E. Fogg*, " The Kinetic Instability of s-Bound Aryloxide in Coordinatively Unsaturated or Labile Complexes of Ruthenium." *Inorg. Chim. Acta.*, **2003**, *345*, 268.

3) J. C. Conrad, G. P. A. Yap, D. E. Fogg*, "A Concise Route to Highly Reactive Ruthenium Metathesis Catalysts Containing a Labile Donor and an *N*-Heterocyclic Carbene (NHC) Ligand", *Organometallics*, **2003**, *22*, 1986.

2) D. Amoroso, J. L. Snelgrove, J.C. Conrad, G.P.A. Yap, D.E. Fogg*, "A Ruthenium Alkylidene Complex Containing Labile Phosphane Donors: One-Step Synthesis from a Commercially Available Precursor." *Advanced Synthesis & Catalysis*, **2002**, *344*, 757.

1) D. E. Fogg*, D. Amoroso, S. D. Drouin, J.L. Snelgrove, J.C. Conrad, F. Zamanian, "Ligand Manipulation and Design for Ruthenium Metathesis and Tandem Metathesis-Hydrogenation Catalysis", *J. Mol. Catal. A*, **2002**, *190*, 177.

Manuscripts in Preparation

J. C. Conrad, C. Carra, D. E. Fogg "Pentabromophenoxide as an Anionic Ligand in Ru-Catalyzed Olefin Metathesis: A DFT Study" submitted.

J. C. Conrad, D. E. Fogg "Highly Efficient Ru-Pseudohalide Catalysts for Olefin Metathesis" in preparation.

J. C. Conrad, J. M. Blacquiere, D. E. Fogg "Carbonate as a chemical trigger for assisted tandem RCM-Isomerization based on well-defined ruthenium complexes" *Organometallics,* submitted.

J. C. Conrad, S. Monfette, D. E. Fogg "The Development of Anionic Ligands in Ru Metathesis Chemistry" (review article) in preparation.

J. C. Conrad, K. Camm, D. E. Fogg "Easily Remved Catalysts for Oleifn Metathesis and the Effect of Reaction Time on Catalyst Removal" in preparation.

J. C. Conrad, D. E. Fogg "Thioaryloxide and Linear Pseudohalides in Ru Metathesis Chemistry" in preparation.

J. C. Conrad, S. Monfette, D. E. Fogg "The Unique Properties of the Pentabromoaryloxide Ligand" in preparation.

J. C. Conrad, J. L Snelgrove, J. Blacquiere, N. Beach, D. E. Fogg "Asymmetric Ru Catalysts for Olefin Metathesis" in preparation.

Patents

D. E. Fogg, J.C. Conrad
"Ruthenium Compounds, Their Production and Use" (fully allowed)
WO 2005012315 (2004)
US 10/855,485
PCT-CA2004/001420